Effects of conformation on the electronic and optical properties of aryleneethynylenes

Simon Richard Rutter

EFFECTS OF CONFORMATION ON THE ELECTRONIC AND OPTICAL PROPERTIES OF ARYLENEETHYNYLENES

Simon Richard Rutter

Department of Chemistry

University of Durham

Durham, U.K.

Submitted in partial fulfilment of the requirements for the degree of Doctor of Philosophy, University of Durham.

March 2007

Declaration

The work described in this thesis was carried out in the Department of Chemistry at the University of Durham between October 2002 and September 2005. This thesis is the work of the author except where acknowledged by reference and has not been submitted for any other degree.

Statement of Copyright

Abstract

Materials based upon the aryleneethynylene skeleton are currently of great interest. The fluorescent and electroluminescent properties of both molecular and polymeric systems has prompted speculation about the suitability of these materials as the emitting layer in electroluminescent devices, while the conjugated π-system has led to the development of molecular wire-like architectures, and materials which display negative differential resistance.

The degree of conjugation in the π-system is dependent on the relative orientation of the aromatic rings. The barrier to rotation about the aryl-alkynyl single bond for phenyleneethynylenes is very low, leading to a continuum of rotational isomers when in solution. Engineering physical control over the conformation of aryleneethynylenes therefore presents a significant challenge.

In this work, a review is presented on the uses, behaviour and synthesis of aryleneethynylenes, followed by an account of the practical work carried out. Initially various series of 1,4-bis(phenylethynyl)benzene (BPEB) analogues containing naphthalene and thiophene moieties were produced. Study of the photophysical behaviour and molecular modelling of these systems suggests that the choice of central ring in a three ring aryleneethynylene system has the greatest effect on the compounds' characteristics. This can be attributed to the π-electrons of the central aromatic ring giving the largest contribution to the frontier orbitals of these compounds.

Conformational control of aryleneethynylenes is then examined. Derivatives of BPEB and 9,10-bis(phenylethynyl)anthracene (BPEA) with bulky alkyl substituents have been synthesised, with the aim of using steric bulk to restrict rotation about the acetylenic bond. Initial attempts at this approach resulted in the additional steric bulk only giving slight conformational restriction in the solid state as well as only having a small effect on the observed photophysics. Subsequently, compounds were successfully synthesised where, in the ground state, the two outer rings were orthogonal to the central ring system, switching off their contribution to the frontier orbitals, and thus leading to significant changes in photophysical behaviour being observed relative to BPEB and BPEA.

Simon Richard Rutter, March 2007

Acknowledgements

Firstly my thanks must go to my supervisor, Dr Andrew Beeby. Thank you for giving me the chance to study for this PhD as well as for all the help and support you have given me along the way!

My thanks must also go to the EPSRC for their financial support including the provision of my PhD studentship, and One NorthEast for financial support through the Nanomaterials UIC during the latter stages of my research.

For their technical assistance I must thank Dr Amber Thompson and Dr Andrés Goeta for their X-ray crystallographic analysis of my compounds. Also Dr Alan Kenwright, Catherine Heffernan and Ian McKeag for NMR assistance, Dr Mike Jones and Lara Turner for mass spectrometry and Jarika Dostal for elemental analysis. Thanks must also be given to Barry Barker and Kelvin Appleby in the electrical workshop and Jim Hodgson and Neil Holmes in the mechanical workshop, as well as the glassblowers Peter Coyne and Malcolm Richardson.

Many thanks to those members of the Beeby group who I've worked alongside throughout the course of my research - Sylvia, Karen, Kate, Laurent, Bex, Ruth and Frances. Thanks for your help in the lab as well as providing a friendly and relaxed atmosphere to work in!

Thanks must also go to the good friends I have made along the way. From my fellow chemists Chris, Kate (again!), and Graham, to all those who I have got to know in the Motor-Sports Society, especially Matt, Shelley and Helen. You have all helped me escape the world of chemistry when away from the lab!

My most important and final thanks must go to those closest to me. First of all to my girlfriend Ally, you most of all have helped me to stay sane through the last two years! Also I must thank my family, particularly Mum, Dad, Em and Grandma, for their advice and support throughout my life but also more especially my time in Durham. Without the love and support you have all given me I wouldn't have got this far. Thank you!

Abbreviations

Ar: Aryl

ADIMET: Acyclic diyne metathesis

Alq_3: Tris(8-hydroxyquinoline)aluminium

BPEA: 9,10-Bis(phenylethynyl)anthracene

BPEB: 1,4-Bis(phenylethynyl)benzene

Bu: Butyl

COSHH: Control of substances hazardous to health

CRDS: Cavity-ring-down spectroscopy

DCM: Dichloromethane

DFT: Density functional theory

DMSO: Dimethyl sulfoxide

DNT: 2,4-Dinitrotoluene

DSC: Differential scanning calorimetry

EDOT: 3,4-Ethylenedioxythiophene

EEM: Emission-excitation matrix

EI: Electron ionisation

EL: Electroluminescent / electroluminescence

EO: Electro-optical

EPA: Solvent mixture of diethyl ether, *iso*-pentane and ethanol in a 5:5:2 ratio (v/v)

Et: Ethyl

ETHBL: Electron-transport and hole-blocking layer

ETM: Electron-transport material

ε: Extinction coefficient

GC-MS: Gas chromatography - mass spectrometry

GPC: Gel permeation chromatography

Grad: Gradient

h: Planck's constant

HOMO: Highest occupied molecular orbital

HTM: Hole-transport material

IC: Internal conversion

ICT: Intramolecular charge transfer

^{i}Pr: *Iso*-propyl

IR: Infrared

ISC: Inter-system crossing

ITO: Indium-tin-oxide

k: Rate constant

L: Ligand

LC: Liquid crystal

LCD: Liquid crystal display

LED: Light emitting diode

LUMO: Lowest unoccupied molecular orbital

λ: Emission wavelength

MALDI-MS: Matrix-assisted laser desorption/ionization - mass spectrometry

MDP: Molecularly doped polymer

Me: Methyl

MP: Melting point

MS: Mass spectrometry

NDR: Negative differential resistance

NMR: Nuclear magnetic resonance

NMP: N-Methylpyrrolidone

OAc: Acetate

OLED: Organic light emitting diode

PEDOT: Poly(3,4-ethylenedioxythiophene)

Ph: Phenyl

PIPES: Piperazine-1,4-bis(2-ethanesulfonic acid)

PMMA: Poly(methyl methacrylate)

POPOP: 1,4-Bis(5-phenyloxazole-3-yl)benzene

PPE: Poly(phenyleneethynylene)

PPV: Poly(*para*-phenylenevinylene)

PQ: Paraquat

PSS: Poly(styrenesulfonate)

PVR: Peak to valley ratio

Φ: Quantum yield

RAM: Random access memory

ROMP: Ring-opening metathesis polymerisation

RTD: Resonant tunnelling diode

η: Refractive index

S_0: Singlet ground state

S_1: First excited singlet state

SAM: Self assembled monolayer

STM: Scanning tunnelling microscope

T_1: First excited triplet state

^{t}Bu: *Tertiary*-butyl

TBDPS: *Tertiary*-butyl diphenylsilyl

TCSPC: Time-correlated single photon counting

TD-DFT: Time-dependent density functional theory

THF: Tetrahydrofuran

THP: Tetrahydropyran

TMS: Trimethylsilyl

TMSA: Trimethylsilyl acetylene

TN: Twisted nematic

TNT: 2,4,6-Trinitrotoluene

TPD: N,N′-Diphenyl-N,N′-bis(3-methylphenyl)-1,1′-biphenyl-4,4′-diamine

TR^3: Time-resolved resonance Raman

τ: Lifetime

UHMW-PE: Ultra-high molecular weight polyethylene

UV: Ultraviolet

v: Volume

VR: Vibrational relaxation

Contents

CHAPTER 1

INTRODUCTION

EFFECTS OF CONFORMATION ON THE ELECTRONIC AND OPTICAL PROPERTIES OF ARYLENEETHYNYLENES

1.1 - Introduction

Aryleneethynylenes are a class of highly conjugated compounds that are made up of alternating aryl-ethynyl-aryl units. The simplest example is diphenylacetylene or tolan, **1**, with another being 1,4-bis(phenylethynyl)benzene or BPEB, **2**. Due to the highly conjugated nature of these compounds they have potential uses as molecular wires and in organic light emitting diodes (OLEDs). Their rigid linear nature can also lead to them displaying liquid crystalline behaviour. The following section will look into this behaviour in more detail.

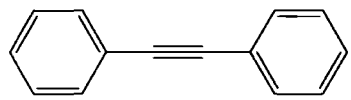

1

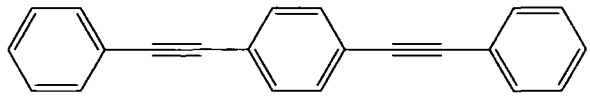

2

1.2 - Uses of Aryleneethynylenes

1.2.1 - Molecular electronics

Computer technology is constantly becoming more and more powerful. In 1968 Gordon Moore predicted that the number of devices on computer chips would double every 18-24 months.[1] The resultant doubling of computational power, known as "Moore's Law," has since then followed that prediction. At the moment this is achieved by a "top-down" approach by the downsizing of the current silicon chip technology. This will encounter problems in the fairly near future as the size of chips reaches the physical limit - for example once the oxide layers on silicon chips reach a thickness of three atoms they become poorly insulating resulting in charge leakage.[2-4]

Due to this problem an alternative approach will soon need to be found. In December 1959 Feynman gave a talk entitled "There is Plenty of Room at the Bottom". In this talk, the first in the field now known as nanotechnology, he considered the possibility of directly manipulating individual atoms to produce miniaturised systems, including

computers.[5] Fifteen years later in 1974 Aviram and Ratner suggested that one way of producing a smaller alternative to silicon chips could be the use of molecules.[6] This so called "bottom up" approach would involve synthesis of molecules that have been designed to perform specific functions. These would then be assembled together to make the desired electronic devices.[3]

Aryleneethynylenes are one of several types of molecule that could find potential use as molecular wires - the simplest of electronic devices. In general, the systems that have been looked at for this application contain alternating single and double/triple bonds. These conjugated molecules can thus conduct electrons through their π-systems. To be of any use in molecular devices, these wires need to be straight and of a defined length.

The initial research into these compounds only studied the properties of bulk materials. The relative difficulty of attaching a single wire into a system in which it can be tested prevented more detailed study. Recently it has become possible to look at individual molecules. One way of doing this is by attaching the molecules onto metal electrodes. This is done by the use of so-called "molecular alligator clips", which are groups that allow the molecule of interest to attach to the surface of the metal. One example of this is to create a compound with a thiol substituent which will attach to a gold surface by the formation of a thiolate. However due to the instability of thiols, these compounds are usually made as thioacetates which can then be converted to the thiol in situ.

The tip of a scanning tunnelling microscope (STM) can be used to measure the current flowing through molecules attached to the electrode via these 'alligator clips'. If molecules of the system of interest can be inserted onto the metal surface surrounded by non conducting molecules, then passing the STM tip across the surface can give information on the conductivity of the wire. When the tip passes over the top of the conducting molecule, an increase will be seen in the current flowing through the tip.[7] One method of doing this has been to insert compounds of interest into grain boundaries within self-assembled monolayers (SAMs) of dodecanethiolate on gold (see Figure 1.1).[4]

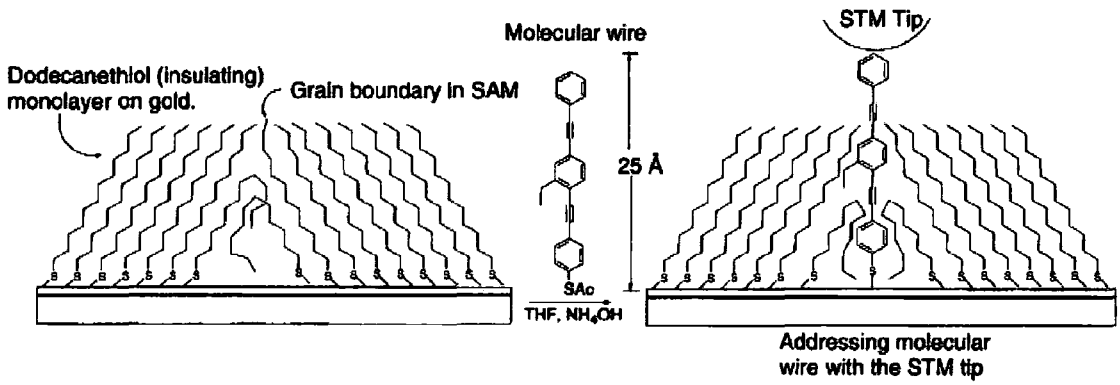

Figure 1.1: Schematic diagram of Tour's approach to insertion of individual aryleneethynylenes into non conducting monolayers on gold to allow conductivity testing.[4]

It has also been possible to insert molecules more selectively onto a surface by using a STM tip to remove alkanethiolates from a SAM in precise positions and then inserting molecular wires (no more than 10 at a time) in their place.[4] Then as a STM tip observing the surface passes over these positions it records an increase in conductance, thus proving that the increase is due to the molecules inserted. This technique does not however allow the properties of individual molecules to be examined.

The methods described above however can be difficult to use well, so molecules are often attached to a metal surface (such as gold) as a SAM rather than individually. Tour and co-workers have studied compounds in this way on a nanopore assembly.[8] In this setup a small surface of evaporated metal that is 30 to 50nm in diameter has a SAM formed on it. An upper metal layer is then evaporated onto this SAM, creating a metal-molecular wire-metal sandwich on which measurements can be performed. The advantage of using such a small monolayer is that it is unlikely to contain any defects, which can lead to shorts in the system.

The first system Tour *et al.* studied in this way, compound **3** (Figure 1.2), showed negative differential resistance (NDR) which is a behaviour seen in an electrical component called a resonant tunnelling diode (RTD). Like a RTD, **3** has two barriers between conducting segments of the molecule (in this case, the CH_2 linkers between the central benzene rings). A compound exhibiting NDR shows a deflection in the current/voltage I(V) plot of a system, as seen in Figure 1.2.

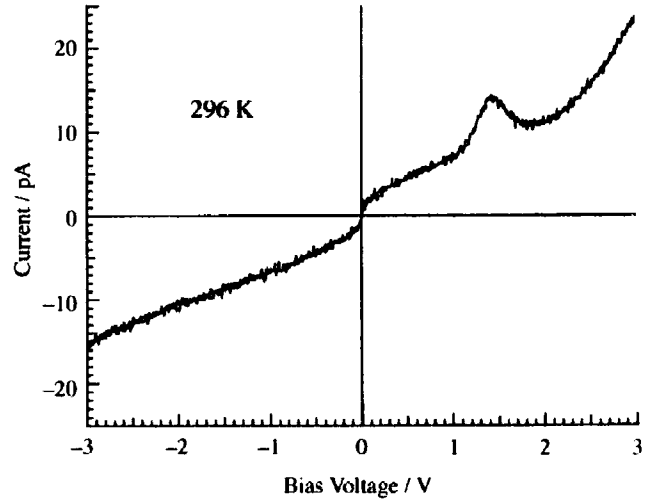

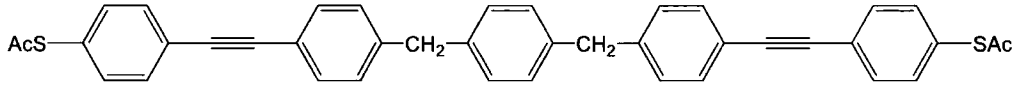

3

Figure 1.2: The NDR behaviour (the peak seen at *ca.* 1.5 V) shown by **3** at 298K.[8]

NDR behaviour is not just seen in compounds containing barriers like **3**, it has also been observed in some fully conjugated aryleneethynylene systems, some examples of which can be seen in Figure 1.3.

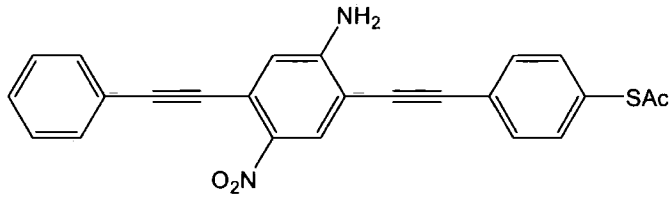

4

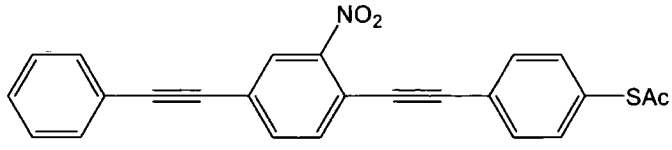

5

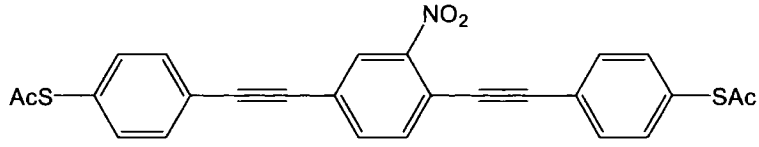

6

Figure 1.3: Examples of fully conjugated aryleneethynylenes that show NDR behaviour.

This RTD type behaviour is potentially of use in memory devices (for example Random Access Memory (RAM) in personal computers), and as such has been the focus of

various studies. The negative differential resistance causes a change from a low to high conductivity state on application of a pulse at a certain voltage. This high conductivity state can then be 'read' by the application of further voltage pulses. A summary of this mechanism can be seen in Figure 1.4. This behaviour leads to the possibility of storing binary data by utilising these off (0) and on (1) states.[9]

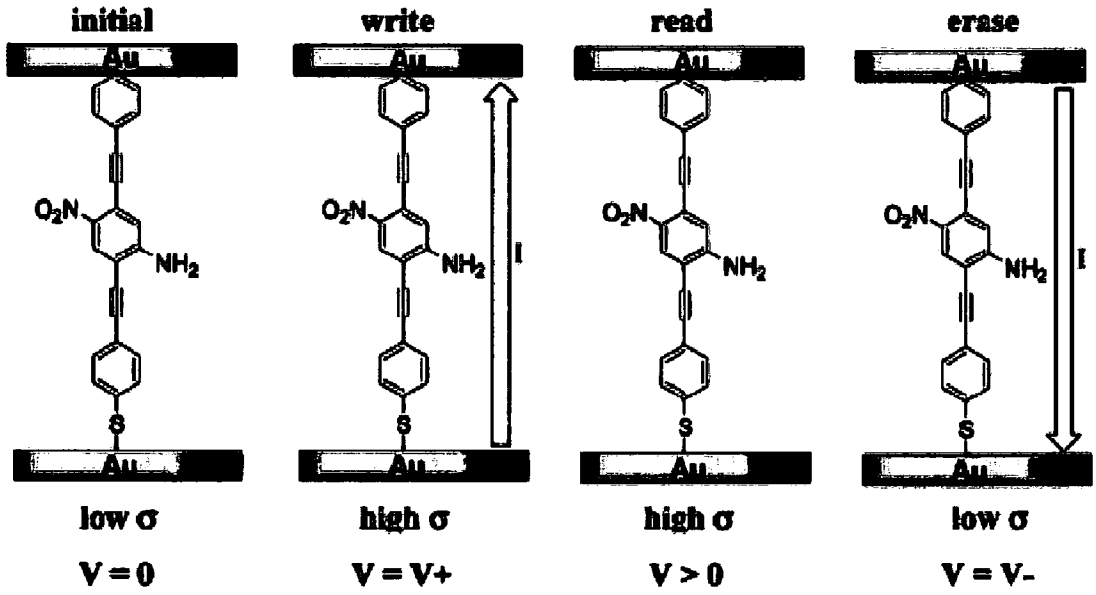

Figure 1.4: Schematic of the use of **4** in a molecular memory storage device.[9]

Examples of the NDR behaviour of compounds **4** and **5** when placed in these systems can be seen in Figure 1.5. **4** displays a large NDR, of around -400 $\mu\Omega cm^2$ with a peak to valley ratio (PVR, which gives an indication of peak current) of 1030:1 at 60 K,[10] however this behaviour is only observed at temperatures up to 260 K. **5** however shows NDR behaviour at room temperature, which makes it a potentially more useful system. The NDR in this system is around -144 $\mu\Omega cm^2$ which persists from low temperature. The PVR at room temperature is vastly reduced down to 1.5:1, although the peak does sharpen down towards lower temperatures.[11] This reduction in PVR with temperature was associated by Chen *et al.* to an increase in inelastic scattering with temperature. Similar behaviour was not observed from an analogue of **5** containing an amino rather than the nitro group, which suggested that the nitro group was responsible for the NDR behaviour observed. [11]

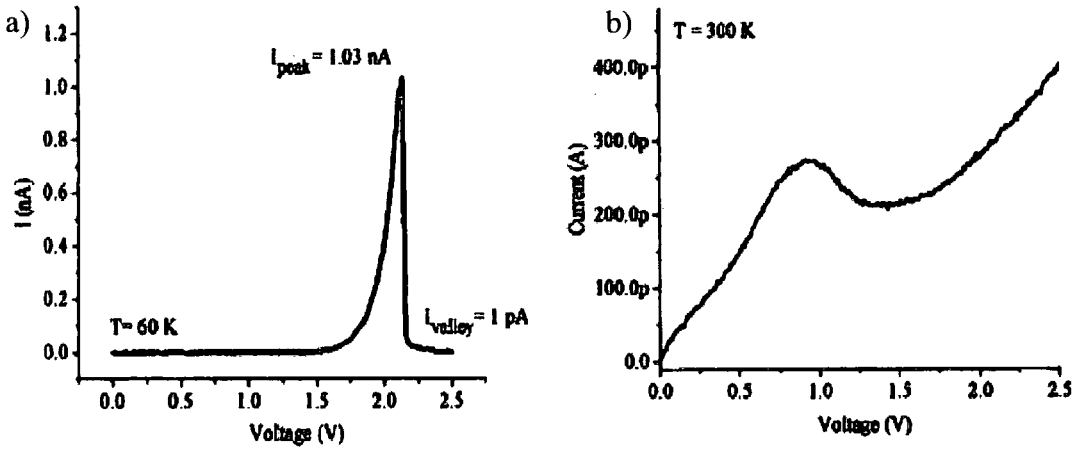

Figure 1.5: NDR profiles for a) **4** at 60K[10] and b) **5** at 300K.[11]

The mechanism by which the NDR occurs is not clear. Záliš *et al.* modelled the behaviour of **4** that had been integrated into a gold nanowire. They found that the peak observed in the I-V plots was down to charge transfer occurring in the molecule. This was due to a reduction from the end chemically bonded to the metal surface that involved the energy level closest to the Fermi energy.[12] Another explanation has been put forwards by Cornil *et al.* who carried out semi-empirical calculations on the electronic behaviour of phenyleneethynylene trimers. These calculations pointed to rotation of the rings leading to a twisted conjugated backbone, with the central ring rotated out of the molecular plane acting as a tunnel barrier.[13] (The twisting of aryleneethynylenes is examined in more detail in section 1.3)

Another way of studying these systems has been to attach a redox active (metal) centre to each end of the molecule, which then acts as a bridge between an electron donor and an electron acceptor. In this type of system the molecule can be studied without the need for integration into a larger system, as the electron to be transferred is generated in situ. For this method to be used there needs to be good overlap between the π-system of the wire and the d-orbitals of the metal, so that the delocalisation of electrons reaches from one metal atom to the other.[14] However as the orbitals of the metal centres are involved in the electron transfer process, the results obtained will be partly down to the metal contribution. It is not possible to say how much of a contribution this is and therefore it cannot be said whether any favourable properties found are down to the metal or wire.

1.2.2 - Organic Light-Emitting Diodes

Aryleneethynylenes have also been studied with respect to use in OLED display technology due to their electronic and photophysical properties. OLED technology presents an alternative to well-established display technologies such as the cathode-ray tube and liquid crystal display (LCD), especially with regard to large-area displays for which these are not well suited.[15] Organic electroluminescent (EL) materials can be cheaper to prepare, more energy efficient and easier to process compared to the more traditional inorganic semiconductor technologies. It has also been possible to make flexible displays by application of EL polymers to suitable substrates.[15] Displays based on organic technology are starting to enter the general marketplace. For example, the first digital camera to feature an OLED display was released by Kodak in 2003,[16] and also the Aston Martin DB9 uses OLEDs for displays in the instrument pack and centre console.[17]

1.2.2.1 - How OLEDs Work

The basic multilayer architectures that can be seen in OLED construction are shown in Figure 1.6. Each layer has a role in the emission of light from one of these devices. On application of an electric field, the hole-transport material (HTM) is oxidised into its HOMO as electrons are extracted by the anode (this can also be thought of as holes being injected into the HTM), and the electron-transport material (ETM) is reduced as the cathode injects electrons into the ETM's LUMO. The charge carriers then migrate under the applied field, and recombine to form singlet and triplet excitons within the emitter. These excited-state species are then able to return to the ground state with the energy being released as light.[18]

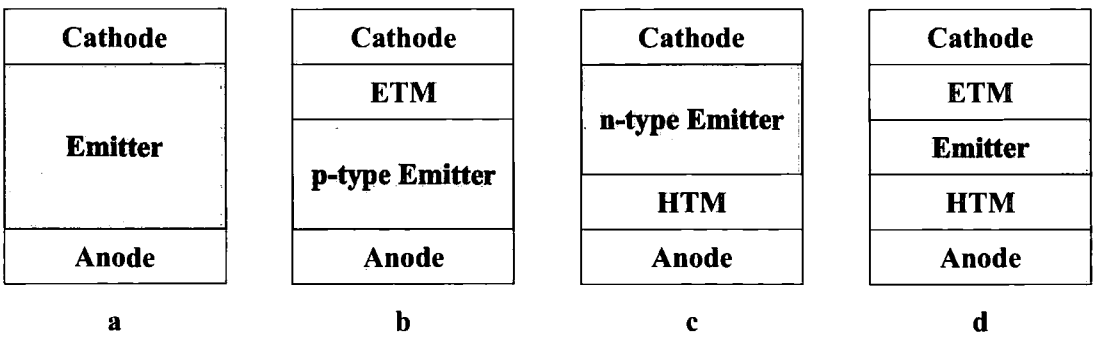

Figure 1.6: Common OLED architectures with a hole-transport material (HTM) and/or an electron transport material (ETM).[19]

The anode is placed onto an optically clear substrate, and must itself be transparent. Hence a transparent conducting anode is used, an example of which is indium-tin-oxide (ITO). The exact construction of a device will depend on the properties of the emitter used in the device construction. The most simple kind of device (as shown in Figure 1.6a) is not necessarily the easiest to achieve. An efficient OLED with this 'single layer' configuration would require an emitter with a high luminescence quantum yield and would need to be able to permit both injection and transport of electrons and holes. This behaviour is very difficult to obtain from most current materials. Most highly luminescent materials of potential use for OLEDs show either p-type (hole-transport) or n-type (electron-transport) characteristics.[19] It is theoretically therefore preferable to use two or more materials (with the architectures shown in Figure 1.6b-d) to allow for efficient light emission, and hole/electron injection and transport.

1.2.2.2 - OLED Development

The generation of light by electrical excitation is known as electroluminescence (EL) and has been known for organic semiconductors since the 1960s when EL was observed from single crystals of anthracene.[20,21] However it was not until the late 1980s that research in this field produced efficient EL devices. Up to this point a drive voltage of around 100V or greater had been needed to achieve a significant output of light, which meant a low power-conversion efficiency.[22] Tang *et al.* were able to obtain efficient emission from multi-layer sublimed molecular devices.[22,23]

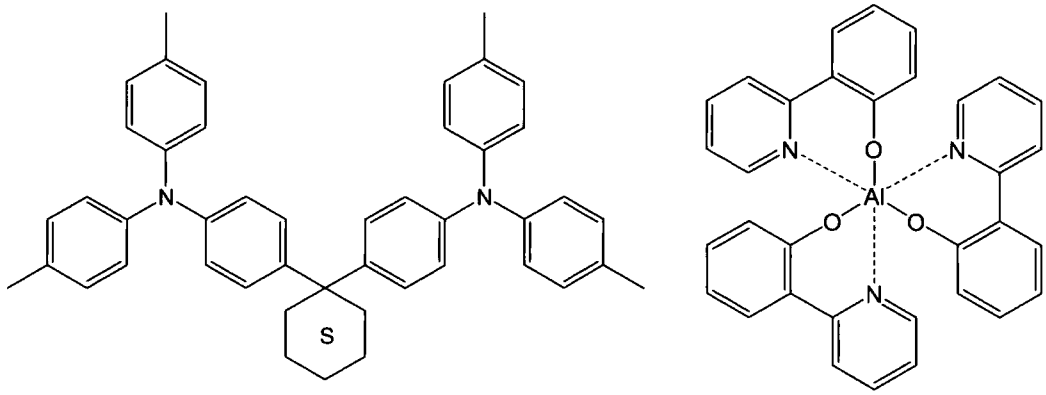

7 **8**

Figure 1.7: Compounds used as organic layers in one of Tang's OLED devices.[22]

Tang's device consisted of an ITO coated glass substrate onto which a thin layer (ca. 750 Å) of an aromatic diamine (**7**, see Figure 1.7) followed by a film (ca. 600 Å) of a fluorescent metal chelate complex were deposited - the first complex reported being 8-hydroxyquinoline aluminium (Alq_3, **8**). An alloy of Mg and Ag (ratio 10:1 respectively) was then added to form the cathode. The device formed was of the type shown in Figure 1.6c, with the diamine providing the hole transport and the Alq_3 transporting the electrons as well as being the emissive layer.

The device produced a measurable amount of green light from a positive voltage of around 2.5 V, which was much lower than that used in previous organic EL studies. They were able to get the diode to a high intensity, with a brightness greater than 1000 cd/m^2 and the device had a luminous efficiency of 1.5 lm/W which compared favourably with the commercially available inorganic LEDs of the time.[22] Further work also showed that they could improve the EL efficiency of the Alq_3 by doping with various fluorescent dyes - coumarin 540 (C540), DCM1 and DCM2. These dyes improved the EL efficiency by a factor of two and also gave a degree of tuning of the colour emitted, with the emission ranging from blue-green to orange-red. The variation in EL emission profiles can be seen in Figure 1.8.

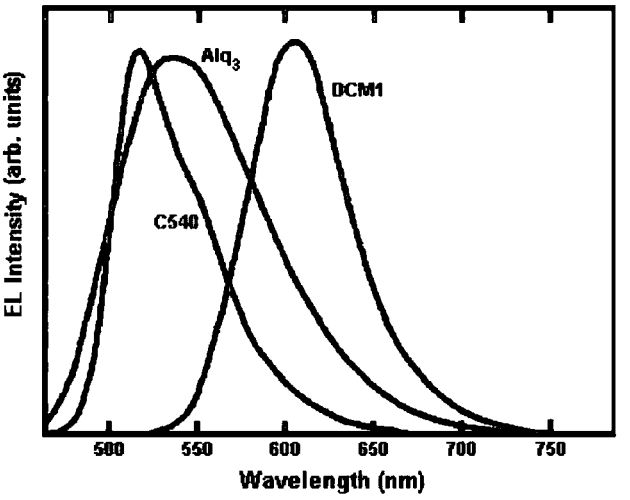

Figure 1.8: EL emission spectra of undoped Alq_3, C540/Alq_3 and DCM1/Alq_3.[23]

This sort of device only has a lifetime of around 100 hours, which is not suitable for practical use. This is due to crystallisation of the organic layers which can damage the contact between the layers leading to degradation of the device.[24]

One way of avoiding this problem was evaluated by Kido *et al.* They created single layer EL devices using molecularly doped polymers (MDPs). These devices consisted of ITO and Mg:Ag electrodes and a layer of the inert and inactive polymer poly(methyl methacrylate) (PMMA, **9**) that had been doped (to 50 wt %) with Alq_3 and TPD (**10**, see Figure 1.9). Application of a voltage across the device led to the emission of green light at around 510 nm.[24]

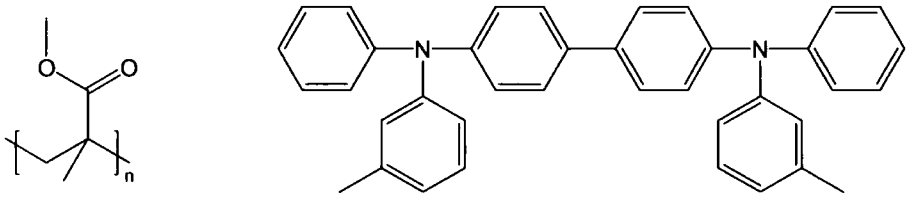

PMMA **9** TPD **10**

Figure 1.9: Structures of molecules PMMA and TPD used in Kido's device.

As in Tang's device the electroluminescence originated from the Alq_3. The TPD did not contribute to the light emission, however it allowed hole injection and transport from the anode into the device without the need for an additional layer.[24]

The next major development after the research of Tang *et al.* was the first use of a conjugated polymer in a device, reported by Friend and coworkers in 1990. They fabricated a single layer device consisting of an electrode deposited on a glass substrate onto which a film of PPV (poly(*p*-phenylene vinylene), **11**) was further deposited with a second electrode then placed on top of the PPV film.[25]

Devices of this type have the advantage that they can be readily fabricated by processing the polymer onto ITO coated glass from solution. Spin coating from solution allows polymer films to be formed with a highly uniform thickness, with a variation of thickness of only a few angstroms over several cm^2. ITO is used as the hole injecting anode due to its relatively high work function, matching the HOMO energy level of PPV, thus facilitating hole injection. Low work function materials like aluminium, magnesium or calcium are used for the cathode. Calcium provides the best match of work function to the polymer's electron affinity, however is commercially undesirable due to its reactivity (especially moisture sensitivity) which would require a very high degree of encapsulation. Aluminium tends to be used as an alternative,

however does not match as well, leading to poor electron injection and hence low efficiency.[15,26]

In general PPVs have poor electron-accepting properties, resulting in an imbalance between electrons and holes in devices, and hence reducing the quantum efficiencies observed. The addition of an ETM layer into the device would increase the efficiency, but like with Tang's multi layer devices this would have the disadvantage of a shorter lifespan for the device, in this case due to the space-charge and tunnelling of accumulated holes resulting in damage to the device.[27]

PPV is not the only polymer type that is suitable for use in EL displays. Other polymers that have been of interest are based on the poly(*p*-phenylene) (**12**) and polythiophene (**13**) frameworks.[28] The structures of these polymers are shown, along with that of PPV in Figure 1.10.

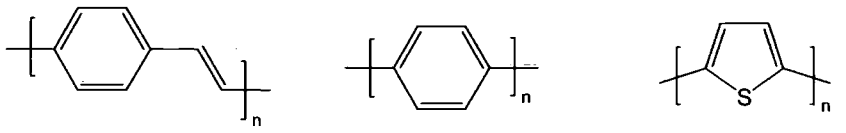

11 **12** **13**

Figure 1.10: Structure of some common polymer frameworks used in OLEDs.

Another major advantage that these organic polymers have over the alternative inorganic semiconductors is the fact that their properties can be tailored by manipulation of their structure. This means that by the addition of substituents, the use of different aromatic rings or the formation of a copolymer, the materials can be changed to give a range of colour emission and also to alter solubility to help with processing.[15]

1.2.2.3 - Aryleneethynylenes in OLEDs

Poly(aryleneethynylene)s have been investigated for use in EL devices, although due to their low solubility and low processability they were not thought suitable for use in device applications.[28] However, with the addition of substituents onto the aryl rings these problems can be overcome.

One successful approach was that of Weder.[29] His group was able to fabricate devices from poly(*p*-phenylene ethynylenes) (PPEs) that had alkoxy substituents on the phenyl rings. Devices were fabricated by spin coating solutions of O-OPPE and EHO-OPPE (structures given in Figure 1.11) onto ITO-coated glass substrates followed by the deposition of a top electrode.[29] The polymers used had number-average molecular weights of around 10,000 g mol^{-1}.

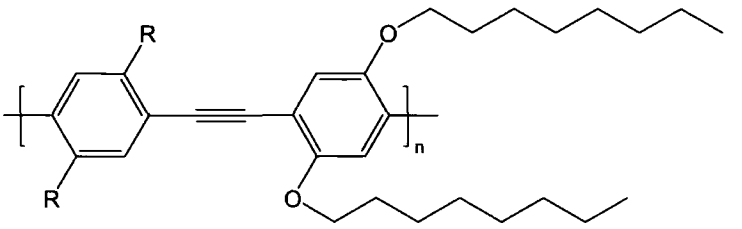

14: R= 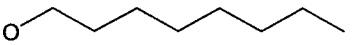

15: R = 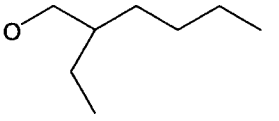

Figure 1.11: Structures of O-OPPE (**14**) and EHO-OPPE (**15**).

Both polymers (**14, 15**) produced devices with nearly identical characteristics, these emitted yellow-green light with a maximum emission wavelength (λ_{max}) of 535 nm. Weder also investigated the effects of using different metals (aluminium, calcium and chromium) as the cathode. The results of this are summarised in Table 1.1. The behaviour observed using these PPE polymers is different from that observed in PPV.[29] As mentioned in Section 1.2.2.2, for a PPV based LED a compromise has to be reached by using less efficient metals (such as aluminium) for the cathode, as opposed to a more efficient, but also more reactive, calcium electrode.[15,26]

Emitting Layer	EHO-OPPE, **15**			O-OPPE, **14**	
Cathode Material	Al	Ca	Cr	Al	Ca
EL Threshold Voltage (V)	10.8	14.5	19.7	11.0	14.2
External Quantum Efficiency (%)	0.035	0.023	0.015	0.032	0.020
Max. Brightness (cd/m^2)	80	38	33	80	35

Table 1.1: EL Characteristics of O-OPPE and EHO-OPPE single layer LEDs with varying cathode.[29]

With Weder's PPE based LED devices however, the reverse is seen with calcium being a less efficient electrode than aluminium. For both cases, the device with the Al

cathode has a threshold voltage for EL of about 3-4 V lower than that seen in the Ca device (and just under 9 V lower than that in a Cr device). The aluminium electrode also leads to a higher external quantum efficiency and maximum brightness than the other alternatives.

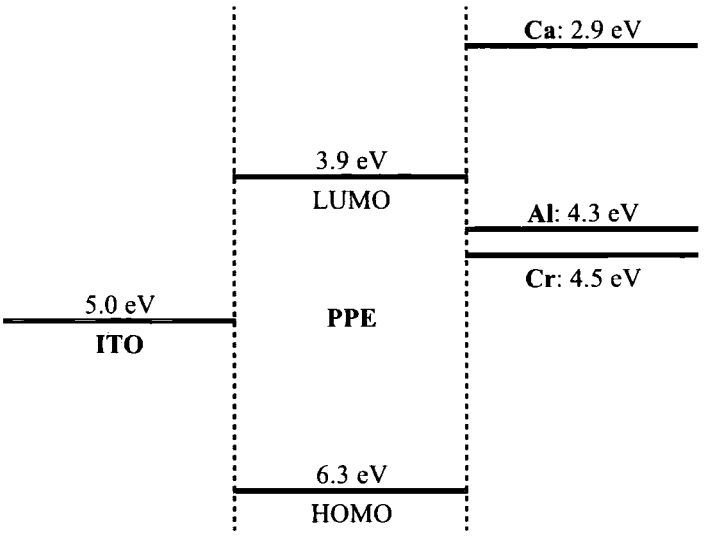

Figure 1.12: Schematic representation of energy levels in a PPE-based single layer LED as determined by Weder using UPS.[29]

This behaviour can, as for the PPV devices, be explained by the energy levels involved in the process. These can be seen in Figure 1.12 (including values as determined by Weder from ultraviolet electron spectroscopy (UPS) measurements). A higher efficiency is seen from the aluminium cathode due to a more balanced charge injection than in the calcium electrode device, where there is no energy barrier to be overcome in the process. Electron injection therefore is easier for these PPE based systems. However hole injection is now an issue instead, with the HOMO being too low in energy for the process to be efficient.[29]

As mentioned previously, the low efficiency of hole injection can be countered in different ways, such as using additional layers or polymer blends. Further work by Weder examined the effects of the addition of a poly-TPD (**16**) into the device to facilitate hole injection, as well as the effects of the addition of the tetrameric spiroquinoxaline - spiro-qux (**17**) as an electron-transport and hole blocking layer (ETHBL). The structures of these are shown in Figure 1.13. Four different devices were compared, the first just contained a single layer of EHO-OPPE with ITO anode and aluminium cathode, the second was a two layer device with a layer of poly-TPD

between the anode and the emitting polymer, the third contained a polymer blend of EHO-OPPE and poly-TPD and the final device had a polymer blend as in the third, but with the addition of a spiro-qux layer between the polymer and the cathode.[30]

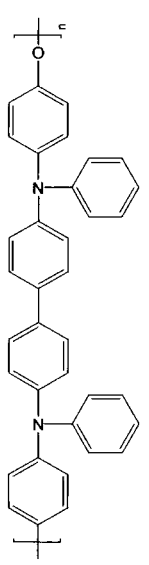

poly-TPD

17

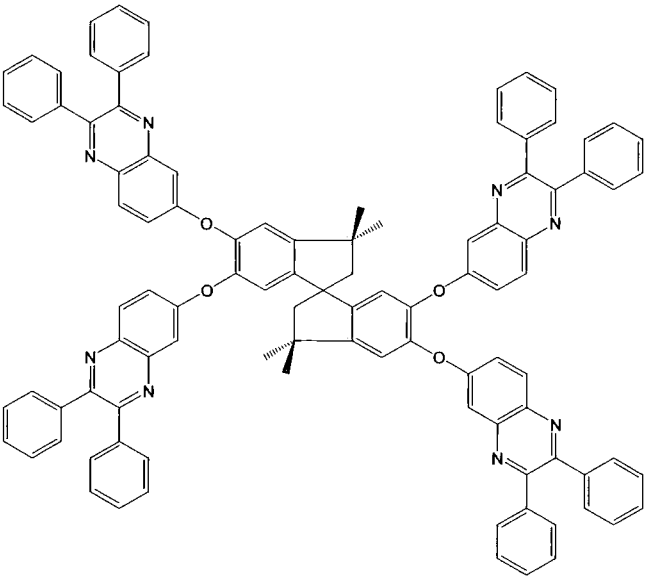

spiro-qux

18

Figure 1.13: The structures of spiro-qux and poly TPD used by Weder to increase the efficiency of EHO-OPPE LED devices.[30]

The addition of the poly-TPD resulted in a more balanced hole injection and transport, leading to an efficiency five times greater than in the pure EHO-OPPE, with both devices 2 and 3 having a similar efficiency. The addition of the spiro-qux layer in device 4 increased the efficiency once again, by a further factor of 7. The major difference in results between devices 2 and 3 was the maximum brightness of the emitted light. The pure EHO-OPPE device gave out a maximum brightness of 4 cd/m^2, the dual layer device 2 improved this to 19 cd/m^2, whereas the polymer blend device had a brightness of 146 cd/m^2. The best overall brightness was observed from the final device, the addition of the ETHBL increasing the maximum brightness to 257 cd/m^2. The improvement in performance *via* the addition of the spiro-qux layer was attributed to one or more of the following factors. Firstly, the Al/spiro-qux interface may have improved electron injection compared to the Al/blend interface in the next brightest device. Also the hole-blocking behaviour of spiro-qux confines charges to the emitting layer, potentially giving higher recombination rates in the blend. This also would lead to charge accumulation at the spiro-qux/blend interface, causing an internal field to be formed, again possibly favouring electron injection. Finally, electron injection may also

be facilitated due to an improved electron transport through the spiro-qux layer into the blend.[30]

OLED research has also been carried out using other PPE systems. One example is the work of Anderson who synthesised an isomeric range of 18 phenylene ethynylene pentamers by varying the postions of the phenylethynyl links at *ortho*, *meta* and *para* positions. Out of these 18 molecules photophysical measurements in solution showed that pentamer **18** (Figure 1.14) was the most emissive and so she chose this to use in an EL device.[31]

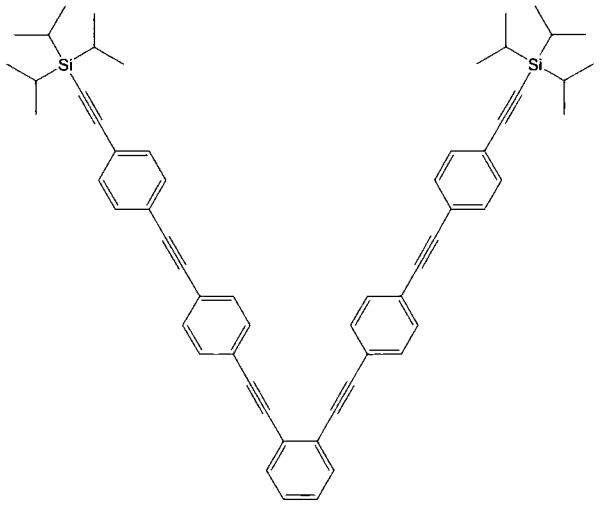

18

Figure 1.14: Phenylethynyl pentamer used by Anderson in an EL device.[31]

A single layer device formed with pentamer **18** between ITO and Al:Li was found to only give faint blue electroluminescence at voltages above 20 V. This poor performance was attributed to a poor match between the electrode work functions and the energy levels of **18**. To counter this a further device was fabricated with a film of PEDOT·PSS, a mixture of the polymers poly(3,4-ethylenedioxythiophene), **19**, and poly(styrenesulfonate), **20**, used as a HTM. This improved the device's performance with a maximum intensity of 5 cd/m^2 at 16V.[31]

Anderson then tried to further improve the efficiency by adding a layer of Alq_3 to improve electron injection. This extra layer appeared to improve the injection of electrons however it changed the colour of the emission to blue-green which was a result of the emission occurring from the interface between **18** and the Alq_3. Over time the colour of the LED changed to a green colour which was attributed to diffusion of the

organic layers.[31] The EL spectra obtained from the two measurable devices are given in Figure 1.15.

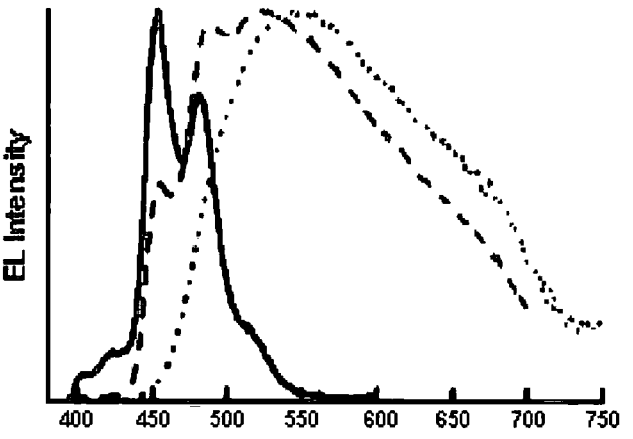

Figure 1.15: Normalised EL spectra from devices based on pentamer **18**. The solid line shows the emission from the ITO/PEDOT/Pentamer/Al:Li system. The other two lines show the emission from the ITO/PEDOT/Pentamer/Alq_3/Al:Li system, the dashed line from initial operation of the diode and the dotted line showing the light emitted after the colour change.

Other aryl groups besides benzene have also been studied for OLED use, one example of which is the use by Lee *et al.* of the fluorene ethynylene pentamer **21** (Figure 1.16) to create a single layer device that emitted bright blue light. They synthesised a range of oligomers containing between two and five fluorene units, the dimer and trimer had photoluminescence (PL) efficiencies of around 50 % with the tetramer and pentamer having just over 60 % efficiency. The pentamer was chosen for the device due to its marginally better PL characteristics.[32]

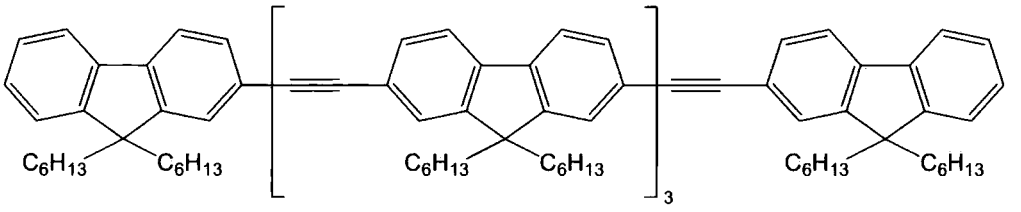

21

Figure 1.16: Fluorene ethynylene pentamer used by Lee *et al.* in a single layer EL device.[32]

The EL spectrum, in chloroform, of **21** has an emission maximum of 424 nm, which is red shifted from the PL maximum which arises at 402 nm. This increase in wavelength indicates that in the solid state there is a strong intermolecular interaction.[32] These two spectra are shown in Figure 1.17.

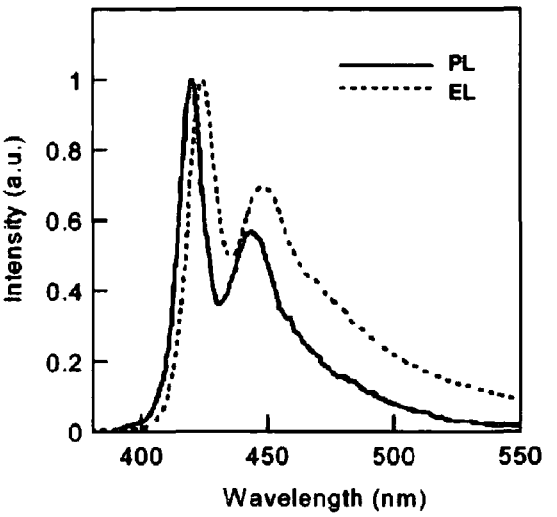

Figure 1.17: Normalised photoluminescence (in chloroform) and electroluminescence spectra of **21**. (Figure adapted from reference 32)

With respect to OLED research aryleneethynylenes have not solely been looked at as being the emissive component in a device. Research has also looked into using molecules based on the arylethynyl framework to improve charge transport in the devices.

Bryce *et al.* studied the use of aryleneethynylenes based around the 2,5-diethynyl-3,6-dimethylpyrazine, **22**, group. These types of compounds are of interest due to the electron deficient nature of the pyrazine molecule. It has been shown that compared to phenylene type compounds, the use of electron deficient groups such as pyridine and pyrimidine improves the electron transport characteristics of a molecule.

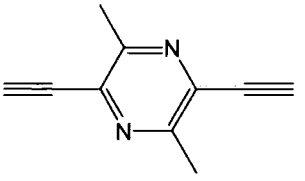

22

They synthesised a range of aryleneethynylenes containing this group and the potential for the use of some of these as electron transport materials was looked into. Single layer devices were fabricated using the pyrazine containing compounds (as well as some phenyl based compounds for comparison) as dopants into a MEH-PPV (**23**) emissive layer that was sandwiched between ITO and Al electrodes.[33] The structure of MEH-PPV and the dopants used are shown in Figure 1.18.

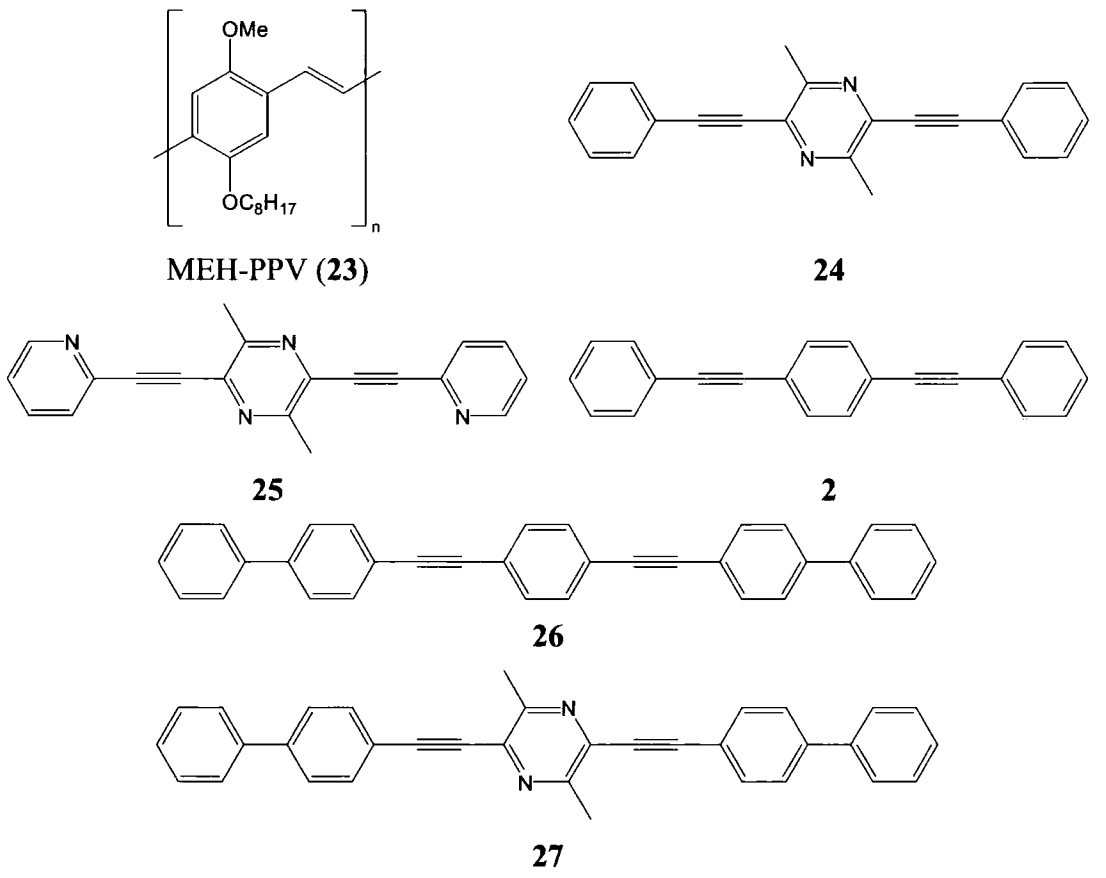

Figure 1.18: Structure of MEH-PPV and the molecules used as dopants by Bryce.[33]

Devices containing molecules **2** and **24-26** as dopants showed no change in performance when compared to a pure undoped MEH-PPV reference. Compound **27**, however, displayed an increase in the device's external quantum efficiency compared to the reference device (an efficiency of 0.07 % compared to *ca.* 0.002 %, at a current density of 10 mA cm^{-3}). This increased efficiency did come at a cost, with the device containing **27** showing a faster degradation of the EL signal with time.[33]

The EL profiles of all devices were very similar, indicating that the emission occurs from the MEH-PPV and not from any of the dopants. The comparison of results between compound **27** and its phenylene analogue, **26**, shows the benefit of the electron

withdrawing pyrazine group. The non-planar biphenyl groups of **27** probably reduce segregation of the dopant in the blend by reducing crystallisation.[33] This is perhaps one reason why the use of compounds **24** and **25**, which contain the same pyrazine unit as **27**, did not also lead to an increase in the EL efficiency.

1.2.3 - Liquid Crystalline Behaviour

Another field that aryleneethynylenes have been studied in is that of liquid crystals (LCs). One area of study within liquid crystals where they have been used is as photoluminescent polarisers within LCD displays. Traditional LCD displays have disadvantages including limited brightness and energy efficiency combined with poor viewing angles. These arise from the use of dichroic sheet polarisers and colour filters which absorb a large fraction of the incident light, converting it into thermal energy.[34,35]

The use of a photoluminescent polariser coupled with an appropriate backlight (eg ultraviolet) and a dichroic mirror (which directs all emitted light towards the person viewing the LCD) allows the construction of ultra-efficient coloured LCDs.[35] Weder *et al.* created devices of the type shown in Figure 1.19, using a commercially available twisted nematic (TN) electro-optical (EO) light valve fitted with a linear sheet polariser as well as a polarised photoluminescent layer excited by an ultraviolet light source.

Figure 1.19: Schematic structure of a LCD device whereby the light emitted by the polarised PL layer is switched.[34]

The PL layer consisted of a uniaxially orientated blend containing 2% (w/w) EHO-OPPE (**15**) in ultrahigh molecular weight polyethylene (UHMW-PE) prepared by solution casting and subsequent tensile drawing, the resultant layer being highly orientated and strongly luminescent. The light emitted from the UV light source is partially absorbed in the polarised EHO-OPPE layer, leading to the emission of

polarised light. This light then either passes through or gets blocked by the TN EO light valve / sheet polariser combination, depending on its switched state. The device as seen in Figure 1.20 had a "bright" state emitting yellow-green light (30 cd m^{-2}) with a "dark" state that was of much lower intensity (4 cd m^{-2}).[34]

Figure 1.20: Photograph of a display device of the type shown in Figure 1.19.[34]

Aryleneethynylenes are not only useful as PL polarisers in LC applications, they have also been shown to display liquid crystalline properties themselves. The first PPE shown to display LC behaviour was reported by Weder in 1997. A solution of **15** in 1,2,4-trichlorobenzene was observed to show a nematic phase at concentrations above 11 vol.-% Solutions of lower concentration were featureless and showed a prominent shear-birefringence. [36]

Molecules like this that show lyotropic behaviour, whereas of potential interest for some advanced electro-optical devices, are less desirable than those displaying thermotropic LC behaviour.[37]

Thermotropic LC phases of PPEs allow the possibility of manipulating the molecular order of the material by external forces such as magnetism. One potential device that this could lead to would be a LED emitting polarised light.[38] Bunz *et al.* demonstrated in 1999 that PPEs could display this thermotropic behaviour when they studied a range of alkyl substituted PPEs, of the type shown in Figure 1.21.[38]

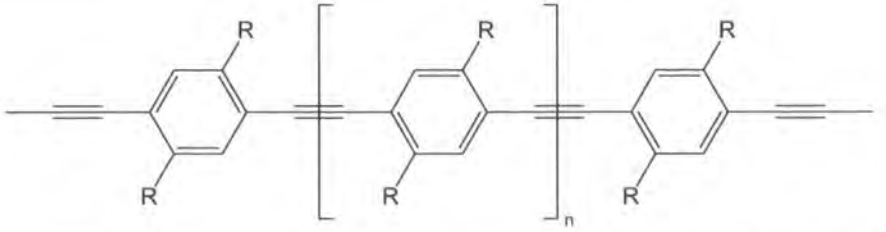

R = hexyl, **28** R=dodecyl, **29** R = 2-ethyl(hexyl), **30**

Figure 1.21: Examples of PPEs studied by Bunz for thermotropic LC behaviour.

28 Was discovered to be a poor choice for studying the thermotropic LC behaviour as it showed an endothermic transition in its differential scanning calorimetry (DSC) trace at 280 °C which was too close to a strong endotherm, > 300 °C, that indicated cross linking. The longer / branched side chains of **29** and **30** allowed the lowering of the transition temperature to more manageable levels, plus allowing the use of a wider range of analytical techniques including polarising microscopy and powder X-ray diffraction.[38]

29 Displayed a transition in its DSC trace at 105 °C upon cooling from 250 °C, which was confirmed by polarising electron microscopy. Above 145 °C the polymer is completely isotropic under crossed polarisers with coexisting isotropic and birefringent domains observed on cooling to 130 °C. Upon further cooling to 105 °C these domains were fully transformed into a Schlieren texture. Some samples of **29** displayed Maltese crosses characteristic of lamellar-nematic or sanidic phases. The Schlieren and Maltese cross structures can be seen in Figure 1.22. All the compounds studied showed a single phase transition upon cooling, in the range 190-280 °C. This transition temperature was found to be dependent on the degree of polymerisation and choice of side chain (higher temperatures were due to smaller side chains and longer polymers).[38]

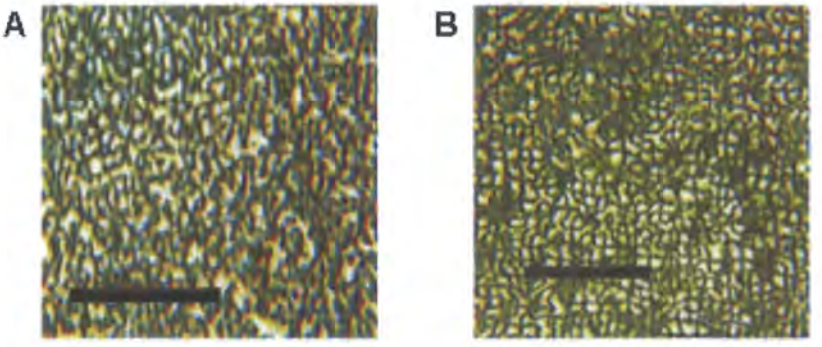

Figure 1.22: Schlieren (A) and Maltese cross (B) structures observed for polymer **29**. Scale bar represents 20 μm.[38]

9-10-Bis(phenylethynyl)anthracene (BPEA, **31**) is another aryleneethynylene compound, derivatives of which have been used to create LC materials. Serrano *et al.* synthesised a range of BPEA derivatives, that were elongated along the long axis of the molecule by the addition of a variety of substituents. They wanted to produce compounds with the same (or improved) properties as BPEA but with better dichroic properties and induced mesomorphic behaviour. This change in properties makes the compounds more compatible with LC mixtures / polymers.[39]

The addition of two ethoxy substituents did not lead to liquid crystalline behaviour, with the resultant compound (**32**, shown in Figure 1.23) melting to an isotropic liquid. Indeed in general the addition of small substituents to BPEA does not lead to LC properties due to the BPEA core having a low length-to-breadth ratio.[39]

Replacement of one of the ethoxy substituents with a decyloxycarbonyl group gave a compound, **33**, that had a significantly decreased melting point and also led to the introduction of a monotropic nematic phase. Also, on cooling, **33** was obtained as a mixture of two crystalline forms, each with different melting points.[39] The replacement of the second ethoxy substituent with another decyloxycarbonyl to yield compound **34** does not give LC behaviour. **34** has a similar melting point to **33**, however it does have a higher degree of symmetry and as such favours organisation in the solid state.[39]

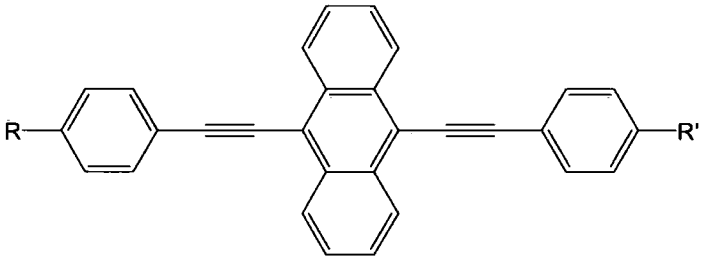

R	R'	Compound
OEt	OEt	**32**
OEt	$COOC_{10}H_{21}$	**33**
$COOC_{10}H_{21}$	$COOC_{10}H_{21}$	**34**
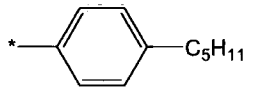	OEt	**35**
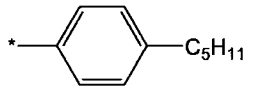	$COOC_{10}H_{21}$	**36**
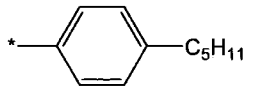	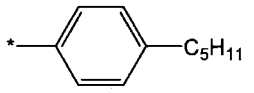	**37**
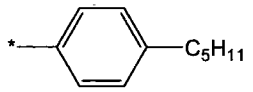	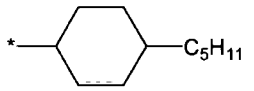	**38**

Figure 1.23: BPEA derivatives studied by Serrano *et al.* for LC behaviour.

Further elongation of the molecule by the addition of a *p*-pentylphenyl ring (compounds **35**, **36**) gave enantiotropic liquid crystals. The extra ring induced a nematic phase over a fairly large temperature range, due to favouring intermolecular interactions along the molecule's long axis and minimizing the hindrance on LC behaviour by the relatively broad anthracene core. **35** showed a nematic mesophase with a relatively low aspect

ratio, whereas **36** gave lower melting and clearing points as well as displaying polymorphism. The use of a second *p*-pentylphenyl substituent, **37**, increased the transition temperatures and gave a shorter nematic phase. With a cyclohexane substituent used in place of the second phenyl ring, compound **38**, the same transition temperatures were observed but polymorphism was introduced.[39]

1.2.4 - Molecular Sensors

The addition of binding sites for analytes capable of quenching fluorescence into a polyaryleneethynylene allows the formation of molecular sensors. A bound analyte acts as a low energy defect site for the polymer and can lead to quenching of the polymer's fluorescence, diminishing the emission observed.[37] The polymer can, therefore, be used to sense if the analyte is present.

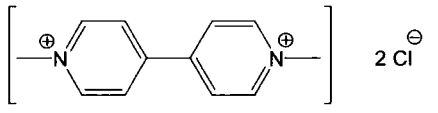

39
Paraquat

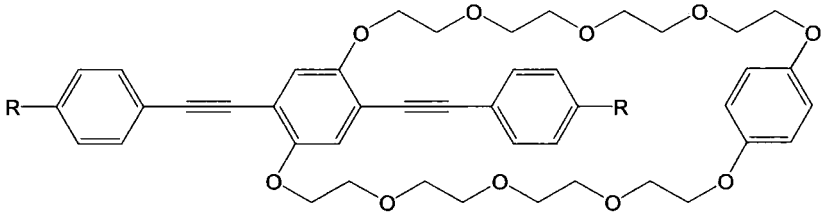

40
Monoreceptor System, R = $OC_{12}H_{25}$

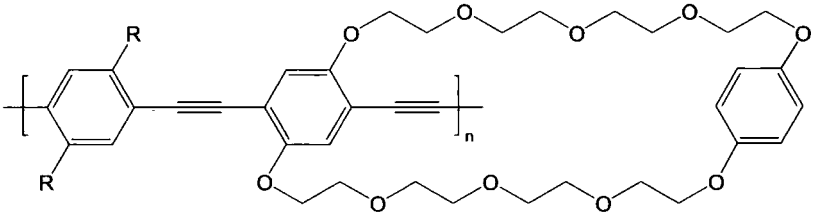

41
Polyreceptor system, R = $CON(C_8H_{17})_2$

Figure 1.24: Structure of paraquat and some example molecular sensors studied by Swager.

Early research into this behaviour in aryleneethynylenes was carried out by Swager. His initial research looked into detecting paraquat (PQ), **39**, via the use of

phenyleneethynylenes with integrated cyclophane receptors.[40,41] Detection of paraquat is of interest as it is used as a herbicide but is also highly toxic to humans and animals.[42]

There are two approaches to molecular sensors, the first is a monoreceptor system where there is a solution of molecules, each containing a single receptor unit. Secondly a polyreceptor system can be used, whereby the receptor units are regularly arranged on the backbone of a conducting polymer. The structure of **39** along with examples of mono- and polyreceptor systems studied by Swager are given in Figure 1.24. The polyreceptor systems show a significant gain in sensitivity over the use of a monoreceptor system. A monoreceptor system like **40** will only see fluorescence quenched in those molecules which have the receptor group complexed with paraquat, resulting in the reduced emission being proportional to the number of filled sites.[40]

In a molecular wire system like **41** however, excitations resulting from the absorption of a photon migrate through the polymer via energy migration. Therefore the excitation "samples" a number of receptor sites along the polymer chain and will be quenched when it encounters a bound site. A schematic band diagram for this process is given in Figure 1.25. Therefore this type of system requires a much lower concentration of analyte in relation to the sensor for total quenching of the fluorescence to be observed. The amount by which the analyte detection is enhanced will be reduced if the diffusion length of the exciton is less than the length of the polymer. This can be due to low mobility and/or short lifetimes.[40] This effect can be seen in the emission profiles in Figure 1.26.

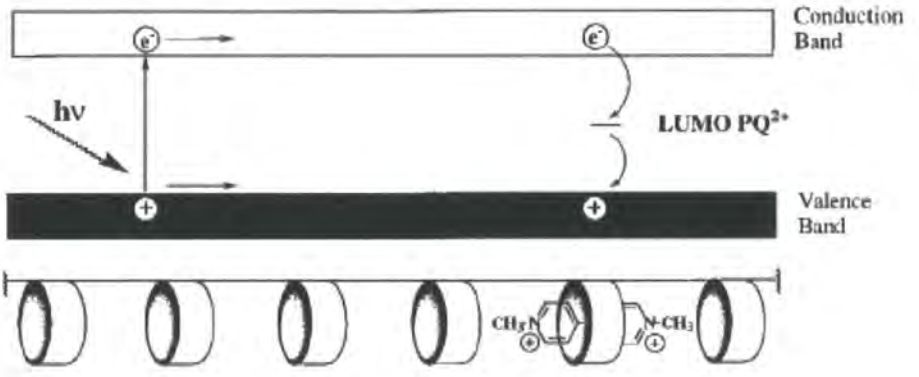

Figure 1.25: Schematic band diagram showing the migration of excitons causing the quenching of fluorescence in a polymeric molecular sensor and subsequent quenching by a bound analyte.[41]

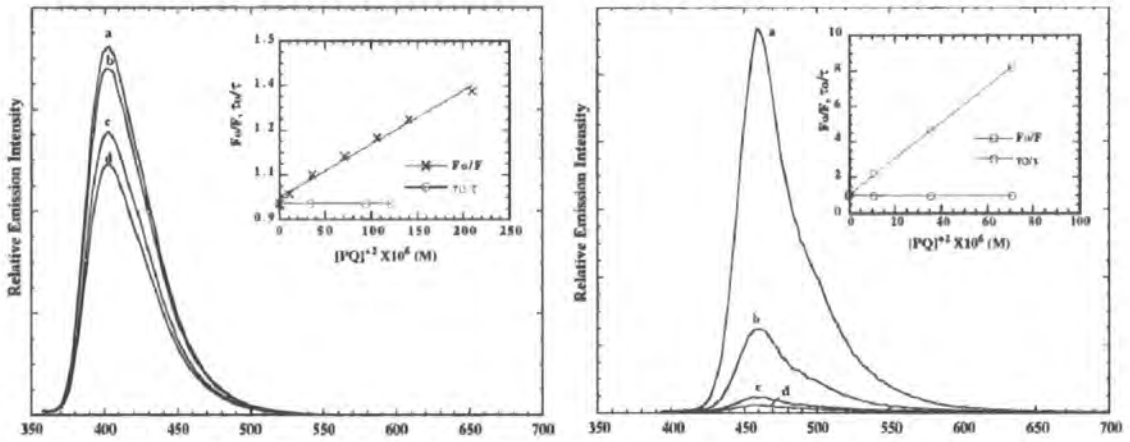

Figure 1.26: Emission spectra of **40** (left) and **41** (right) as a function of added paraquat (PQ^{2+}). Curves labelled to indicate amount of PQ^{2+} added. (a) 0, (b) 3.56×10^{-5} M, (c) 2.10×10^{-4} M, (d) 3.45×10^{-4} M. Stern-Volmer plots are shown as inserts.[41]

Swager's analysis of the Stern-Volmer plots shown in Figure 1.26 gave an improvement for the quenching of the polymeric species (**41**, M_n = 65,000) by paraquat of a factor of 65 in comparison to **40**. Further increasing of the polymer's molecular weight did not give any significant improvement in performance due to the ca. 0.5 ns lifetime of **41**, combined with the probable limiting of exciton mobility by conformational disorder in solution. Also it was found that the fluorescence lifetime (τ) of both systems does not vary with analyte concentration, indicating that only static quenching was being observed.[41]

Swager has also investigated a system which can be used to detect 2,4,6-trinitrotoluene (TNT, **42**) and 2,4-dinitrotoluene (DNT, **43**). Detection of these molecules is of interest due to the fact that they are the principle components in the vast number of unexploded land mines around the world. The detection of land mines by using a chemical sensor in addition to metal detectors should allow more efficient detection, reducing the number of false positives that metal detecting alone produces.[43]

The aryleneethynylene polymer **44** containing pentiptycene (shown in Figure 1.27) shows a high sensitivity for detection of the vapours of these two explosive compounds. The rigid three dimensional nature of the pentiptycene molecule helps prevent π-stacking (which can lead to self quenching) or excimer formation in thin films, which can otherwise reduce the fluorescence quantum yields observed for solid state systems.[44]

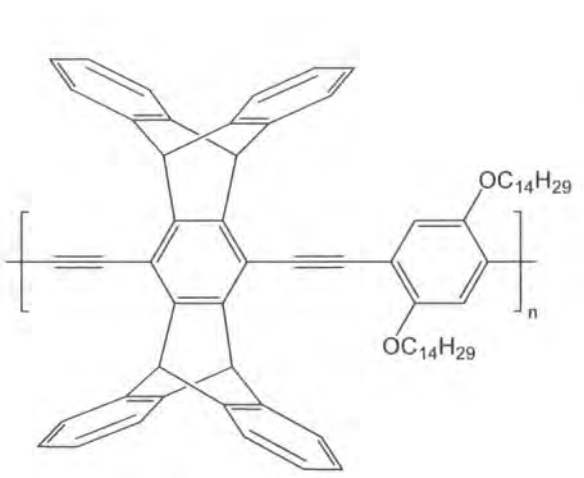

44

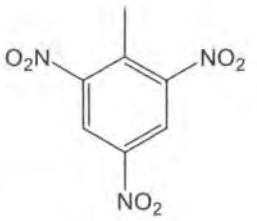

TNT, **42**

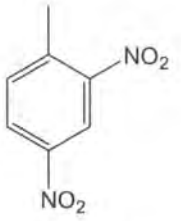

DNT, **43**

Figure 1.27: Pentiptycene containing polymer, **44**, used as a sensor for TNT and DNT (structures also given).

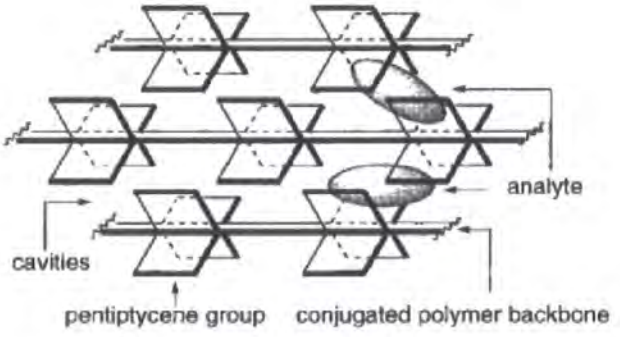

Figure 1.28: Schematic diagram showing the porosity of polymer **44** that results from the rigid pentiptycene groups.[43]

The three dimensional nature of the pentiptycene group also has the advantage of adding a degree of porosity to films of the polymer. This helps negate to some extent the problem faced by dense polymer films, which can prevent rapid diffusion of analytes into the material. The porosity is a result of the rigid pentiptycene groups providing cavities for analyte binding within the polymer.[43] This porosity is shown schematically in Figure 1.28.

Polymer **44** shows a fast fluorescence response on exposure to vapours of DNT and TNT. As seen in Figure 1.29, on exposure to TNT a 25 ± 5 Å film of **44** shows a fluorescence quenching of 50 ± 5 % within 30 s, increasing to 75 ± 5 % at one minute. This response is even faster on exposure to DNT with 91 ± 2 % quenching of the fluorescence at 30s, increasing to 95 ± 2 % at one minute. This increase in the speed of

quenching can be attributed to DNT having a higher equilibrium vapour pressure than TNT.[44]

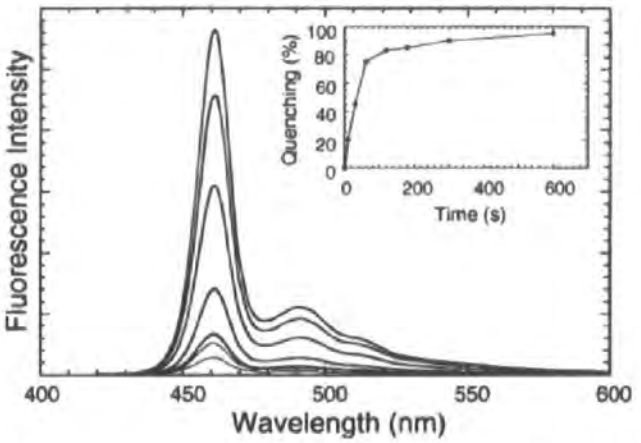

Figure 1.29: Time dependent fluorescent spectra of a thin film of **44** (thickness 25 ± 5 Å) upon exposure to TNT vapour at 0, 10, 30, 60, 120, 180, 300 and 600 s (top to bottom) with the fluorescence quenching against time as an insert.[44]

The fluorescence quenching was found to be dependent on the thickness of the film used. As mentioned previously the fluorescence quenching of **44** by DNT is 95 ± 2 % at one minute in a 25 Å film. This drops to 75 ± 5 % in a 200 Å film, and even further to 35 ± 5 % in a 2500 Å film, suggesting that the porosity of the films is somewhat limited towards these analytes. The porosity of the films is affected by the size of the cavities and the strength of the interactions between analyte and receptor, with the strong interactions between TNT/DNT and **44** likely to be reducing mobility within the films.[43] These systems have since been developed into ICx Nomadics' Fido portable explosives detector.[45]

Bunz has developed systems that can be used to detect various metal ions. The cruciform phenyleneethynylene-phenylenevinylene systems **45** and **46** display differing fluorescence profiles dependent on the ions present. These systems have a HOMO that is situated on the distyrylbenzene branch whereas their LUMO's are located on the bisaryleethynyl part of the molecule. Due to this, the intramolecular charge-transfer emission and absorption of these compounds is dependent on factors such as solvent polarity. Bunz found that, dependent on the metal ion present (and its binding preference) the optical properties of **45** and **46** were changed by switching of the intramolecular charge-transfer band.[46]

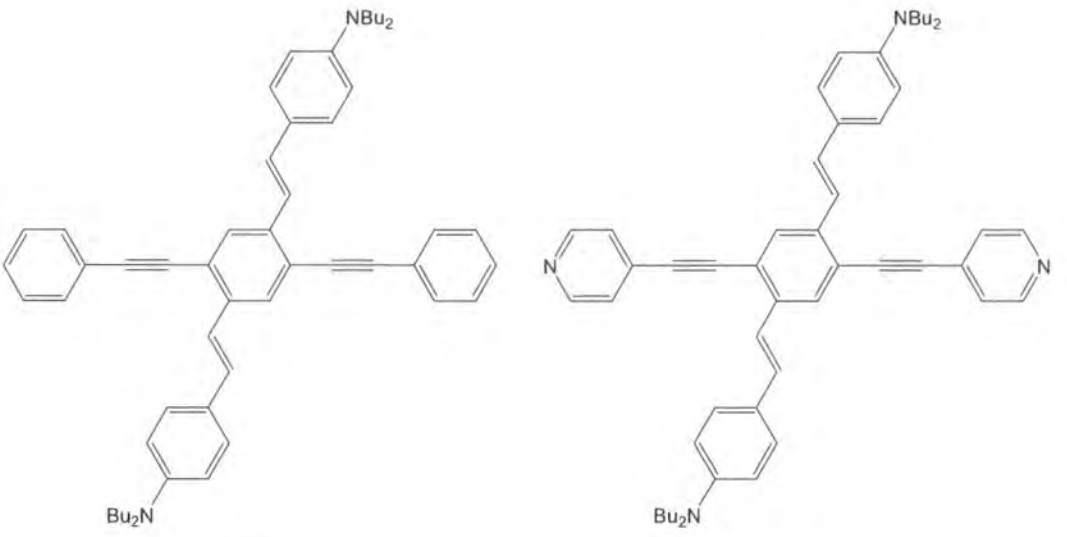

45 **46**

Figure 1.30: Molecular sensors for metal ions developed by Bunz.[46]

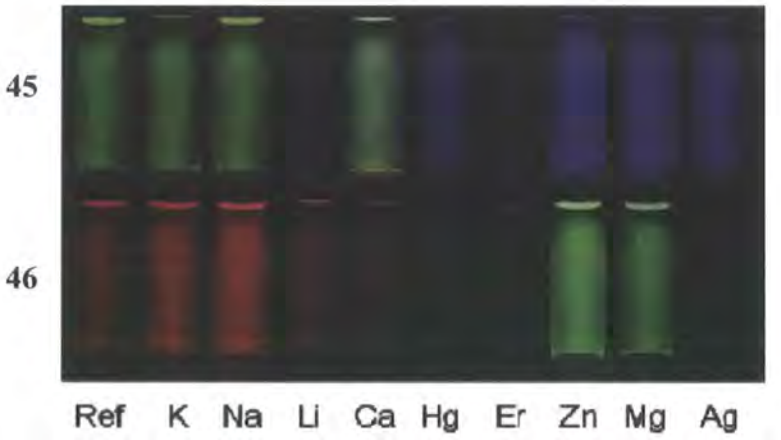

Figure 1.31: Emission of **45** and **46** upon addition of different metal salts in dichloromethane.[46]

The responses observed for these two compounds can be seen in Figure 1.31. Neither compound shows a response to K or Na ions. Other ions tested affect the fluorescence of the systems in differing ways, the emission is either seen to be quenched, for example with the addition of Er, or blue shifted, for example with the addition of Zn. One interesting result is the behaviour observed by the addition of Ag ions, quenching the fluorescence when it can coordinate to the pyridine end of the molecule (in **46**), however when there is just the aniline moiety present, **45**, the emission is seen to be blue shifted. These systems cannot be used to detect the presence of a specific metal ion, however they, along with differentially substituted variants, could be used to make up a sensor array with the responses of the various different 'sensors' being used to determine the analyte present.[46]

Another area investigated by Bunz has been the sensing of lead ions by the use of water soluble carboxylate-substituted PPEs. Detection of heavy metals like lead and mercury is of importance in aqueous environments due to their role as environmental pollutants. Bunz found that the fluorescence quenching of the polymeric system **47** was highly selective and sensitive with respect to lead ions. As with Swager's systems mentioned previously the polymeric system was much more sensitive towards analytes when compared to the monomeric variant **48**.[47]

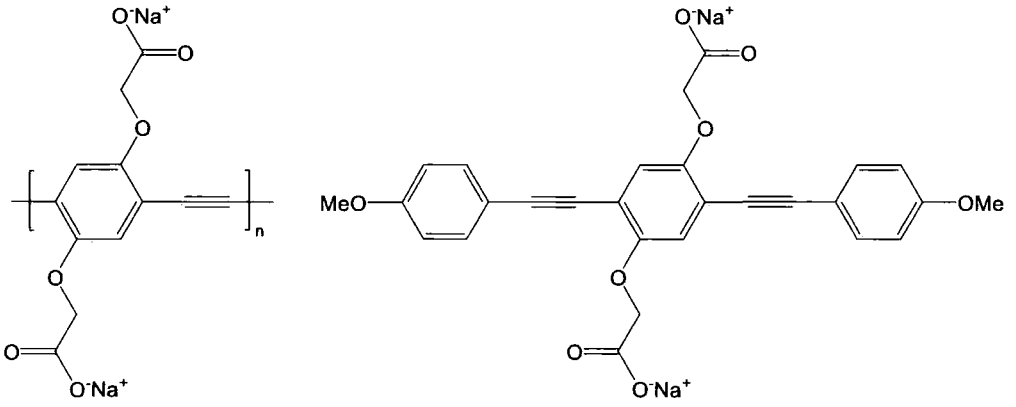

47 **48**

Figure 1.32: Compounds used by Bunz to detect lead ions.[47]

Emission was observed to be quenched by the addition of transition metal salts to solutions of either **47** or **48** in both phosphate buffer and a piperazine-1,4-bis-(2-ethanesulfonic acid) (PIPES, **49**) buffer. These buffers are used in biological experiments, however PIPES is generally preferred for the sensing of trace metal ions in cells due to the potential of phosphates to interfere with the metal ions present. Indeed it was found that, in general, the PIPES buffer led to better binding of the metal ions to these sensory systems in the quenching experiments. Compound **48** only shows a moderate response to the presence of metal ions, with Stern-Volmer constants of around 10-700. Polymer **47** however displays a much larger response, with Stern-Volmer constants 40 to 70 times greater observed in the presence of metal ions such as zinc, copper and manganese. The presence of lead however shows an even greater response, with a Stern-Volmer constant of up to 8.8×10^5, an enhancement of the response of up to 1500 times that seen for the **48** system.[47]

This large enhancement can be attributed to the manner in which the Pb^{2+} ions coordinate to these systems. In the monomeric system the ions bind to a single

carboxylate 'arm' of **48** with the other carboxylate group too far away for interaction and the solutions generally being too dilute for interactions with more than one sensor molecule. In the polymeric system, **47**, the carboxylate groups on adjacent monomer units are close enough for a multivalent bonding between the Pb^{2+} ions and the sensor molecules. This multivalent bonding is not seen in the other metal systems tested and leads to **47** being much more sensitive towards lead than the other metals.[47]

1.3 - Physical and Electronic Structure of Aryleneethynylenes

1.3.1 - Ground State

An interesting feature of these types of compound is the ease with which there can be rotation about the single bonds between the aryl and ethynyl groups. The barrier to rotation has been estimated at around 1.4 $kJmol^{-1}$.[48] This rotation gives rise to conformations of the molecules that are either coplanar or twisted (see Figure 1.33) and the low energy barrier gives rise to an equilibrium between the two forms.

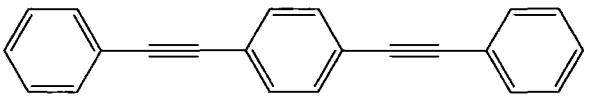

Coplanar Form

Twisted Form

Figure 1.33: Conformations of BPEB.

Theoretical work by Levitus *et al.*[49] examined the rotational potential of **2** in both the ground and excited states using an AM1 method, as shown in Figure 1.34. The barrier to rotation is greater in the excited state than the ground state, leading to a planar S_1 state being energetically favoured over a twisted one.

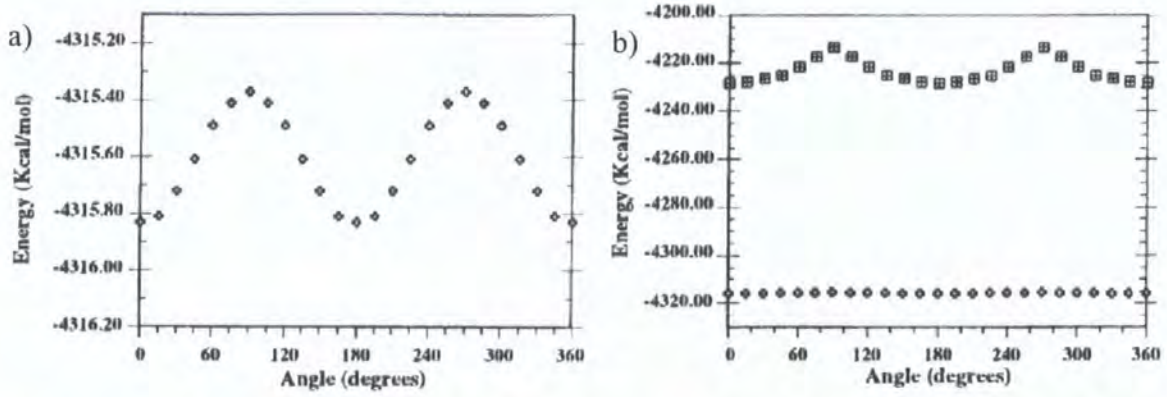

Figure 1.34: Ground state potential calculated for the central phenyl ring of 2 in a) the ground state and b) ground and first excited singlet state. Adapted from reference 49.

More recently Wrede *et al.* have been able to carry out the first experiment to determine the torsional barrier height of **2** by the use of cavity ring-down spectroscopy (CRDS). CRDS measures the rate of absorption of a light pulse contained between two highly reflective mirrors that form a stable optical cavity. This approach allowed them to obtain high-resolution absorption spectra of jet-cooled BPEB for the first absorption band. From this the torsional transitions within the $\pi \leftarrow \pi^*$ transition could be resolved. The experiment determined the symmetric and asymmetric vibration frequencies to be 23.00 ± 0.07 and 13.00 ± 0.05 cm^{-1} respectively.[50]

These vibrational frequencies were used to successfully simulate the torsional spectra for these modes by using simple periodic potentials. Due to the low temperature in the molecular beam, an exact figure for the torsional barrier could not be determined and the barrier height could only be estimated. The estimated value obtained for the barrier was between 220 and 235 cm^{-1}, which is approximately 2.7 kJ mol^{-1}.[50] This value is higher than that of **1** which is 202 cm^{-1},[51] which indicated that the additional long-range π-conjugation in the three ring system of **2** compared to the two ring system **1** has a small stiffening effect on the torsional motion.[50]

The alkyne bond can be thought of as having cylindrical symmetry, which helps to maintain conjugation throughout the molecule from one aromatic ring to the next even though their aromatic planes may not be of the same orientation.[49] The amount of conjugation along the molecule will, however, still be affected by twisting of the aromatic rings out of the overall plane of the molecule, with less conjugation leading to lower conductivity. Therefore it may be possible to produce a molecular switch if a

molecule were to be designed where the conformation can be controlled (and hence also the conductivity).[52]

The monolayer studies of Tour *et al.* that were mentioned in section 1.2.1 have shown potential evidence for this change in conductivity with conformation. On crystallisation at low temperatures (around 20-40K) in the SAM, phenyleneethynylenes have a tendency to pack in a fishbone structure with the phenyl rings perpendicular to each other along each molecule. A plot of current against temperature for these systems, obtained using a nanopore system, shows a pronounced drop in conductance at these lower temperatures. This is down to a decrease in the π-orbital overlap and hence a drop in conductivity caused by the rings being locked out of the molecular plane. At higher temperatures the molecules are free to rotate allowing conformations which have better overlap. The nanopore system consisted of a small surface of gold, onto which a SAM of phenyleneethynylene molecules (*ca.* 1000) was formed. A top contact of titanium was then evaporated onto the SAM layer, giving a metal-SAM-metal "sandwich" through which the measurements could be recorded.[8]

1.3.2 - Excited States

The molecular and electronic structures of the excited state of these compounds have not been well studied. However it is important to gain a better knowledge of these to be able to understand the behaviour described in section 1.2.

1.3.2.1 - Excited State of Molecules and Luminescence

When energy is absorbed by a molecule (e.g. through electrical or photophysical stimulation), electrons in the ground state can be promoted (excited) into a higher energy level. These electrons can then relax back down to the ground state, and in some cases release energy in the form of light, in a process known as luminescence. The light emitted by luminescence is sometimes called "cold light" as no heat is released in the process.

Luminescence can also be categorised by the manner in which the excited state is formed. Photoluminescence occurs when light is absorbed by a molecule, in

electroluminescence the excited state is formed by passing an electric current through the material. Chemiluminescence occurs when a reaction releases energy as light rather than heat (a process used in 'glow-sticks') and bioluminescence occurs from a biological source (for example in special organs of deep sea fish used to help attract prey).

Photoluminescence can be subdivided into two processes, fluorescence and phosphorescence. Fluorescence results from a transition between two states of the same multiplicity (normally singlet-singlet). Here the electron involved in the transition is of opposite spin an unpaired electron in the ground state giving an allowed transition, with a transition lifetime of the order of nanoseconds.[53] Therefore to the naked eye it appears that light is only emitted whilst the sample is being excited.

In phosphorescence the emission results from a triplet excited state. In the triplet state the two unpaired electrons have parallel spin orientation, and so the transition down to the ground state is spin-forbidden. As a result the process is slow and emission lifetimes are typically anything from milliseconds to many seconds.[53]

The processes involved in luminescence are usually illustrated with a Jabłoński diagram (named after Prof. Alexander Jabłoński (1898-1980)). A typical example of one of these is given in Figure 1.35. In this diagram the vertical scale represents energy, whilst the horizontal scale has no specific meaning and is just used as an easy way of distinguishing between states of differing spin multiplicity. The singlet ground state, first excited state and higher excited states are denoted as S_0, S_1 and S_n respectively. The triplet excited states are denoted in a similar way with 'T' replacing 'S,' but with the lowest energy triplet denoted as T_1.

Each of the electronic states has its own vibrational manifold which results from the motion of the nuclei in the molecule in that particular electronic state. In multinuclear systems there is a high density of these vibrational levels, causing overlap of the excited states, leading to continuous spectra being observed. Typically in aromatic hydrocarbons vibrational fine structure is observed in the transition. This arises from the coupling of the electronic transition to a vibrational mode in which the nuclear motion gives rise to a geometry more like that of the excited electronic state.[53]

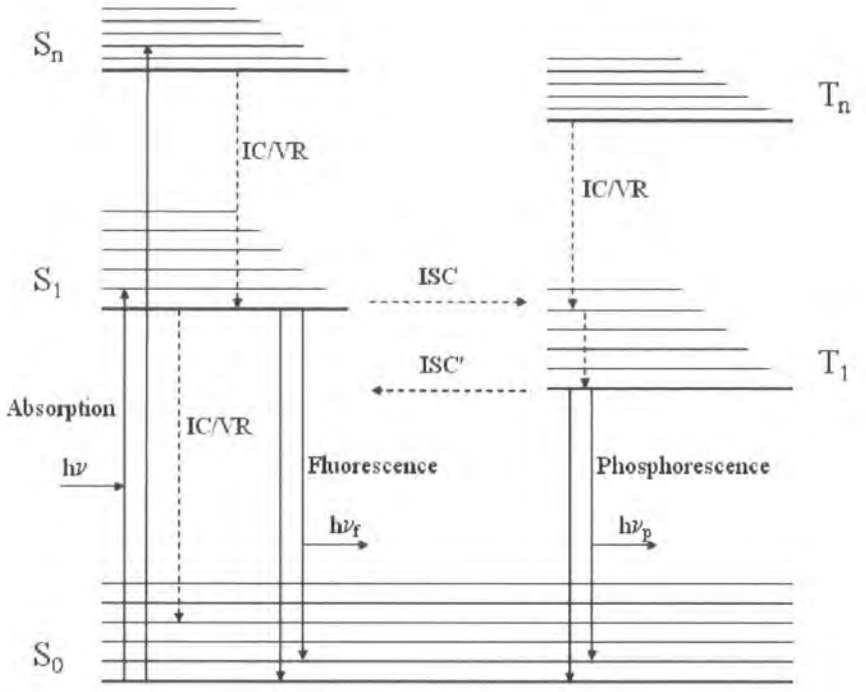

Figure 1.35: An example of a typical Jabłoński diagram (adapted from ref 53).

The absorption of a photon of light promotes a molecule from the ground state into a higher singlet energy level. This transition arises from the promotion of an electron from an occupied orbital to an unoccupied one, with the S_1 state arising from the lowest energy transition, LUMO←HOMO. The molecule then relaxes down to lowest vibrational excited state of S_1 by two non-radiative processes. These are IC (Internal Conversion) to a lower excited state or VR (Vibrational relaxation) where the molecule loses vibrational energy by (i) collisions with solvent molecules in solution or by (ii) interactions with the vibrational motions of a solid matrix. These processes are very rapid, typically occurring in under 10^{-12} s, which is much faster than the alternative ($S_2 \rightarrow S_0$) radiative decay, and as a result no $S_2 \rightarrow S_0$ emission is observed. As fluorescence lifetimes are typically between 10^{-8} s and 10^{-12} s, these processes are usually complete before emission commences. Then the molecule will relax to the ground state (though not necessarily to the lowest energy vibrational state) with the energy lost being released as light. This behaviour was first noted by Kasha in 1950 and can be summarised as, "The emitting level of a given multiplicity is the lowest excited state of that multiplicity"[54]. This is now known as Kasha's rule.

As the excitation does not have a large effect on the geometry of the molecule the spacing of the vibrational states are similar for both S_0 and S_1. This leads to the fluorescence emission spectra being similar (albeit reversed) in shape to the absorption spectra.[53]

Exceptions are known to Kasha's rule, the first of which to be reported was azulene, **50**.[55,56] Beer and Longuet-Higgins found that in azulene, emission is observed from the S_2 level rather than the expected S_1 level. This was attributed to the large energy difference between the S_1 and S_2 levels (a separation of 14,300 cm^{-1}) resulting in a low probability of non radiative transitions compared with the probability of a radiative transition.

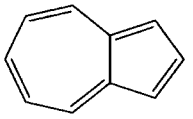

50

Before phosphorescence can occur there needs to be a further non-radiative process called intersystem crossing (ISC). This is slower than VR and IC with a rate of ~ $10^8 s^{-1}$. In this process there is a spin conversion from the singlet to a triplet state of the same multiplicity and energy. The lowest vibrational state of T_1 is usually at lower energy than the corresponding singlet state, causing phosphorescence to be red shifted in relation to fluorescence for the same molecule.[53] As already mentioned in this section, this process is slower than fluorescence due to the transition being forbidden.

The fluorescence of a particular molecule can be influenced by external factors, one of which is the effect of the solvent used. In general the solvent in which a molecule is dissolved leads to the relaxing down (by VR) of electrons that have been excited by absorption into higher energy levels to the lowest S_1 level. This means that in general the fluorescence is red-shifted in relation to the light absorbed. Depending on the solvent used the fluorescence can be shifted to yet longer wavelength (lower energy). This is because polar solvent molecules can potentially stabilise the excited state, lowering it in energy. The more polar the solvent that is used, the greater this relaxation is, and thus the more red-shifted is the spectrum. Molecules that are themselves polar will be affected by this to a large extent, whilst non-polar molecules are much less susceptible.[53] This process is illustrated in Figure 1.36.

Absorption takes place from the ground state to an excited state that has the same solvation shell as the ground state. However this solvation shell is unstable due to the different electronic distribution of the excited state compared to the ground state. This is then followed by a reorientation of the solvent molecules to a more stable, and lower energy state. Emission from this state then gives the ground state molecule in the excited state solvation shell, which then reorientates back into the more stable ground state solvation shell.[57]

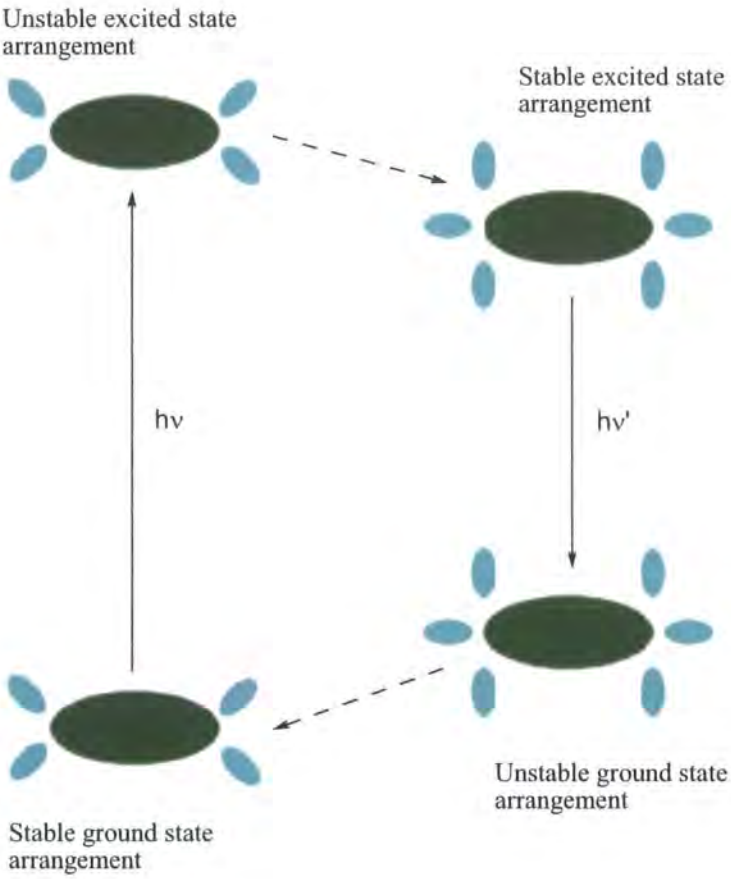

Figure 1.36: Schematic diagram showing the effect of solvation on the processes involved in fluorescence (absorption on left, emission on right). The molecule being excited is illustrated in green with the solvent molecules shown in blue. Adapted from reference 57.

Fluorescence is also affected via the process of quenching. Quenching results in the intensity of the fluorescence being reduced. There are a range of mechanisms by which this process can occur. Firstly there is a process called collisional quenching. This occurs when the fluorophore in the excited state comes into contact with another molecule (called the quencher) in solution. During the encounter the quencher deactivates the S_1 state of the fluorophore by a variety of methods, which can include

electron transfer or spin-orbit coupling and ISC to the triplet state (the latter occurs when the quencher is e.g. molecular oxygen or a halogen).

Another type of quenching is static quenching where the quencher forms a non-fluorescent complex with the fluorophore in the ground state. There are also a variety of other non-molecular mechanisms for quenching, for example the incident light being attenuated by either the fluorophore itself or by another absorbing species in solution.[53]

1.3.2.2 - Excited State of Tolan

Tolan, **1**, is not a good model for these systems as it displays unusual behaviour. Higher oligomers are more similar in behaviour, and hence tend to be more useful models for the polymeric or longer oligomeric systems.

In the electronic structure of **1** the S_1 and S_2 levels are very close in energy. The S_2, rather than the S_1, level is involved in the excitation and emission processes. The S_2 level can also undergo activated non-radiative decay to the non-emissive S_1 state via internal conversion (IC), however it then undergoes rapid activationless intersystem crossing (ISC) to the first triplet state (T_1), where it can further relax via ISC to the ground state.[58] A summary of these processes can be seen in Figure 1.37.

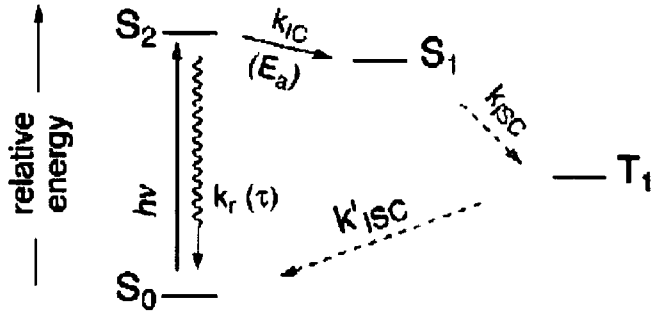

τ / ps	k_r / s^{-1}	E_a / cm^{-1}	k_{nr} / s^{-1}
10	3.9×10^8	610	9.5×10^{10}

Figure 1.37: Energy diagram level depicting the energy processes observed for **1** (τ = fluorescence lifetime, k_r = radiative rate constant, E_a = activation energy of IC, k_{nr} = non radiative decay rate constant). [58]

The structures of the S_2 and S_1 energy states of **1** are also markedly different. As discussed earlier in this chapter, Ishibashi and Hamaguchi have shown that in the S_2 state the molecule retains the linear acetylenic structure of the ground state. Using IR / Raman spectroscopy they also they found that the central C–C stretch of the S_1 state occurs at 1567 cm^{-1}, which is in the region of the spectrum associated with a C=C stretch.[59] This is a significant change in conformation, and they suggested that the S_1 state of tolan has an alkene-like bent structure, which would mean that the $S_2 \rightarrow S_1$ IC process must involve a structural change, akin to an isomerisation. Further work using picosecond transient IR suggested that in the S_1 state, the molecule adopts a symmetrical trans structure.[60]

1.3.2.3 - Higher Order Oligomers

Sluch *et al.* have stated that the first excited state of phenyleneethynylenes are strongly influenced by quinoidal and cumulenic electronic configurations (see Figure 1.38).[61] They based this hypothesis on theoretical work such as that of Karabunarliev *et al.*[62] and Levitus *et al.*[49]

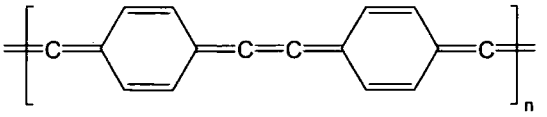

Figure 1.38: Cumulenic structure seen in excited state of poly(phenyleneethynylenes) according to Sluch *et al.*[61]

Molecular modelling of these compounds allows the electronic structure to be determined and the electronic transitions / energies predicted. TD-DFT calculations indicate that the first excited state is accessed *via* a LUMO←HOMO transition. The calculations also allow theoretical diagrams of these molecular orbitals to be visualised for compounds being studied. As shown in Figure 1.39, the HOMO of BPEB (**2**) ties in with the phenylacetylenic framework, whereas the LUMO is more representative of the cumulenic form.[63]

Experimentally, however, there has been no evidence to support Sluch's hypothesis. Indeed, time-resolved resonance Raman (TR^3) studies carried out by Beeby *et al.*[63] showed that in the S_1 state **2** retains significant acetylenic character.

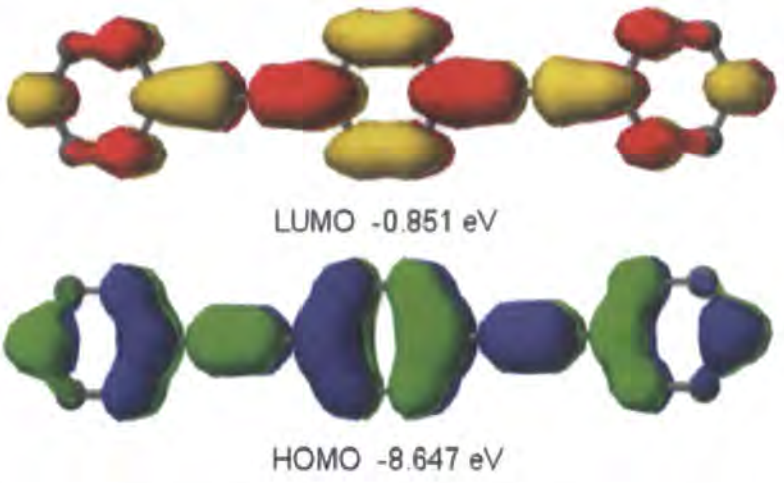

Figure 1.39: Diagram showing the LUMO and HOMO of **2**. Calculated using CAChe 5.0, with a MOPAC/PM3 level calculation.[63]

The TR^3 spectrum of the S_1 state of **2** in cyclohexane has bands at 2128, 1588, 1138 and 999 cm^{-1}. The intensity of these bands increases by around 20-25% in the first 50 ps after excitation, after which the Raman signal decays with a lifetime that matches that of the S_1 state. This early change was attributed to a reorientation within the excited state changing the electronic structure and Raman excitation profiles.[63] A comparison between this spectrum and the ground state spectrum can be seen in Figure 1.40.

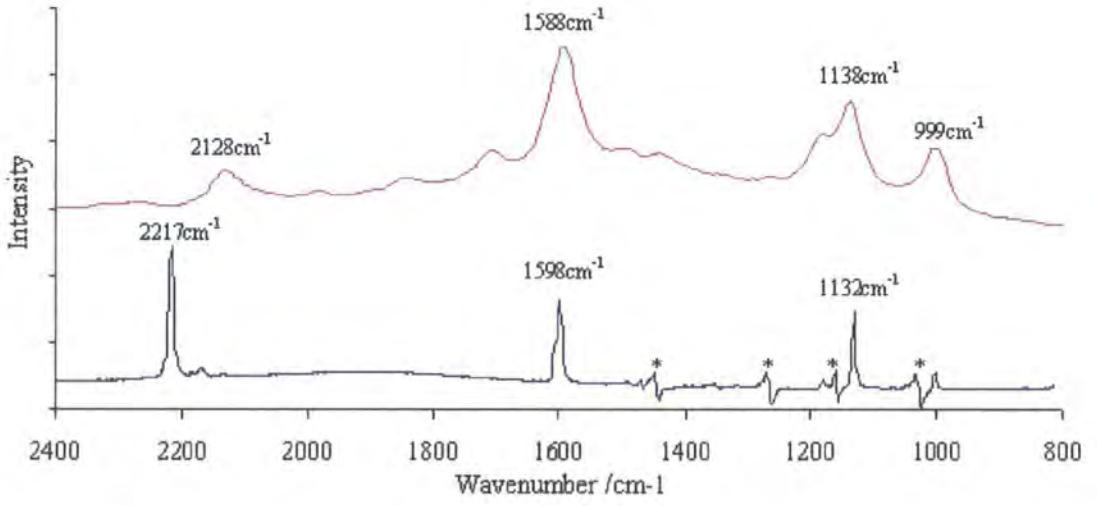

Figure 1.40: Resonance Raman spectrum of S_1 State of **2** 50 ps after pump (pump 267 nm, probe 588nm) (—) compared to the ground state non-resonance Raman spectrum (probe = 532 nm) (—). * = mis-cancelled solvent bands.[63]

The ground state Raman spectrum of BPEB shows major bands at 2217, 1598 and 1132cm^{-1}. For this spectrum the band at 2217cm^{-1} had previously been associated with the symmetric C≡C stretching mode of the acetylene groups, the band at 1598cm^{-1} with

the symmetric stretch of the three aromatic rings along the long axis of the molecule, and the band at 1132 cm^{-1} results from a symmetric C–H bending mode. A weaker band is also observed at 999 cm^{-1} attributed to an aromatic ring breathing mode.[64] However this weaker band is obscured by the mis-cancellation of the solvent in Figure 1.40.

The bands in the Raman spectra of the S_1 and ground state Raman spectra have, with the exception of band associated with the ethynyl group, similar wavenumbers which indicates there is little change in the bond order and structure of the two states. The greatest change on excitation is the shift of the acetylenic band by -89 cm^{-1}. This is consistent with observations made by Ishibashi and Hamaguchi on **1**, where they found a 118 cm^{-1} shift to lower wavenumber upon excitation from the S_0 to S_2 state of tolan.[59] This decrease in wavenumber shows a weakening of the C≡C bond in the excited state, however it still has a "triple" bond order and retains its linearity.

More significantly, if the excited state were to be cumulenic a characteristic band for the butatriene, or cumulene linkage (>C=C=C=C<) would be expected to be visible in the spectrum. The symmetrical stretching vibration of this linkage shows a strong signal in the Raman spectrum at around 2040 cm^{-1}, with an increase in conjugation leading to a further decrease in the wavenumber.[65] In **2**, however, this signal is not observed, which led Beeby *et al.* to conclude that in the excited state there is no significant cumulenic character.[63]

They also noted that, given that there are a large number of lower lying occupied molecular orbitals that contribute to the acetylenic and aromatic nature of **2**, it is not too surprising that the fact that the promotion of a single electron from the HOMO to the LUMO does not lead to a significant change in the bond order of the molecule as these two orbitals only have a small contribution to the overall C≡C bond.[63]

1.3.3 - Effect of Conformation

Changes in the effective conjugation of the molecule will affect its photophysical properties via a change in its HOMO-LUMO gap. Therefore it is possible to also study the effect of conformation via, for example, the use of absorption and fluorescence spectroscopy.[66]

Studies have been carried out on BPEB to see if there is any evidence for it forming discrete configurational isomers. Levitus *et al.*[49] claimed to have found such evidence, reporting a wavelength dependent emission spectrum and fluorescence lifetime. They mentioned the presence of two discrete spectral profiles as opposed to a smooth transition from one spectral profile, this behaviour, if real, would have indicated two spectroscopically distinct species in solution. However, subsequent work proved that these observations arose due to impurities in the sample used.[66,67] This demonstrates that care has to be taken when obtaining data as even traces of impurity can lead to erroneous results.

Levitus and Garcia-Garibay also carried out a theoretical study into the effect of the conformation of the similar molecule BPEA, **31**. Their work compared the planar and perpendicular conformers via semi empirical calculations producing theoretical UV-vis spectra for each of these (which can be seen in Figure 1.41). Of the two conformations, the calculations showed that the planar conformation is more stable than perpendicular one, however the energy difference between the two forms was only 1.42 kJ mol^{-1}. This gives a low barrier to rotation (like that in BPEB as mentioned in section 1.3.2.3), and leads to free intramolecular rotation at room temperature.[68]

The calculated transitions for the UV-vis spectra were all found to have transition dipole moments parallel to one of the molecule's principle axes. For some of these transitions, the energy of the transitions and the corresponding oscillator strengths depend on the dihedral angle formed between the anthracene plane and the plane of the phenyl groups. This is seen most obviously in the lowest energy transition (which is polarised along the long axis of the molecule) for which the calculations predict a blue shift of 32 nm going from the planar to twisted conformers, with the oscillator strength being reduced by 35 %. The relative positions of the transitions are in good agreement with the observed UV-Vis spectrum of BPEA, albeit that the theoretical spectra are blue shifted by 30-50 nm compared to the observed spectrum.[68]

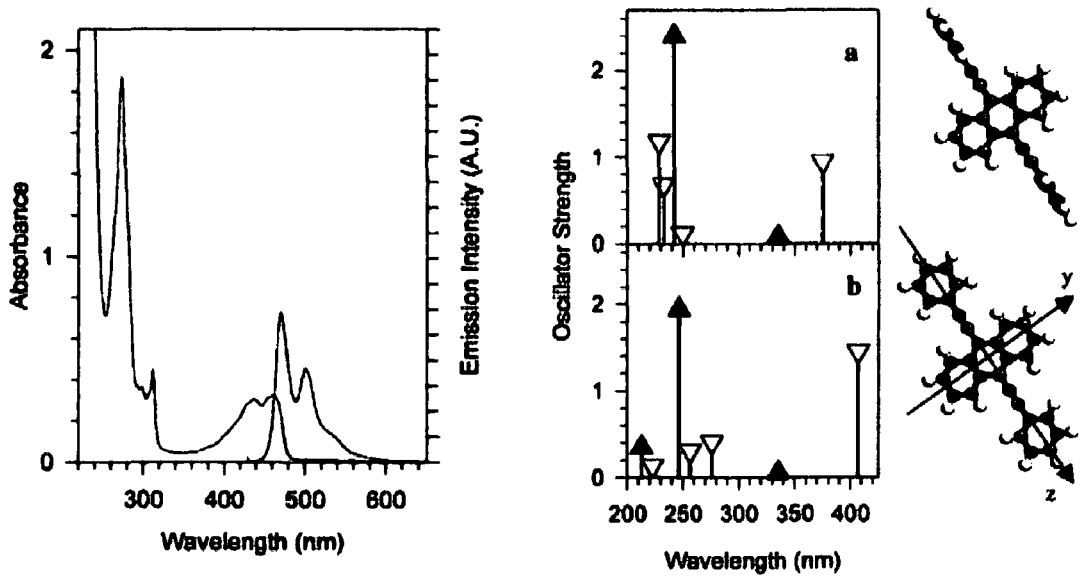

Figure 1.41: UV-Vis and fluorescence spectra of **31** in cyclohexane at room temperature (left hand side) and the calculated UV-Vis spectrum for the two conformations of BPEA shown on the far right. ▽: z-axis polarised transition, ▲: y-axis polarised transition. (Adapted from reference 68)

This calculated variation in behaviour according to conformation, to some extent accounts for why the visible band in the UV-vis spectrum of BPEA lacks the vibrational resolution that is observed in the fluorescence spectrum. This effect will be compounded by the range of conformations existing in the solution, further decreasing the resolution observed.[68]

Beeby *et al.* examined the excitation and emission spectra of **2** at both low and room temperatures. The spectra they obtained are shown in Figure 1.42. The room temperature excitation spectrum has very little vibrational structure, which is due, as in the anthracene case just described, to a range of conformers in solution decreasing the resolution. Cooling the system down to 77 K the excitation spectrum sees a significant increase in absorption at the red edge and an increase in resolution, becoming closer to a mirror image of the observed emission (which also shows a slight increase in vibrational resolution). There was still a continuum of conformers being observed at this low temperature, however the conformers were now longer lived with the rate of rotation of the phenyl rings being comparable to the fluorescence lifetime. This was proposed to limit the range of conformers observed with the planar form being more favoured, however the low barrier to rotation in the ground state is still too low for kT to limit the system to a planar conformation.

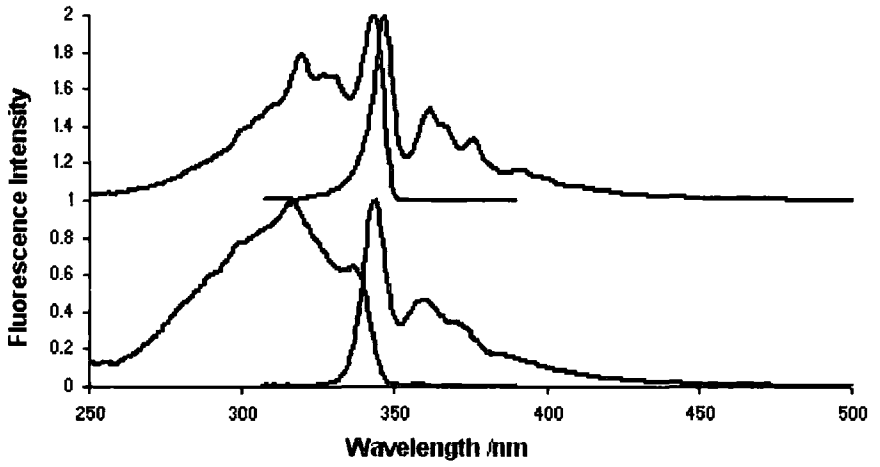

Figure 1.42: Normalised, corrected fluorescence excitation and emission spectra of **2** in EPA at 77 K (upper trace) and 298 K (lower trace) determined with excitation at 320 nm and emission at 360 nm. Adapted from reference 66.

Control of the conformation of aryleneethynylenes can be difficult due to this low barrier to rotation coupled with the physical distance between the aromatic rings. Groups such as those of Bunz and Crisp have used intramolecular tethers between the aromatic rings, such as in compound **51**, to restrict the rotation about the C≡C bond.[69-72]

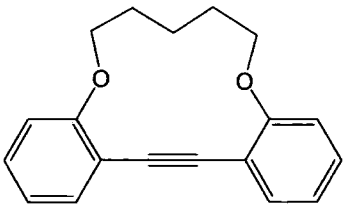

51

These approaches are not ideal however, due to the fact that the majority of the systems are based on tolan, which (as mentioned in section 1.3.2.2) is not a suitable model for longer chain oligomers or polymers. Also, the tethers used have oxygen atoms attached to the phenyl rings which contribute to the molecule's electronic structure. This research is examined in more detail in Chapter 4.

1.4 - Synthetic Approaches Towards Aryleneethynylenes

1.4.1 - Original Approach

The first route used to synthesise phenyleneethynylenes involved the halogenation - dehydrohalogenation of an alkene. A phenylenevinylene, **52**, was reacted with bromine, thus brominating each of the vinylene groups, **53**, followed by a dehydrobromination reaction to form the corresponding phenyleneethynylene, **54**.[73,74] An overview of this process is shown in Scheme 1.1.

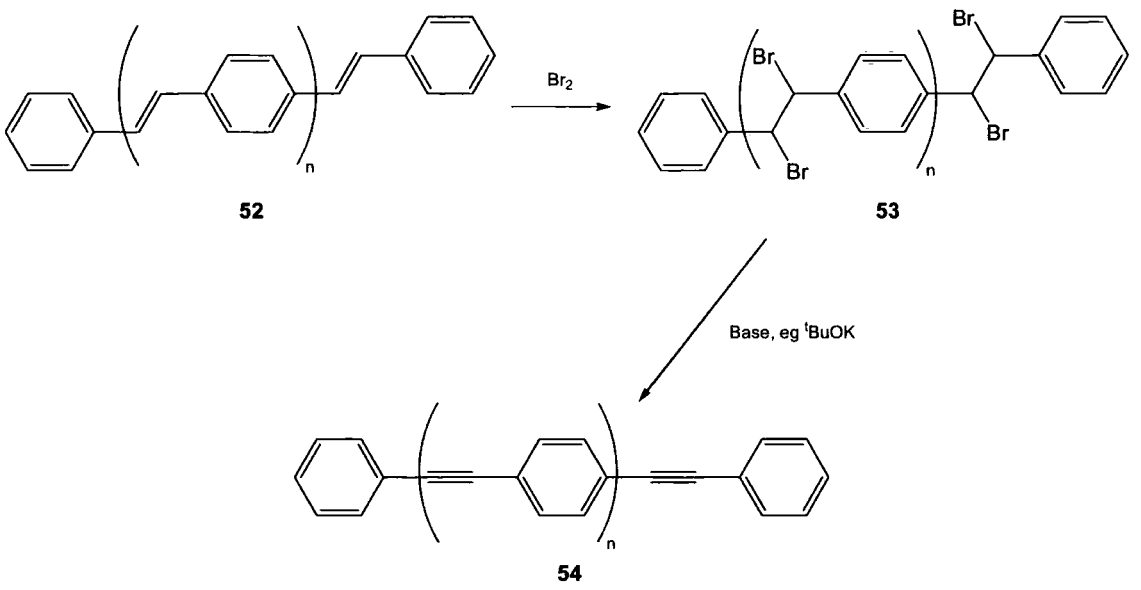

Scheme 1.1: Formation of phenyleneethynylene via the dehydrobromination of a phenylenevinylene.[74]

This route however initially requires the formation of the phenylenevinylene via a Wittig or similar reaction. Also it is essential that, when this route is used, complete bromination and dehydrobromination occurs in order to eliminate the possibility of alkene impurities.

1.4.2 - The Stephens-Castro Reaction

Stephens and Castro found in 1963 that it was possible to obtain tolan based systems by reacting aryl iodides with copper acetylides. The reaction was carried out in pyridine at

reflux under nitrogen.[75,76] If any oxygen is present in the reaction mixture, the acetylene couples oxidatively to give a diyne product.

The copper acetylide was formed by pouring a solution of cuprous iodide in aqueous ammonia into a solution of the arylacetylene in ethanol, yielding the acetylide as a yellow precipitate.[76] Their proposed reaction mechanism is given in Scheme 1.2, where the reaction proceeds *via* a copper complex intermediate.

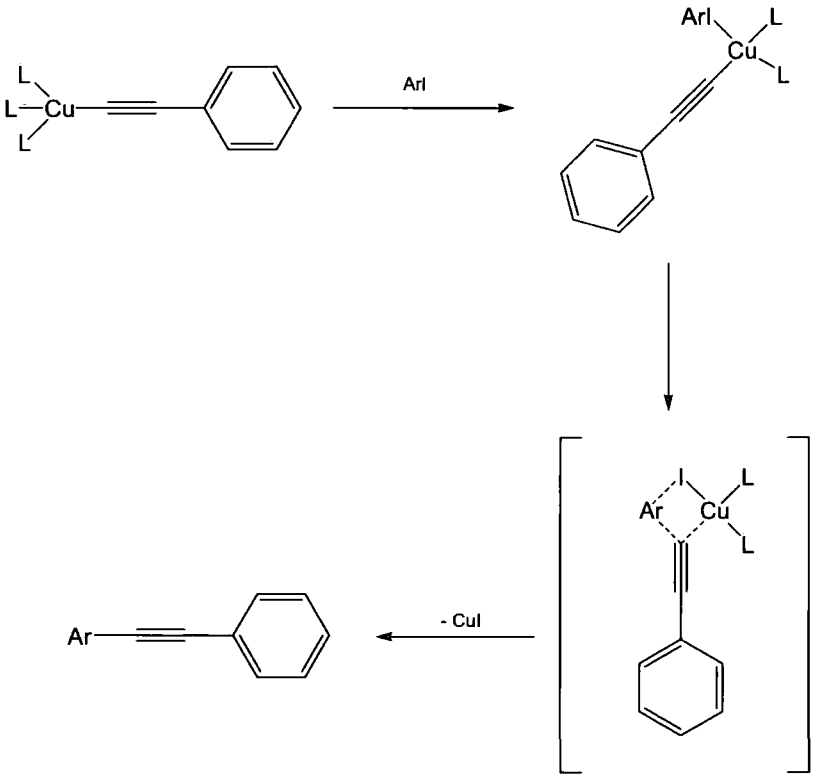

Scheme 1.2: Method proposed by Stephens and Castro for the substitution of aryl iodides with copper acetylides.[76]

Stephens and Castro found that if the aryl iodide has an *ortho* nucleophilic substituent then the reaction did not lead to the substituted tolan product. Instead, a cyclisation reaction leading to the corresponding heterocycle occurs. No cyclisation is observed when the substituted tolan is exposed to copper iodide and copper acetylide in refluxing pyridine, and therefore the cyclisation must occur in the same complex as the substitution.[76] An example of this reaction is given in Scheme 1.3.

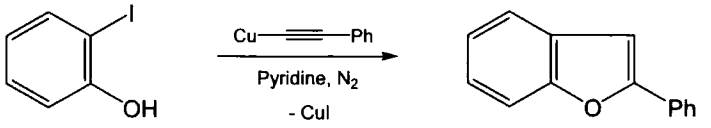

55 56

Scheme 1.3: Example of Stephens-Castro reaction on an *ortho* substituted aryl halide leading to a heterocyclic product.[76]

In 1964, Bacon and Hill studied a variety of substitution reactions between aryl halides and cuprous salts of the type ArX + CuY → ArY + CuX. In this work they found that the ease of displacement of a halogen atom from the aryl ring follows the order I > Br > Cl >> F.[77] This work was followed up in 1966 by Castro *et al.* who found that this same sequence applies in the substitution of the aryl halides by copper acetylides.[78]

One major problem with the Stephens-Castro approach is the nature of copper acetylides. These compounds can act as contact explosives, therefore they need to be treated carefully and should never be allowed to dry out reducing the practicality of this approach.[79]

1.4.3 - The Sonogashira Coupling Reaction

The most common route now employed in synthesising aryleneethynylenes is *via* a palladium catalysed cross coupling reaction first reported by Sonogashira *et al.* in 1975.[80] This *Sonogashira Coupling* proceeds via the catalytic cycle shown in Figure 1.43. The reaction involves the coupling of terminal acetylenes with aryl and vinyl halides in the presence of a catalytic amount of copper iodide and a palladium complex. Many Pd(0) and Pd(II) complexes can be used, but the one that Sonogashira *et al.* used was bis-(triphenylphosphine)palladium dichloride.

The Sonogashira reaction must be done under an inert atmosphere of nitrogen or argon, as any oxygen present can lead to excessive homocoupling of the acetylene. Some homocoupling does occur to a small extent in the reaction, during the in situ formation of the active catalyst, the Pd(0) containing species, $Pd(PPh_3)_2$. Any oxygen present can re-oxidise this back to a Pd(II) species which will then cause more of the diacetylene to be formed. If the homocoupling product cannot be tolerated then its formation can be eliminated by the use of Pd(0) catalysts, such as $Pd(PPh_3)_4$, which typically require more careful handling due to their greater air sensitivity. [37]

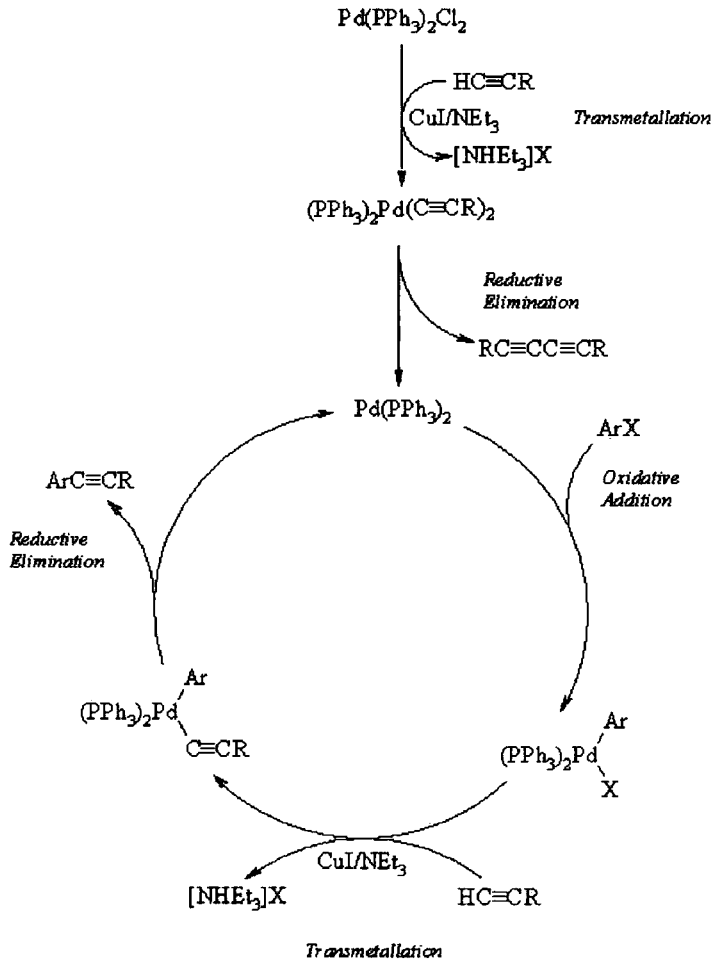

Figure 1.43: Catalytic cycle for the Sonogashira coupling reaction (Adapted from reference 80).

The choice of aryl halide can also affect the coupling. The reaction will proceed with both aryl iodides and aryl bromides, although the iodides react considerably faster with the oxidative addition step being much more facile than with bromides. Also in general couplings involving aryl bromides require elevated temperatures whereas those involving iodides can be carried out at room temperature. Therefore, if they are available, aryl iodides are the preferred substrates in the Sonogashira coupling.[37]

Due to the potential problem of homocoupling in the Sonogashira reaction, Elangovan *et al.* devised a methodology where the reaction was performed under a dilute atmosphere of hydrogen in nitrogen/argon, which they report as reducing the overall yield of the homocoupled product.[81] This route in general is not required, as long as freshly distilled solvents are used and the reaction mixture is vigorously degassed to remove any oxygen present before the addition of the palladium catalyst.

The catalyst used is usually homogeneous. This can lead to palladium contamination in the product which can be problematic. Also, this makes recovery of the catalyst difficult, to the extent that it is usually not carried out. Study has gone into looking towards the development of heterogeneous catalysis methods for this reaction, such as using solid-supported palladium. One example of this is using palladium on charcoal, which is widely used as a heterogeneous catalyst for hydrogenation reactions.

Novák *et al.*[82] have studied reactions using a solid-supported catalyst over a range of aromatic halides, such as the highly reactive 2-bromopyridine and the less reactive 4-chlorobenzonitrile. These were reacted with simple alkynes in a variety of solvents. They found that the polarity of the solvent can play an important role in the reaction, and overall report good yields of product. They suggest that the active species in the reaction is palladium (0) that is leached into the solution during the reaction, but is then returned to the surface of the charcoal at the end of the reaction. Re-use of the catalyst showed slightly less reactivity, due to some of the palladium remaining in solution (the contamination is still vastly reduced from using a homogeneous catalyst).

1.4.4 - Quinone Attack Approach

Another route to aryl-ethynyl frameworks makes use of the electrophilicity of the carbonyl carbon centres in quinones - work in this area has been largely focused on the di-alkylation of large aromatics and the preparation of mono-acetylenic compounds. The synthesis of BPEB-type compounds by this route has been less well documented.[83]

The addition of a lithium acetylide or Grignard to a quinone in solution results in the formation of an acetylene substituted diol.[84-86] Subsequent reduction of the diol with, for example, tin (II) or hydroiodic acid leads to the desired arylacetylene product. An example of this approach can be seen in Scheme 1.4, which shows the steps in converting anthraquinone, **57**, to BPEA.

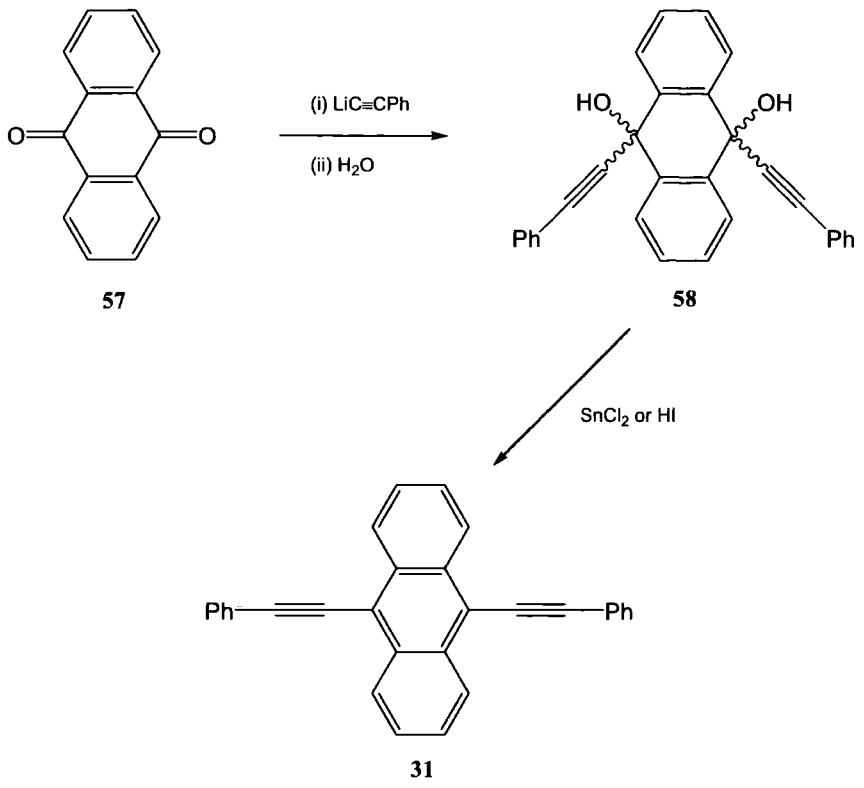

Scheme 1.4: Preparation of BPEA from anthraquinone.[87]

The addition product contains a mixture of *cis* and *trans* isomers, the ratio of which is dependent on several factors, for example the polarity of the solvent used and the reaction time.[87] The ratios formed are not overly important to the overall synthesis, as both isomers yield the same product upon reduction reaction. Reductions are usually carried out on the crude diol without having to chromatographically separate the individual isomers.[83,87]

This methodology has been use to make di-ethynyl systems based on phenyl, naphthyl, and other aryl systems, up to the work of Payne *et al.* on hexacene and heptacene systems.[88] Some further examples of compounds prepared by this route are given in Figure 1.44.

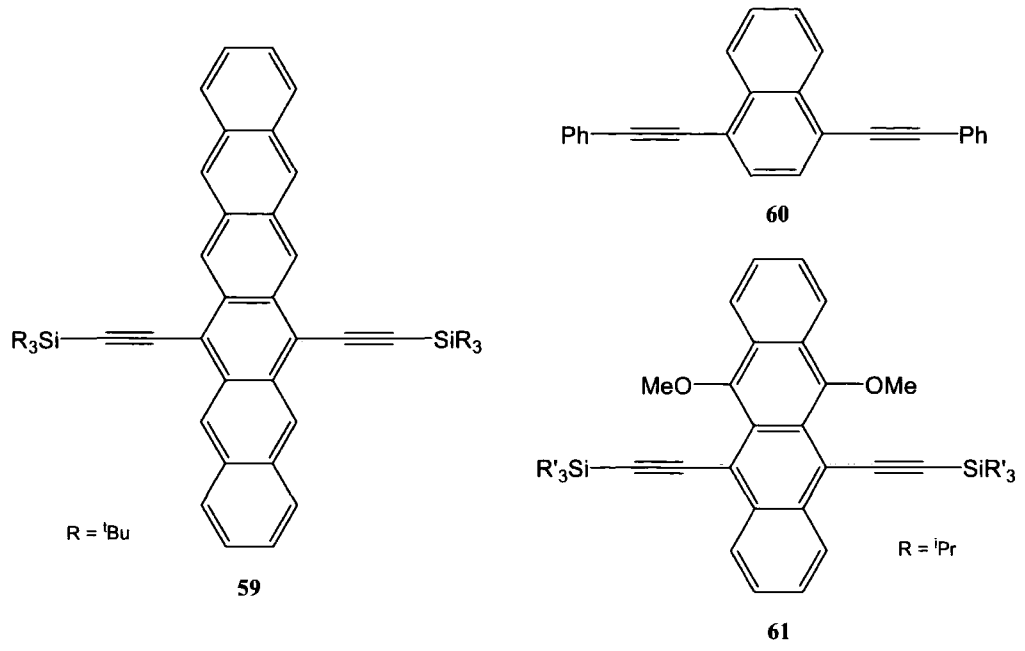

Figure 1.44: Example of further diethynyl compounds that have been synthesised from a quinine based starting material.[83,88,89]

Swager and co-workers have made a range of compounds using this reaction that just contain a single acetylene group. This approach used one equivalent of the lithium acetylide followed by the reduction of the mono-substituted intermediate to the acetylenic-phenol in situ.[90,91] An example of this is shown in Scheme 1.5, with the addition of one equivalent of TMSA to 1,4-triptycene quinone, **62**.

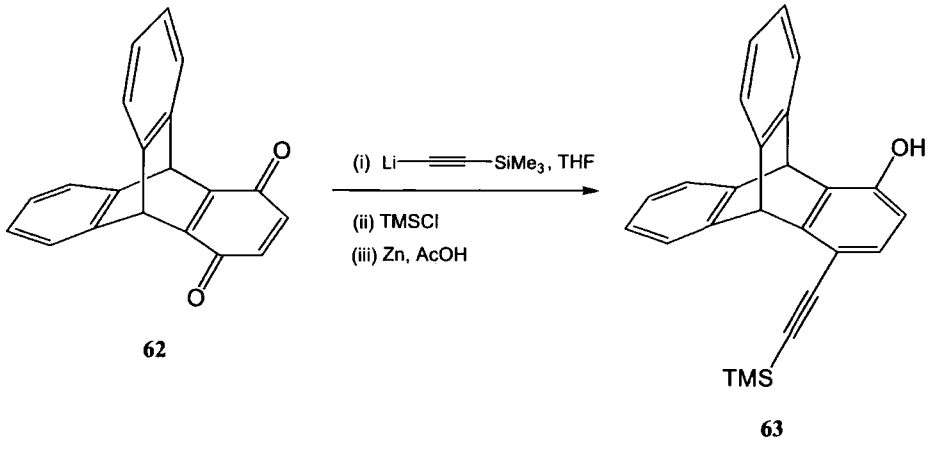

Scheme 1.5: Addition of a single acetylenic group to 1,4-triptycene quinone.[91]

Srinivasan *et al.* observed that the addition of two equivalents of lithium acetylide to *p*-benzoquinone, **64**, occurs in a stepwise manner. Carrying out the reaction at -78 °C will only yield the mono-addition product, **65**. The addition of the second acetylide

molecule only progresses when the solution had been warmed to above -40 °C.[92,93] This behaviour is useful as it allows the formation of differentially substituted products.

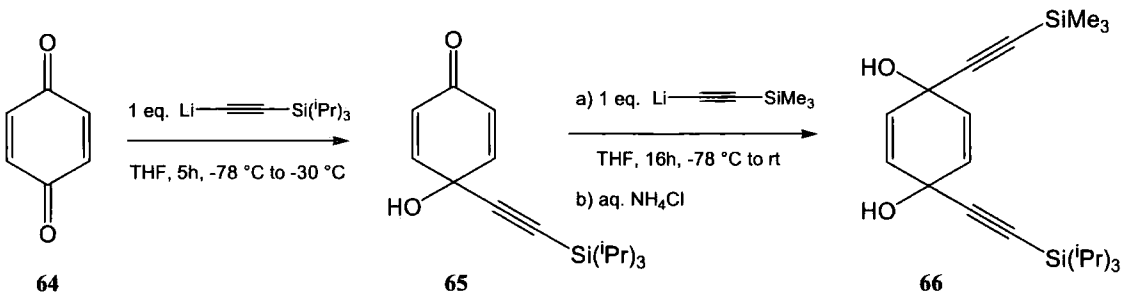

64 **65** **66**

Scheme 1.6: Differential addition to benzoquinone.[93]

An example of the differential addition to benzoquinone carried out by Sankararaman and Srinivasan is given in Scheme 1.6. Initially, one equivalent of lithium triisopropylsilylacetylide was added at -78 °C before stirring for 5 hours at -30 °C. The solution was then cooled once again to -78 °C before the addition of a further equivalent of lithium trimethylsilylacetylide. The solution was subsequently warmed to room temperature and stirred for a further 16 hours. This yielded the final differentially substituted diol, **66**, as a mixture of isomers with a *cis-trans* ratio of 1:2 and an overall yield of 90 %.

This behaviour was utilised by Lydon *et al.* for a 'one pot' synthesis of unsymmetrical phenyleneethynylenes **67** & **68**. This method is potentially very useful as it provides a more facile route in to making these sorts of compounds, which otherwise require a series of Sonogashira couplings of the acetylenes to 1-bromo-4-iodobenzene.[83]

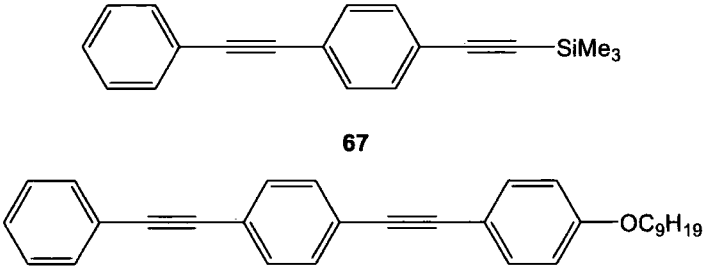

67 **68**

Figure 1.45: Unsymmetrical phenyleneethynylenes, **67** & **68**, synthesised by Lydon *et al.* from a benzoquinone starting material.[83]

The addition of the alkyne can also be carried out by reacting the quinone with an alkynyl Grignard reagent.[94,95] For example, Anthony *et al.* reacted pentacenequinone, **69**, with a range of acetylenic Grignards, many giving the product in high yield.[95] This reaction is illustrated in Scheme 1.7.

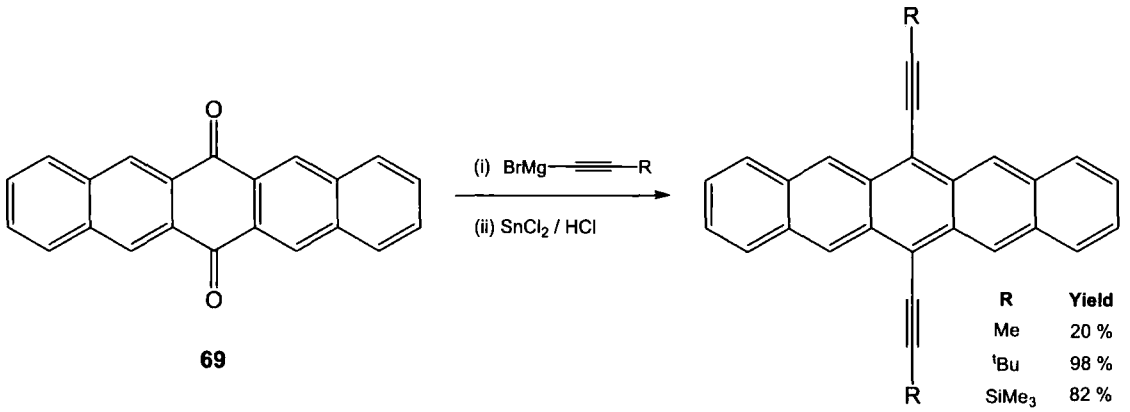

69 **70**

Scheme 1.7: Reaction of several alkynyl Grignard reagents with pentacenequinone.[95]

This Grignard approach is less commonly used, with the alkynyl lithium route being more widely used.

1.4.5 - Alkyne Metathesis

Bunz has developed a method of synthesising PPEs by an alkyne metathesis route, during which the C≡C bonds are formed, in contrast to the other routes that have been described above, where the single carbon-carbon bond is formed between the aryl ring and the alkyne triple bond. This method can be advantageous for the synthesis of high molecular weight PPEs in comparison with the methods using palladium catalysis. Polymers created via a palladium-catalysed route can contain diyne defects, especially if oxygen has not been totally excluded from the reaction vessel. Also, the Sonogashira type reactions can lead to PPEs with ill-defined end groups due to dehalogenation and phosphonium salt formation.[96]

Alkyne metathesis was first reported by Mortreux in 1974, when they observed the disproportionation of methyltolan to tolan and dimethyltolan via a catalyst formed in situ from molybdenum hexacarbonyl and resorcinol as shown in Scheme 1.8.[97]

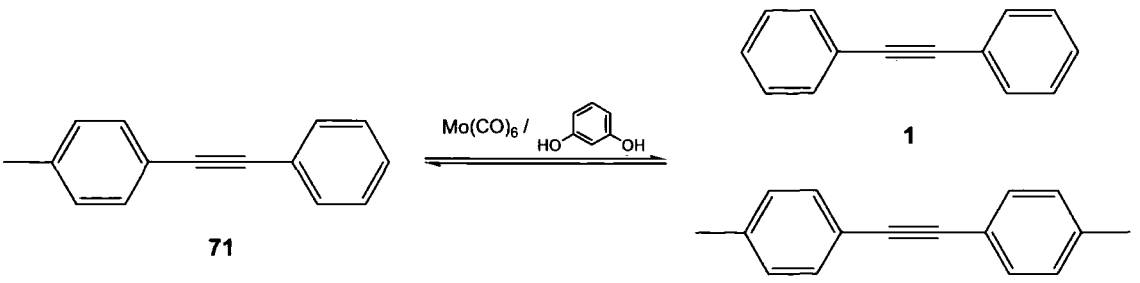

71 1 72

Scheme 1.8: Mortreux's alkyne metathesis catalyst causing disproportionation of 4-methyltolan, **71**, into tolan, **1**, and 4,4'-dimethyltolan, **72**.

Bunz used a tungsten-carbyne catalyst, **73**, to perform an acyclic diyne metathesis (ADIMET) reaction to form a PPE.[98] The catalyst was developed by Schrock in 1989,[99] and subsequently used by Schrock[100] and Bazan[101] to form C≡C bonds via a ring opening metathesis (ROMP) reaction.

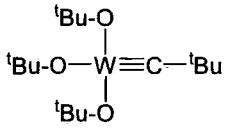

73

The ADIMET reaction requires the use of disubstituted alkynes as the tungsten carbine complexes preferentially polymerise 1-alkynes.[98] The monomer used by Bunz, **74**, was treated with the Schrock catalyst in dried solvents in an inert atmosphere, and was left to react for 12-16 hours at an elevated temperature. The reaction, shown in Scheme 1.9, gave defect-free polymer **75** in high yields. The degree of polymerisation obtained was almost 100 repeating units, making this route competitive with alternative Pd catalysed routes.[37]

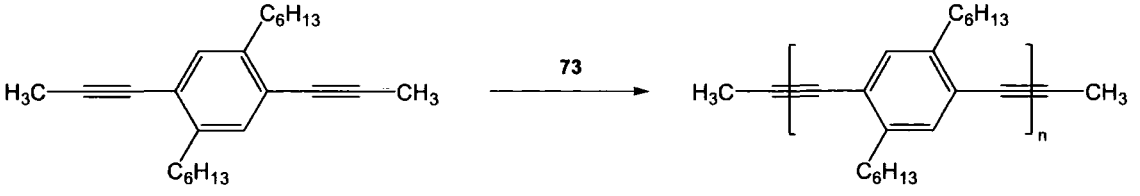

74 75

Scheme 1.9: Formation via alkyne metathesis of **75** using a Schrock catalyst.

Using the Schrock catalyst, **73**, however is not ideal. Despite being highly active it is not available off the shelf (and so requires synthesis), and is very sensitive towards air and water. Therefore the preparation of PPEs with **73** as a catalyst is not very practical. The systems developed by Mortreux do, however, work with off the shelf solvents (non-dried and non-purified) although give only a moderate yield of products.[37]

Mortreux type systems were investigated by Mori, using a mixture of $Mo(CO)_6$ and 4-chlorophenol as the catalyst, to synthesise a range of unsymmetrical alkynes - although their obtained yields were overall not high.[102,103] Bunz later optimised the conditions of this approach for the metathesis of propynylated arenes (example shown in Scheme 1.10). The reaction temperature was increased from 110 °C to 140 °C (with 1,2-dichlorobenzene as solvent) and the reaction was carried out under a steady stream of nitrogen to remove the butyne formed by the reaction. This approach improved the efficiency of the reaction by driving the equilibrium towards the desired products, as well as creating an anhydrous environment for the reaction to proceed under.[104]

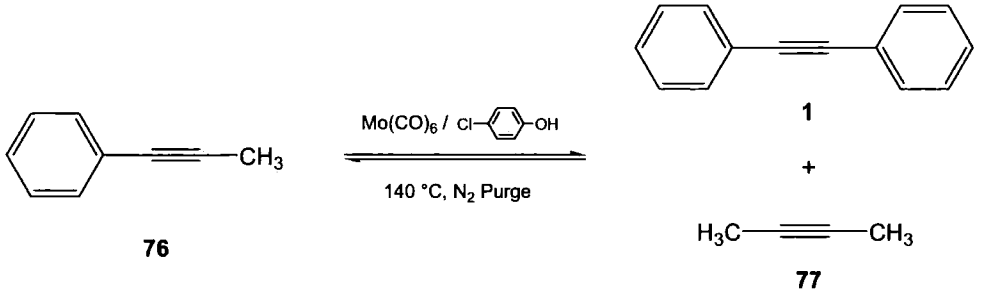

Scheme 1.10: Example of Bunz's optimised alkyne metathesis reaction.

Bunz carried out this method using a wide range of propynylated arenes; the optimal amount of catalyst was found to be 5 molar % of $Mo(CO)_6$ and 30 molar % of 4-chlorophenol, and the optimum reaction time was 12-16 hours. The yields obtained for some of the resultant products are given in Table 1.2. It was found that the substituents on the aryl rings as well as the aryl systems used had an effect on the efficiency of the reaction. The addition of *para* alkyl groups did not increase the yield in relation to the reaction with the unsubstituted propynylbenzene, however the addition of *meta* or *ortho* alkyl groups gave almost quantitative yields from the metathesis reaction, as did the use of 1-propynylnaphthalene. This was attributed in the *ortho* case to the alkyl groups giving a slight amount of steric shielding to the propynyl group, suppressing side reactions and protecting the final product.[104]

Ar	Yield (%)	Ar	Yield (%)	Ar	Yield (%)
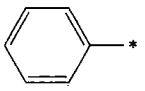	82	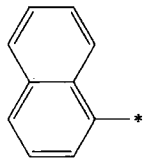	95	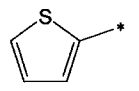	0
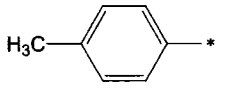	78	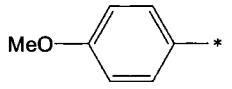	72	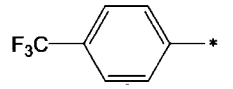	49
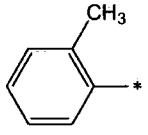	96	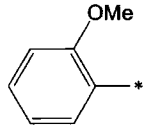	0	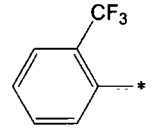	25

Table 1.2: Yields of a range of Ar-C≡C-Ar compounds from Bunz's optimised alkyne metathesis reaction.

The addition of alkoxy and hydroxy substituents decreased the efficiency of the system. Methoxy and ester substituents that are in *para* or *meta* positions, as well as hydroxyl substituents in the *para* position, react to give yields that are lower than for the propynylbenzene system though still in synthetically useful amounts. If these groups are positioned *ortho* to the propynyl group however, the reaction does not proceed, most probably due to internal coordination to the active molybdenum containing species. It was found that in general the use of substituents with free electron pairs gave lower yields. Also the use of the electron accepting CF_3 group decreased the coupling efficiency with the *para* substituted species, giving greater yields than the *ortho* or *meta* variants. Finally, it was observed that the use of heterocyclic arenes such as thiophene did not undergo any reaction at all, with isolation of the starting material at the end of the reaction period.[104]

This modified Mortreux catalytic system was also used by Bunz to prepare PPEs such as **75** by the ADIMET reaction. It was found that a range of alkyl substituted monomers formed the corresponding polymers in high yield. The main difference in performance of the monomers in the reaction was dependent on the solubility of the final polymer. For example isopentyl and cyclohexyl substituents form relatively insoluble products, and therefore resulted in the formation of oligomers rather than polymers with around 20-40 repeating units. Hexyl substituents gave a greater amount of solubility with up to 100 repeat units. The highest molecular weight polymers were obtained using dodecyl substituted monomers reacting at 150 °C for 24 hours. The polymers formed were all bright yellow in colour. At temperatures greater than 150 °C

it was found that the resultant polymers had a brownish or greyish appearance, which was indicative of defect structures in the polymer chains affecting the conjugated system.[105]

This approach was also used, with modification, to create an alkoxy substituted PPE, in near quantitative yield. As shown in Scheme 1.11, the ADIMET reaction on isopentyloxy substituted monomer **78** proceeded only in low yield when 4-chlorophenol is used in the catalytic system. Also, this approach gave only oligomers with relatively low molecular weights (around 8 repeating units in length). Bunz found that by using 4-(trifluromethyl)phenol instead of the 4-chlorophenol and increasing the amount of $Mo(CO)_6$ from 5 to 10 molar %, the reaction proceeded with much improved efficiency, and a greater than 99 % yield. The length of polymer formed was unclear, however, with ^1H NMR spectroscopy giving the number of repeat units as around 20. Gel permeation chromatography (GPC) gave a chain length of 65 repeat units. This discrepancy in the length values was attributed to the possible aggregation of **79** in the dilute DCM solution used in the GPC process.[105]

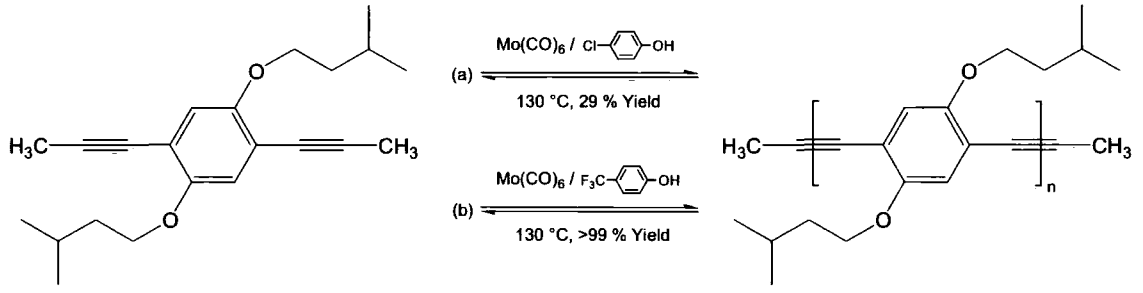

78 **79**

Scheme 1.11: Dependence of choice of phenol in the Mortreux type catalytic system on the efficiency of the ADIMET reaction on alkoxy substituted monomer **78**.

1.4.6 - Corey-Fuchs Reaction

In 1972 Corey and Fuchs reported an efficient two step process to convert aldehydes to acetylenes via chain extension. This 'Corey-Fuchs' reaction, illustrated in Scheme 1.12, proceeds by firstly reacting the aldehyde with carbontetrabromide and triphenylphosphine to form a dibromoolefin. This can then be reacted on with *n*-butyllithium and subsequently quenched with water to form a terminal acetylene.[106]

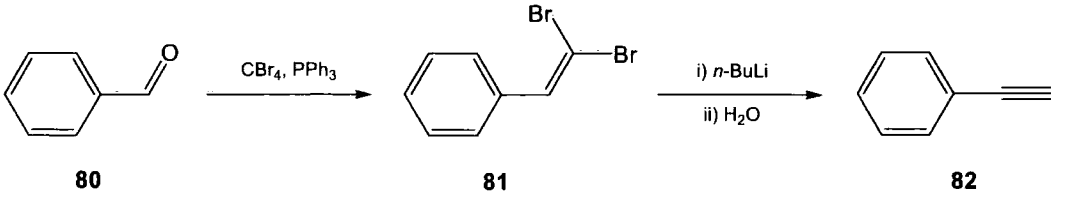

80 81 82

Scheme 1.12: Corey-Fuchs reaction to convert benzaldehyde to phenylacetylene.

Alternatively this route can be used to synthesise a range of acetylenic compounds by treating the intermediate lithium acetylide formed in the second stage of the process with reagents such as carbon halides, aldehydes, ketones and epoxides. For example the addition of carbon dioxide will give the product R-C≡C-CO_2H.[106]

1.5 - Aims and Objectives

As discussed in section 1.3.3, the approaches that have previously been used to control the conformation of aryleneethynylenes have not been ideal for forming model compounds to investigate in detail the effect of conformation on the electronic behaviour of longer chain compounds. Also, the use of tethers bound to the phenyl rings via oxygen atoms gives an increase in contributions to the molecule's electronic structure.

This work aims firstly to study various series of aryleneethynylenes based on the BPEB framework as shown by the schematic in Figure 1.46. These series are formed from combinations of phenyl and non-phenyl aromatic ring systems. These series will be examined by a combination of photophysical and theoretical techniques to examine the effect that the changes of ring systems used have on the resultant compounds' behaviour.

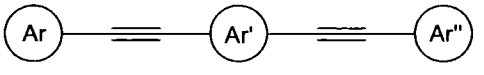

Figure 1.46: Schematic representation of BPEB derivatives

This thesis will also investigate novel derivatives of BPEB that utilise sterically demanding sigma bonded alkyl groups to potentially control the conformation along the long axis of the molecule. If the groups have sufficient bulk then it is expected that the

system will be most thermodynamically stable when the middle ring of the system lies around 90° to the plane of the molecule. This is represented in Scheme 1.13.

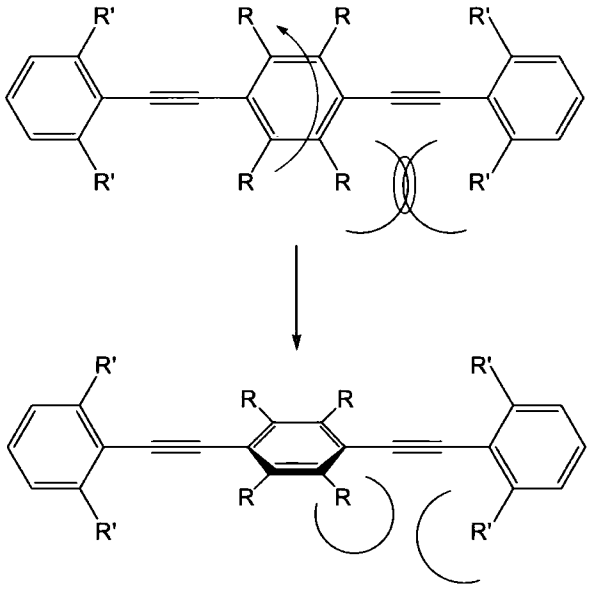

Scheme 1.13: Schematic representation of how steric bulk should favour rotation of the centre ring of a BPEB type system out of the plane of the molecule.

Photophysical studies on the resultant compounds both at high and low temperatures, combined with molecular modelling, should allow an insight into the electronic behaviour of these restricted rotation systems.

The research carried out in these areas is discussed in subsequent chapters. *Chapter Three* examines the synthesis and subsequent studies of series of three-ring aryleneethynylene systems. The attempts to sterically restrict rotation about the acetylenic bond in both BPEB and BPEA type systems are described in *Chapter Four*, detailing the increasing levels of steric bulk introduced in the pursuit of a 'twisted' conformation. *Chapter Five* summarises the work carried out and details some potential future work and *Chapter Six* gives experimental details of all the syntheses carried out.

1.6 - References

1. G. E. Moore, *Electronics*, 1965, ***38***, 114-117.
2. P. A. Packan, *Science*, 1999, ***285***, 2079-2081.
3. N. Robertson and C. A. McGowan, *Chem. Soc. Rev.*, 2003, ***32***, 96-103.
4. J. M. Tour, *Accounts Chem. Res.*, 2000, ***33***, 791-804.
5. Transcript of talk by R. P. Feynman in December 1959 available at http://www.its.caltech.edu/~feynman/plenty.html,
6. A. Aviram and M. A. Ratner, *Chem. Phys. Lett.*, 1974, ***29***, 277-283.
7. M. T. Cygan, T. D. Dunbar, J. J. Arnold, L. A. Bumm, N. F. Shedlock, T. P. Burgin, L. Jones, D. L. Allara, J. M. Tour and P. S. Weiss, *J. Am. Chem. Soc.*, 1998, ***120***, 2721-2732.
8. J. M. Tour, A. M. Rawlett, M. Kozaki, Y. X. Yao, R. C. Jagessar, S. M. Dirk, D. W. Price, M. A. Reed, C. W. Zhou, J. Chen, W. Y. Wang and I. Campbell, *Chem.-Eur. J.*, 2001, *7*, 5118-5134.
9. M. A. Reed, J. Chen, A. M. Rawlett, D. W. Price and J. M. Tour, *Appl. Phys. Lett.*, 2001, ***78***, 3735-3737.
10. J. Chen, M. A. Reed, A. M. Rawlett and J. M. Tour, *Science*, 1999, ***286***, 1550-1552.
11. J. Chen, W. Wang, M. A. Reed, A. M. Rawlett, D. W. Price and J. M. Tour, *Appl. Phys. Lett.*, 2000, *77*, 1224-1226.
12. S. Záliš, I. Kratochvilova, A. Zambova, J. Mbindyo, T. E. Mallouk and T. S. Mayer, *Eur. Phys. J. E*, 2005, ***18***, 201-206.
13. J. Cornil, Y. Karzazi and J. L. Bredas, *J. Am. Chem. Soc.*, 2002, ***124***, 3516-3517.
14. J. P. Launay, *Chem. Soc. Rev.*, 2001, ***30***, 386-397.
15. A. Kraft, A. C. Grimsdale and A. B. Holmes, *Angew. Chem.-Int. Edit.*, 1998, ***37***, 402-428.
16. http://www.kodak.com/US/en/corp/pressReleases/pr20030302-13.shtml,
17. http://www.astonmartin.co.uk/ENG/thecars/db9/engineeredquality,
18. J. G. C. Veinot and T. J. Marks, *Accounts Chem. Res.*, 2005, ***38***, 632-643.
19. A. P. Kulkarni, C. J. Tonzola, A. Babel and S. A. Jenekhe, *Chem. Mat.*, 2004, ***16***, 4556-4573.
20. M. Pope, P. Magnante and H. P. Kallmann, *J. Chem. Phys.*, 1963, ***38***, 2042-&.
21. W. Helfrich and W. G. Schneider, *Phys. Rev. Lett.*, 1965, ***14***, 229-231.
22. C. W. Tang and S. A. VanSlyke, *Appl. Phys. Lett.*, 1987, ***51***, 913-915.
23. C. W. Tang, S. A. VanSlyke and C. H. Chen, *J. Appl. Phys.*, 1989, ***65***, 3610-3616.
24. J. Kido, M. Kohda, K. Okuyama and K. Nagai, *Appl. Phys. Lett.*, 1992, ***61***, 761-763.
25. J. H. Burroughes, D. D. C. Bradley, A. R. Brown, R. N. Marks, K. Mackay, R. H. Friend, P. L. Burns and A. B. Holmes, *Nature*, 1990, ***347***, 539-541.
26. R. H. Friend, R. W. Gymer, A. B. Holmes, J. H. Burroughes, R. N. Marks, C. Taliani, D. D. C. Bradley, D. A. Dos Santos, J. L. Bredas, M. Logdlund and W. R. Salaneck, *Nature*, 1999, ***397***, 121-128.
27. H. Meng, W. L. Yu and W. Huang, *Macromolecules*, 1999, ***32***, 8841-8847.
28. E. Arias-Marin, J. C. Arnault, D. Guillon, T. Maillou, J. Le Moigne, B. Geffroy and J. M. Nunzi, *Langmuir*, 2000, ***16***, 4309-4318.
29. A. Montali, P. Smith and C. Weder, *Synth. Met.*, 1998, ***97***, 123-126.
30. C. Schmitz, P. Posch, M. Thelakkat, H. W. Schmidt, A. Montali, K. Feldman, P. Smith and C. Weder, *Adv. Funct. Mater.*, 2001, ***11***, 41-46.
31. S. Anderson, *Chem.-Eur. J.*, 2001, *7*, 4706-4714.

32. S. H. Lee, T. Nakamura and T. Tsutsui, *Org. Lett.*, 2001, ***3***, 2005-2007.
33. L. Zhao, I. F. Perepichka, F. Turksoy, A. S. Batsanov, A. Beeby, K. S. Findlay and M. R. Bryce, *New J. Chem.*, 2004, ***28***, 912-918.
34. C. Weder, C. Sarwa, A. Montali, G. Bastiaansen and P. Smith, *Science*, 1998, ***279***, 835-837.
35. A. Montali, G. Bastiaansen, P. Smith and C. Weder, *Nature*, 1998, ***392***, 261-264.
36. D. Steiger, P. Smith and C. Weder, *Macromol. Rapid Commun.*, 1997, ***18***, 643-649.
37. U. H. F. Bunz, *Chem. Rev.*, 2000, ***100***, 1605-1644.
38. L. Kloppenburg, D. Jones, J. B. Claridge, H. C. zur Loye and U. H. F. Bunz, *Macromolecules*, 1999, ***32***, 4460-4463.
39. R. Giménez, M. Piñol and J. L. Serrano, *Chem. Mat.*, 2004, ***16***, 1377-1383.
40. Q. Zhou and T. M. Swager, *J. Am. Chem. Soc.*, 1995, ***117***, 12593-12602.
41. T. M. Swager, *Accounts Chem. Res.*, 1998, ***31***, 201-207.
42. http://en.wikipedia.org/wiki/Paraquat,
43. J. S. Yang and T. M. Swager, *J. Am. Chem. Soc.*, 1998, ***120***, 11864-11873.
44. J. S. Yang and T. M. Swager, *J. Am. Chem. Soc.*, 1998, ***120***, 5321-5322.
45. http://www.nomadics.com/_media/documents/pdf/Fido_Brochure.pdf, http://web.mit.edu/tswager/www/Current%20Research-PEMW.htm,
46. J. N. Wilson and U. H. F. Bunz, *J. Am. Chem. Soc.*, 2005, ***127***, 4124-4125.
47. I. B. Kim, A. Dunkhorst, J. Gilbert and U. H. F. Bunz, *Macromolecules*, 2005, ***38***, 4560-4562.
48. A. V. Abramenkov, A. Almenningen, B. N. Cyvin, S. J. Cyvin, T. Jonvik, L. S. Khaikin, C. Romming and L. V. Vilkov, *Acta Chem. Scand. A*, 1988, ***42***, 674-684.
49. M. Levitus, K. Schmieder, H. Ricks, K. D. Shimizu, U. H. F. Bunz and M. A. Garcia-Garibay, *J. Am. Chem. Soc.*, 2001, ***123***, 4259-4265.
50. S. J. Greaves, E. L. Flynn, E. L. Futcher, E. Wrede, D. P. Lydon, P. J. Low, S. R. Rutter and A. Beeby, *J. Phys. Chem. A*, 2006, ***110***, 2114-2121.
51. K. Okuyama, T. Hasegawa, M. Ito and N. Mikami, *J. Phys. Chem.*, 1984, ***88***, 1711-1716.
52. Z. J. Donhauser, B. A. Mantooth, K. F. Kelly, L. A. Bumm, J. D. Monnell, J. J. Stapleton, D. W. Price, A. M. Rawlett, D. L. Allara, J. M. Tour and P. S. Weiss, *Science*, 2001, ***292***, 2303-2307.
53. J. R. Lakowicz, *Principles of Fluorescence Spectroscopy*, 2nd ed.; Kluwer Academic: New York, 1999.
54. M. Kasha, *Discuss. Faraday Soc.*, 1950, 14-19.
55. M. Beer and H. C. Longuet-Higgins, *J. Chem. Phys.*, 1955, ***23***, 1390-1391.
56. K. M. Bark and R. K. Forcé, *J. Phys. Chem.*, 1989, ***93***, 7985-7988.
57. *Course Book (S341). Photochemistry: Light, Chemical Change and Life. Block 3: Colour*; The Open University. ISBN 0335 161031.
58. S. A. McFarland and N. S. Finney, *J. Am. Chem. Soc.*, 2002, ***124***, 1178-1179.
59. T. Ishibashi and H. Hamaguchi, *J. Phys. Chem. A*, 1998, ***102***, 2263-2269.
60. T. Ishibashi, H. Okamoto and H. Hamaguchi, *Chem. Phys. Lett.*, 2000, ***325***, 212-218.
61. M. I. Sluch, A. Godt, U. H. F. Bunz and M. A. Berg, *J. Am. Chem. Soc.*, 2001, ***123***, 6447-6448.
62. S. Karabunarliev, M. Baumgarten and K. Mullen, *J. Phys. Chem. A*, 2000, ***104***, 8236-8243.
63. A. Beeby, K. S. Findlay, P. J. Low, T. B. Marder, P. Matousek, A. W. Parker, S. R. Rutter and M. Towrie, *Chem. Commun.*, 2003, 2406-2407.

64. Z. Chernia, T. Livneh, I. Pri-Bar and J. E. Koresh, *Vib. Spectrosc.*, 2001, ***25***, 119-131.
65. M. Kijima, I. Kinoshita and H. Shirakawa, *Synth. Met.*, 1999, ***101***, 145-148.
66. A. Beeby, K. Findlay, P. J. Low and T. B. Marder, *J. Am. Chem. Soc.*, 2002, ***124***, 8280-8284.
67. M. Levitus, K. Schmieder, H. Ricks, K. D. Shimizu, U. H. F. Bunz and M. A. Garcia-Garibay, *J. Am. Chem. Soc.*, 2002, ***124***, 8181-8181.
68. M. Levitus and M. A. Garcia-Garibay, *J. Phys. Chem. A*, 2000, ***104***, 8632-8637.
69. G. Brizius and U. H. F. Bunz, *Org. Lett.*, 2002, ***4***, 2829-2831.
70. G. Brizius, K. Billingsley, M. D. Smith and U. H. F. Bunz, *Org. Lett.*, 2003, ***5***, 3951-3954.
71. G. T. Crisp and T. P. Bubner, *Tetrahedron*, 1997, ***53***, 11881-11898.
72. G. T. Crisp and T. P. Bubner, *Tetrahedron*, 1997, ***53***, 11899-11912.
73. G. Drefahl and G. Plötner, *Chem. Ber.*, 1958, ***91***, 1280-1285.
74. P. F. H. Schwab, M. D. Levin and J. Michl, *Chem. Rev.*, 1999, ***99***, 1863-1933.
75. R. D. Stephens and C. E. Castro, *J. Org. Chem.*, 1963, ***28***, 2163.
76. R. D. Stephens and C. E. Castro, *J. Org. Chem.*, 1963, ***28***, 3313-3315.
77. R. G. R. Bacon and H. A. O. Hill, *J. Chem. Soc.*, 1964, 1097-1107.
78. C. E. Castro, E. J. Gaughan and D. C. Owsley, *J. Org. Chem.*, 1966, ***31***, 4071-4078.
79. P. G. Urben, *Bretherick's Handbook of Reactive Chemical Hazards Vol 1*, 5th ed.; Butterworth-Heinemann Ltd: Oxford, 1995.
80. K. Sonogashira, Y. Tohda and N. Hagihara, *Tetrahedron Lett.*, 1975, 4467-4470.
81. A. Elangovan, Y. H. Wang and T. I. Ho, *Org. Lett.*, 2003, ***5***, 1841-1844.
82. Z. Novák, A. Szabó, J. Répási and A. Kotschy, *J. Org. Chem.*, 2003, ***68***, 3327-3329.
83. D. P. Lydon, L. Porres, A. Beeby, T. B. Marder and P. J. Low, *New J. Chem.*, 2005, ***29***, 972-976.
84. D. R. Maulding and B. G. Roberts, *J. Org. Chem.*, 1969, ***34***, 1734-&.
85. P. J. Hanhela and D. B. Paul, *Aust. J. Chem.*, 1981, ***34***, 1701-1717.
86. W. Ried, W. Donner and W. Schlegelmilch, *Chem. Ber.*, 1961, ***94***, 1051-1058.
87. P. J. Hanhela and D. B. Paul, *Aust. J. Chem.*, 1981, ***34***, 1669-1685.
88. M. M. Payne, S. R. Parkin and J. E. Anthony, *J. Am. Chem. Soc.*, 2005, ***127***, 8028-8029.
89. S. A. Odom, S. R. Parkin and J. E. Anthony, *Org. Lett.*, 2003, ***5***, 4245-4248.
90. Q. Zhou and T. M. Swager, *J. Org. Chem.*, 1995, ***60***, 7096-7100.
91. T. M. Long and T. M. Swager, *J. Mater. Chem.*, 2002, ***12***, 3407-3412.
92. M. Srinivasan, S. Sankararaman, H. Hopf and B. Varghese, *Eur. J. Org. Chem.*, 2003, 660-665.
93. S. Sankararaman and M. Srinivasan, *Org. Biomol. Chem.*, 2003, ***1***, 2388-2392.
94. G. Rio, *Ann. Chim.*, 1954, ***9***, 182.
95. J. E. Anthony, D. L. Eaton and S. R. Parkin, *Org. Lett.*, 2002, ***4***, 15-18.
96. U. H. F. Bunz, *Accounts Chem. Res.*, 2001, ***34***, 998-1010.
97. A. Mortreux and M. Blanchard, *J. Chem. Soc.-Chem. Commun.*, 1974, 786-787.
98. K. Weiss, A. Michel, E. M. Auth, U. H. F. Bunz, T. Mangel and K. Mullen, *Angew. Chem.-Int. Edit. Engl.*, 1997, ***36***, 506-509.
99. R. R. Schrock, D. N. Clark, J. Sancho, J. H. Wengrovius, S. M. Rocklage and S. F. Pedersen, *Organometallics*, 1982, ***1***, 1645-1651.
100. S. A. Krouse and R. R. Schrock, *Macromolecules*, 1989, ***22***, 2569-2576.
101. X. P. Zhang and G. C. Bazan, *Macromolecules*, 1994, ***27***, 4627-4628.
102. N. Kaneta, T. Hirai and M. Mori, *Chem. Lett.*, 1995, 627-628.

103. N. Kaneta, K. Hikichi, S. Asaka, M. Uemura and M. Mori, *Chem. Lett.*, 1995, 1055-1056.
104. N. G. Pschirer and U. H. F. Bunz, *Tetrahedron Lett.*, 1999, ***40***, 2481-2484.
105. L. Kloppenburg, D. Jones and U. H. F. Bunz, *Macromolecules*, 1999, ***32***, 4194-4203.
106. E. J. Corey and P. L. Fuchs, *Tetrahedron Lett.*, 1972, 3769-3772.

CHAPTER 2

EXPERIMENTAL TECHNIQUES

2.1 - Introduction

This chapter describes the experimental techniques as well as the instrumentation used to obtain the photophysical measurements described in chapters 3 and 4. Information is also given on the software used in the theoretical, molecular modelling calculations.

2.2 - UV-Visible Absorption Spectroscopy

UV-Visible absorption spectra were recorded over an appropriate wavelength range using an ATI Unicam UV-2 spectrophotometer and quartz cuvettes. Assuming the Beer-Lambert law, the absorption of light can be related to the concentration of the absorbing species present in solution using equation 2.1, where I_0 is the intensity of incident light, I_t is the intensity of transmitted light, A is the absorbance at a particular wavelength, ε is the molar extinction coefficient ($dm^3mol^{-1}cm^{-1}$), c is the concentration (mol dm^{-3}) of the absorbing species and l is the pathlength of the cuvette (cm).

$$\log_{10}\left(\frac{I_o}{I_t}\right) = A = \varepsilon\, c\, l \qquad 2.1$$

2.3 - Steady-State Fluorescence Spectroscopy

2.3.1 - Spectra

Emission and excitation spectra were recorded using a Perkin Elmer LS-50B luminescence spectrometer or a Jobin-Yvon Horiba Fluorolog 3-22 Tau-3 spectrofluorimeter with a right angle illumination method. The spectra obtained were corrected for the spectral response of the appropriate machine. A schematic of the Fluorolog is shown in Figure 2.1.

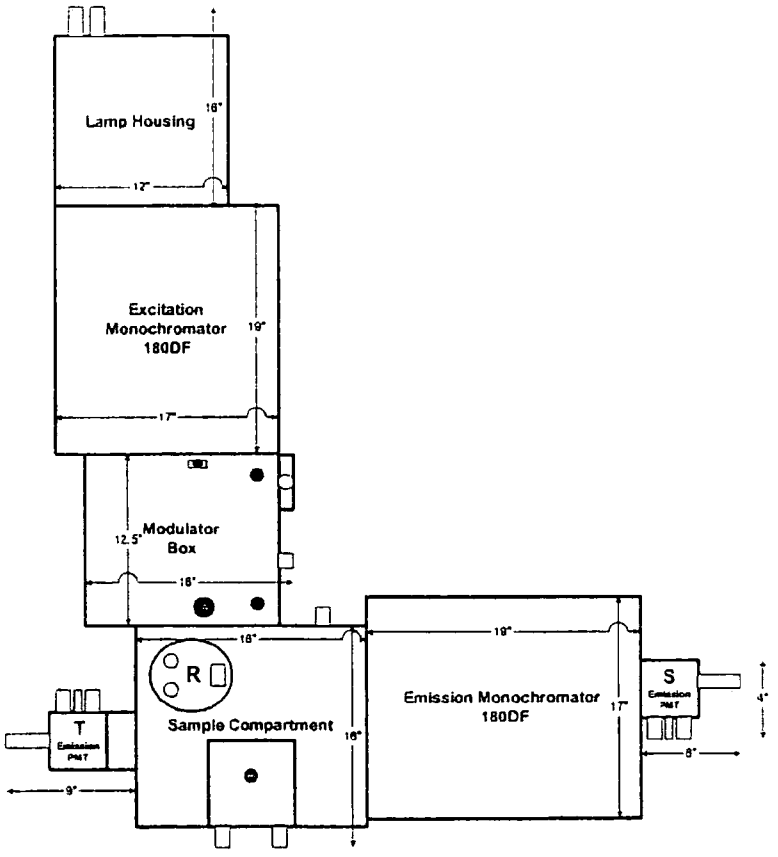

Figure 2.1: Schematic of the Fluorolog-3 Model FL-3-22-T, double excitation / double emission lifetime spectrofluorometer with T-side detector.[1]

2.3.2 - Fluorescence Quantum Yields

The fluorescence quantum yield, Φ, is defined as the ratio of photons absorbed by a molecule that are then emitted through fluorescence. The fluorescence quantum yields were recorded using the method of Williams *et al.*[2] which uses well known characterised standard samples with known Φ values. Solutions of the standard and test samples that have identical absorbance at the same excitation wavelength can be taken as absorbing the same number of photons. Thus a ratio of the integrated fluorescence intensities of the two solutions can be used to obtain the ratio of the quantum yield values and hence the Φ of the test sample.[3]

Standard samples used were 1,4-bis(5-phenyloxazole-2-yl)benzene (POPOP, Φ = 0.97),[4] quinine sulphate (Φ = 0.54),[5] norharmane (Φ = 0.58),[6] coumarin 153 (Φ = 0.38)[5] and acridine orange (Φ = 0.20).[7] Complementary pairs of standards are used when doing measurements as this allows cross-calibration of them, ensuring both are

behaving as expected. Measurement of fluorescence data over a range of five different absorbances (all below 0.1 in a 1 cm cell) is carried out to ensure the absence of concentration effects such as self-quenching. A plot of the integrated fluorescence intensity against absorbance can then be obtained, the gradient of the graphs allowing the value of Φ to be calculated using equation 2.2 (Grad = gradient, η = the refractive index of the solvent and the subscripts X and ST denote the test sample and the standard respectively)

$$\Phi_X = \Phi_{ST}\left(\frac{Grad_X}{Grad_{ST}}\right)\left(\frac{\eta_X^2}{\eta_{ST}^2}\right) \qquad 2.2$$

2.4 - Low Temperature Measurements

All low temperature measurements were obtained using an Oxford Instruments DN 1704 Optical Cryostat, cooled by liquid nitrogen. Samples in EPA were held in 1 cm pathlength Spectrosil cuvettes. EPA is a mixture of diethyl ether, isopentane and ethanol in a ratio of 5:5:2 (v/v) that forms a stable transparent glass on cooling to 77 K.[8] Temperature control was obtained via the use of an Oxford Instruments ITC-601 temperature controller, with samples given 15-30 minutes to equilibrate at a temperature before data was collected.

2.5 - Fluorescence Lifetimes

Lifetimes were obtained *via* the time-correlated single-photon counting technique.[9] The method described by Beeby *et al.*[10] was used. Samples were excited by pulsed light from IBH Nanoled diodes at 295, 334 or 371 nm, the wavelength chosen was dependent on the samples absorption profile. Emission was collected at 90° to the source of excitation and the emission wavelength selected by a monochromator (Jobin Yvon Triax 190). Fluorescence detection was obtained using a photomultiplier tube (IBH Model TBX-04) that was linked to a time-to-amplitude converter (Ortec 567) and a multichannel analyser (E.G. & G. Trump Card and Maestro for Windows v 5.10). Fluorescence decays were recorded to a minimum of 10,000 counts in the peak channel of the pulse height analyser and the data transferred to PC for analysis in Microsoft Excel *via* the method of iterative reconvolution and nonlinear least squares fitting.

The emission lifetime of a species in a single excited state follows a single exponential decay curve. To obtain the lifetime from the data, the decay can be fitted to a single exponential function, shown in equation 2.3 (t is the time, I(t) is the intensity of light at time t, A_1 is a constant and τ_1 is the lifetime of the species).

$$I(t)=A_1\exp\left(\frac{-t}{\tau_1}\right) \qquad 2.3$$

The quality of a calculated fit was judged *via* the use of statistical parameters. These were the Durbin-Watson parameter, the reduced χ^2 and both the random and auto-correlated residuals. Figure 2.2 shows a typical decay and fit along with the calculated residual.

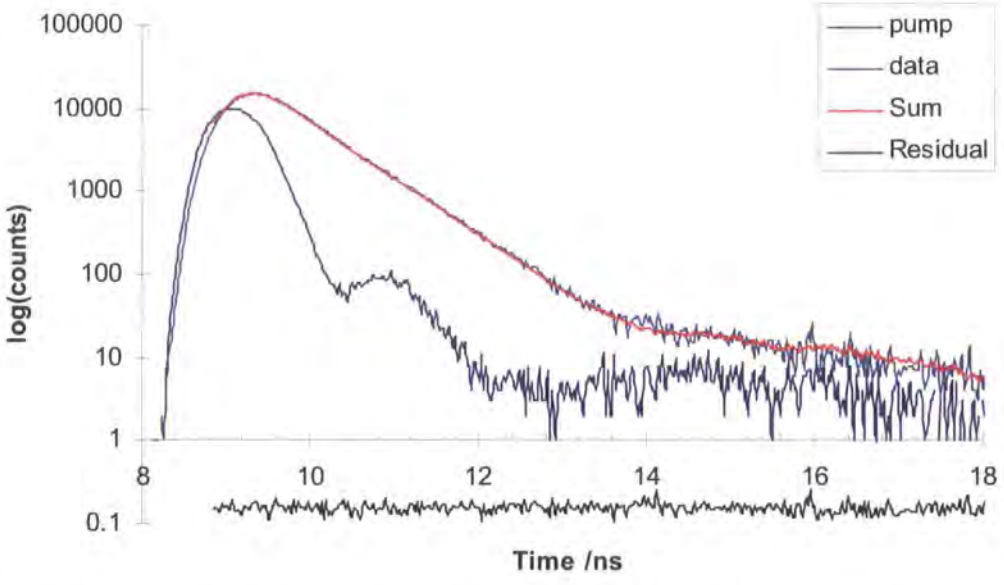

Figure 2.2: Example of a typical single exponential fit used to obtain a fluorescence lifetime.

2.6 - Calculations

Molecular modelling was carried out on a PC using both Fujitsu CAChe Ver 6.1.10 and Gaussian-03W, Revision C.02.[11] In CAChe structures were first optimised using semi-empirical methods (MOPAC, PM5) after which the electronic transitions were calculated using ZINDO INDO-S. Gaussian was used for TD-DFT calculations using in general the B3LYP/6-311g(2d,p) level of theory.

2.7 - References

1. *Jobin Yvon-Spex Fluorolog Tau-3 Lifetime System Hardware Operation Manual*, 1999.
2. A. T. R. Williams, S. A. Winfield and J. N. Miller, *Analyst*, 1983, ***108***, 1067-1071.
3. Jobin Yvon Ltd, *A Guide to Recording Fluorescence Quantum Yields*,
4. J. R. Lakowicz, *Principles of Fluorescence Spectroscopy*, 2nd ed.; Kluwer Academic: New York, 1999.
5. W. H. Melhuish, *J. Phys. Chem.*, 1961, ***65***, 229-235.
6. A. Pardo, D. Reyman, J. M. L. Poyato and F. Medina, *J. Lumines.*, 1992, ***51***, 269-274.
7. B. Soep, M. Martin, A. Kellmann and Lindqvis.L, *Chem. Phys. Lett.*, 1972, ***13***, 241-244.
8. J. C. Scaiano, *Handbook of Organic Photochemistry*; CRC Press, 1989; Vol. 2.
9. D. V. O'Connor and D. Phillips, *Time Correlated Single Photon Counting*; Academic Press: London, 1984.
10. A. Beeby, S. FitzGerald and C. F. Stanley, *Photochem. Photobiol.*, 2001, ***74***, 566-569.
11. Gaussian 03, Revision C.02, M. J. Frisch, G. W. Trucks, H. B. Schlegel, G. E. Scuseria, M. A. Robb, J. R. Cheeseman, J. A. M. Jr., T. Vreven, K. N. Kudin, J. C. Burant, J. M. Millam, S. S. Iyengar, J. Tomasi, V. Barone, B. Mennucci, M. Cossi, G. Scalmani, N. Rega, G. A. Petersson, H. Nakatsuji, M. Hada, M. Ehara, K. Toyota, R. Fukuda, J. Hasegawa, M. Ishida, T. Nakajima, Y. Honda, O. Kitao, H. Nakai, M. Klene, X. Li, J. E. Knox, H. P. Hratchian, J. B. Cross, C. Adamo, J. Jaramillo, R. Gomperts, R. E. Stratmann, O. Yazyev, A. J. Austin, R. Cammi, C. Pomelli, J. W. Ochterski, P. Y. Ayala, K. Morokuma, G. A. Voth, P. Salvador, J. J. Dannenberg, V. G. Zakrzewski, S. Dapprich, A. D. Daniels, M. C. Strain, O. Farkas, D. K. Malick, A. D. Rabuck, K. Raghavachari, J. B. Foresman, J. V. Ortiz, Q. Cui, A. G. Baboul, S. Clifford, J. Cioslowski, B. B. Stefanov, G. Liu, A. Liashenko, P. Piskorz, I. Komaromi, R. L. Martin, D. J. Fox, T. Keith, M. A. Al-Laham, C. Y. Peng, A. Nanayakkara, M. Challacombe, P. M. W. Gill, B. Johnson, W. Chen, M. W. Wong, C. Gonzalez and J. A. Pople, Gaussian, Inc., Wallingford CT, 2004,

CHAPTER 3

SYNTHETIC AND PHOTOPHYSICAL STUDY OF ARYLENEETHYNYLENE SERIES

3.1 - Introduction

To date, research into aryleneethynylenes has not been carried out in great detail towards the synthetic and photophysical study of a series of three ring analogues to BPEB (as shown in Figure 3.1). Whereas many compounds of this type have been synthesised the majority of research has been concerned with only individual members of a potential series. It was of interest therefore to examine some series of three ring systems to see the effect of changing the rings present.

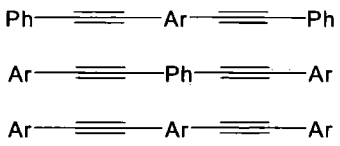

Figure 3.1: Series of three ring aryleneethynylene systems, Ar = non-phenyl arene.

3.2 - Naphthalene systems

3.2.1 - Introduction

Of the three ring phenyl-naphthyl series shown in Figure 3.2, only **60** has been reported as a known compound.[1,2] Only substituted analogues of **83** have been made, whereas there is no reported derivative of **84**.

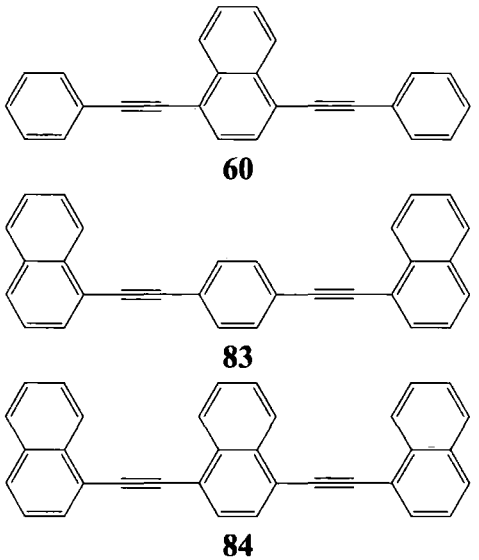

60 **83** **84**

Figure 3.2: Phenyl-Naphthyl three ring aryleneethynylene series.

Compound **60** was first reported in 1981 by Hanhela and Paul,[1] who synthesised it in 22 % yield by the reaction of naphthoquinone, **85**, with lithium phenylacetylide in dioxan and subsequent reduction of the formed diol by $SnCl_2$, (Scheme 3.1). The low yield was attributed to the formation of unwanted products such as **86**, as the reaction conditions used led to the attack of the naphthalene ring system by lithium phenylacetylide *via* an oxidative coupling.

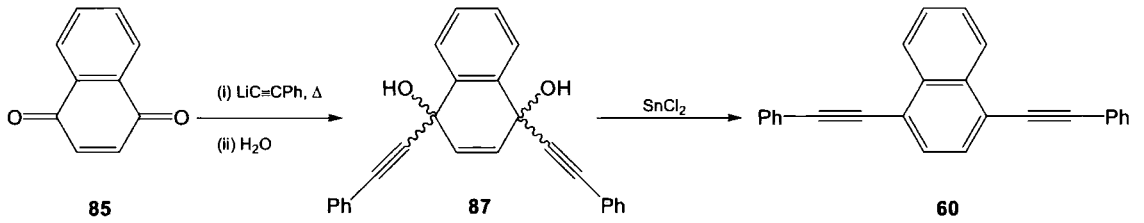

Scheme 3.1: Hanhela and Paul's synthetic route to **60**.

The route described above also allowed the synthesis of the dichloro derivative **88** from 2,3-dichloronaphthoquinone in a 15 % yield. The diol intermediate could not be reduced by tin (II) chloride, thus potassium iodide and sodium hypophosphite were employed. They also attempted synthesis of the dimethoxy derivative, **89**, however, the reaction did not proceed as they expected, with lithium phenylacetylide attacking the 2,3-dimethoxynaphthoquinone at one of the methoxy groups before attacking the quinone to give the mixture of products shown in Figure 3.4.[1]

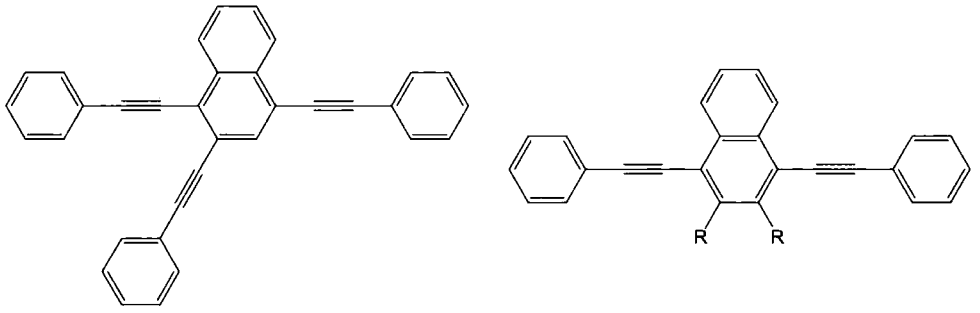

86

R = Cl, **88**
R = OMe, **89**

Figure 3.3: Side product of elevated temperature formation of **60** from 1,4-naphthoquinone plus further derivatives of **60** whose syntheses were attempted by Hanhela and Paul.[1]

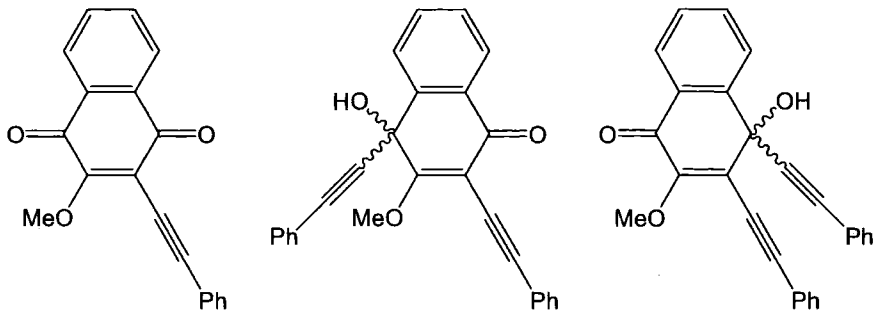

90 **91** **92**

Figure 3.4: Products from Hanhela and Paul's attempted synthesis of **89**.[1]

In 2005 Lydon *et al.* were able to optimise the synthesis of **60** using this approach. Whereas Hanhela and Paul carried out the reaction in dioxan at reflux,[1] Lydon *et al.* utilised temperatures between -70 °C and room temperature with THF used as the solvent. This approach gave the desired product in 76 % yield.[2]

Hanhela and Paul carried out only limited luminescence studies on **60** and **88**. The fluorescence emission spectra were obtained in dimethyl phthalate solution, and are shown in Figure 3.5. The emission profile of **60** shows some evidence of vibrational structure with peaks observed at 394 and 415 nm and a reported quantum yield of 1.00 ± 0.07. The spectrum of **88** is very similar, although red shifted by 12 nm in relation to **60**. **88** Is a less efficient emitter with a reduced quantum yield however of 0.41 ± 0.07.[1,3]

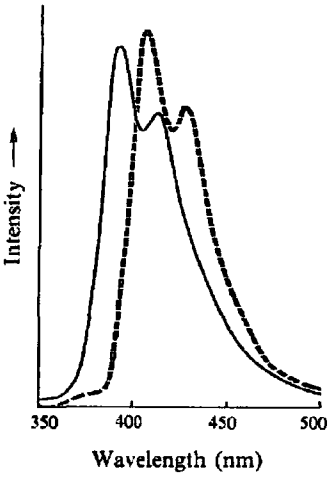

Figure 3.5: Emission spectra of **60** (—) & **88** (---) in dimethyl phthalate solution. Adapted from ref 1.

The use of **60** and **88** in a chemiluminescence reaction was also investigated. Emission was observed from 10^{-3} M solutions of the compounds in dimethyl phthalate that also contained bis(2,4,6-trichlorophenyl) oxalate and hydrogen peroxide (both 0.01 M). The

oxidation of the diaryl oxalate by the peroxide caused the excitation and subsequent emission from the fluorescent compounds. Emission was observed at 419 nm for **60** and 430 nm for **88**.[1]

Rodríguez and Tejedor have reported the synthesis of **83** derivatives *via* a Sonogashira coupling route (see Scheme 3.2) where the coupling of diiodobenzene to substituted 1-ethynylnaphthalenes proceeded readily. The compounds synthesised are shown in Figure 3.6.[4-6]

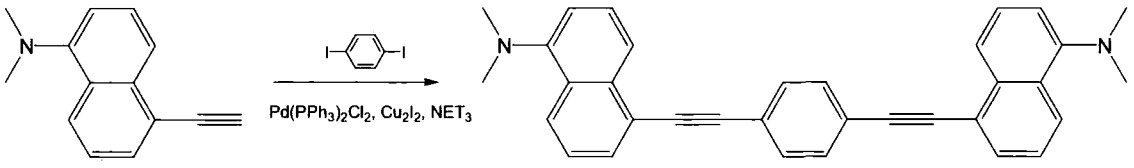

93 **94** 90 %

Scheme 3.2: Sonogashira coupling route to **94**, a substituted derivative of **83**.[4,5]

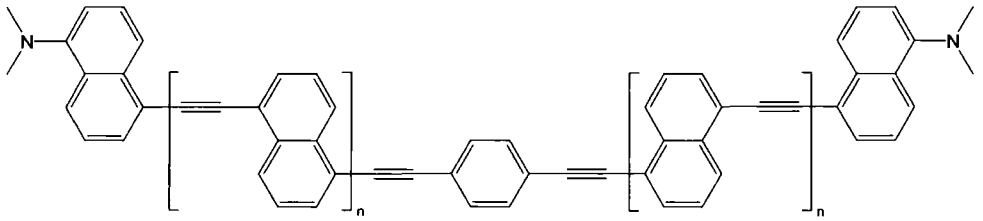

n = 0, **94**
n = 1, **95**
n = 2, **96**

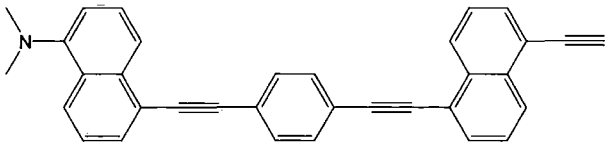

97

Figure 3.6: Derivatives of **83** synthesised by Rodríguez and Tejedor.[4-6]

Compounds **95** and **96** involved a more complex synthesis due to their larger number of arylethynyl units. **95** was synthesised as follows (Scheme 3.3). Initially 1,5-dinitronaphthalene, **98**, was reduced to **99** and **100**, followed by diazotisation reactions to convert the aniline groups to the corresponding iodides **101** and **104**. The nitro group of **101** was reduced with stannous chloride before being treated with sodium cyanoborohydride and formic acid to give compound **102**. The next step involved a Sonogashira coupling of **102** with 2-methyl-3-butyn-2-ol followed by deprotection of

the acetylene to give **103**. Another Sonogashira coupling was carried out between **104** and one equivalent of 2-methyl-3-butyn-2-ol to give **105**.

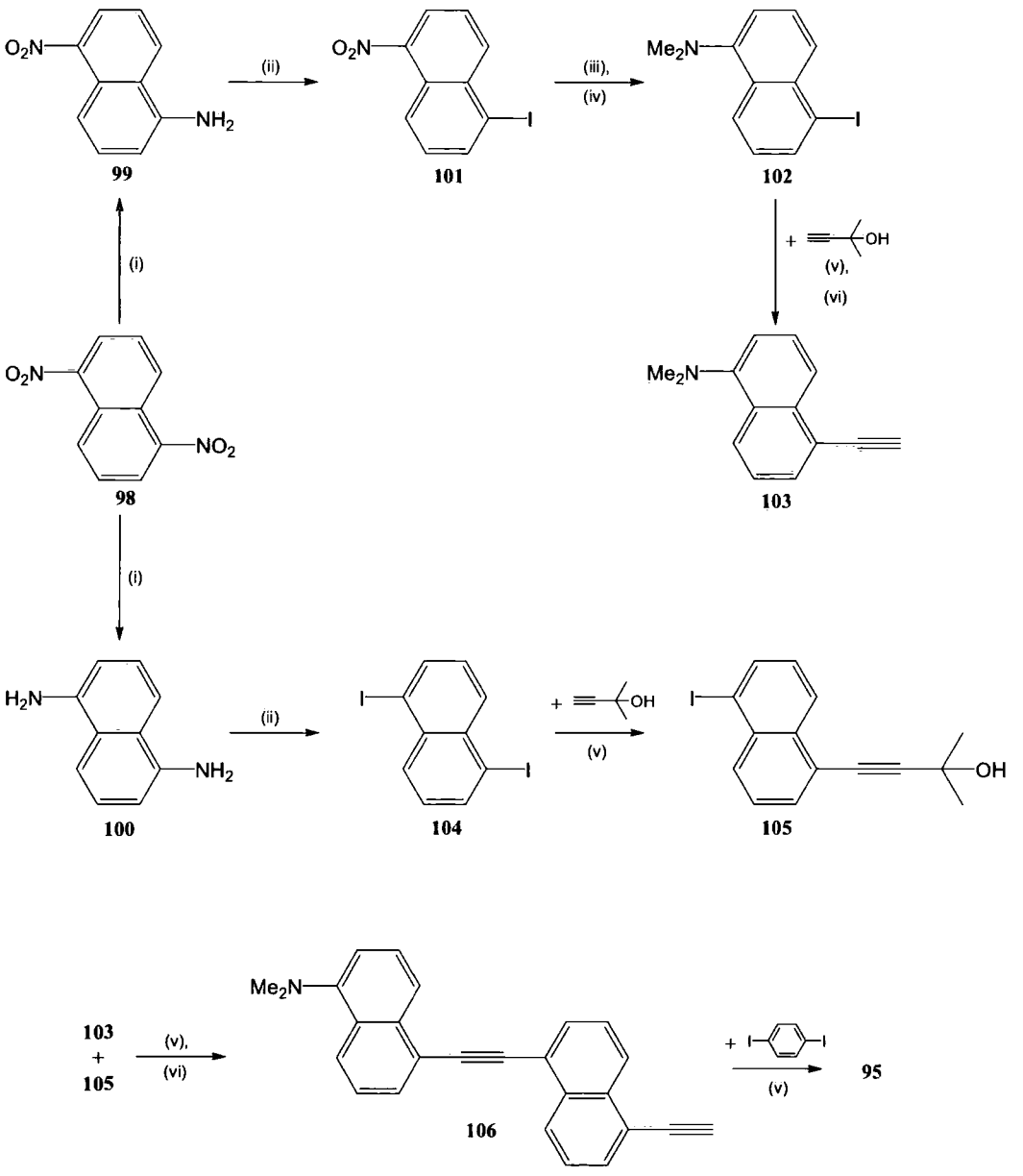

Scheme 3.3: Rodriguez and Tejedor's synthetic route to **95**. Reagents and conditions: (i) Na_2S, NH_4OH, Δ; (ii) $NaNO_2$, H_2SO_4, KI; (iii) $SnCl_2.2H_2O$, EtOAc, Δ; (iv) HCO_2H, MeCN, $NaBH_3CN$, glacial acetic acid; (v) $Pd(PPh_3)_2Cl_2$, Cu_2I_2, NEt_3; (vi) NaOH, toluene, Δ.[4,5]

They then carried out a further coupling reaction, this time between **103** and **105**, which after a successive deprotection step gave **106**. The last stage of the synthesis involved a Sonogashira coupling of **106** with 1,4-diiodobenzene to give **95** with a 81 % yield for this final step.

Attempts to grow single crystals of **97** failed, preventing structural studies of the compound. However, they were able to obtain suitable crystals of the picrate complex of **97**, the structure obtained is shown in Figure 3.7. In these crystals **97** adopts a structure where the naphthalene rings are rotated 180° in relation to each other (the *anti* rotamer) and the central benzene ring is rotated out of the naphthalene plane by 28.6°.

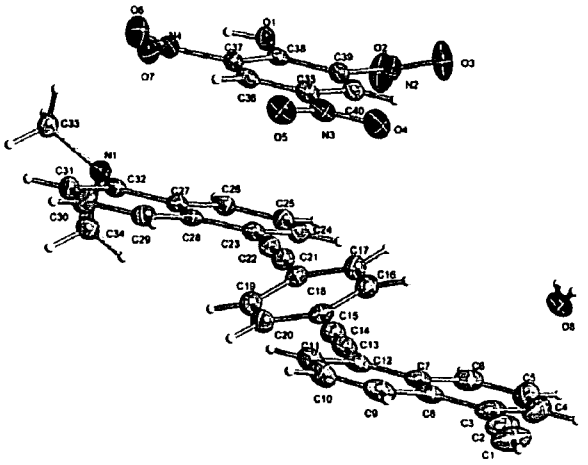

Figure 3.7: Crystal structure of the picrate complex of **97** (1:1 complex).[6]

Photophysical studies were also carried out by Rodríguez and Tejedor on all four of the **83** derivatives, the spectra of compounds **94** to **96** obtained are shown in Figure 3.8.[5] From Table 3.1 it can be seen that all of compounds **94** - **97** have very similar maxima, both for their absorbance and emission spectra - with the length of conjugation having little effect on these values. An increase in conjugation did, however, give greater extinction coefficients and decreased quantum yields.[5,6]

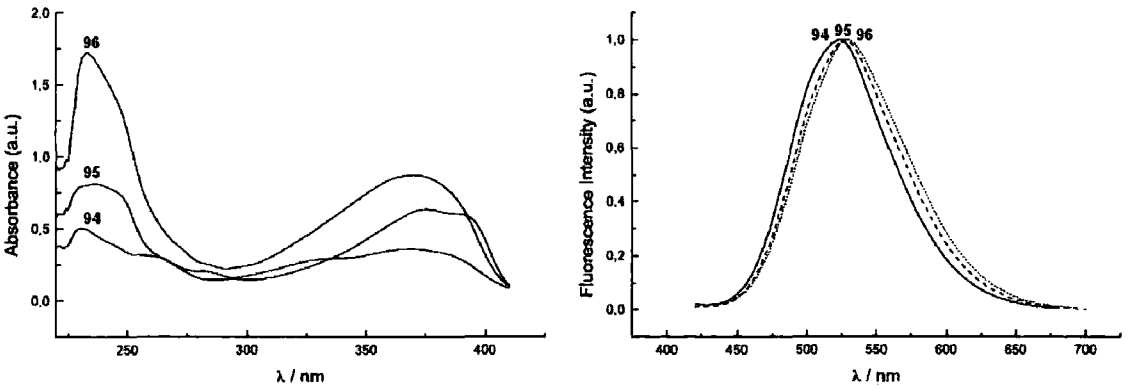

Figure 3.8: Absorption (left) and emission (right) spectra for compounds **94** - **96** in DCM at room temperature.[5]

All of the compounds exhibit large Stokes shifts (1587 cm^{-1} for **97**) and relatively low quantum yields, and this can be attributed to the presence of the dimethylamino group leading to intramolecular charge transfer (ICT) states.[6]

Compound	Abs λ_{max} (nm)	ε ($M^{-1}cm^{-1}$)	Fluor λ_{max} (nm)	Φ_f
94	369	36,200	524	0.30
95	375	60,300	528	0.15
96	371	87,500	529	0.08
97	364	69,450	526	0.20

Table 3.1: Selected photophysical properties for compounds **94** - **97** in DCM at room temperature.[5,6]

1,4-Bis(1-hydroxynaphthalen-5-ylethynyl)benzene, **98**, was synthesised in good yield by Liu *et al.* *via* a Sonogashira coupling reaction as an intermediate towards the construction of the rotaxane shown in Figure 3.9. The location of the two cyclobis(paraquat-*p*-phenylene) rings can be controlled either chemically or electrochemically *via* redox processes, with the distance between the rings changing between 4.2 and 1.4 nm. This action mimics the contraction and extension of skeletal muscle but on a smaller scale. Development of systems like this could be used to perform larger-scale mechanical work with a number of these "molecular muscles" working together to provide movement.[7]

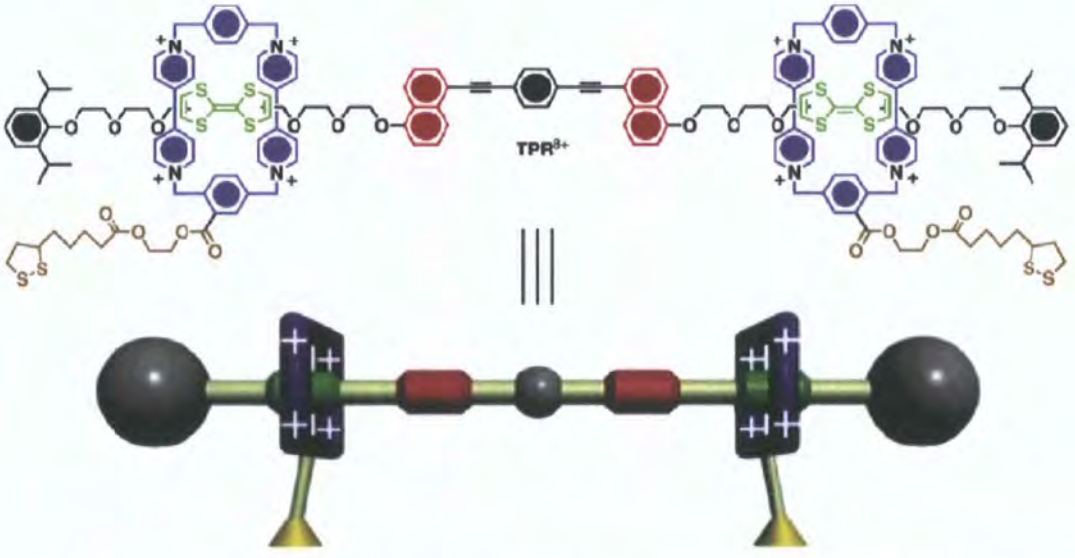

Figure 3.9: Structural formula and graphical representation of Liu *et al.*'s disulfide-tethered molecular muscle.[7]

The aim of the work described below was to prepare a series of BPEB analogues containing the naphthalene moiety and to compare their photophysical properties.

3.2.2 - Synthesis

Although commercially available, 1,4-dibromonaphthalene, **107**, is rather expensive. Thus, for this work it was decided to prepare it using the method of Cakmak *et al.*[8] by the treatment of naphthalene, **108**, in DCM solution with bromine at -10 °C. After three days at this temperature **107** was obtained in good yield.

Synthesis of the aryleneethynylene series was carried out using standard Sonogashira methodology, and is summarised in Figure 3.10. **60** was synthesised by coupling the dibromonaphthalene with phenylacetylene. Subsequent purification, by passing through a silica column with a hexane/DCM eluent followed by recrystallisation, led to the desired product in 85 % yield. 1,4-diiodobenzene, **109**, was coupled to 1-ethynylnaphthalene, **110**, to obtain **83** in 54 % yield after purification. Finally, **84** was synthesised *via* the coupling of **107** and **110** with a 29 % yield after purification.

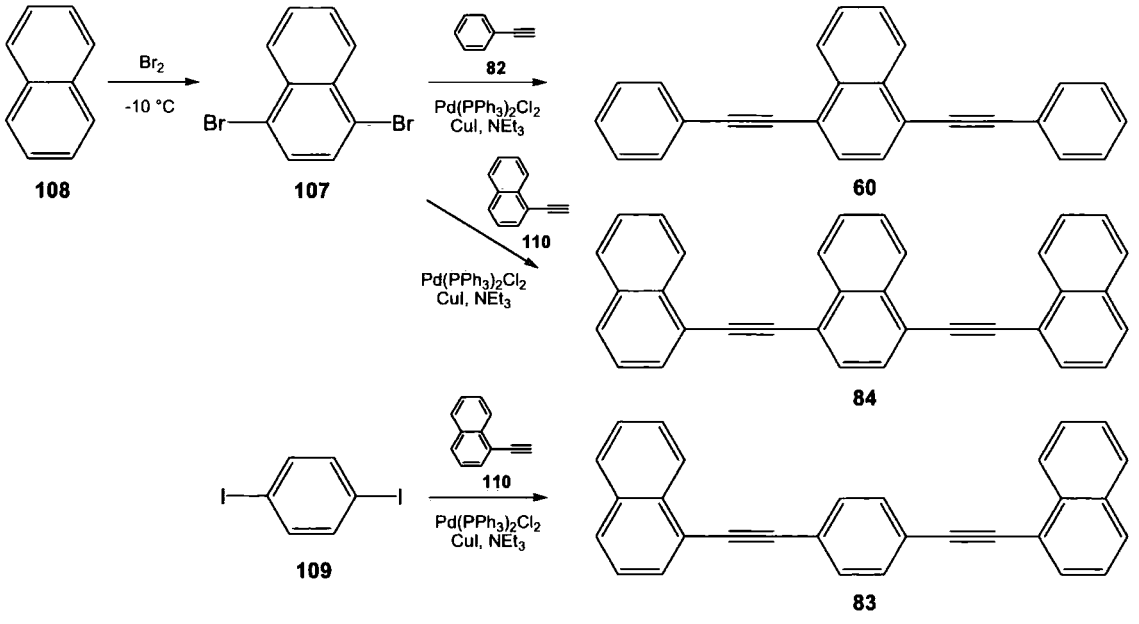

Figure 3.10: Synthetic route to compounds **60**, **83** and **84**.

Crystals were obtained for all three compounds, however only those of **83** proved to be of sufficient quality for X-ray analysis. The resultant structure obtained shows the molecule adopting the *anti*-rotamer with the two naphthalene rings rotated 180° in relation to each other. Also, the central phenyl ring is twisted out of the plane of the

molecule by 17°. This corresponds well with the structure obtained by Rodríguez and Tejedor for the picrate complex of **97**, albeit with a smaller angle for the central ring, suggesting that the presence of the picric acid molecule in the complex did not have a large effect on the conformation of **97**.

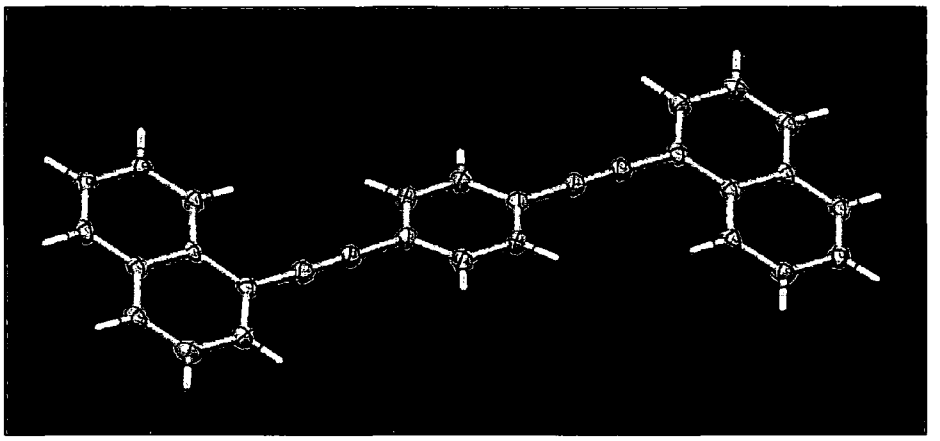

Figure 3.11: Structure of **83** determined by X-ray crystallography.

3.2.3 - Photophysics

Emission and excitation spectra were obtained for compounds **60**, **83** and **84**, these are shown in Figure 3.12. The emission spectrum obtained for **60** is blue shifted by *ca.* 10 nm in relation to that observed by Hanhela and Paul (Figure 3.5) but otherwise shows a similar profile, confirming their result.

The room temperature spectra of compounds **60**, **83** and **84** are all red shifted in relation to BPEB, but otherwise have similar profiles. The excitation spectra are broad and free of significant vibrational structure, due to the averaging of a continuum of rotational conformers in solution. The emission spectra show a greater amount of vibronic structure due to a planarisation of the molecule before emission.

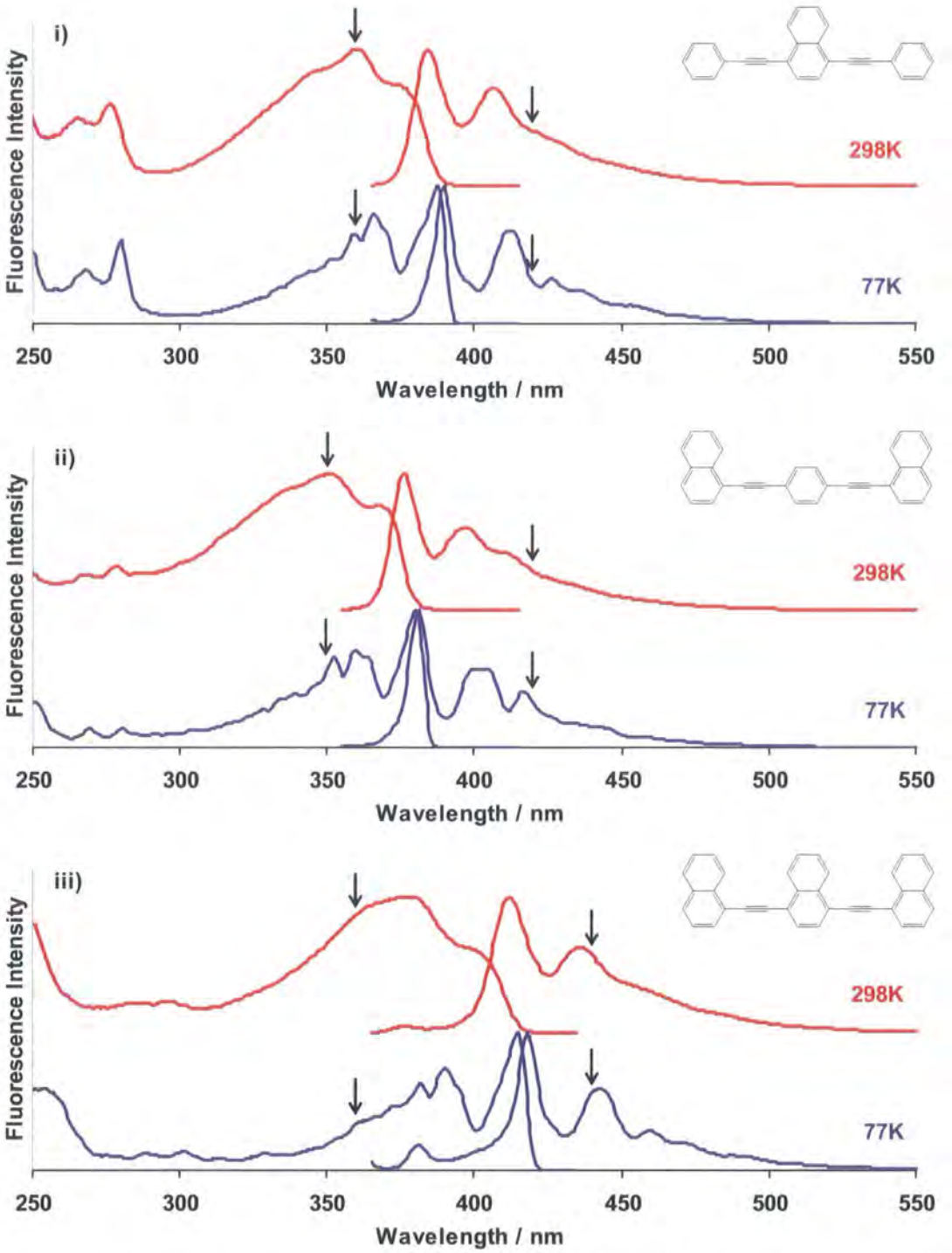

Figure 3.12: Normalised, emission-excitation spectra of i) **60** (λ_{ex} = 360 nm, λ_{em} = 420 nm), ii) **83** (λ_{ex} = 350 nm, λ_{em} = 420 nm) and iii) **84** (λ_{ex} = 360 nm, λ_{em} = 440 nm) in EPA at 298 and 77 K (Arrows on spectra denote emission and excitation wavelengths).

	Excitation Features (nm)		Emission Features (nm)	
	298K	77K	298K	77K
60	360, 375	359, 366, 388	384, 406	390, 412, 426
83	351, 367	353, 360, 380	376, 397, 412	381, 404, 417
84	375, 401	382, 390, 415	412, 436	381, 418, 442

Table 3.2: Summary of features on emission-excitation spectra of **60**, **83** and **84**.

The fluorescence spectra at low temperature also behave, in general, in a similar way to that of BPEB. The excitation spectra see the appearance of vibrational structure plus a strengthening of the signal at the red edge, they also become more like a mirror image of the emission spectra which show a sharpening of the vibrational structure.

The low temperature emission spectrum of **84**, however, shows an extra band at 381 nm. This is likely to arise from a restriction of the rotation about the acetylenic bonds due to steric interactions between the hydrogens in the 5 and 8 positions on the naphthalene rings adjacent to the C≡C bonds, as illustrated in Figure 3.13. This means that when adjacent naphthalene rings are in a similar orientation the molecule cannot fully planarise. This conformational restriction means that not all of the molecules are able to reorient to a planar conformation before emission occurs, causing there to be more than one emitting species present. Restriction of rotation about acetylene bonds in aryleneethynylenes is examined in greater detail in Chapter 4.

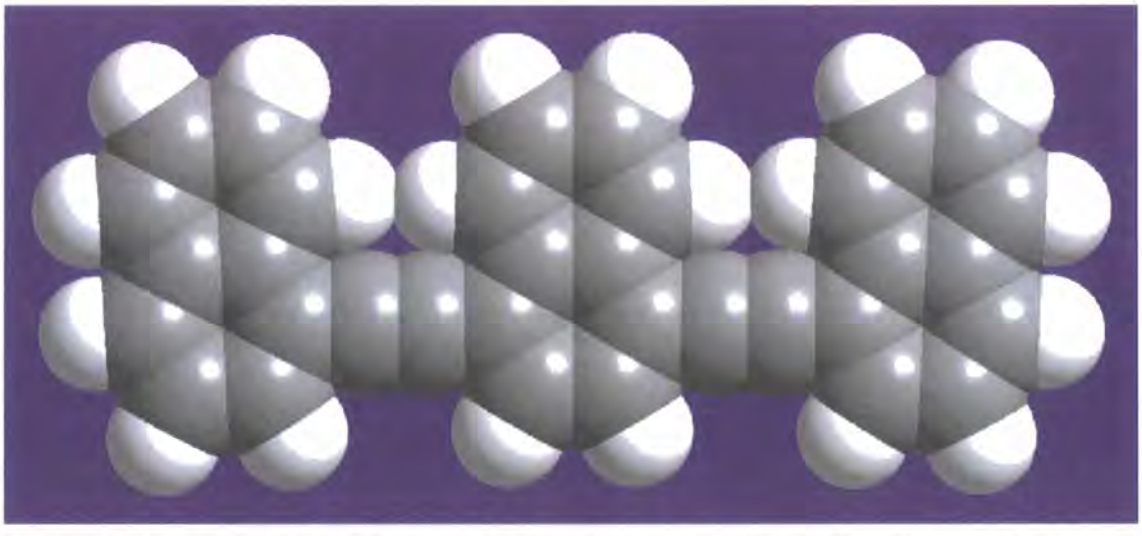

Figure 3.13: Space filling diagram of **84** to show steric interactions between hydrogen atoms adjacent to the acetylenic bond.

The absorption spectra of compounds **60**, **83** and **84** all closely resemble the corresponding fluorescence excitation spectra. This similarity is illustrated in Figure 3.14, using **60** as an example. The near identical spectra show that only the species involved in fluorescence are absorbing in solution, confirming the sample's purity.

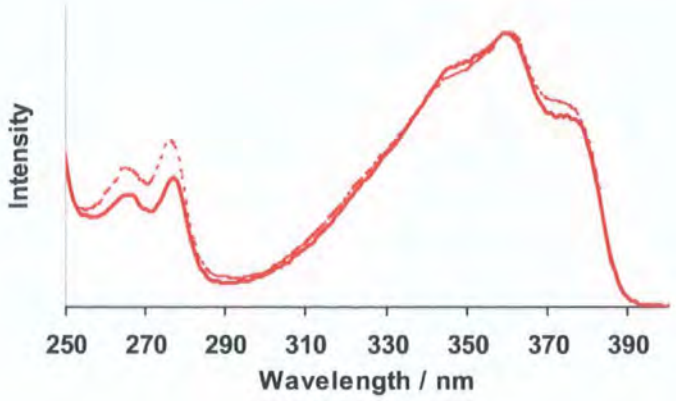

Figure 3.14: Comparison of the absorbance (solid) and fluorescence excitation (dotted) spectra of **60** in EPA.

Extinction coefficients, fluorescence quantum yields, lifetimes and fluorescence rate constants were obtained for each of the three compounds (see Table 3.3). It appears that the rate of fluorescence is dependent on the central ring system, with the rate constants of the two molecules with a central naphthalene (**60** and **84**) being very similar to each other but smaller than that of **83** with its central benzene ring which is very similar to that of BPEB.

Compound	ε / 10^3 $dm^3mol^{-1}cm^{-1}$ (λ / nm)	$\Phi_f \pm 0.05$	τ_f / ns ($\pm$ 0.1)	k_f / ns^{-1}
2	58.0 (320)[9]	0.79[10]	0.68[10]	1.16
60	46.4 (361)	0.73	0.98	0.74
83	26.6 (351)	0.91	0.80	1.14
84	34.7 (381)	0.85	1.17	0.73

Table 3.3: Photophysical data for compounds **60**, **83** and **84** compared to BPEB. Lifetimes obtained by Time Correlated Single Photon Counting (TCSPC). All measurements carried out in cyclohexane solution at 298K. ($k_f = \Phi_f / \tau_f$)

The central ring also appears to have a greater effect on the fluorescence of a system than the overall degree of possible conjugation in a molecule. The number of aromatic 6-membered rings in the compounds investigated increases in the order **60** < **83** < **84** (with 4, 5 and 6 rings respectively). If the molecular orbitals involved in the photophysical processes were located evenly over the entire molecule, it would be expected that the red shift in the fluorescence spectra relative to BPEB would increase in this same order. However, the increase in the red shift relative to **2** shows the following order; **83** < **60** < **84** (shifts of *ca.* 34, 42 and 64 respectively). This suggests

that the molecular orbitals have a higher contribution from the central aryl group as opposed to the external ring systems.

It was therefore of interest to examine the molecular orbitals involved in further detail. To this end, molecular modelling was used to visualise these using CAChe. The structures of **60** and **83** were first optimised using semi-empirical methods (MOPAC, PM5) before their electronic transitions were calculated using ZINDO (INDO-S). Both molecules were found to have the lowest energy transition (to the first excited state) arising from a LUMO ← HOMO transition. **83** was calculated to have a higher energy transition appearing at 331 nm compared to that of **60** which has its simulated transition appearing at 342 nm. The order of these predicted bands matches the observed photophysical results.

The calculated frontier orbitals obtained for **60** and **83** are shown in Figure 3.15. It can be seen from these that the central ring systems have a larger influence on the HOMO and LUMO than the outer rings where the magnitude of contribution from the atomic orbitals is visibly lower. This result matches the hypothesis obtained from the relative positions of the emission obtained from these compounds.

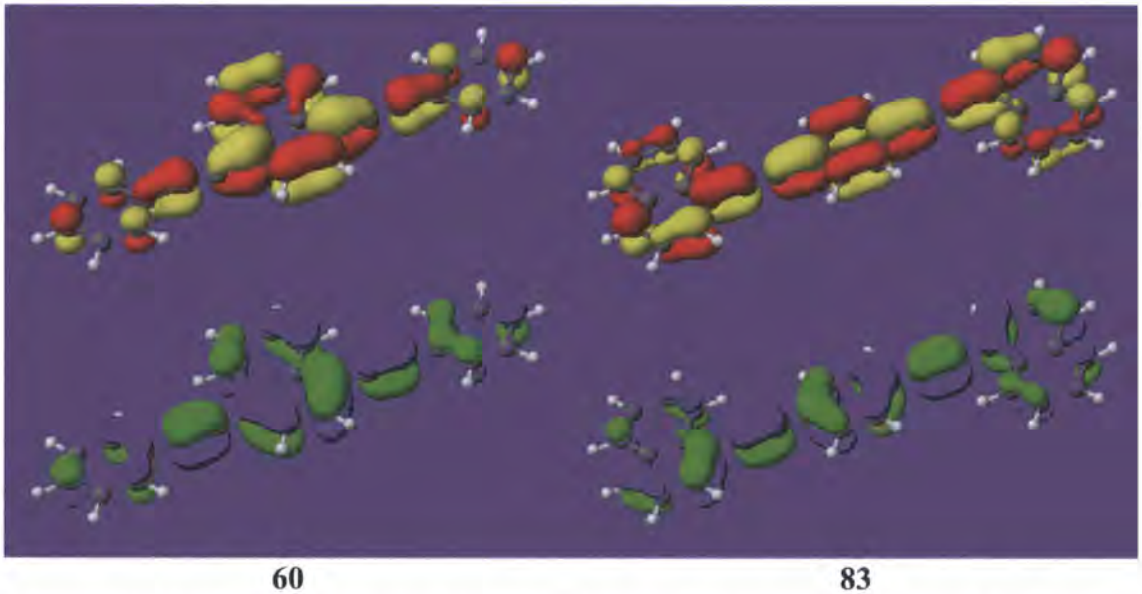

60 **83**

Figure 3.15: HOMOs (blue/green) and LUMOs (red/yellow) for compounds **60** and **83**, calculated using CAChe.

3.2.4 - Conclusions

The studies described above on the naphthalene containing series of BPEB derivatives **60**, **83** and **84** have shown that these compounds behave in a similar way to BPEB. Structurally the compounds display free rotation about the acetylenic groups, with the lowest energy conformations formed when the aromatic ring systems lie in the same plane.

Absorbance and emission of light from these compounds are similar in profile, albeit red shifted in relation to BPEB with the central ring system having the largest contribution to the HOMOs and LUMOs of **60**, **83** and **84**, and hence also to the degree of red shift observed. The behaviour observed at 77 K in an EPA glass for **60**, **83** and **84** was also similar to that of BPEB, with the appearance of vibrational structure in the excitation spectrum, including a strengthening of the signal at the red edge, as well as a sharpening of the observed emission spectrum.

The only deviation from this behaviour was observed for compound **84** at 77 K. Here a peak was observed at the blue edge of the low temperature emission spectrum suggesting the emergence of a separate emitting species in the viscous glass. This extra species was attributed to some molecules present where adjacent naphthalene rings were in a similar orientation. At low temperature, the steric interactions between the hydrogen atoms in the 5 and 8 positions of the naphthalene moieties prevent full planarisation of the molecule before emission occurs.

3.3 - Thiophene Systems

3.3.1 - Introduction

There has been more extensive research into three ring aryleneethynylenes containing thiophene rings, than for the naphthalene systems described above. The series of thiophene containing systems that are of interest is shown in Figure 3.16.

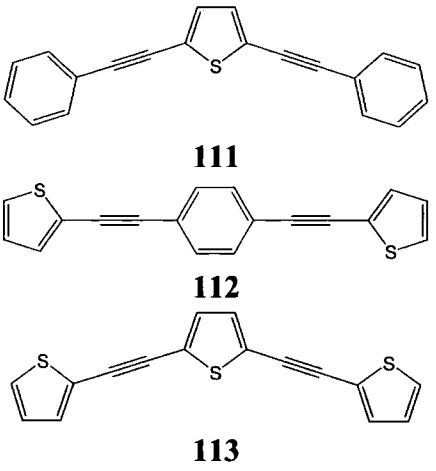

111

112

113

Figure 3.16: Phenyl-thienyl three ring aryleneethynylene series.

111 Was first reported in 1984 by Sanechika *et al.*, where it was obtained *via* a palladium catalysed cross coupling reaction (Scheme 3.4). Phenylacetylene was reacted with ethylmagnesium bromide to form the Grignard, before the addition of 2,5-dibromothiophene plus palladium (II) acetate and triphenylphosphine. After reacting for two hours the product was obtained in 76 % yield after extraction and purification. They noted that **111** gave a bluish purple emission under UV light, however no formal luminescence studies were undertaken.[11]

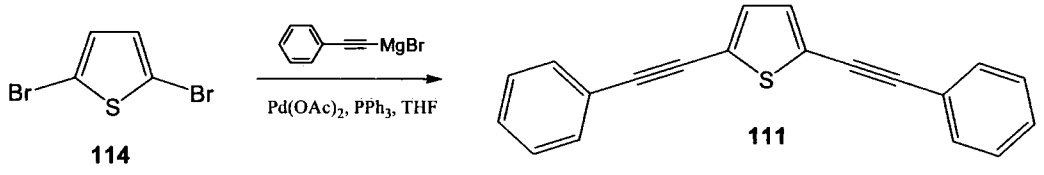

114 **111**

Scheme 3.4: Sanechika *et al.*'s synthesis of **111**.[11]

Freeman *et al.* were next to report the synthesis of **111**, using an approach where a cyclisation reaction was used to form the thiophene ring. A diketone, **115**, was thionated *via* the addition of a Steliou reagent (Scheme 3.5). The reaction using the Steliou reagent involves treating a bis(tri(alkyl/aryl)tin sulphide with boron trichloride in the presence of a carbonyl-containing compound.[12,13] Three different tin sulfides were tested for their reactivity in the reaction, and the yield was found to be essentially independent of which one was chosen.[12]

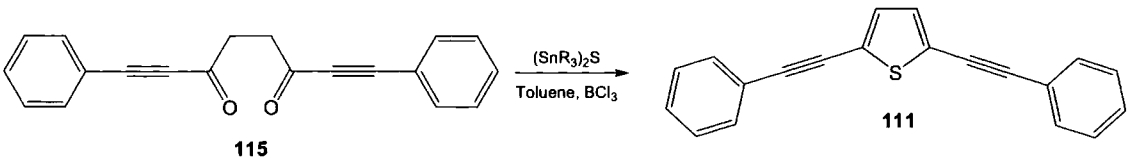

Scheme 3.5: Freeman *et al.*'s synthesis of **111**. R = Bu, C_6H_{12}, Ph. Yields = 84, 89 and 92 % respectively.[12]

The synthetic route to the precursor **115** involved the 7-step process outlined in Scheme 3.6. This route allows the formation of asymmetric aryleneethynylenes, with the addition of different lithium acetylides possible. To this end, Freeman *et al.* also reacted **120** with $LiC{\equiv}CCH_3$ in THF at -78 °C (rising to 0 °C) to form 2-(phenylethynyl)-5-(prop-1-ynyl)thiophene, **123**.

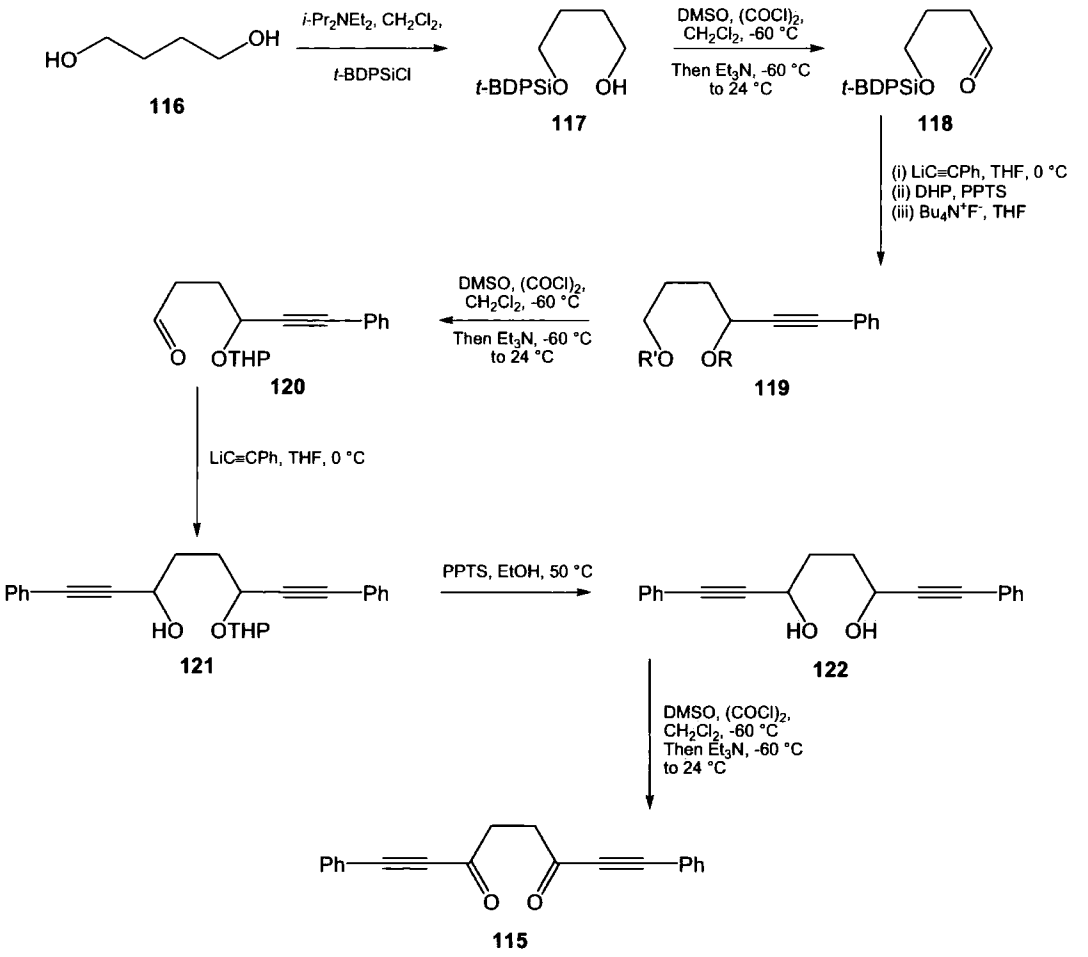

Scheme 3.6: Freeman *et al.*'s synthetic route to diketone used in the synthesis of **111**. (In compound **119** - R, R′ = mixture of H, TBDPS; THP, TBDPS and THP, H).[12]

Tormos *et al.* reported the synthesis of a series of ethynylthiophene oligomers, including the three-thiophene system, **113**, *via* the use of $Pd(PPh_3)_2Cl_2$ catalysed Sonogashira coupling methodology. As can be seen from Table 3.4, **113** was obtained

in greatest yield, with the other chain lengths being obtained less efficiently. The UV-Vis absorption of the oligomer series was examined, observing an increase in the maximum absorption with an increase in molecule (and therefore conjugation) length.[14]

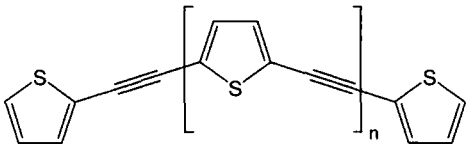

	n	Yield / %	λ_{max} / nm
124	0	33	317
113	1	85	360
125	2	17	377
126	3	26	400

Table 3.4: Overall yields and absorption maxima for ethynylthiophene oligomers synthesised by Tormos *et al.*[14]

This observed increase in the wavelength of the absorption maximum with the number of repeating units in a thienylethynyl chain was also examined by Pearson and Tour who studied this effect over a wider range of chain lengths for compounds of the type **127**. As can be seen from Figure 3.17 they found that by the formation of the octamer (n = 7) the system was almost at saturation, with an increase in size to the 16-mer causing only a small increase in absorption maximum.[15]

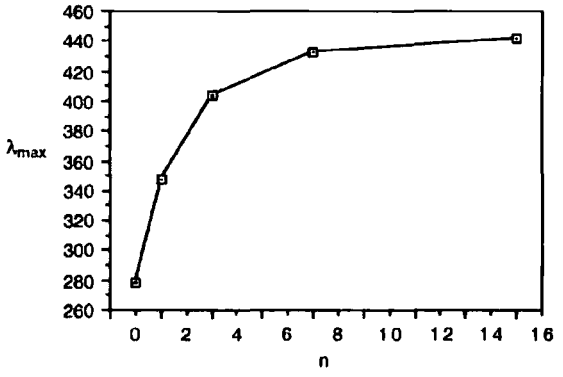

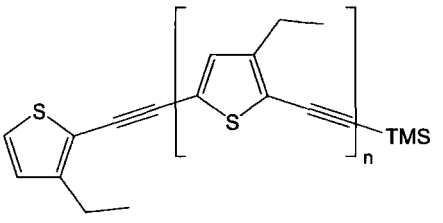

127

Figure 3.17: The effect of the chain length of thienylethynyl systems on their absorbance maxima.[15]

The main objective of Pearson and Tour's research was the synthesis of potential molecular wires complete with thioacetate "alligator clips." Thienylethynyl oligomers were produced that were capped at either one or both ends by *para*-thioacetate substituted phenyl rings, thus having the potential to attach to gold surfaces. The

simplest compound of this type was **133**, a substituted analogue of **111**, the synthetic approach to which is shown in Scheme 3.7.

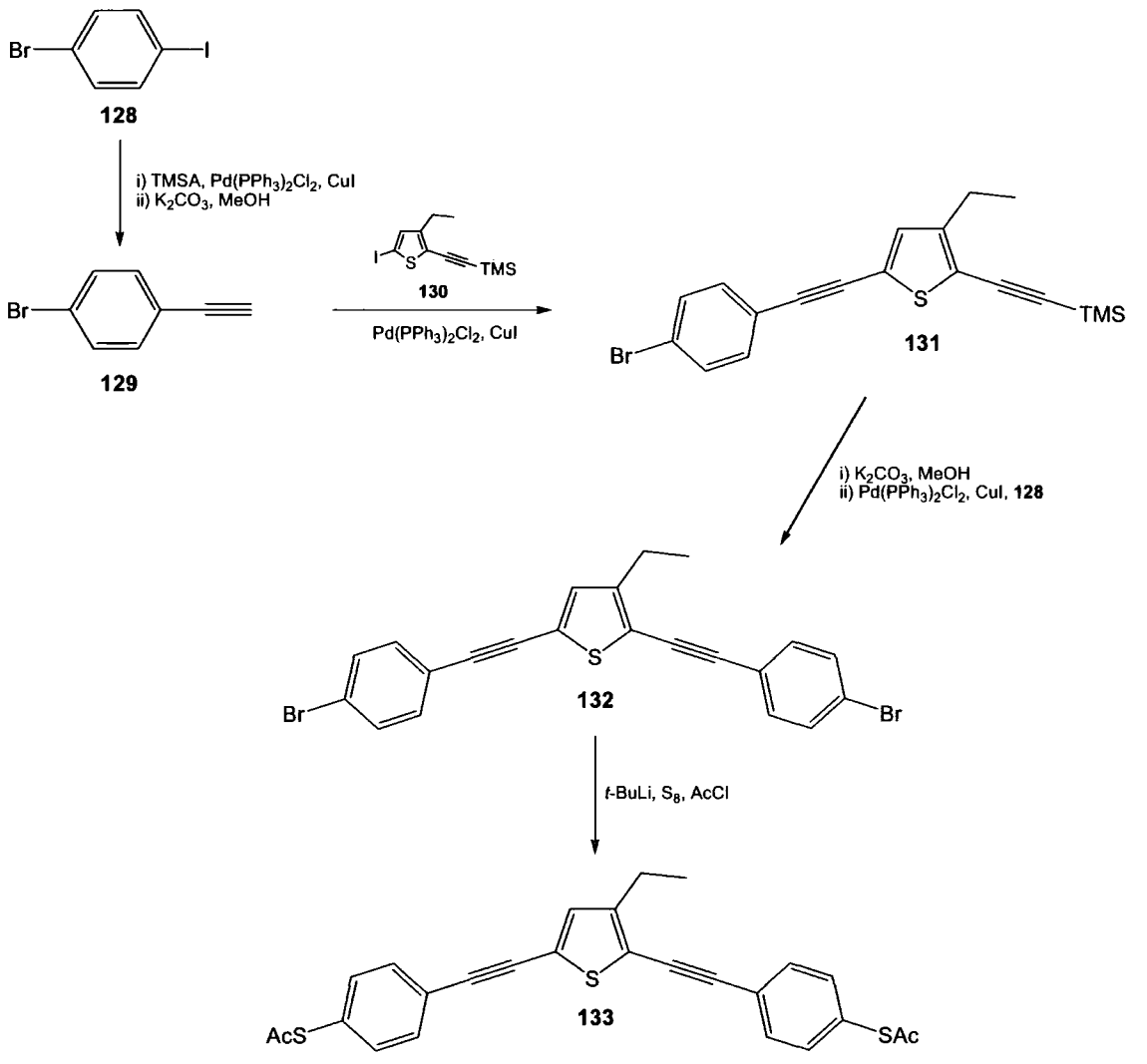

Scheme 3.7: Pearson and Tour's synthesis of **133**, an "alligator clip" substituted derivative of **111**.

In 1997 Zimmer *et al.* described the synthesis of **111** - **113**, as well as carrying out some basic spectroscopic studies. They used a Sonogashira coupling approach, as shown in Scheme 3.8, using a tetrakis(triphenylphosphine)palladium (0) catalyst to obtain the compounds in good yield (**111**, 75 %; **112**, 75 %; **113**, 60 %).[16]

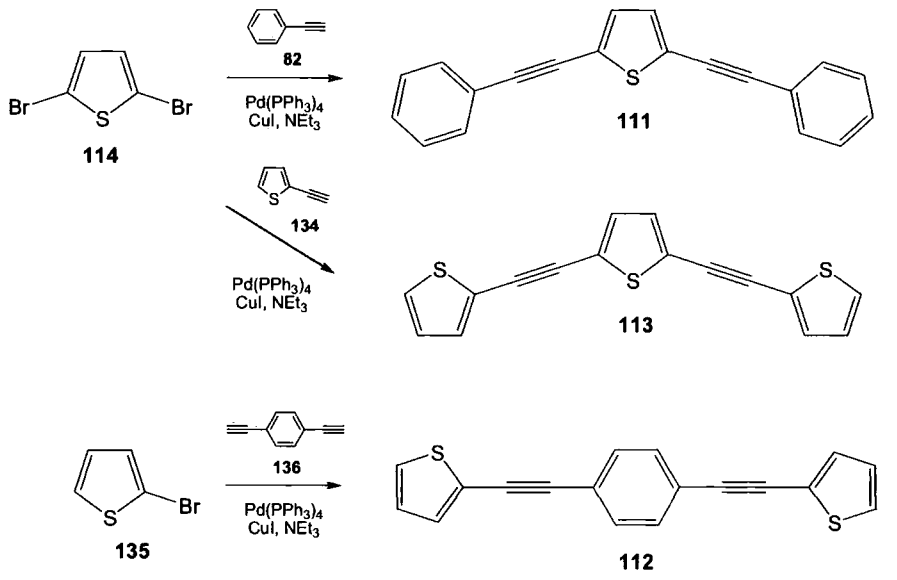

Scheme 3.8: Zimmer *et al.*'s synthesis of compounds **111** - **113**.[16]

Zimmer *et al.* obtained the absorbance spectra for the three compounds above as well as calculating their extinction coefficients, (Table 3.5). The extinction coefficient for **112** (central phenyl ring) was found to be roughly double that of the other two molecules (which have a central thiophene ring).[16]

Compound	Abs λ_{max} / nm	ε / $M^{-1}cm^{-1}$
111	349	33,100
112	340	76,200
113	366	39,300

Table 3.5: Absorbance characteristics for compounds **111** to **113**.[16]

It was also noted that the chromophores of both **111** and **112** contained phenyl and thienyl units, but Zimmer was unable to explain why **112** showed an absorbance maximum at lower wavelength. It was stated that theoretical calculations were being carried out to help gain a better understanding, although nothing has been presented in the literature.[16] This behaviour is likely to be similar to that observed in section 3.2.3 for the naphthalene containing systems, but will be discussed later.

Variable temperature behaviour, as shown in Figure 3.18 of 3-hexyl-2,5-bis((3-hexyl thiophen-2-yl)ethynyl)thiophene, **137**, a derivative of **113**, was examined by Li *et al.* They observed that the shoulder at the red edge of the absorbance (*ca.* 400 nm) became more pronounced as the temperature was lowered. At -198 °C this feature was clearly

resolved into a separate peak in the spectrum, along with a general sharpening of the spectrum, behaviour which is similar to that seen for BPEB as mentioned in section 1.3.3.[17,18]

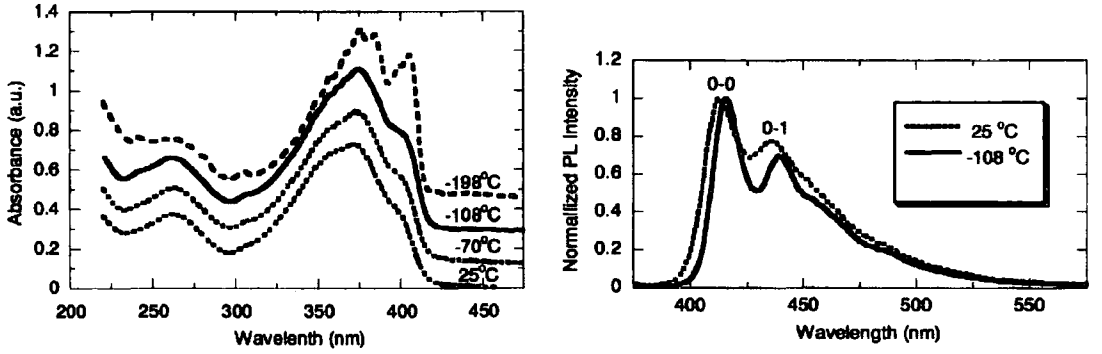

Figure 3.18: Variable temperature absorbance (left, offset for clarity) and emission spectra (right) for **137** obtained in THF (25, -70, -108 °C) and EPA (-198 °C).[18]

The emission spectrum was observed to have a low quantum yield of 0.06 at room temperature.[17] Lowering the temperature to -108°C caused the spectrum to be red shifted by approximately 3 nm in relation to that observed at 25 °C. The two bands in the emission spectrum at *ca.* 416 and 439, which they respectively assigned to the 0-0 and 0-1 transitions, became more pronounced with the lowering of temperature.[18]

Rodríguez *et al.* synthesised and studied the photophysical properties of a series of compounds based on the **111** framework, extending the conjugation with further phenylethynyl units, as shown in Figure 3.19.[19,20]

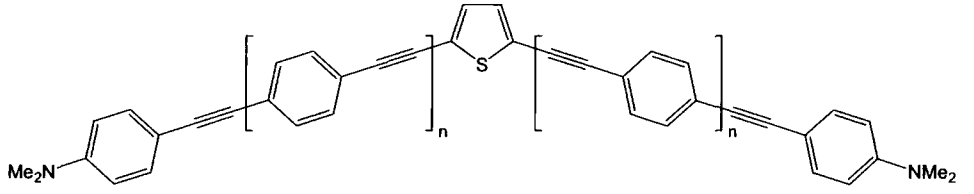

n = 0 (**138a**), 1 (**138b**)

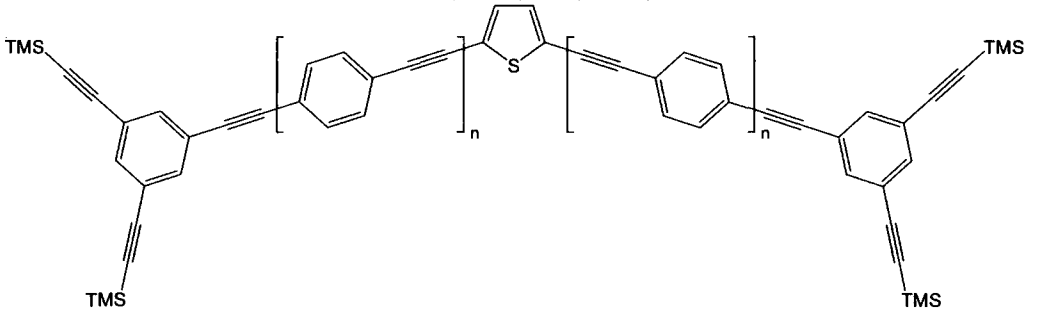

n = 0 (**139a**), 1 (**139b**), 2 (**139c**)

Figure 3.19: Phenyl/thienylethynyl compounds synthesised by Rodríguez *et al.*[19]

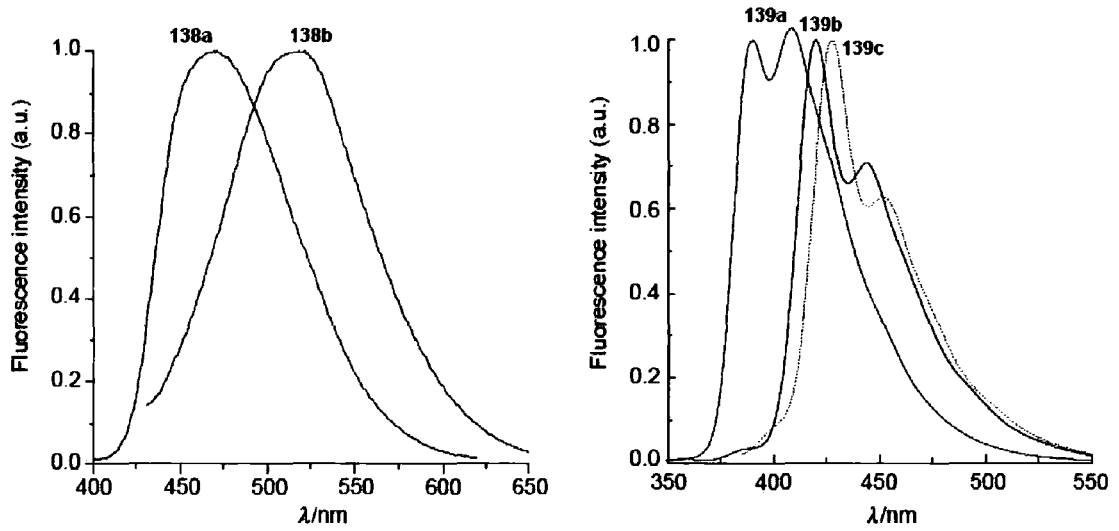

Figure 3.20: Normalised emission spectra for compounds **#138a-b** (left) and **#139a-c** (right) in DCM at room temperature.[20]

	UV-Vis λ_{max} / nm	ε $M^{-1}cm^{-1}$	Fluor. λ_{max} / nm	Φ_f		UV-Vis λ_{max} / nm	ε $M^{-1}cm^{-1}$	Fluor. λ_{max} / nm	Φ_f
138a	385	57,500	456	0.23	**139a**	355	46,900	391, 410	0.20
138b	393	104,320	512	0.30	**139b**	379	78,900	421, 447	0.42
					139c	377	113,000	429, 454	0.54

Table 3.6: Photophysical properties of Rodríguez *et al.*'s phenyl/thienylethynyl compounds.[19]

Increasing in the number of aromatic rings in the oligomeric chain affects the photophysical behaviour of compounds **138a-b** and **139a-c** (see Figure 3.20, Table 3.6). Comparing the uv-visible absorption spectra of **138a** and **138b** it can be seen that there is a red shift of *ca.* 10 nm when the number of rings is increased from 3 to 5, as well as an increase in the extinction coefficient due to the extended conjugation.[19]

Compounds **139a** and **139b** also show similar behaviour, albeit with a larger increase (of *ca.* 25 nm) in absorbance maximum on increasing the number of rings from 3 to 5. A further lengthening of the molecule to 7 rings in **139c** led to a 2 nm blue shift of the absorbance maximum relative to **139b**. The extinction coefficient, however, did still increase with molecule length.[19]

The dimethylamino terminated compounds **138a** and **138b** displayed a single band in their fluorescence emission spectra devoid of any vibrational structure. The more conjugated system **138b**, showed a more red shifted emission relative to that of **138a**. The increase in the number of arene rings in the molecule's backbone also led to an increase in fluorescence quantum yield.[20]

Compounds **139a-c** on the other hand gave emission profiles that did contain some vibronic structure with two peaks seen in the spectral profile. The fluorescence maximum of **139a** occurred at the lower energy of the two peaks, whereas compounds **139b** and **139c** displayed an emission maximum with their respective higher energy bands. Increasing the number of aryl rings in the molecule's backbone from 3 to 5 (**139a** to **139b**) gave a 30 nm red shift in the position of the emission, whereas a further increase to 7 rings (**139c**) only led to a *ca.* 10 nm shift. Again increasing the length of the molecule led to an increase in the quantum yield.[20]

Campbell *et al.* have shown that *n*-alkyl and *n*-alkoxy derivatives of **111** display nematic liquid crystalline behaviour. The observed crystal ↔ nematic and nematic ↔ isotropic transitions are shown in Table 3.7. They found that, in general, the melting and clearing points of these systems decreased with an increase in the length of the alkyl/alkoxy chains. This was attributed to the longer alkyl chains having an increased number of conformations compared to the shorter chains, which have the effect of diluting the attractive van der Waals forces between the aromatic rings. Another observation they made was that the alkoxy derivatives have higher transition temperatures than their corresponding alkyl analogues. This was down to the increase in van der Waals forces from the presence of the oxygen atoms, as well as an increase in the effective size of the rigid molecular core.[21]

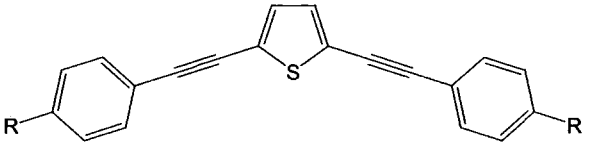

R	Cr ↔ N	N ↔ I	R	Cr ↔ N	N ↔ I
C_3H_7	88	112	OC_3H_7	136	174
C_4H_9	72	81	OC_4H_9	95	168
C_5H_{11}	59	94	OC_5H_{11}	87	139
C_6H_{13}	51	69	OC_6H_{13}	81	137
C_7H_{15}	42	83	OC_7H_{15}	79	126

Table 3.7: Transition temperatures (°C) for *n*-alkyl and *n*-alkoxy derivatives of **111**. (Phases: Cr = crystal, N = nematic, I = isotropic).[21]

3,4-Ethylenedioxythiophene (EDOT, **140**) is a derivative of thiophene that is of interest in the field of conducting polymers. The ether groups at the β,β′ positions on **140** give a strong electron donating effect, as well as preventing the formation of unwanted α-β′

linkages on polymerisation as well as leading to a high reactivity at the free α,α′ positions.[22]

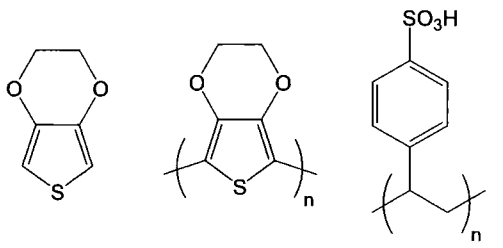

140 **19** **141**

Figure 3.21: Structure of compounds **140**, **19** and **141**.

The polymeric form of EDOT (PEDOT, **19**) displays high conductivity and has good optical transparency in the visible region, as well as a low oxidation potential and moderate bandgap that lead to good stability in the oxidised charged state. Pure **19** is insoluble, though this can be circumvented by the use of a water-soluble polyelectrolyte (poly(styrenesulfonic acid), **141**) as the charge-balancing dopant during polymerisation, leading to a polymeric mixture PEDOT/PSS which displays the same properties as PEDOT. The properties of this material have led to several applications including anti-static coatings and as hole injection layers in OLEDs.[22,23]

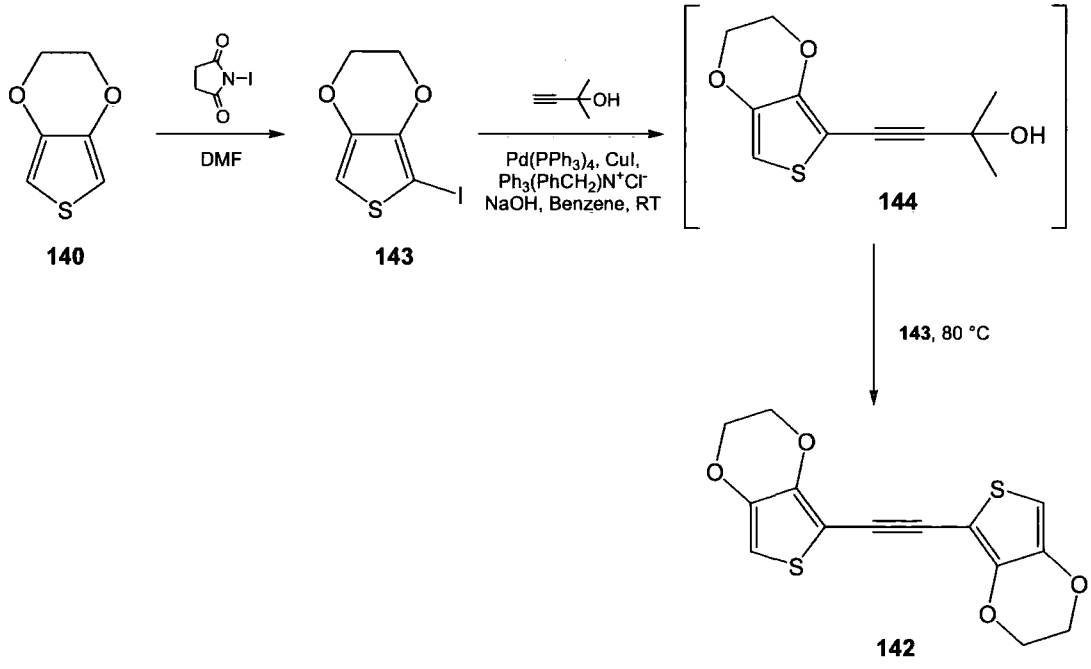

140 **143** **144** **142**

Scheme 3.9: Zotti *et al.*'s synthetic route to the EDOT containing tolan derivative **142**.

There have been few published examples of ethynylated EDOT systems. Zotti *et al.* reported the synthesis of the analogue of tolan, di(3,4-ethylenedioxythiophen-2-yl)acetylene (**142**). They first iodinated **140** with *N*-iodosuccinimide before coupling the resultant product with 2-methyl-3-butyn-2-ol under phase transfer conditions using a synthetic methodology first reported by Carpita *et al* as shown in Scheme 3.9.[24,25]

142 And the analogous di(thiophen-2-yl)acetylene (**124**) both show a single oxidation process when studied by cyclic voltammetry. As seen in Table 3.8, the oxidation peak potential for **142** is lower than that of **124**, mirroring the lower oxidation potential of PEDOT compared to polythiophene. **142** also has an absorbance maximum that is red shifted by 16 nm in relation to that of **124**.

	monomer		polymer	
	E_p / V	λ_{max}	E^0 / V	λ_{max}
142	1.07	312	0.45	400
124	0.75	328	0.25	490

Table 3.8: Electrochemical and absorption data for the monomers (E_p = oxidation peak potential) and polymers (E^0 = redox potential) of **142** and **124**.[24]

Potential cycling over the peak potential of **142** and **124** gives the formation of a polymer *via* anodic coupling, as summarised in Scheme 3.10. The resultant polymer of **142** displays a higher redox potential and absorbance maximum compared to that of **124**.[24]

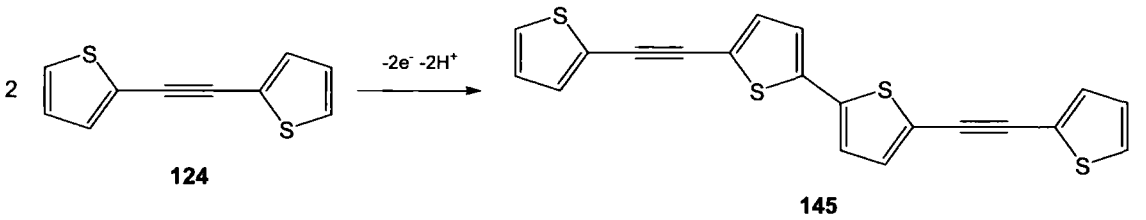

124 **145**

Scheme 3.10: Anodic coupling of the **124** monomer (Adapted from reference 24).

The only other reported ethynyl substituted EDOT derivative was reported by Li *et al.* in the formation of porphyrin-acetylene-thiophene molecular wires like **146**, shown in Figure 3.22. The polymers were produced as well-defined fibres in the form of totally linear strands with a thickness of *ca.* 4 nm and up to 2.5 μm in length. Cyclic

voltammetry on this material showed an oxidation of the zinc-porphyrin moiety around 0.6-0.9 V, with the di-EDOT being oxidised at potentials greater than 1 V.[26]

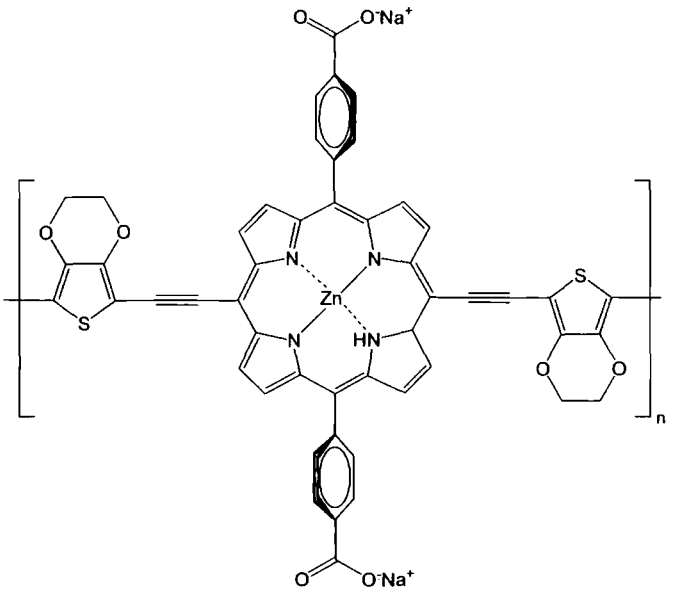

146

Figure 3.22: Molecular wire, **146**, containing EDOT-acetylene moiety synthesised by Li *et al.*[26]

Oligothiophenes have been shown to display an increase in electron delocalisation and electron affinity through the incorporation of a thiophene-1,1-dioxide (**147**) moiety with theoretical calculations showing a decrease in the HOMO-LUMO energy gap.[27,28]

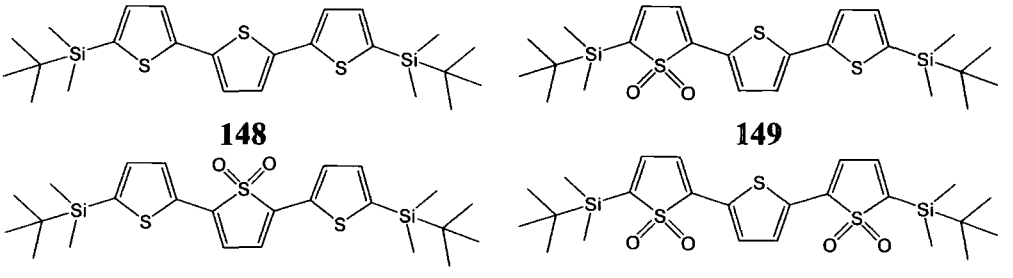

148 **149**

150 **151**

Compound	**148**	**149**	**150**	**151**
UV-Vis λ_{max} /nm	370	460	440	460

Figure 3.23: Structure and absorbance maxima of thiophene trimers incorporating **147** synthesised by Barbarella *et al.*[28]

Barbarella *et al.* have studied a range of oligothiophenes containing this group, examples of which can be seen in Figure 3.23. Measurements of the UV-visible absorbance maxima showed that the incorporation of the **147** moiety caused the

maximum absorbance of the compounds to occur at markedly longer wavelengths than the simple tri-thiophene oligomer.[28]

The only reported aryleneethynylene containing an ethynyl substituted thiophene-1,1-dioxide unit was reported by Yamamoto *et al.* who synthesised the polyaryleneethynylene variant **152** *via* the route shown in Scheme 3.11. The polymer however was insoluble thus no photophysical studies were able to be carried out.[29]

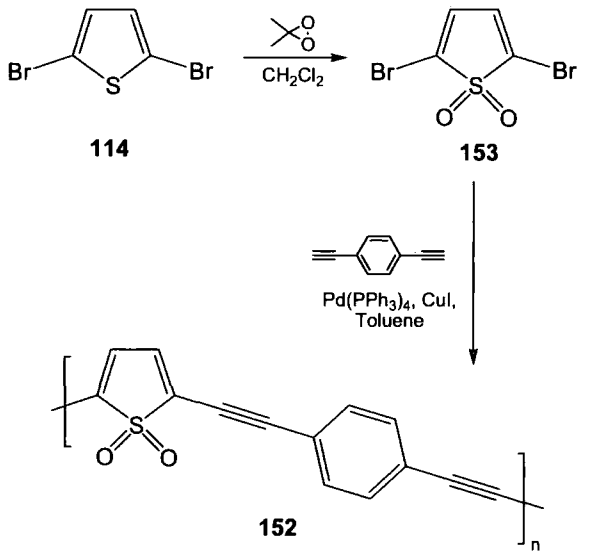

Scheme 3.11: Yamamoto's synthesis of a polyaryleneethynylene containing a thiophene-1,1-dioxide unit.[29]

3.3.2 - Synthesis

2-Ethynylthiophene, **134**, was synthesised using the route shown in Scheme 3.12. Sonogashira methodology was used to couple 2-bromothiophene and TMSA and the subsequent product was deprotected by stirring with potassium carbonate in methanol.

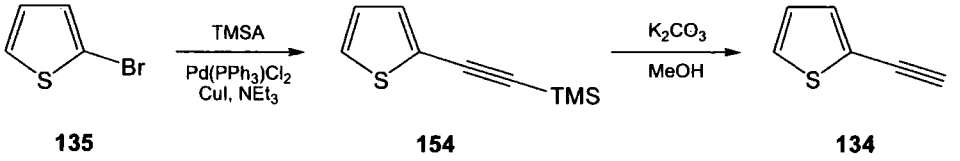

Scheme 3.12: Synthesis of 2-ethynylthiophene.

Compounds **111** - **113** were synthesised using the approach of Zimmer *et al.* described previously in this section, replacing the air sensitive palladium (0) complex with the

easier to process $Pd(PPh_3)_2Cl_2$. After purification the compounds were obtained in 81, 89 and 86 % yields respectively. Crystals of sufficient quality were obtained for all three compounds and so X-ray crystallography was carried out to obtain their solid state structures.

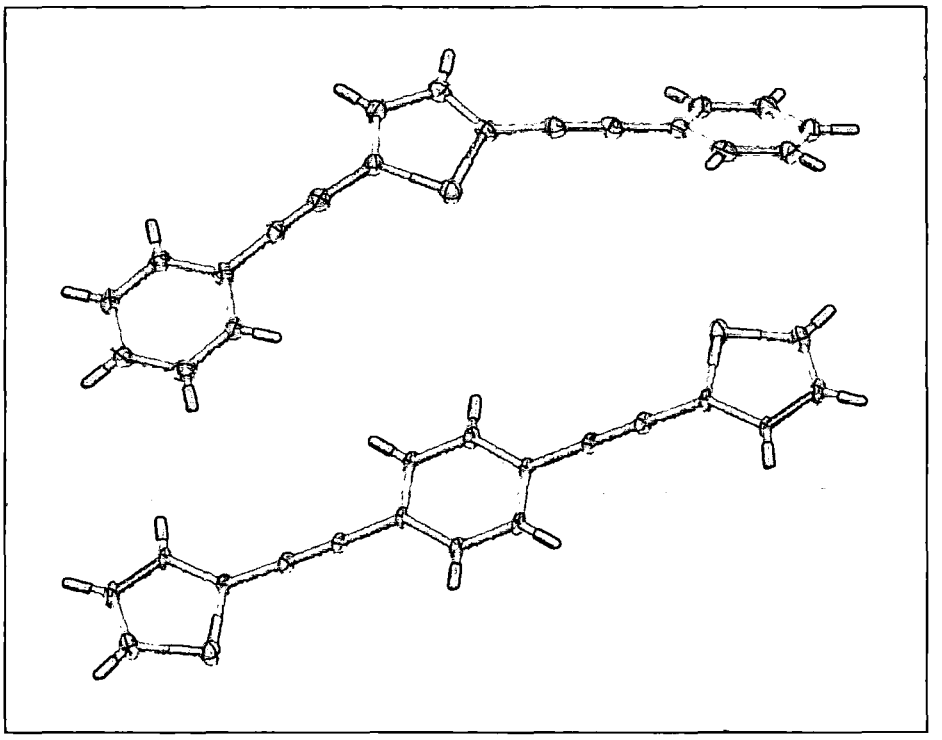

Figure 3.24: Structure of **111** (top) and **112** (bottom) determined by X-ray crystallography.

The structures obtained for **111** and **112** are shown in Figure 3.24. The two phenyl rings in compound **111** are in different orientations relative to the central thiophene group. One phenyl ring is rotated at an angle of *ca.* 30° relative to the thiophene, with the other essentially untwisted. There is also an overall bend evident along the long axis of the molecule. Compound **112** on the other hand has a planar structure similar to that of BPEB. The one thing of note in the structure of **112** is that the thiophene rings are rotated 180° in relation to each other with the sulphur atoms pointing in opposite directions.

Compound **113** has a more complex crystal structure, with two different conformations present in the solid state, Figure 3.25. In the first conformation the outer thiophene rings are rotated by different amounts in relation to the central thiophene ring, with angles of 59° and 149°. In the second conformation one outer ring is rotated by an

angle of 27° relative to the central ring, the other ring displays a degree of disorder and is twisted by either 5° or 175°.

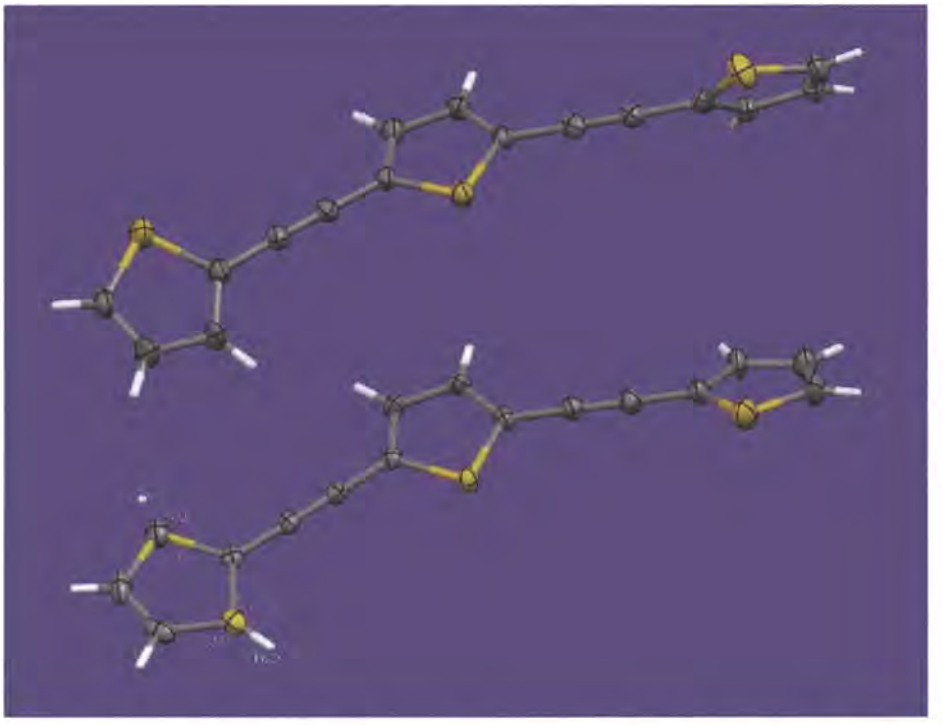

Figure 3.25: Structure of the different conformations of **113** present in the solid state, determined by X-ray crystallography.

A further asymmetrical compound, **155**, was also synthesised, the route to this compound is shown in Scheme 3.13. 1-bromo-4-iodobenzene was reacted with 1 equivalent of phenylacetylene using a Sonogashira coupling. After purification the product, **156**, was reacted on in another coupling reaction, this time with 2-ethynylthiophene to obtain the final product in 63 % overall yield.

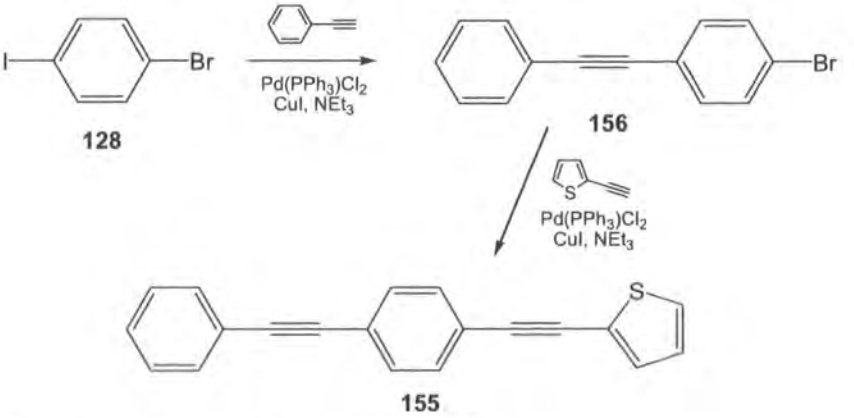

Scheme 3.13: Synthetic approach to compound **155**.

In addition to the series of thiophene-2-ylethynylenes mentioned above, a novel, analogous, series of compounds was synthesised using the EDOT unit. These compounds are shown in Figure 3.26.

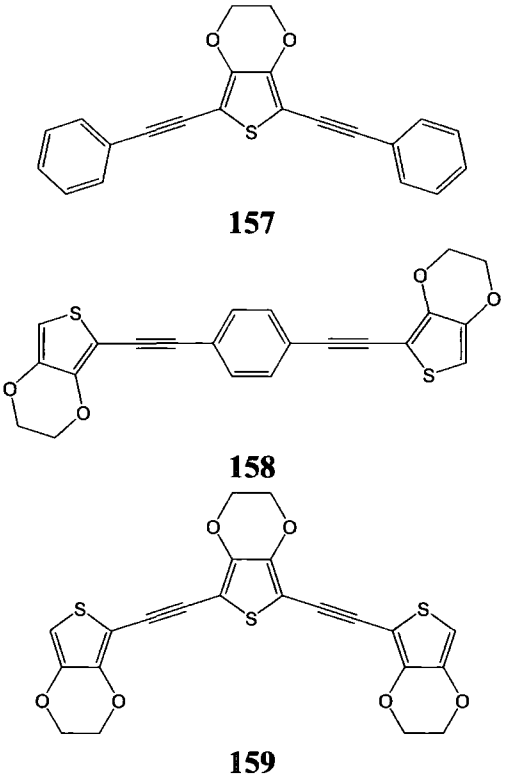

157

158

159

Figure 3.26: Synthesised series of EDOT containing aryleneethynylenes.

Firstly the method of Zotti *et al.*[24] was used to synthesise 3,4-ethylenedioxy-2-iodo thiophene (**143**) and 2,5-diiodo-3,4-ethylenedioxythiophene (**160**) by reacting one and two equivalents respectively of *N*-iodosuccinimide with 3,4-ethylenedioxythiophene using DMF as the solvent.

The rest of the synthesis of compounds **157** - **159** was carried out using standard Sonogashira methodology. Firstly **143** was coupled to TMSA, before a deprotection step gave 3,4-ethylenedioxy-2-ethynylthiophene, **161**, using the same route as shown in Scheme 3.12. Synthesis of the final compounds was then carried out *via* the same approach Zimmer *et al.* used for compounds **111**- **113**, as shown in Scheme 3.8, albeit with a $Pd(PPh_3)_2Cl_2$ catalyst. Crystals were obtained for **157** - **159** however only those of **157** proved sufficient for study by X-ray crystallography (Figure 3.27). This revealed that in the solid state **157** does not adopt a planar conformation with the phenyl rings twisted out of the plane of the thiophene ring by 24° and 81°.

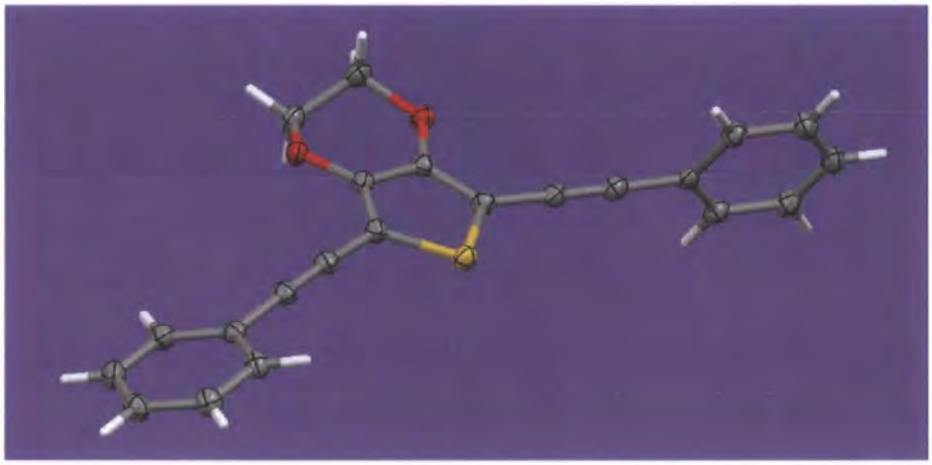

Figure 3.27: Structure of **157** determined by X-ray crystallography.

3.3.3 - Photophysics

Emission-excitation spectra were obtained for compounds **111** - **113** and **155** at room temperature in cyclohexane. The excitation spectra of these compounds are red shifted but similar in profile in relation to BPEB, with the maximum of the broad featureless absorption bands of **111** - **113** corresponding well to those observed by Zimmer *et al.*[16]

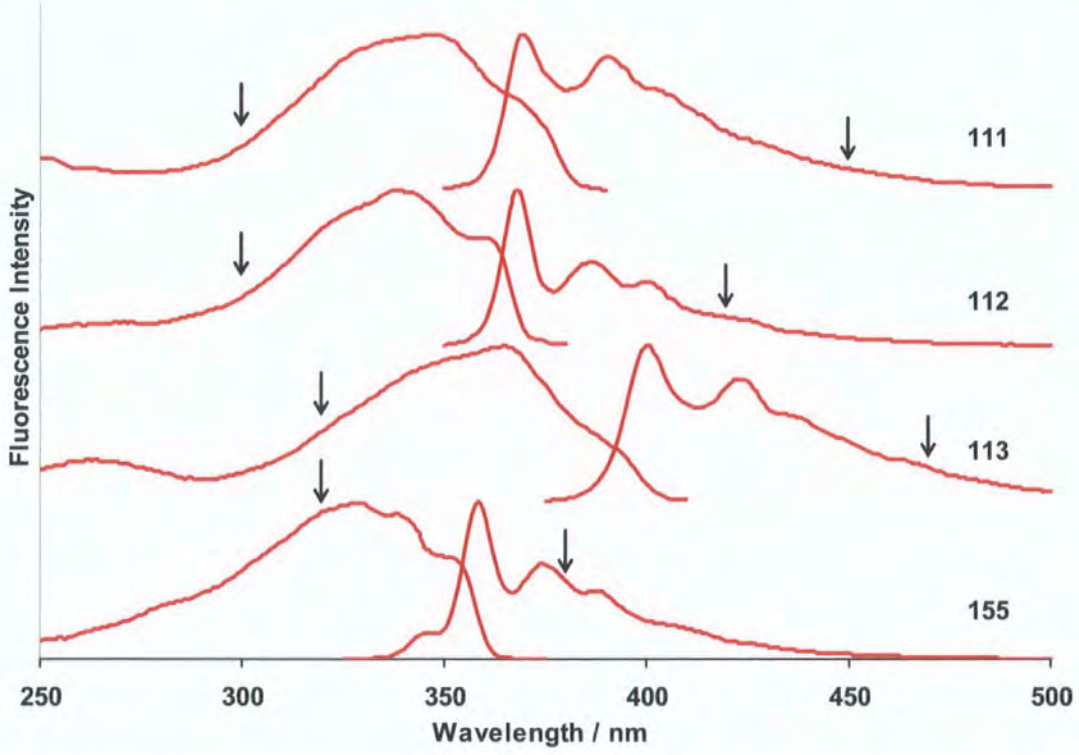

Figure 3.28: Normalised, emission-excitation spectra of **111** (λ_{ex} = 300 nm, λ_{em} = 450 nm), **112** (λ_{ex} = 300 nm, λ_{em} = 420 nm), **113** (λ_{ex} = 325 nm, λ_{em} = 470 nm) in EtOH and **155** (λ_{ex} = 320 nm, λ_{em} = 380 nm) in C_6H_{12} at 298 K (Arrows on spectra denote emission and excitation wavelengths).

	Excitation Features (nm)	Emission Features (nm)
111	348, 370	369, 390
112	338, 360	368, 386, 400
113	365, 392	401, 424
155	328, 338, 353	347, 358, 374, 388

Table 3.9: Summary of features on emission-excitation spectra of **111** - **113** and **155**.

The emission spectra of the compounds show a greater degree of vibronic structure than the excitation spectra, and mirror the behaviour of BPEB (albeit they are relatively red shifted). The profiles of the emission spectra of **112** and **155** are similar to that of BPEB, although with that of **155** showing a slight shoulder on the blue edge of the spectrum at 347 nm. Compounds **111** and **113**, however, show a profile with a relatively more intense second band which is similar in magnitude to the highest energy band.

The compounds with a central phenyl ring show a smaller red shift in relation to BPEB than those with a central thiophene ring. This could be interpreted as the thiophene moiety leading to relatively lower energy transitions than benzene. As such, the relative positions of the spectra of **111** (one thiophene ring, two phenyl, lower energy) and **112** (two thiophene rings, one phenyl, higher energy) may appear anomalous. However, as observed for the naphthalene compounds, it appears that the choice of central ring has a larger effect on the observed photophysical behaviour than that of the external rings.

The emission-excitation spectra of **111** were also recorded in EPA at 298 and 77 K, as shown in Figure 3.29. The spectra recorded at 298 K are very similar to those in cyclohexane, although the position of the spectra are shifted by approx. 4-6 nm, the excitation spectrum being blue shifted and the emission spectrum being red shifted. This suggests the more polar solvent leads to a slightly higher band gap than the non-polar cyclohexane.

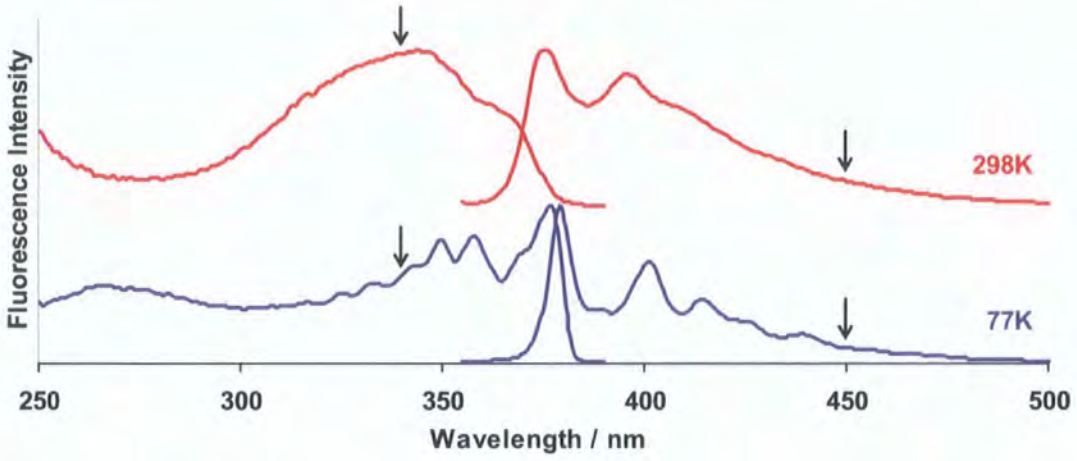

Figure 3.29: Normalised, emission-excitation spectra of **111** in EPA at 298 and 77 K (λ_{ex} = 340 nm, λ_{em} = 450 nm, denoted by arrows on spectra).

	Excitation Features (nm)	Emission Features (nm)
298K	344, 368	376, 396
77K	350, 358, 377	379, 401, 415

Table 3.10: Summary of features on emission-excitation spectra of **111** at 298 and 77 K in EPA.

Upon cooling the system down to 77 K, **111** displays similar behaviour to that observed for BPEB. The excitation spectrum gains vibronic structure and there is a strengthening of the signal at its red edge. The emission spectrum shows a sharpening of the vibronic structure with the excitation spectrum now more like a mirror image of the emission.

The observed effect of the central ring on the behaviour of the thiophene containing systems also shows up in their photophysical parameters. As can be seen from Table 3.11 the photoluminescence quantum yields of **111** and **112** are similar (and approximately ¼ of that observed for **2**, Table 3.3), with that of **112** being slightly higher. These two compounds also show a reduced fluorescence lifetime compared to BPEB, with **111** showing a longer fluorescence decay. Examination of the fluorescence rate constant shows that emission from **111** (phenyl central ring) occurs at approximately the same rate as from **2** but twice as fast as that from **112** (thienyl central ring).

Compound	ε / 10^3 $dm^3mol^{-1}cm^{-1}$ (λ / nm)	$\Phi_f \pm 0.05$	τ_f / ns (± 0.1)	k_f / ns^{-1}
111	41.6 (348)	0.16	0.29	0.55
112	42.1 (342)	0.21	0.19	1.10
113	36.0 (355)	0.06	0.12	0.50
155	36.5 (328)	0.16	0.20	0.80

Table 3.11: Photophysical data for compounds **111** - **113** and **155**. Lifetimes obtained by TCSPC. All measurements carried out in cyclohexane solution at 298K. ($k_f = \Phi_f / \tau_f$)

The other compound with a thienyl central ring, **113**, shows a more reduced quantum yield compared to the other thiophene containing compounds as well as a reduced fluorescence lifetime with a rate constant similar to **111**. The rate of fluorescence from the asymmetric system, **155**, is lower than seen for BPEB and **112**, so it is not solely the central ring that determines the rate of emission, although it does appear that a central phenyl ring leads to faster emission than a central thiophene ring. Caution must be taken with this result however as the errors observed in the values of Φ_f and τ_f lead to a larger error in the calculated k_f.

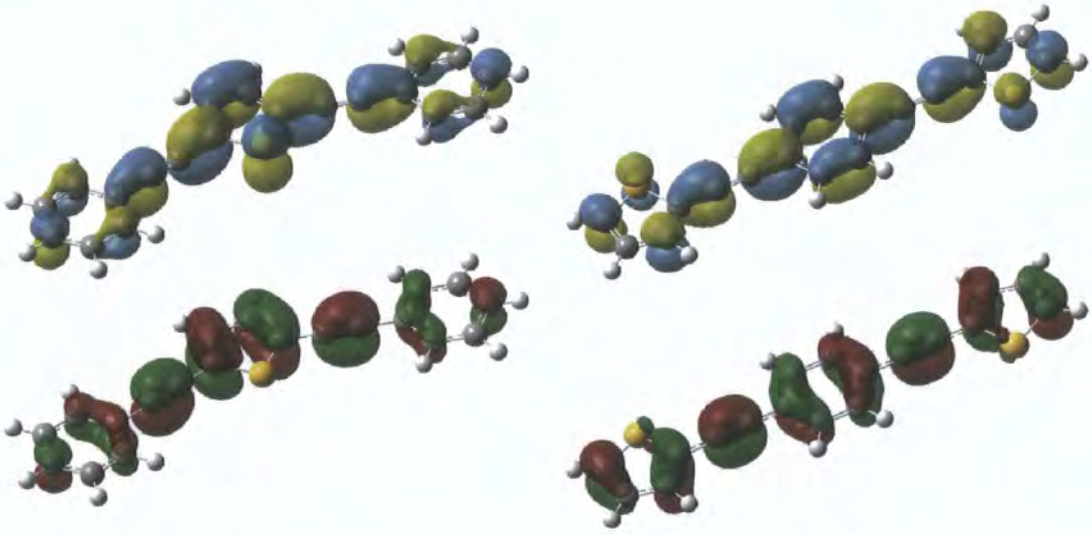

111 **112**

Figure 3.30: Comparison between the HOMO (red/green) and LUMO (blue/yellow) of compounds **111** and **112**. MOs visualised using a TD-DFT calculation with a B3LYP/6-311g(2d,p) level of theory (Gaussian 03W)[30].

Molecular modelling using DFT allows the reasoning for this to be seen. The simulations showed that the first excited state arises from a LUMO ← HOMO transition. Visualisation of these frontier orbitals allows it to be seen that, as found with

the naphthalene compounds described in section 3.2, the molecular orbitals have less presence on the external rings compared to the central ring.

The simulation does not totally agree with the observed behaviour. The calculated LUMO ← HOMO transitions arise at energies equivalent to 316 nm for **111** and 382 nm for **112**, whereas in the observed results it is **112** that has spectra at lower wavelength. The reason for this disparity is unclear.

The photophysics of the EDOT series of compounds was also studied, the spectra obtained are shown in Figure 3.31.

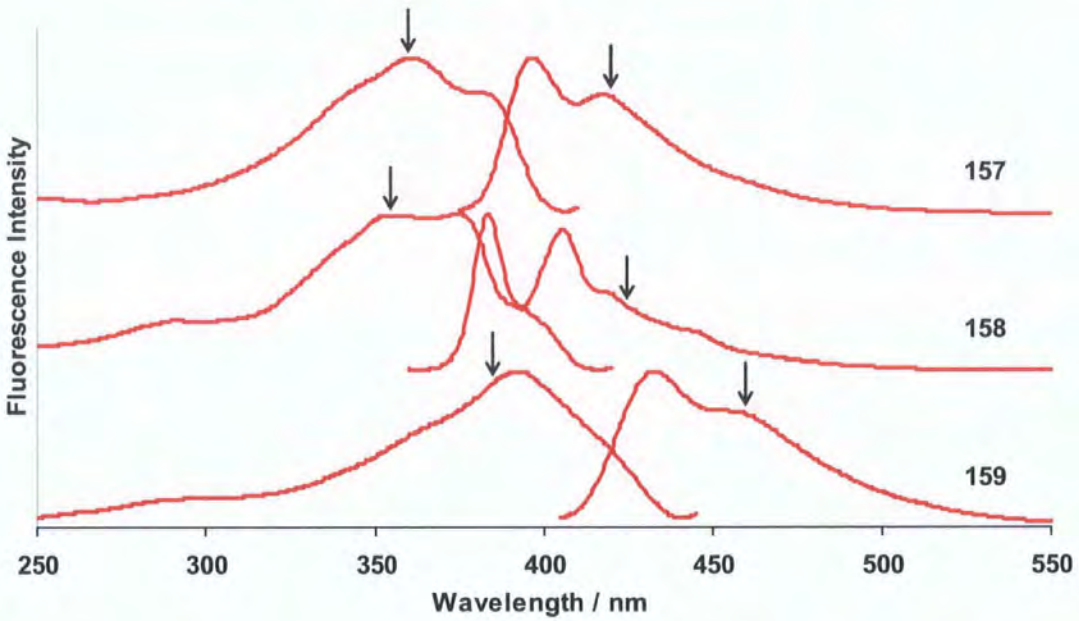

Figure 3.31: Normalised, emission-excitation spectra of **157** (λ_{ex} = 360 nm, λ_{em} = 420 nm), **158** (λ_{ex} = 340 nm, λ_{em} = 425 nm) and **159** (λ_{ex} = 385 nm, λ_{em} = 460 nm) in DCM at 298 K (Arrows on spectra denote emission and excitation wavelengths).

	Excitation Features (nm)	Emission Features (nm)
157	361, 382	397, 418
158	358, 374, 396	384, 406, 419
159	393	433, 459

Table 3.12: Summary of features on emission-excitation spectra of **157** - **159**.

The excitation spectra of **157** is similar in profile to that of **2**. Compounds **158** and **159** still show broad bands with little vibronic structure, but the profiles have a different

shape. The wavelength at which maximum absorbance is observed increases with the number of EDOT moieties present in the molecule, with **157**<**158**<**159** (361, 374 and 393 nm respectively).

The emission spectra of the three compounds have superficially similar profiles to that of **2**, with two main emission maxima observed. **157** and **158** show two distinct bands, those of **157** separated by 1265 cm^{-1} and those of **158** separated by 1411 cm^{-1}. The bands in **158** are sharper, leading to better distinction between the peaks than for those of **157**. The second band in **159** is less easy to distinguish, occurring more as a shoulder on the side of the main emission band.

Compound	ε / 10^3 $dm^3mol^{-1}cm^{-1}$ (λ / nm)	$\Phi_f \pm 0.05$	τ_f / ns ($\pm$ 0.1)	k_f / ns^{-1}
157	49.2 (361)	0.10	0.26	0.38
158	39.7 (374)	0.17	0.21	0.81
159	43.2 (393)	0.014	-	-

Table 3.13: Photophysical data for compounds **157** - **159**. Lifetimes obtained by TCSPC. All measurements carried out in DCM solution at 298K. ($k_f = \Phi_f / \tau_f$)

Examining the photophysical parameters for these compounds, as shown in Table 3.13, it can be seen that they have differing photoluminescence quantum yields. **159** has a very low quantum yield of around 1 % which did not allow its lifetime to be measured reliably *via* the TCSPC technique. Compounds **157** and **158** have quantum yields of around 10 and 17 % respectively, which are small compared to compounds such as BPEB and BPEA and unsurprisingly are similar to those observed for compounds **#111** to **#113** (Table 3.11). **157** and **158** have similar fluorescence lifetimes, with **158** showing a greater rate of emission due to its increased quantum yield. Again these lifetimes are more like those of **111** - **113** than those of **2**.

DTF calculations show that, as seen for **111** earlier, the first excited state of **157** occurs from a LUMO ← HOMO transition arising at 401 nm. This is at a lower energy than that of **111**, indicative of the lowered bandgap found in these systems due to the presence of the β,β′ ether groups. Indeed, visualisation of the orbitals involved in the first excited state (Figure 3.32) shows the incorporation of the ether oxygen atoms into electronic structure of both the HOMO and LUMO.

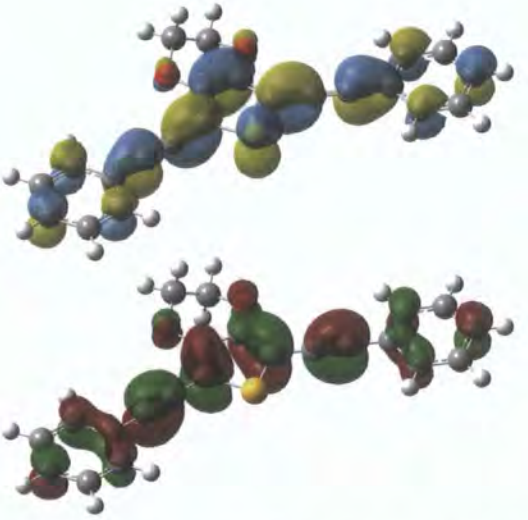

Figure 3.32: Comparison between the HOMO (red/green) and LUMO (blue/yellow) of compound **157**. MOs visualised using a TD-DFT calculation with a B3LYP/6-311g(2d,p) level of theory (Gaussian 03W)[30]

No synthesis was carried out of systems based on the thiophene-1,1-dioxide unit, however theoretical analysis was carried out on 2,5-bis(phenylethynyl)thiophene-1,1-dioxide, **162**.

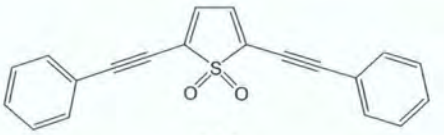

162

These calculations revealed that incorporation of the **147** unit changes the electronic behaviour of the molecule when compared to **111**. There is a reduced bandgap with the first excited state occurring from a lower energy transition at 478 nm. This first excited state does not occur solely from a LUMO ← HOMO transition, there is also a second (LUMO+1) ← (HOMO-2) transition present, albeit with a lower contribution.

Visualisation of the orbitals involved, as shown in Figure 3.33, shows that the HOMO and LUMO of **162** are similar to those of **111**, with the HOMO located on the hydrocarbon section of the molecule, not on the SO_2 unit with the LUMO spread over the whole molecule (with a small contribution from the oxygen atoms).

The HOMO-2 and LUMO+1 are located on the centre of the molecule, with only a small contribution from the external phenyl rings in the former. These orbitals show a larger contribution from the oxygen atoms than the HOMO and LUMO. It would be of

interest to see how this behaviour affects the photophysical spectra obtained, however this must be left to future work in this area.

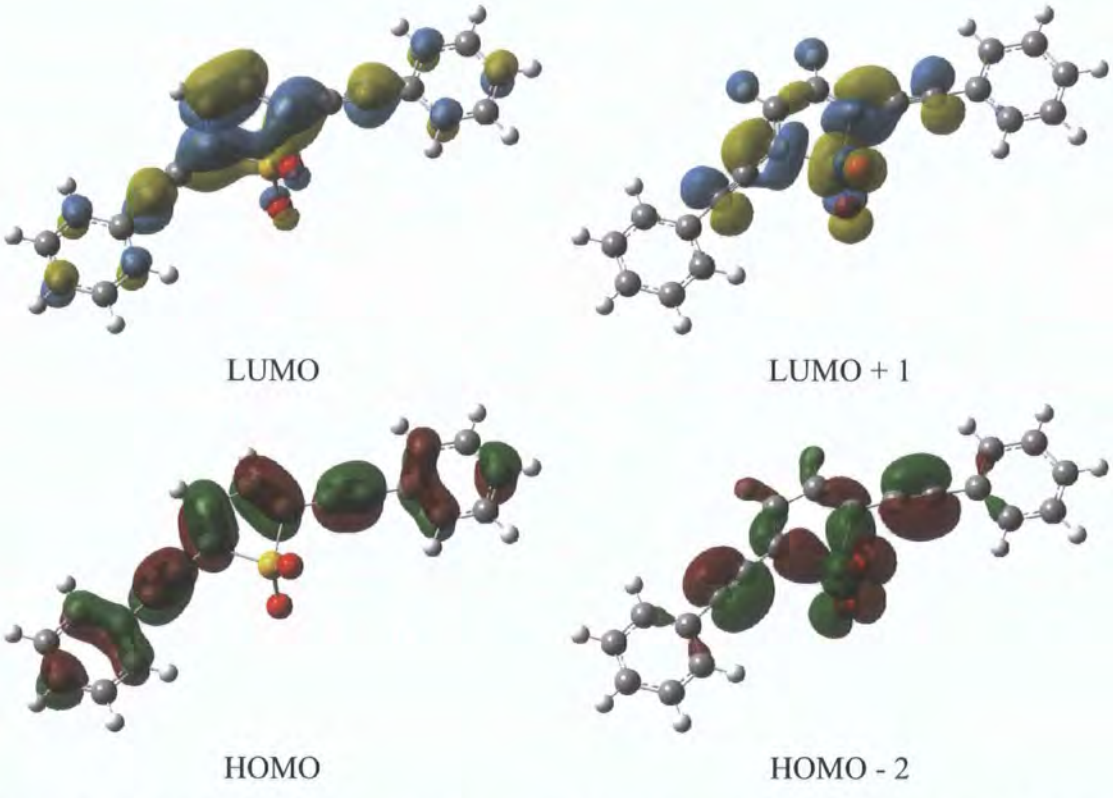

Figure 3.33: Molecular orbitals of involved in the transition to the first excited state of **162**. MOs visualised using a TD-DFT calculation with a B3LYP/6-311g(2d,p) level of theory (Gaussian 03W).[30]

3.3.4 - Conclusions

The emission and excitation spectra of the thiophene containing series of compounds **111** - **113** and **155** are similar to those of BPEB. In solution at room temperature the excitation spectra of these compounds are broad with little vibronic structure, whereas the emission spectra having a greater amount of vibronic structure. The low temperature spectra of **111** show the emergence of vibronic structure in the excitation spectrum as well as a sharpening of the structure observed for the emission spectrum. The low temperature spectra of the other compounds were not obtained, however it is expected that these would show similar behaviour.

As seen for the series of compounds containing naphthalene (Section 3.2), the choice of central ring has the largest effect on the observed photophysical behaviour. Theoretical

studies of the molecular orbitals involved in the fluorescence process (the HOMO and LUMO) supported this finding. These orbitals are located over the entire molecule, however the largest contribution to the HOMO and LUMO is from the centre of the molecule with the outer rings giving a lesser contribution.

These compounds do however have lower quantum yields than BPEB, with a maximum value of 0.21 observed for **112**, and the lowest value seen for **113** (0.06). The rate of fluorescence of compounds **111** - **113** is roughly of the same order of magnitude as that of BPEB, which, combined with the low quantum yields, leads to shorter fluorescence lifetimes.

The inclusion of the EDOT moiety in place of the thiophene ring (compounds **157** - **159**) gave behaviour similar to that just described. The inclusion of the ether groups at the 3 and 4 positions of the thiophene ring leads to lower energy transitions (and hence red shifted spectra) being observed for compounds **157** - **159** compared to **111** - **113** and **155**. These EDOT compounds have low fluorescence quantum yields and lifetimes, with the broad structureless excitation spectra and emission spectra that show a degree of vibronic structure. The structure in the emission spectra is however generally less distinct than observed for the thiophene series.

Theoretical studies gave similar results to those previously described in this chapter. The visualised HOMO and LUMO of **157** show that, as expected from the previous results, the main contribution to these orbitals comes from the central ring system.

Compound **162** was not synthesised, but was studied *via* molecular modelling. Again it was found that the central ring plays a larger role in the photophysical processes than the two outer rings, though it was found that as well as the LUMO ← HOMO transition there is also a contribution from the LUMO+1 and HOMO-2 orbitals. It was predicted that this compound should have lower energy transitions (red shifted spectra) compared to the thiophene compounds. However this will need an analogous series of compounds to be synthesised before this can be checked against experimental results.

3.4 - References

1. P. J. Hanhela and D. B. Paul, *Aust. J. Chem.*, 1981, ***34***, 1687-1700.
2. D. P. Lydon, L. Porres, A. Beeby, T. B. Marder and P. J. Low, *New J. Chem.*, 2005, ***29***, 972-976.
3. P. J. Hanhela and D. B. Paul, *Aust. J. Chem.*, 1984, ***37***, 553-559.
4. J. G. Rodríguez and J. L. Tejedor, *Tetrahedron Lett.*, 2003, ***44***, 2691-2693.
5. J. G. Rodríguez and J. L. Tejedor, *Tetrahedron*, 2005, ***61***, 3033-3043.
6. J. G. Rodríguez and J. L. Tejedor, *Eur. J. Org. Chem.*, 2005, 360-367.
7. Y. Liu, A. H. Flood, P. A. Bonvallett, S. A. Vignon, B. H. Northrop, H. R. Tseng, J. O. Jeppesen, T. J. Huang, B. Brough, M. Baller, S. Magonov, S. D. Solares, W. A. Goddard, C. M. Ho and J. F. Stoddart, *J. Am. Chem. Soc.*, 2005, ***127***, 9745-9759.
8. O. Cakmak, I. Demirtas and H. T. Balaydin, *Tetrahedron*, 2002, ***58***, 5603-5609.
9. A. Beeby, K. Findlay, P. J. Low and T. B. Marder, *J. Am. Chem. Soc.*, 2002, ***124***, 8280-8284.
10. U. W. Grummt, E. Birckner, E. Klemm, D. A. M. Egbe and B. Heise, *J. Phys. Org. Chem.*, 2000, ***13***, 112-126.
11. K. Sanechika, T. Yamamoto and A. Yamamoto, *Bull. Chem. Soc. Jpn.*, 1984, ***57***, 752-755.
12. F. Freeman, D. S. H. L. Kim and E. Rodriguez, *J. Org. Chem.*, 1992, ***57***, 1722-1727.
13. K. Steliou and M. Mrani, *J. Am. Chem. Soc.*, 1982, ***104***, 3104-3106.
14. G. V. Tormos, P. N. Nugara, M. V. Lakshmikantham and M. P. Cava, *Synth. Met.*, 1993, ***53***, 271-281.
15. D. L. Pearson and J. M. Tour, *J. Org. Chem.*, 1997, ***62***, 1376-1387.
16. H. Zimmer, K. Sudsuansri, H. B. Mark and B. Ziegler, *Phosphorus Sulfur Silicon Relat. Elem.*, 1997, ***122***, 269-286.
17. J. Li and Y. Pang, *Macromolecules*, 1997, ***30***, 7487-7492.
18. J. Li, L. Liao and Y. Pang, *Tetrahedron Lett.*, 2002, ***43***, 391-394.
19. J. G. Rodríguez, A. Lafuente, L. Rubio and J. Esquivias, *Tetrahedron Lett.*, 2004, ***45***, 7061-7064.
20. J. G. Rodríguez, J. Esquivias, A. Lafuente and L. Rubio, *Tetrahedron*, 2006, ***62***, 3112-3122.
21. N. L. Campbell, W. L. Duffy, G. I. Thomas, J. H. Wild, S. M. Kelly, K. Bartle, M. O'Neill, V. Minter and R. P. Tuffin, *J. Mater. Chem.*, 2002, ***12***, 2706-2721.
22. J. Roncali, P. Blanchard and P. Frère, *J. Mater. Chem.*, 2005, ***15***, 1589-1610.
23. B. L. Groenendaal, F. Jonas, D. Freitag, H. Pielartzik and J. R. Reynolds, *Adv. Mater.*, 2000, ***12***, 481-494.
24. G. Zotti, G. Schiavon, S. Zecchin and A. Berlin, *Synth. Met.*, 1998, ***97***, 245-254.
25. A. Carpita, A. Lessi and R. Rossi, *Synthesis*, 1984, 571-572.
26. G. T. Li, T. Y. Wang, A. Schulz, S. Bhosale, M. Lauer, P. Espindola, J. Heinze and J. H. Fuhrhop, *Chem. Commun.*, 2004, 552-553.
27. G. Barbarella, O. Pudova, C. Arbizzani, M. Mastragostino and A. Bongini, *J. Org. Chem.*, 1998, ***63***, 1742-1745.
28. G. Barbarella, L. Favaretto, G. Sotgiu, M. Zambianchi, L. Antolini, O. Pudova and A. Bongini, *J. Org. Chem.*, 1998, ***63***, 5497-5506.
29. T. Yamamoto, I. Nurulla, H. Hayashi and H. Koinuma, *Synth. Met.*, 1999, ***107***, 137-141.
30. Gaussian 03, Revision C.02, M. J. Frisch, G. W. Trucks, H. B. Schlegel, G. E. Scuseria, M. A. Robb, J. R. Cheeseman, J. A. M. Jr., T. Vreven, K. N. Kudin, J.

C. Burant, J. M. Millam, S. S. Iyengar, J. Tomasi, V. Barone, B. Mennucci, M. Cossi, G. Scalmani, N. Rega, G. A. Petersson, H. Nakatsuji, M. Hada, M. Ehara, K. Toyota, R. Fukuda, J. Hasegawa, M. Ishida, T. Nakajima, Y. Honda, O. Kitao, H. Nakai, M. Klene, X. Li, J. E. Knox, H. P. Hratchian, J. B. Cross, C. Adamo, J. Jaramillo, R. Gomperts, R. E. Stratmann, O. Yazyev, A. J. Austin, R. Cammi, C. Pomelli, J. W. Ochterski, P. Y. Ayala, K. Morokuma, G. A. Voth, P. Salvador, J. J. Dannenberg, V. G. Zakrzewski, S. Dapprich, A. D. Daniels, M. C. Strain, O. Farkas, D. K. Malick, A. D. Rabuck, K. Raghavachari, J. B. Foresman, J. V. Ortiz, Q. Cui, A. G. Baboul, S. Clifford, J. Cioslowski, B. B. Stefanov, G. Liu, A. Liashenko, P. Piskorz, I. Komaromi, R. L. Martin, D. J. Fox, T. Keith, M. A. Al-Laham, C. Y. Peng, A. Nanayakkara, M. Challacombe, P. M. W. Gill, B. Johnson, W. Chen, M. W. Wong, C. Gonzalez and J. A. Pople, Gaussian, Inc., Wallingford CT, 2004,

CHAPTER 4

CONFORMATIONAL RESTRICTION OF ARYLENEETHYNYLENES *VIA* THE ADDITION OF STERIC BULK

4.1 - Introduction

In aryleneethynylenes, the low barrier to rotation round the carbon-carbon triple bond and the physical distance between the rings has presented a significant challenge to engineering control of their conformation. Various research groups have concentrated on trying to surmount these problems by the use of intramolecular tethers between the aromatic rings, examples of which can be seen in Figure 4.1.

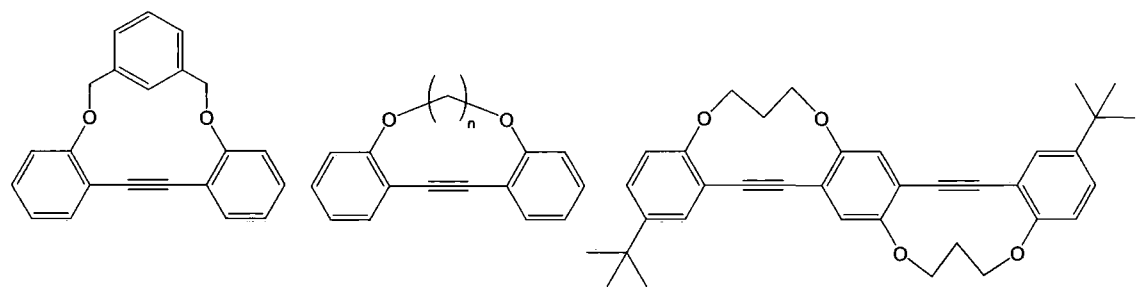

163 164 165

Figure 4.1: Examples of the use of tethers in literature to restrict rotation.

This approach has its disadvantages. Firstly, the work has mostly been concerned with systems based on the two ring system, tolan, **1**, with work being carried out by the groups of Bunz and Crisp.[1-3] As described in Section 1.3.2.2, however, these systems are not a good model for the longer chain oligomers due to the anomalous photophysical behaviour of tolan. The electronic structure of tolan means that the S_1 and S_2 levels are very close in energy and it is the S_2 level which dominates the excitation and emission processes.[4] A more suitable choice of model system therefore needs to have three or more rings in the aryleneethynylene chain. The only work to date on these more extended systems has been carried out by Crisp and Bubner, where they synthesised compound **165** as well as a four ring system.[5]

There are two different synthetic approaches towards forming these tethered aryleneethynylene systems. The first involves the formation of a tether, followed by the closure of the macrocycle by forming the ethynyl bond. In the second, substituted tolan is first synthesised, followed by the closure of the macrocyclic ring by introducing the tether.

Bunz *et al.* utilised the first approach, *via* an alkyne metathesis reaction using a preactivated molybdenum catalyst. Their synthetic approach involved an optimised version of the reaction first reported by Mortreux and Blanchard,[1,6] involving initially heating a catalytic mixture of $Mo(CO)_6$ and 4-chlorophenol in *ortho*-dichlorobenzene along with an excess of 3-hexyne at 130 °C in a sealed tube for an hour. After purging the reaction vessel for an hour with nitrogen the precursor compound was then added and the reaction mixture was stirred for another 24 hours at 130 °C. A summary of this reaction can be seen in Scheme 4.1.[1]

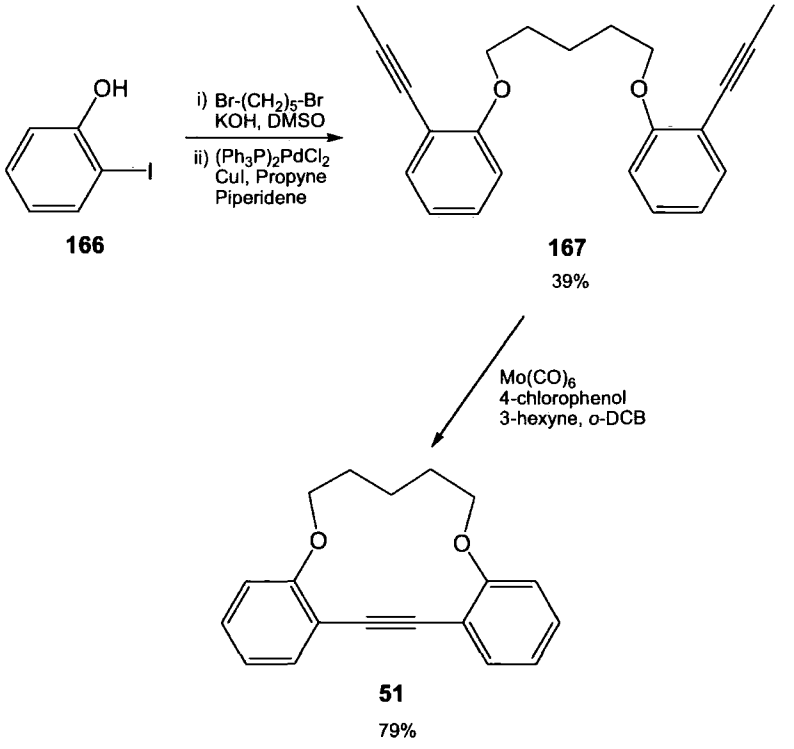

Scheme 4.1: Bunz *et al.*'s synthetic route into tethered tolan systems.[1]

As well as compound **51**, Bunz *et al.* also synthesised macrocycles with tethers incorporating 3 and 12 methylene units, however for these compounds the cyclisation step only gave 5% and 8% yields respectively, which indicates a correlation between the chain length and the overall yield.[1] This is, of course, to be expected for an intramolecular reaction. Small rings are less favoured due to an increase in strain in the molecule giving a less stable transition state in their formation. Large rings are also unfavourable as there is a reduced likelihood of a conformation being formed where the ends of the molecular chain can meet in a ring-closing reaction.[7] The effect of these tethers on the rotation around the acetylene bond in the tolan was not discussed.

Besides utilising the alkoxy chains Bunz *et al.* also attempted to engineer more twist by adding a degree of rigidity into the tether with the use of a benzene ring as in compound **163** (Table 4.1).[2] They carried out ab initio calculations (RHF, 6-31G** basis set) with the benzene ring connected to the cycle in *ortho* (**168**), *meta* (**163**) and *para* (**169**) positions. These calculations suggested that once synthesised, the compounds should be significantly twisted (see α values in Table 4.1). The calculation results for **163** and **169** gave a single observed minimum, however **168** showed two (0 ° and ca. 60 °) minima, with the twisted form slightly more stable. Other calculations were carried out using different theoretical approaches. Calculations at an AM1 level agreed with this result, whereas a B3LYP approach gave a different result, finding the planar form to be more stable. The barrier between the two possible conformers was calculated to be between 17 and 29 kJ mol^{-1} dependent on the level of theory used.[2]

Compound	**170**	**168**	**171**	**163**	**169***
Structure	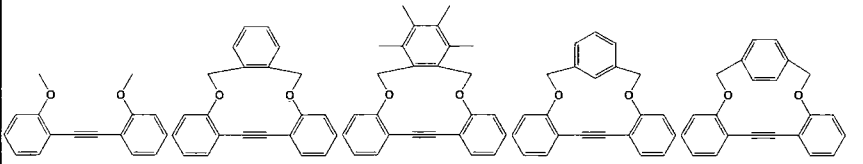				
Total Yield (%)	-	10.1	5.0	7.9	-
α_{theory} (°)	-	0 & 58.82	-	39.12	88.02
$\alpha_{crystal}$ (°)	-	26.6	29.9	-	-
UV λ_{max} (nm)	330	313	315	309	-
ε at λ_{max}	-	20,000	21,700	17,300	-
Fluor. Max (nm)	348	352	350	350	-
Φ	0.45	0.12	0.10	0.69	-

Table 4.1: Theoretical and practical data for compounds **163** and **168** - **171**. Spectroscopic data obtained in chloroform solution.[2] *__169__ was unable to be synthesised and so only theoretical studies were carried out on it. α is the twist angle about the acetylene bond.

Synthetically Bunz *et al.* were able to utilise the same approach as shown in Scheme 4.1 to obtain **163** and **168**, albeit substituting 1,2- and 1,3-bis(bromomethyl)benzene respectively for the dibromopentane. The para derivative, **169**, could not be ring closed,

despite trying a variety of reaction conditions. They were able to obtain single crystals of **168** as well as a similar compound **171** (which had four methyl substituents on the bridging benzene ring) and X-ray crystallography revealed that there was indeed a twist in these two compounds, although in the ortho isomer, **168**, the observed twist angle was lower than predicted by theory, see Table 4.1. These two compounds were the only compounds for which Bunz *et al.* reported the degree of twist out of the plane around the acetylene bond.

Photophysical studies of Bunz's tethered compounds show a pronounced 15-20 nm blue shift in the absorbance maximum compared to the non-restricted analogue, **170**, however, their fluorescence spectra are all very similar, resulting in an increased S_1-S_0 optical gap (see Figure 4.2). Also the two compounds that were shown to be twisted in the solid state (**168** and **171**) have a significantly reduced fluorescence quantum yield. Both of these results demonstrate that an increased torsional angle has a direct effect on both the electronic energy levels and optical properties of these types of systems.[2]

It is unfortunate however that Bunz *et al.* were not able to obtain a crystal structure of **163**, as this showed an increase in quantum yield compared to **170**. However this suggests that **163** favours a more planar conformation, with perhaps the restriction on rotation having a positive effect on the compounds ability to fluoresce.

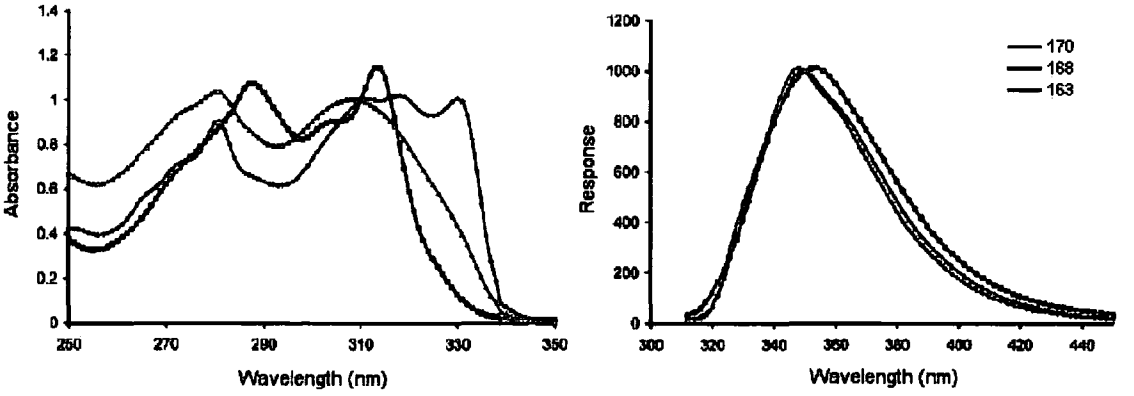

Figure 4.2: Absorption (left) and normalised fluorescence (right) spectra in chloroform of compounds **163**, **168**, **170**.[2]

Crisp & Bubner initially attempted the preparation of tethered systems *via* ring closure at the alkyne using various conditions. They were able to prepare compound **172**, but this approach, shown in Scheme 4.2, provided only a very low yield of the desired

product (7-10 %), and they hence sought an alternative method that would be more generally applicable and give an improved yield.[3]

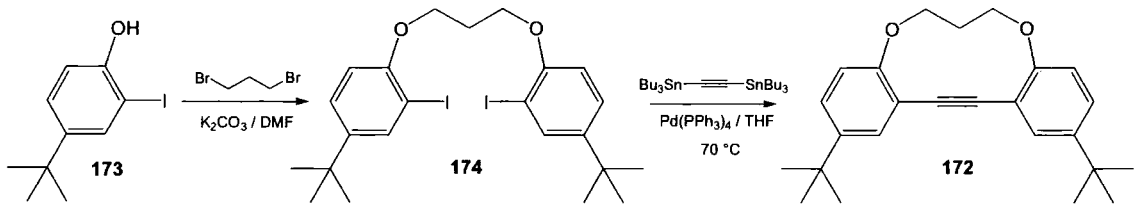

Scheme 4.2: Crisp's palladium catalysed approach to forming a sterically constrained species.[3]

The approach Crisp & Bubner used involved the use of a Mitsunobu reaction[8] to close the macrocyclic ring at one of the alkyl-aryl ether positions. This approach involved the initial formation of the non-restricted tolan which was then cyclised by reacting with DEAD and PPh_3. A summary of this approach can be seen in Scheme 4.3.[3]

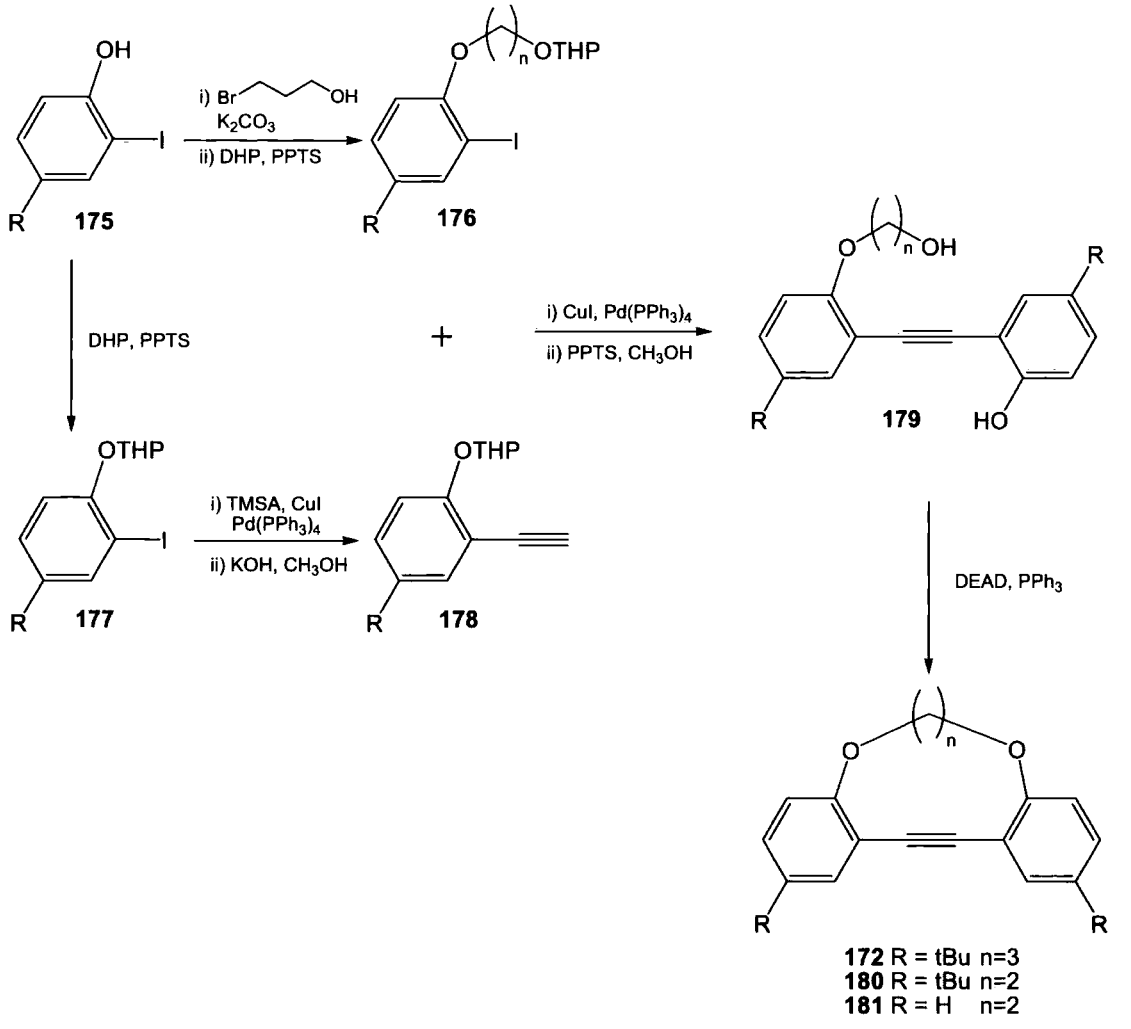

Scheme 4.3: Use of the Mitsunobu reaction to form rotationally restricted tolans.[3]

This approach also meant Crisp & Bubner were not restricted to forming the two ring species. They were also able to use the same ring closing methodology to form the three ring species **165** as well as the analogous four ring species. They also attempted to make the five ring species, but reported that the limited solubility of the material prevented this.[5] Crystals suitable for X-ray crystallography were only to be produced for **165** which showed a torsional angle between the rings of 26°.

When investigating their photophysical properties, Crisp found that the behaviour of these compounds is affected by the restriction of rotation around the acetylene bond. The tethering of the rings causes the compounds to display a sharpening of the absorbance spectra, with a combined increase in extinction coefficient compared to corresponding non tethered compounds along with a small shift in the λ_{max}.[3,5]

Tethered tolan systems have been used by McFarland and Finney to use the effect of conformational restriction on fluorescence in a chemosensor for metal ions. It was initially noted that compounds **182** and **183** displayed similar absorbance spectra but the emission spectra were found to differ, with a four-fold increase in the emission intensity of **183** compared to **182**.

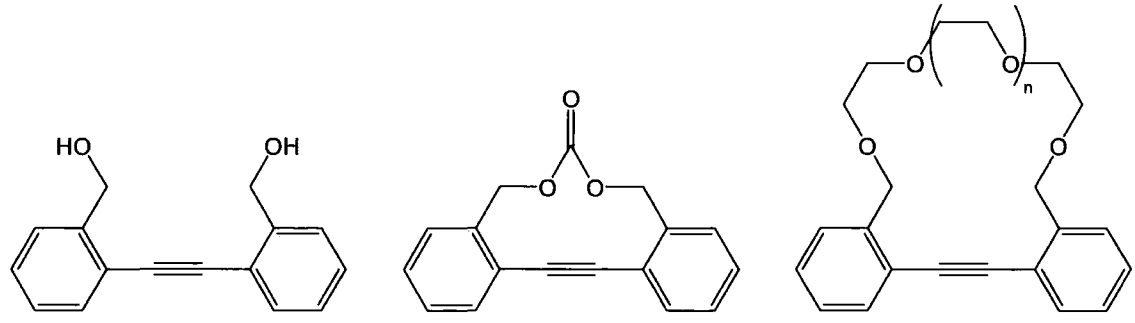

182 **183** **184a**, n = 1 **184b**, n = 2 **184c**, n = 3

Figure 4.3: Tolan systems studied by McFarland and Finney.[4]

Compound	Φ_f	τ_f / ps	k_f / s^{-1}
1	0.004	10	3.9×10^8
182	0.009	20	4.6×10^8
183	0.036	87	4.0×10^8

Table 4.2: Photophysical data for **1**, **182** and **183**.[4]

McFarland and Finney also studied the photophysical parameters of these two compounds, next to **1** as a reference. They found that **182** has a slightly enhanced fluorescence compared to tolan, however **183** shows a significant difference. Compound **183** displayed an approximately four-fold increase in the quantum yield and fluorescence lifetime compared to **182**, with the rate constant of fluorescence staying relatively similar. The restriction of rotation in **183** was not affecting the fluorescence process, but it was reducing the amount of the excited state energy that was lost through non-radiative processes.[4]

Compounds **184a-c** were designed to take this phenomenon into account. The coordination of a metal ion into the crown ether bridge between the phenyl rings was found to restrict the rotation about the C≡C bond. For example, the addition of an excess of lithium ions to a solution of **184a** in acetonitrile, shown in Figure 4.4, gave an enhancement to the fluorescence by a factor of approximately 5.[4]

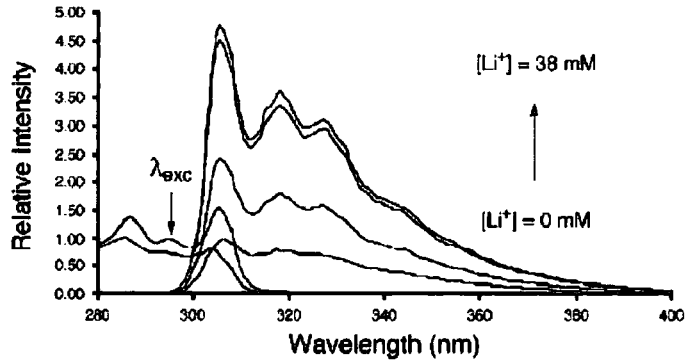

Figure 4.4: Titration of **184a** with $LiClO_4$ in CH_3CN.[4]

It was found that **184a** showed the best selectivity, with a strong preference for Li^+ and Ca^{2+} ions, with **184b** and **184c** being less selective. Also the addition of trifluoroacetic acid had no effect on the emission or excitation spectra which allowed McFarland and Finney to rule out the possibility of there being any electron or charge-transfer processes contributing to this response. The enhancement of fluorescence was occurring solely due to the compounds being restricted into a planar structure by the bound metal ion.[4]

The approaches of Bunz and Crisp have a disadvantage as the tethers all include an oxygen atom attached to aromatic rings. This has an angle dependent conjugation to the π-system from its lone pairs of electrons which affects the electronic structure of the

compounds. This effect is shown in Figure 4.5, which shows a comparison between the HOMO and LUMO of bis(2-hydroxyphenyl)acetylene, **185**, and bis(2-methylphenyl) acetylene, **186**, calculated using CAChe 6.1.10 with a PM5 wavefunction. Here it can be clearly seen that both frontier orbitals are located in part on the oxygen atom of **185**, whereas in **186** there is no contribution from the methyl substituent to either orbital.

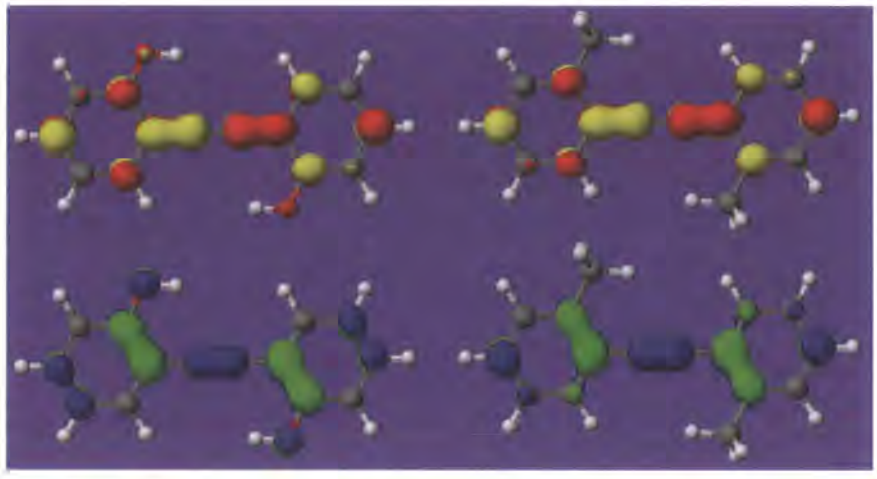

185 **186**

Figure 4.5: HOMO (blue/green) and LUMO (red/yellow) for **185** and **186** calculated in CAChe using a PM5 wavefunction to demonstrate the effect of an oxygen atom attached to an phenyl ring on the electronic structure of aryleneethynylenes.

It is therefore of interest to be able to restrict rotation about the acetylenic bond *via* a different approach. It was decided that the use of sterically demanding, sigma bonded hydrocarbon groups should have a smaller effect on the compounds' electronic structure and should provide a better way of controlling conformation in aryleneethynylenes. Previous work synthesised the decamethyl derivative of BPEB, **187**.[9]

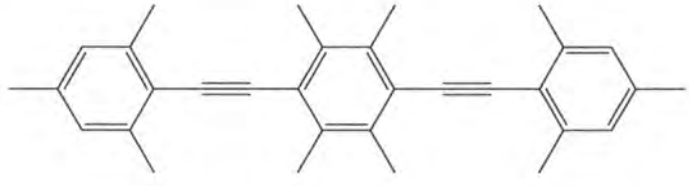

187

Further investigation of this compound, however, shows that the addition of methyl groups does not provide enough steric interaction to affect intramolecular rotation. As can be seen from the 3D space filling model shown in Figure 4.6, the van der Waals'

radii of the hydrogen atoms on the methyl groups ortho to the double bond do not overlap. There is simply too large a distance between the two methyl groups to provide any hindrance to rotation. Indeed, the photoluminescence behaviour of **187** is virtually identical to that of BPEB, albeit with a slight red shift due to the electron donating nature of the methyl groups. This shift is also predicted by TD-DFT calculations using a B3LYP/6-311g(2d,p) level of theory (Gaussian O3W)[10], which predict that the theoretical lowest energy transition ($S_1 \leftrightarrow S_0$) is found at 359 nm for BPEB and at 382 nm for **187**.

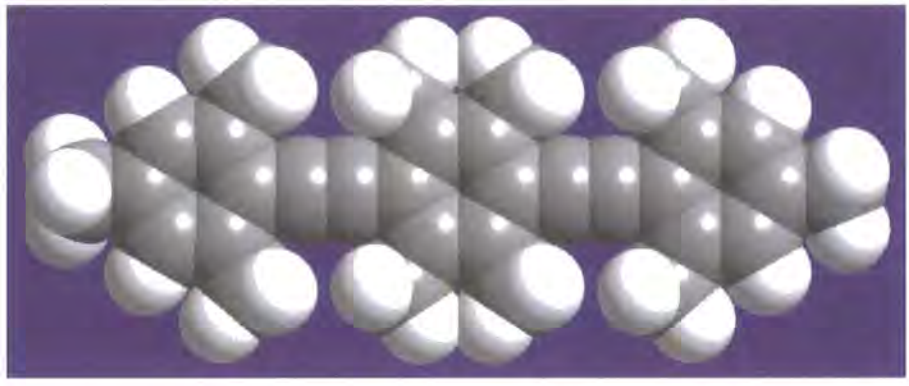

Figure 4.6: Space filling model of compound **187**. Structure optimised using a DFT calculation with a B3LYP/6-311g(2d,p) level of theory (Gaussian 03W)[10].

The rest of this chapter will detail the synthesis and subsequent photophysical analysis of novel derivatives of BPEB which seek to induce conformational control by using steric bulk to engineer twist into aryleneethynylene systems.

4.2 - Synthesis

The incorporation of methyl substituents ortho to the ethynyl unit in **187** does not provide sufficient steric interaction, hence an approach was needed to utilise more sterically demanding side groups. The first compounds proposed for synthesis were the previously unreported 1,4-bis(2-*tert*-butylphenylethynyl)benzene, **188**, and 1,4-bis(2-*tert*-butylphenylethynyl)durene, **189**. These compounds use the more bulky *tert*-butyl side groups which molecular models indicate will lead to an increased steric interaction. Scheme 4.4 shows a retrosynthetic analysis of compound **189**.

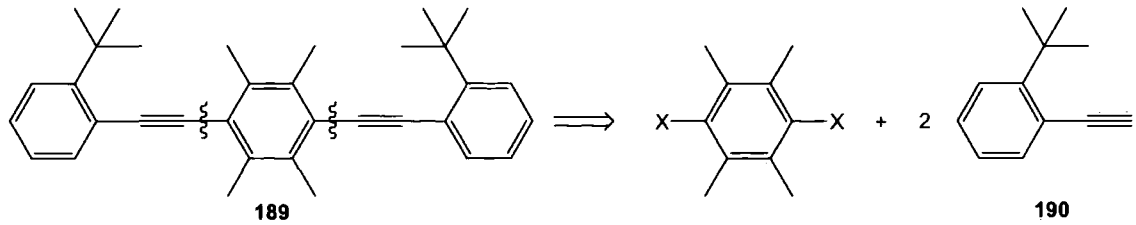

Scheme 4.4: Retrosynthesis of 1,4-bis(2-*tert*-butylphenylethynyl)durene. (X = Br / I)

The first stage of the synthesis was to prepare 2-*tert*-butyl phenylacetylene, **190**. The initial step of this reaction was a diazotisation, carried out in order to convert the commercially available 2-*tert*-butylaniline, **191**, into 1-*tert*-butyl-2-iodobenzene, **192**, using the method described by Lesslie and Mayer.[11] This was then converted into the acetylene by coupling to trimethylsilylacetylene (TMSA) using standard Sonogashira coupling methodology,[12] followed by deprotection. No synthetic approach to **190** has been described in the literature, however it is not a novel compound and its use has been reported in a synthesis by Fogel *et al.*[13]

A further Sonogashira coupling was then used to couple the acetylene **190** to 1,4-diiodobenzene, **109**, and 1,4-diiododurene, **193**,[9] to give compounds **188** and **189** in good yield. A summary of the overall synthesis can be seen in Scheme 4.5.

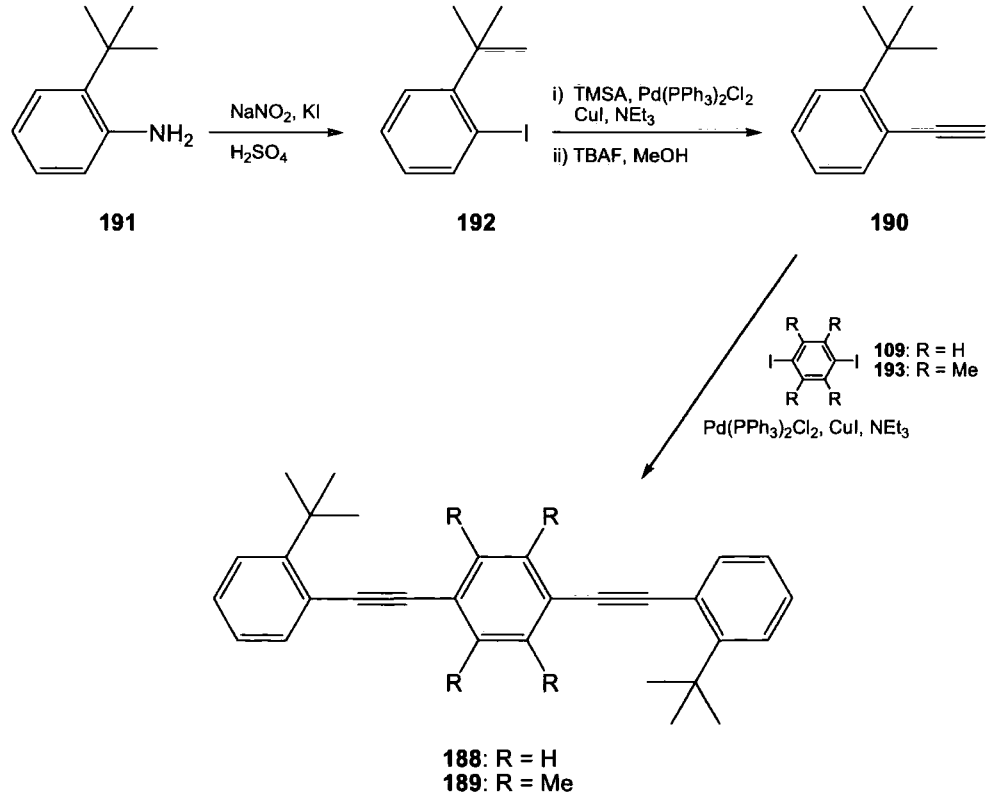

Scheme 4.5: Synthetic approach to compounds **188** and **189**.

Single crystals of **188** and **189** were grown and X-ray crystallography (Figure 4.7) showed only a small twist of the centre ring out of the plane of the molecule of 12° and 10° respectively. Close examination of the structure reveals that some of the steric strain is relieved by bending of the acetylenic group. It must be more energy efficient therefore for the molecule to flex in this way as opposed to forming a structure where the outer rings fully rotate out of the plane of the central ring.

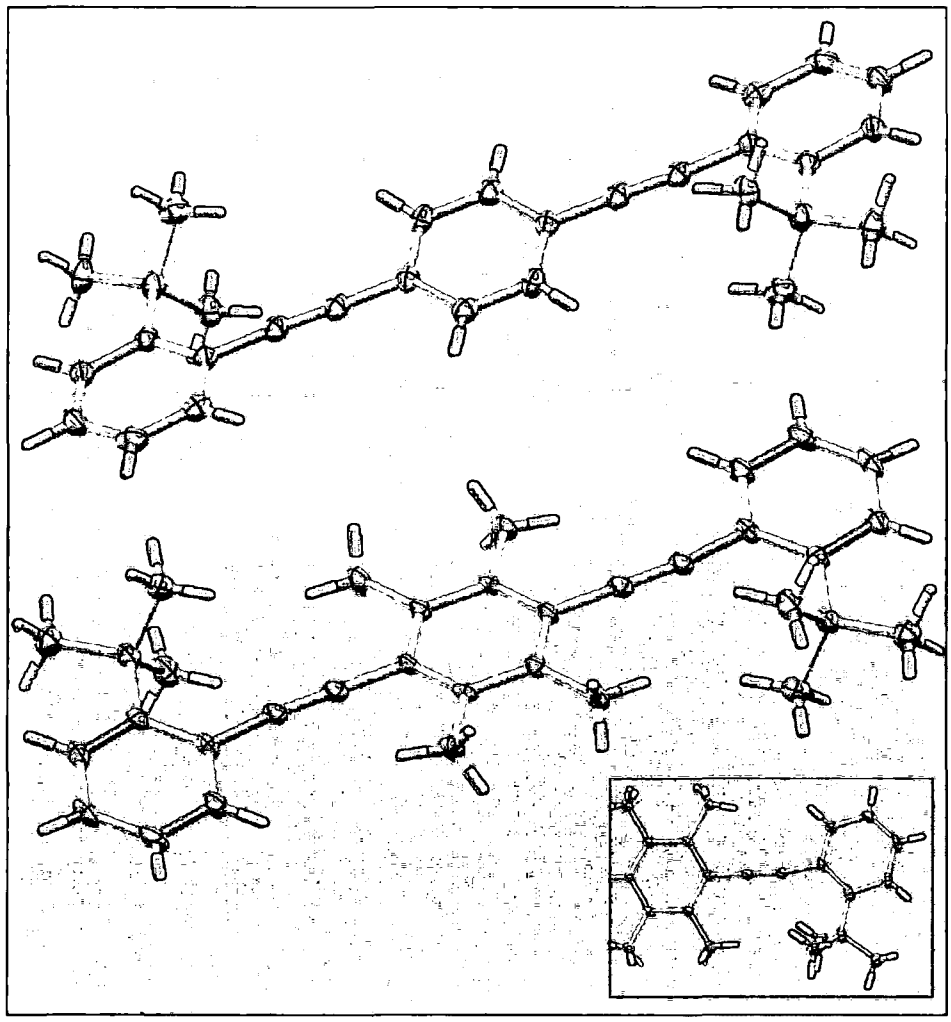

Figure 4.7: Structure of **188** (top) and **189** (bottom) determined by X-ray crystallography. Inset illustrates the bending of the acetylenic bond to reduce strain observed in **189**.

This result, coupled with the photophysical behaviour of **189** and **189** (see section 4.3) suggested that there is enough bulk to have some effect on the conformation of these compounds, however there is not enough overall steric hindrance in the molecules to fully restrict rotation about the acetylene bond due to the molecule being able to bend. It was decided therefore that bulk was required in both of the *ortho* positions on the

outer rings to counter this bending. The next approach therefore involved the use of two *iso*-propyl groups next to the triple bond.

This approach required a slightly more complex synthetic route to obtain the desired phenylacetylene derivative, **200**. Sonogashira coupling of TMSA to 2-bromo-1,3,5-triisopropylbenzene, **194**, did not proceed readily, attributed to the reacting centre between two isopropyl groups being shielded by steric hindrance, reducing reactivity. As a result a more elaborate route, starting from the commercially available ketone, **195**, was used, as seen in Scheme 4.6. The initial reduction of **195** to the secondary alcohol, **196**, with $LiAlH_4$ was carried out using the method described by Delair *et al.*[14] The resulting alcohol was then converted to the alkyne using an adaptation of a procedure by Knorr *et al.*[15] This involved the initial dehydration of **196** to the styrene, **197**, by heating with potassium hydrogensulfate. A bromination reaction was then carried out to form **198** before two successive dehydrobromination steps (*via* the styrene intermediate **199**) finally gave **200** in 53 % overall yield.

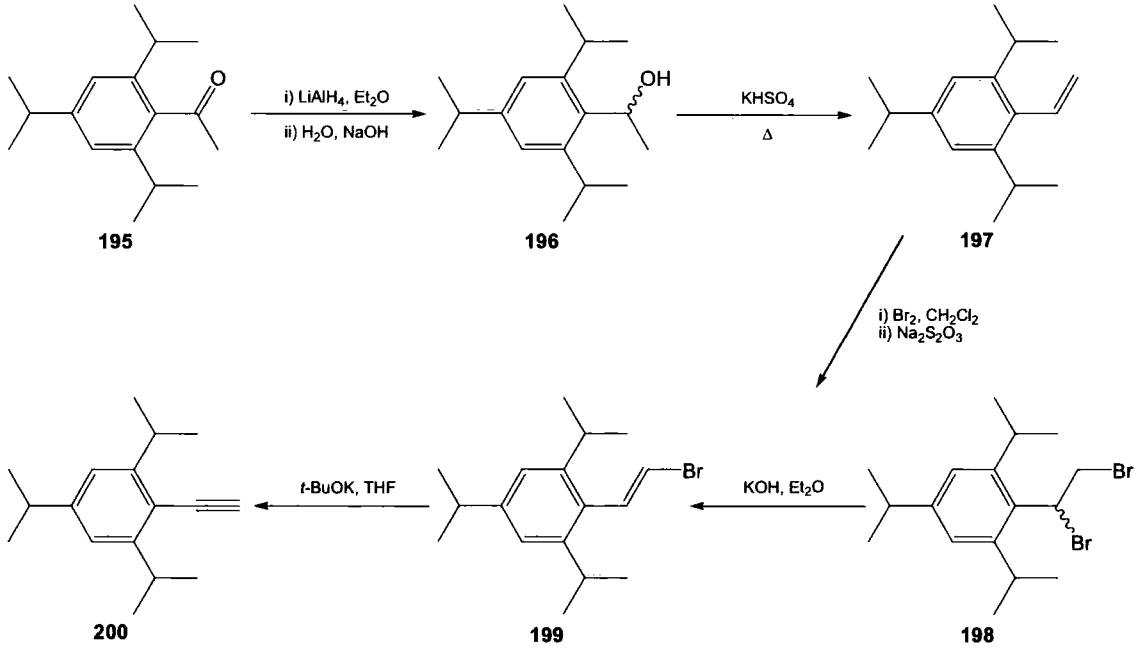

Scheme 4.6: Synthetic scheme for the preparation of 2,4,6-tri-*iso*-propylphenylacetylene.

Once the desired acetylene, **200**, had been synthesised, this coupled readily with **109** and **193** under normal Sonogashira conditions to give compounds **201** and **202**. Single crystals were grown of these compounds, and their structures determined by X-ray crystallography (Figure 4.8), which indicated that neither of these compounds displayed a significant twist in the molecule in the solid state. In practice, it is seen that the *iso*-

propyl group is not significantly more sterically demanding than a methyl group with angles of 26° and 18° observed for **201** and **202** respectively. This is because in order to remove potential strain the *iso*-propyl groups rotate, with the lone hydrogen pointing towards the centre of the molecule. Once again, the photophysical data (see section 4.3) supported the fact that there is insufficient steric hindrance in these two compounds to restrict the rotation of the rings about the alkyne unit.

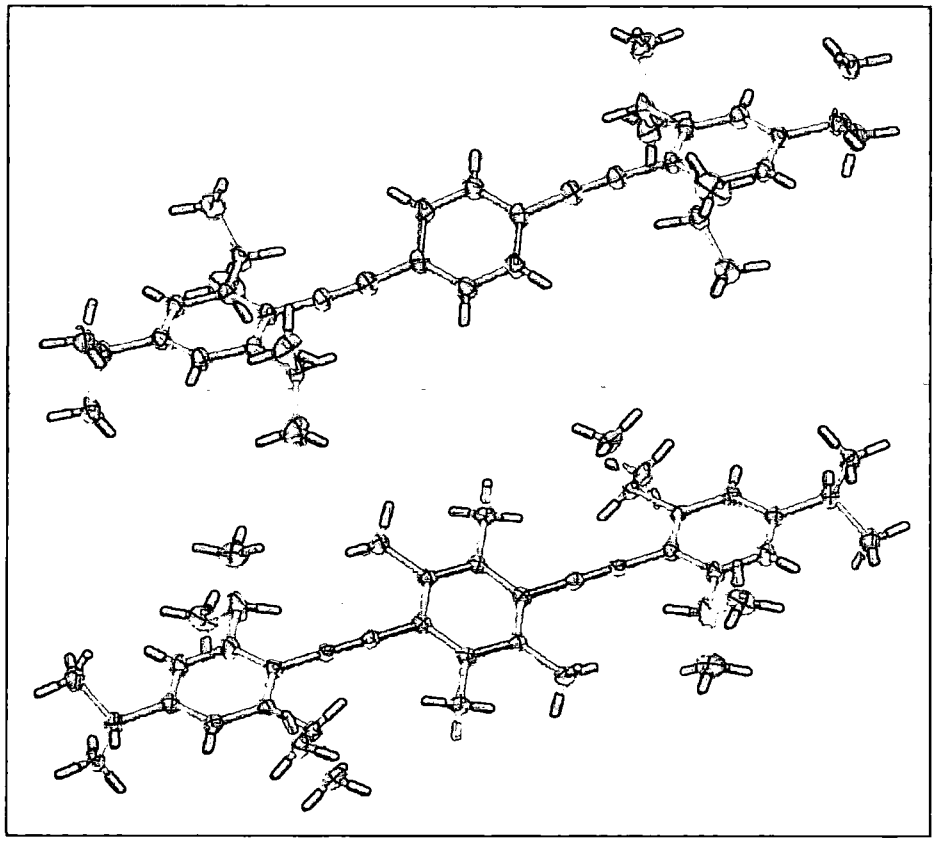

Figure 4.8: Structure of **201** (top) and **202** (bottom) determined by X-ray crystallography.

It was necessary, therefore, to increase the bulk yet further, which could be achieved by the incorporation of two *tert*-butyl groups in the ortho position instead of the *iso*-propyl groups. The added steric bulk of the two adjacent *tert*-butyl groups meant that neither of the previously employed routes to the phenyl acetylene (using either Sonogashira coupling or the method used to produce the 2,4,6-tri-*iso*-propylphenylacetylene) would work.

2,4,6-Tri-*tert*-butylphenylacetylene, **203**, has been previously made by a pre-Sonogashira copper-acetylide reaction by Zimmerman and Dodd[16] and this method was adapted here. The commercial aryl bromide, **204**, was converted to the iodide, **205**,

which was then reacted with copper (I) ethylpropiolate to form ethyl 3-(2,4,6-tri-*tert*-butylphenyl)propiolate, **206**. This stage had to be carried out with extra care due to the potentially explosive nature of copper acetylides.[17] **206** was then converted to the propiolic acid, **207**, by reacting with potassium hydroxide in ethanol.

In the final stage the literature method used a steam distillation process, which proved difficult to replicate, particularly on a small scale. However it was noted that **207** had a reported melting point of 200 °C with decomposition. On investigation of this, it was discovered that the decomposition product was the desired acetylene, thus fusion of the acid provided a much more straight forward and clean method of preparing the material. The reaction scheme to the acetylene is shown in Scheme 4.7.

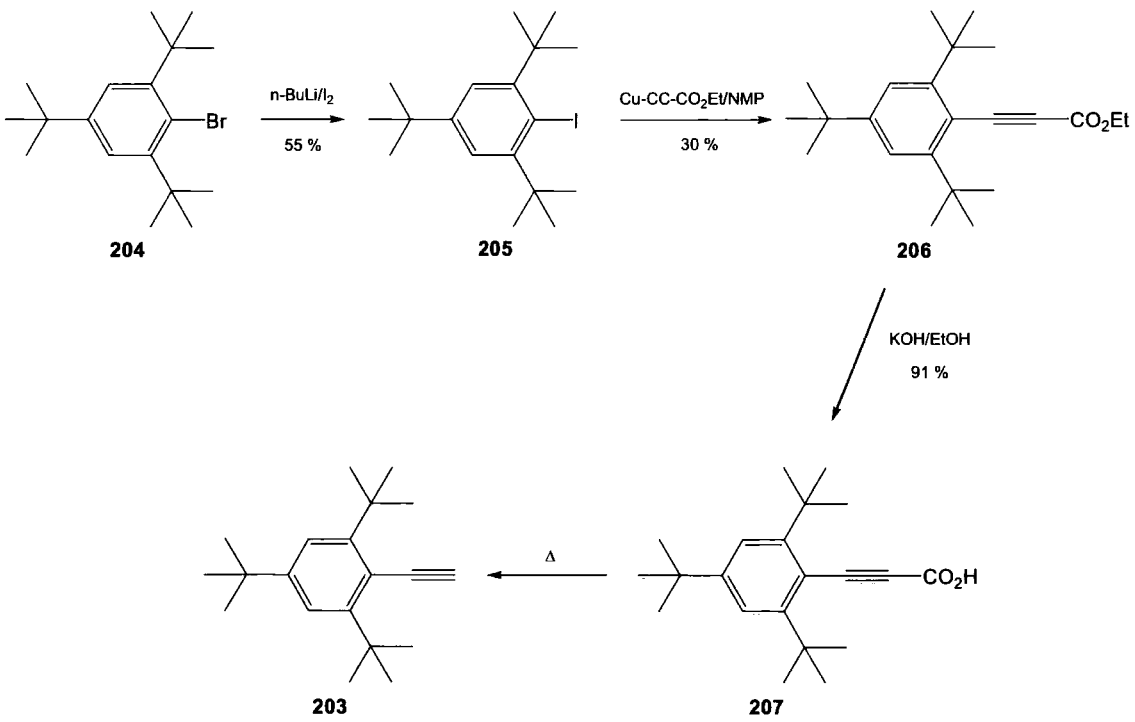

Scheme 4.7: Synthetic scheme for the synthesis of 2,4,6-tri-*iso*-propylphenylacetylene.

Once the acetylene had been synthesised, it proved straightforward to couple it to **109** using normal Sonogashira coupling to give compound **208**. Coupling of the acetylene to 1,4-diiododurene however was not as straightforward, as the standard conditions did not produce a viable yield of product. Instead, the Sonogashira reaction mixture had to be heated at 70 °C for two and a half days in a sealed Schlenk tube with a Pd(0) catalyst, which gave **209** in good yield. The sealed vessel gave an increase in pressure for the reaction, as well as helping to prevent any oxygen seeping into the system over

the extended reaction period. The need for these more extreme conditions was most likely caused by the increased amount of steric bulk in the system.

X-ray crystallography (Figure 4.9) reveals that the bulk of the two *tert*-butyl groups adjacent to the acetylene bond is sufficient to engineer a twisted conformation in the solid state. **208** is the least twisted of the two compounds, with the central unsubstituted phenyl ring at an angle of 35° to the plane of the molecule. The structure of **209** is more significant, with the central durene ring twisted out of the plane by nearly 90°. The photophysical data (see section 4.3) supports the crystallographic findings, this time seeing a definite change (especially for **209**) in behaviour compared to BPEB.

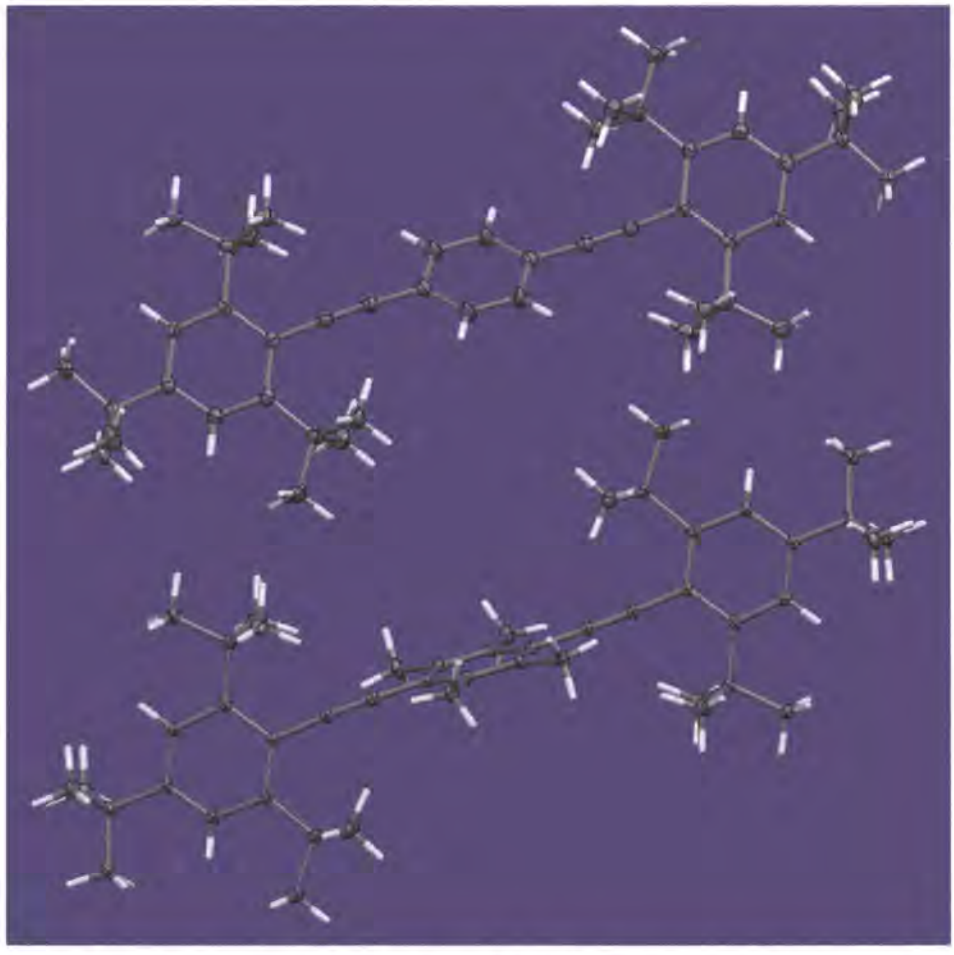

Figure 4.9: Structure of **208** (top) and **209** (bottom) determined by X-ray crystallography.

No conformationally restricted aryleneethynylenes have yet been reported that are based on a non-phenylethynyl framework. Therefore, the study of different types of system was of interest. The central anthracene unit in BPEA has protons in the 1,8 positions (as shown in Figure 4.10) that can provide steric interactions with *ortho* substituents on

the external phenyl rings in a similar way to the methyl protons in durene. Indeed, X-ray crystallography shows that in the solid state BPEA adopts a conformation whereby the outer phenyl rings are twisted out of the plane of the anthracene by 24.7°.[18,19]

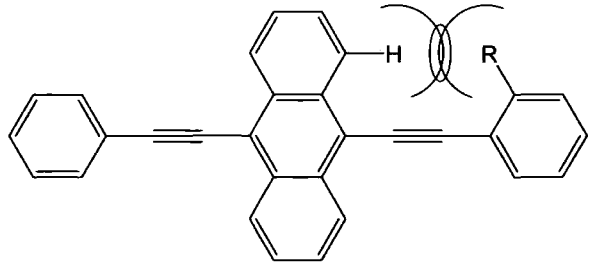

Figure 4.10: Representation of the steric interaction in BPEA between the 1,8 protons of anthracene and *ortho* substituents on the phenyl rings.

A series of compounds analogous to the previously described BPEB variants were synthesised (Figure 4.11). 9,10-dibromoanthracene **210** was reacted with **190** and **200** overnight under Sonogashira conditions at elevated temperature to form **211** and **212** in 60 % and 28 % yield respectively. As with the formation of **209**, the steric bulk present in the reaction prevented the formation of **213** under regular Sonogashira conditions, again requiring the reaction to be carried out in a sealed tube over two and a half days, giving a yield of 31 %.

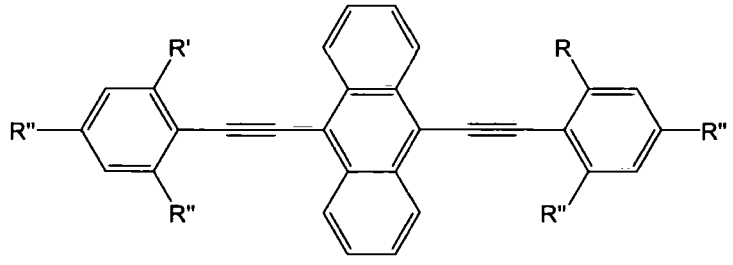

	R	R'	R"
211	^{t}Bu	^{t}Bu	H
212	^{i}Pr	^{i}Pr	^{i}Pr
213	^{t}Bu	^{t}Bu	^{t}Bu
214	^{t}Bu	H	H

Figure 4.11: BPEA analogues synthesised to try to restrict rotation about the ethynyl bond.

Crystals were successfully grown for **211** and **212** for X-ray crystallography, however it was not possible to obtain crystals of **213**. The solid state structure of **211** was found to be different to that of the BPEB analogue **189**, in **211** the molecule does not bend to relieve strain and the 'outer' benzene rings lie orthogonal to the plane of the anthracene. The structure of **212** was found, however, to be analogous to that of **202**, with an almost planar structure (angle between rings *ca.* 12°) and the *iso*-propyl groups rotating so that the lone hydrogen points towards the anthracene (Figure 4.12).

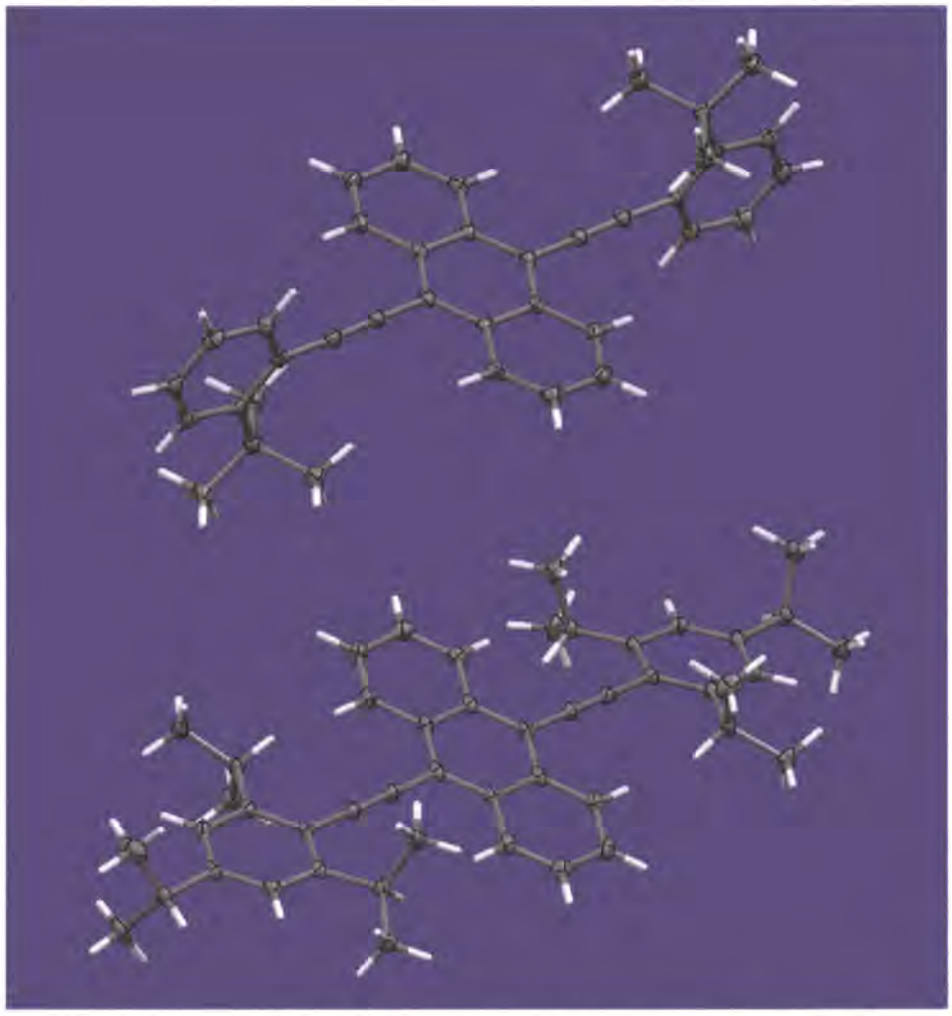

Figure 4.12: Structure of **211** (top) and **212** (bottom) determined by X-ray crystallography.

It is unfortunate that **213** was unable to be studied by X-ray crystallography. The crystals (and solid powder) of the other derivatives of BPEA are orange in colour, whereas **213** is yellow. This difference in appearance gives a clue that it has decreased conjugation compared to the other derivatives and a crystal structure could have potentially helped to understand the cause of this. This difference in electronic structure is also evident in the photophysical behaviour of **213**, being markedly different to that of the other BPEA derivatives, this is examined further in the next section.

With **211** showing an orthogonal twist out of the plane, **214** was synthesised with the aim of creating a molecule that was only 'half-twisted.' This synthesis required two successive couplings as shown in Scheme 4.8. Firstly **210** was reacted with just under 1 equivalent of phenylacetylene using regular Sonogashira conditions to form the 'mono-substituted' compound **215** in a 60 % yield. This was then coupled to 2-tertbutyl-

phenylacetylene, again using regular Sonogashira conditions, to give **214** in 64 % yield (an overall yield of 38 % for the two steps).

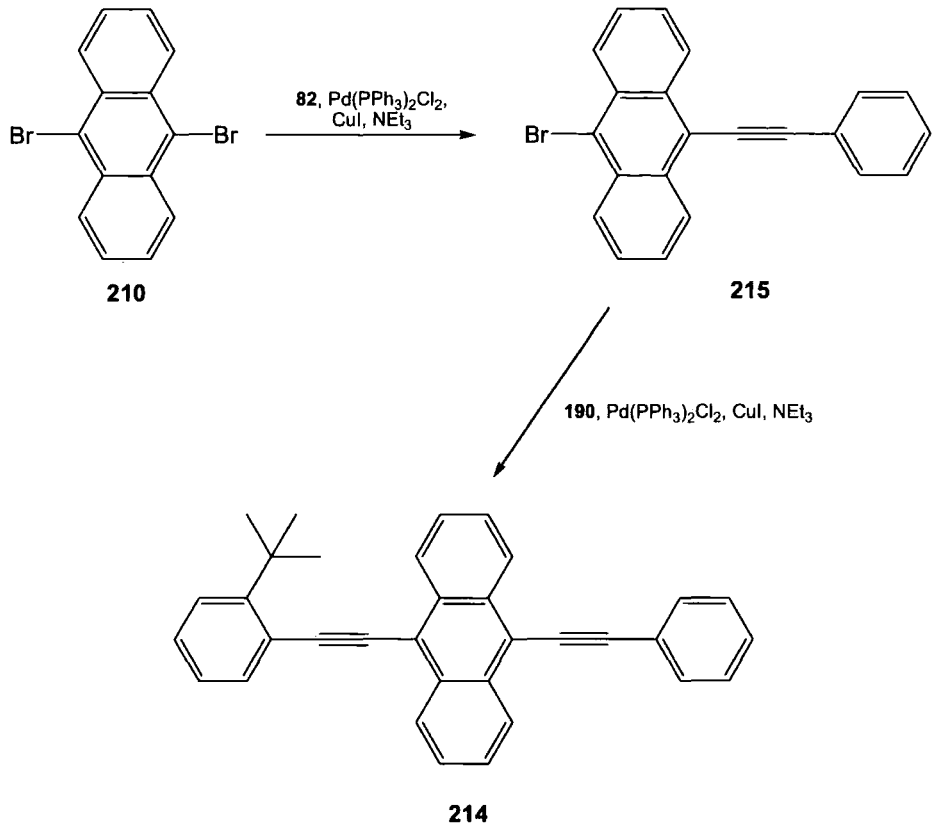

Scheme 4.8: Synthetic route to the asymmetric compound **214**.

X-ray crystallography (Figure 4.13) revealed that the solid state structure does not display the 'half-twisted' conformation that was aimed for. Small angles of twist are observed (*ca.* 20°), with the unsubstituted phenyl ring twisted in the opposite direction to the 2-*tert*-butylphenyl ring, relative to the plane of the anthracene moiety. Also it can be seen that, as with the analogous compound **189**, steric strain from presence of the *tert*-butyl group is relieved by bending of the acetylene group as opposed to a significant twist in the molecule.

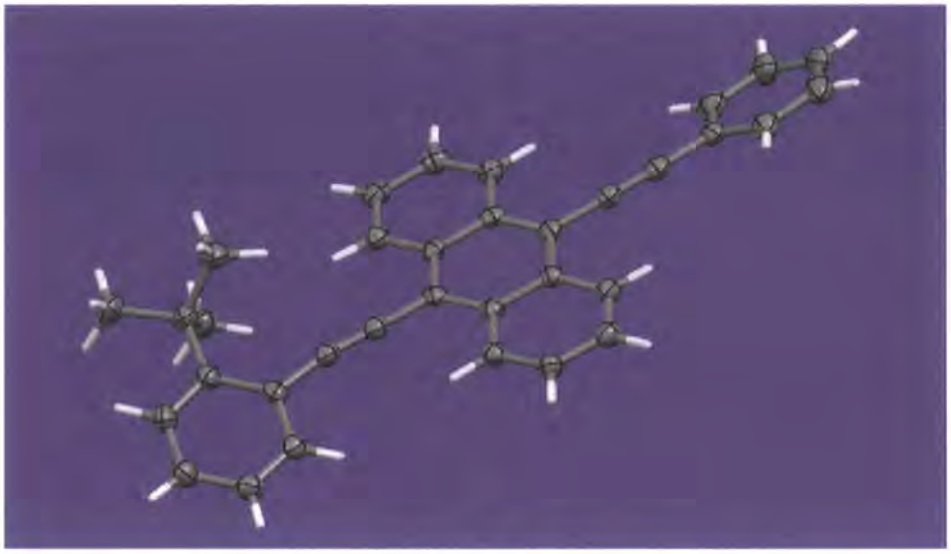

Figure 4.13: Structure of **214** determined by X-ray crystallography.

With the addition of *ortho tert*-butyl groups being observed to have an effect on the conformation of these types of system, it was wondered if different groups could be found to give the same result. To investigate this compounds were prepared where *tert*-butyl groups were replaced with trimethylsilane. TMS was chosen as it is a bulkier group than ^{t}Bu, but retains the sigma bonded character.

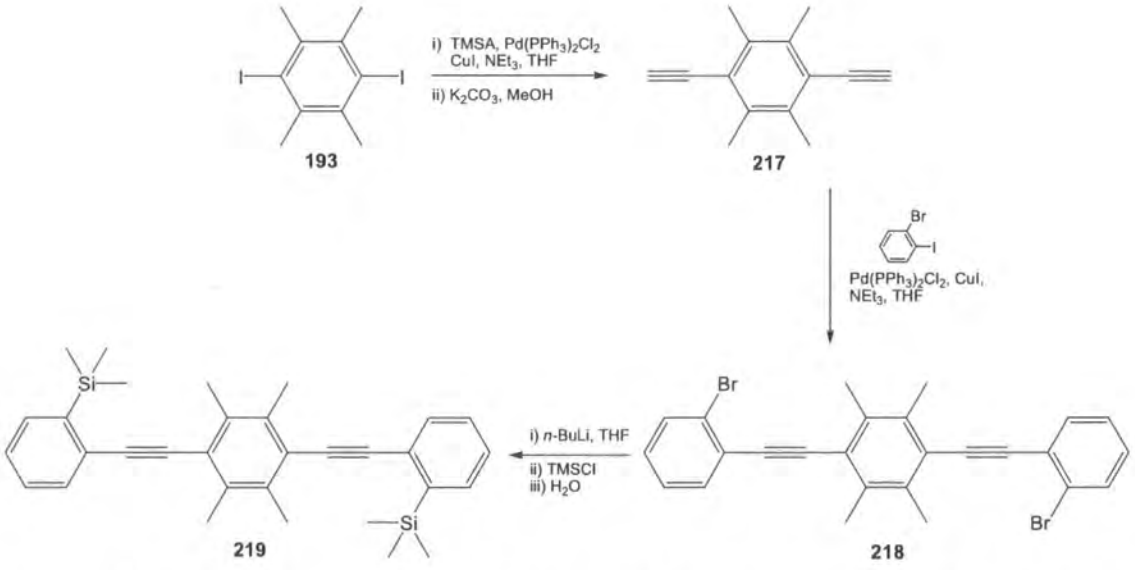

Scheme 4.9: Synthetic route used to obtain 1,4-bis((2-trimethylsilyl)phenylethynyl) durene.

The initial approach was to synthesise **219**, which is an analogous compound to **189**, with TMS replacing the *tert*-butyl groups. The route (Scheme 4.9) initially involved the synthesis of 1,4-bisethynyldurene, **217**, by coupling an excess of TMSA with **193** *via* standard Sonogashira methodology, followed by deprotection of the resultant

acetylene, **216**, with potassium carbonate in methanol. A further Sonogashira coupling was then carried out on this using 2-iodobromobenzene to obtain 1,4-bis((2-bromophenylethynyl)durene, **218**.

The dibromo compound **218** was then dissolved in THF and *n*-butyllithium was added at reduced temperature. Chloro trimethylsilane was added to this mixture after 20 minutes and the solution was subsequently allowed to warm to room temperature before being quenched by the addition of water. The desired product, **219**, was extracted into DCM and subsequently purified by passing through a silica column with a hexane eluent.

Crystals of **219** suitable for X-ray crystallography were obtained, and the solid state structure was determined (Figure 4.14). This structure is similar to that found for **189**, however the outer phenyl rings in **219** are twisted out of the molecular plane to a larger extent than in **189**, although the angle is still relatively small (26.3°). Also, as in **189**, the molecule bends to relieve the steric hindrance rather than twisting fully out of the plane.

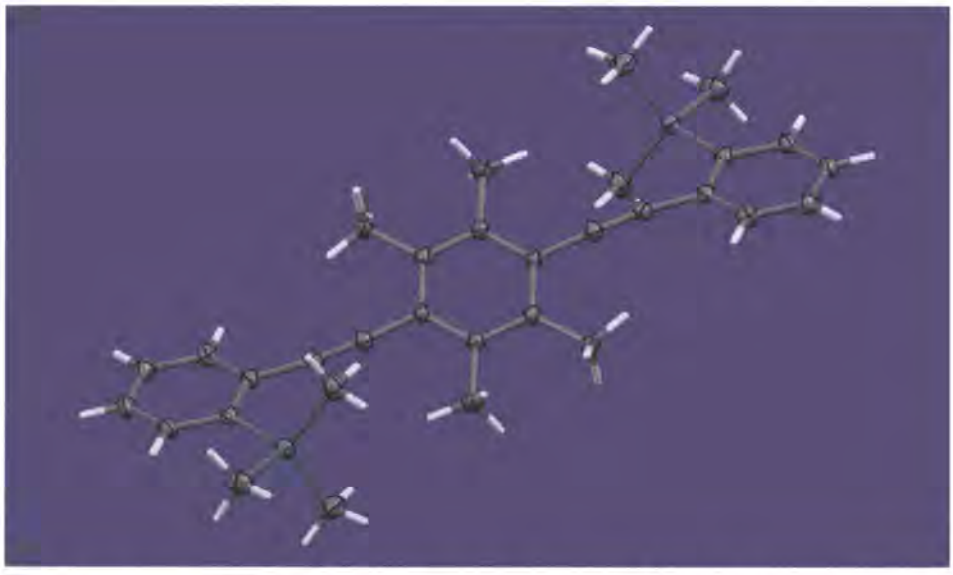

Figure 4.14: Structure of **219** determined by X-ray crystallography.

With one TMS group *ortho* to the acetylene bond giving a compound with a similar structure to the *tert*-butyl derivative, the next step was to synthesise a compound with two *ortho* TMS groups. The first stage of this was to make 2-ethynyl-1,3-bis(trimethylsilyl)benzene, **220**, via the route shown in Scheme 4.10. The approach

used was based on that of Yamaguchi *et al.*[20] Firstly phenylacetylene was lithiated then quenched with TMSCl to form the TMS protected acetylene, **221**. This was subsequently treated at -78 °C with the LICKOR 'superbase' (a mixture of *n*-butyllithium and potassium *tert*-butoxide) in THF before the addition of TMSCl, leading to the formation of 1-trimethylsilyl-2-(trimethylsilylethynyl)benzene, **222**. A second treatment with the LICKOR base and TMSCl gave 1,3-bis(trimethylsilyl)-2-(trimethylsilylethynyl)benzene, **223**, which was then deprotected using TBAF dissolved in methanol to give **220**.

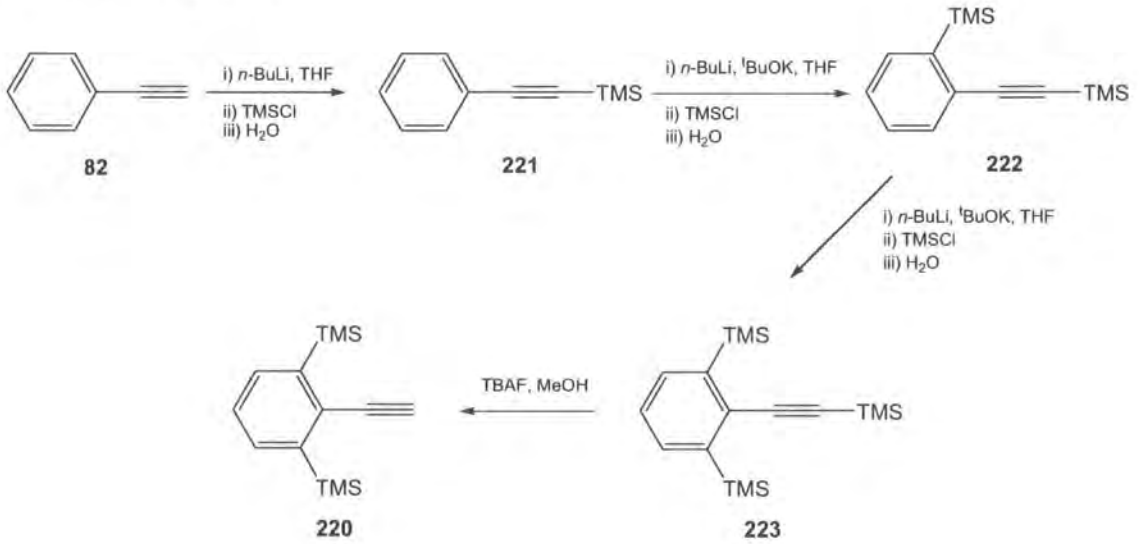

Scheme 4.10: Synthetic route to 2-ethynyl-1,3-bis(trimethylsilyl)benzene.

Formation of a three ring system from this acetylene, was not possible using standard Sonogashira conditions. However it proved possible to synthesise 1,4-bis(2,6-bis(trimethylsilyl)phenylethynyl) benzene, **224**, in 56.5 % yield by carrying out a Sonogashira coupling of **220** and 1,4-diiodobenzene in a sealed tube at 70 °C overnight. Unfortunately the crystal structure could not be obtained as it did not prove possible to obtain crystals suitable for X-ray analysis.

The attempted reaction to obtain 1,4-bis(2,6-bis(trimethylsilyl)phenylethynyl)durene, **225**, by using a closed tube Sonogashira coupling between **220** and **193** did not proceed effectively. After being left to react for several days the reaction had not proceeded in sufficient yield to allow separation from unwanted side products and unfortunately no further work to optimise the conditions was possible.

4.3 - Photophysics

The crystallographic data points towards there being differing degrees of conformational restriction in these compounds in the solid state. However this does not give the whole picture. The solid-state structure represents a static system in which overall free energy is reduced. The observed structure may be governed by factors such as packing effects, and thus may not reliably represent the structure in solution. UV-Vis absorption and fluorescence spectroscopy allow the study of these systems in solution providing further insight into their structure.

4.3.1 - Photophysical Properties

Photophysical studies were carried out to examine the effect of the bulky side groups on the structure of the previously described compounds when in solution. Previous studies in the literature have shown that, due to the free rotation about the acetylenic bond, at room temperature the absorption spectra in solution of non-hindered aryleneethynylenes, such as BPEB, are broad and relatively featureless. This results from a continuum of conformers present in solution that are all absorbing the incident light, with the spectrum observed being a composite of all the conformers present. The molecules planarise before emitting light, and so the observed emission spectra show vibronic structure due to the continuum no longer being present.[21-23]

In an EPA glass at low temperature the planar conformation is more favoured. However, the barrier to rotation about the acetylenic bond is still too low for kT to restrict the molecule to the planar conformation. This behaviour reduces the number of conformations present, thus leading to the appearance of vibronic structure in the spectrum which becomes more like a mirror image of the emission spectrum. The latter exhibiting a slight increase in vibronic resolution at low temperature.[23]

A more detailed examination of this photophysical behaviour is given in Chapter 1. The rest of this section will first examine the photophysical behaviour of the alkyl substituted BPEB derivatives before moving on to look at the other systems studied.

4.3.1.1 - BPEB Derivatives

Absorption, and fluorescence emission / excitation spectra of the synthesised BPEB derivatives were obtained in EPA at both room temperature and in an EPA glass at 77 K. It can be seen from Figure 4.15 that the profiles of the absorption spectra obtained for **189** closely resemble those of the fluorescence excitation spectra, albeit with the absorption spectra relatively red shifted by around 10 nm.

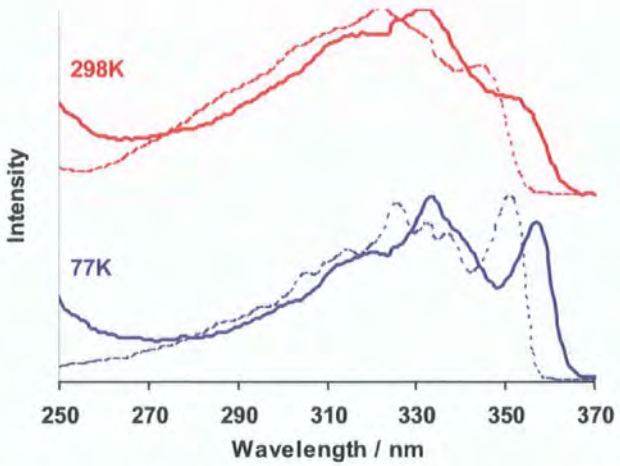

Figure 4.15: Normalised absorption (solid lines) and fluorescence excitation (dotted lines) spectra of **189** in EPA at 298 and 77 K.

This similarity in the profiles is indicative that the samples are pure with the light only being absorbed by the emitting species. This similarity was observed for all the compounds and from here on, only the excitation spectra will be given.

As can be seen from Figure 4.16, the emission and excitation profiles of **188** and **189** in solution at room temperature are very similar to those for the parent compound BPEB, apart from a slight red shift due to the effect of the alkyl groups. When in the transparent glass formed by EPA at 77 K the excitation spectrum also shows the same trend as BPEB, the spectral features sharpen and the red edge of the spectrum becomes pronounced due to an increased population of the lower energy, more planarised conformations.

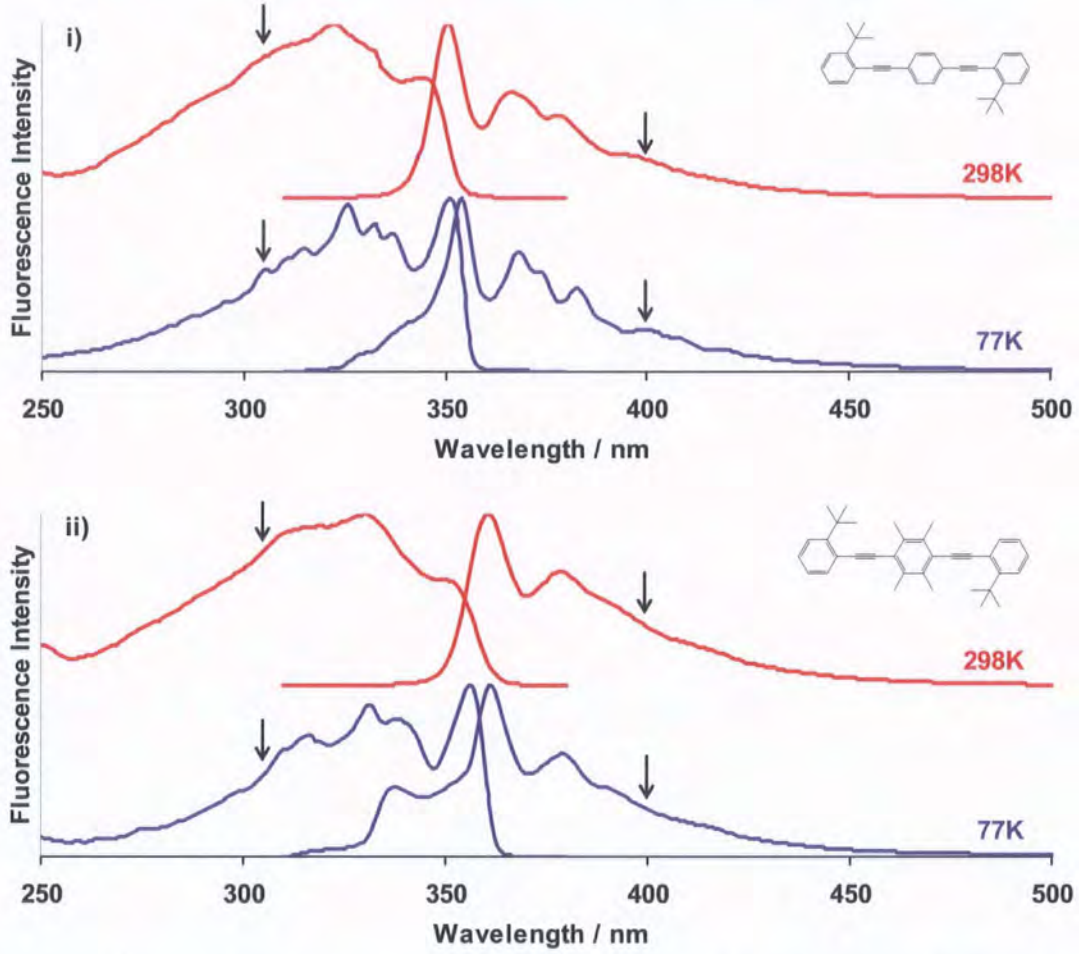

Figure 4.16: Normalised Fluorescence emission-excitation spectra of i) **188** and ii) **189** at 298 K and 77 K in EPA. (λ_{ex} = 305 nm, λ_{em} = 400 nm, denoted by arrows on spectra)

	Excitation Features (nm)		Emission Features (nm)	
	298K	77K	298K	77K
188	323, 344	326, 351	350, 366, 378	338, 354, 369, 384
189	330, 351	317, 331, 356	361, 378	338, 361, 379

Table 4.3: Summary of features on emission-excitation spectra of **188** and **189**.

The emission profiles, however, see a departure from what is observed in BPEB. A new feature in the spectrum is observed for both compounds, at *ca.* 338 nm. For **188** this is as a shoulder at the blue end of the emission profile, whereas for **189** a new distinct peak, blue shifted in relation to the 0,0 transition at 361 nm, is observed. Since these effects are only seen in viscous, low temperature glasses, it is likely that these new features occur due to emission from a twisted conformation that has not planarised before the emission has taken place. Further investigation of this was not possible as wavelength limits prevented the use of time-resolved spectroscopy.

The homogeneity of the fluorescence spectrum allows an insight into whether the compound being studied displays multiple emission characteristics. To test this a range of emission spectra were obtained for **189** over a range of excitation wavelengths between 250 and 380 nm at both 298 and 77 K. The emission-excitation matrices (EEMs) arising from this study are shown in Figure 4.17.

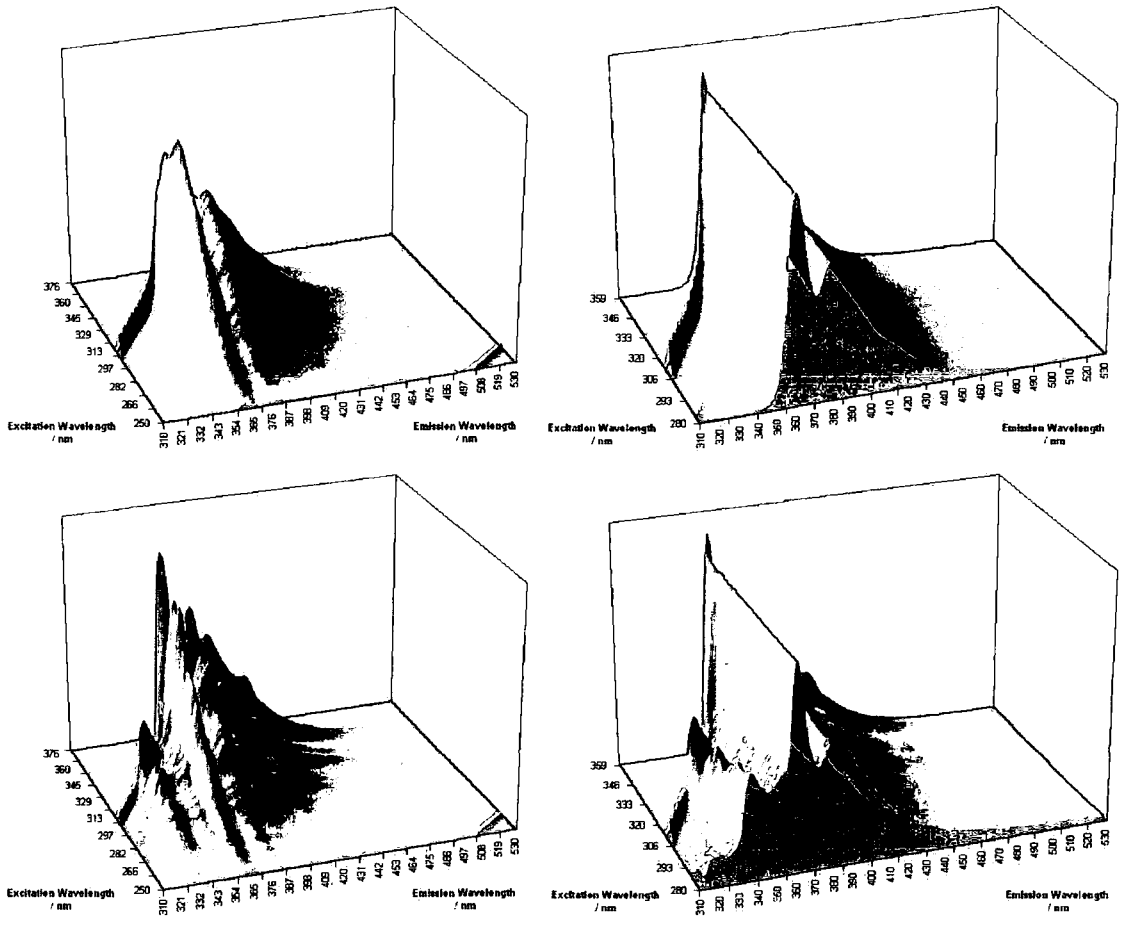

Figure 4.17: Fluorescence Em-Ex matrices of **189** in EPA at 298 K (green spectra) and 77 K (blue spectra). The left hand EEMs show the observed spectra, whilst those on the right are normalised over the excitation wavelength range of 280-360 nm. The diagonal rows of peaks arise from the first and second order scatter of the incident light.

At room temperature the emission of **189** in EPA is homogenous with the profile of the emitted light being independent of the excitation wavelength. This is due to the presence of a single emitting species in the excited state. In the EPA glass however the emission profile varies with excitation, most notably for the feature that appears at the blue edge of the emission spectrum at low temperature. This lack of homogeneity confirms that there is more than one emitting species at low temperature, although the

majority of the observed emission is still occurring from the planarised excited state species.

TD-DFT calculations give a lowest energy conformation of **189** that is very similar to that observed in the crystal structure. The calculated structure is bent to relieve steric interactions and also has the central ring twisted out of the plane of the molecule by *ca.* 15°. The calculations were also used to compare the frontier orbitals of **189** with those of compound **2**. The HOMO and LUMO of the two compounds, shown in Figure 4.18, are very similar, the main difference occurring visually due to the bending observed in **189**.

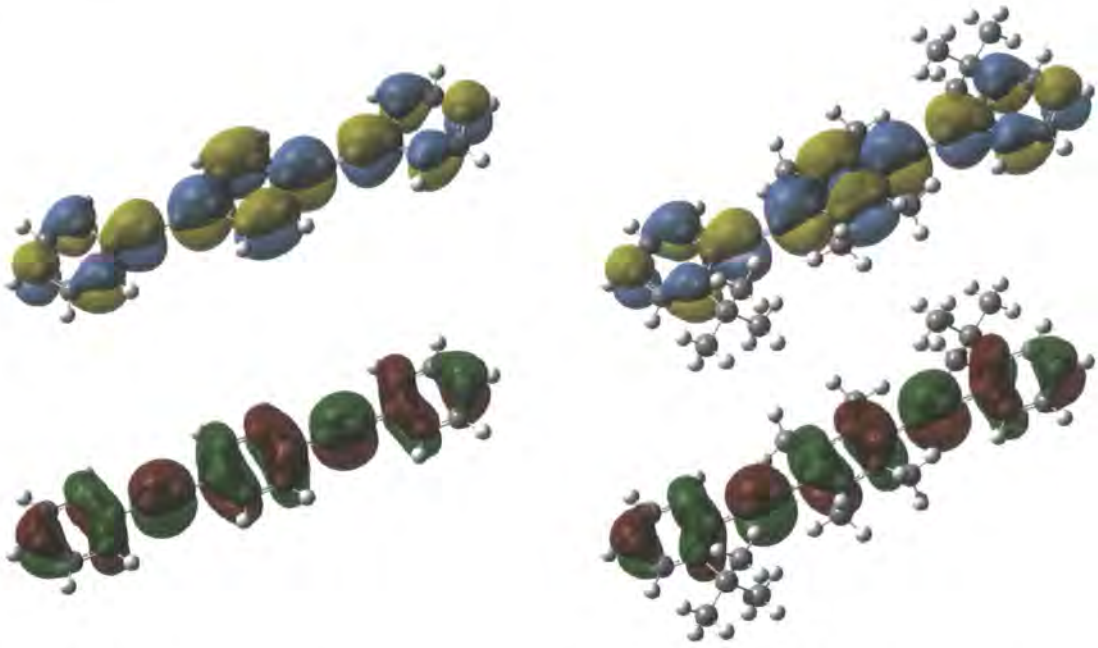

Figure 4.18: Comparison between the HOMO (red/green) and LUMO (blue/yellow) of compounds **2** (left) and **189** (right). MOs visualised using a TD-DFT calculation with a B3LYP/6-311g(2d,p) level of theory (Gaussian 03W)[10].

The calculation also shows that, like for BPEB the first excited state of **189** arises from the LUMO ← HOMO transition. As seen earlier for compound **187**, **189** shows slightly red shifted emission and excitation spectra when compared to **2** due to the alkyl substituents. The calculations confirm this, showing the first excited state at a slightly lower energy for **189** with the transition appearing at 366 nm, compared to the 359 nm transition seen for BPEB.

The photophysical results, as well as the TD-DFT calculations help to confirm the observations from the crystal structure. The addition of a single *tert*-butyl group adjacent to the carbon-carbon triple bond has only a small effect on the conformation of

a phenylethynyl system, with the solution state spectra only showing a small degree of rotational restriction observed when in a low temperature glass.

In the solid state the addition of two *iso*-propyl groups *ortho* to the acetylene bond had little effect on the conformation of the molecule, with the crystal structure showing the *iso*-propyl group rotating to relieve strain. The emission excitation profiles of **201** and **202**, shown in Figure 4.19, are, as in the bis-*tert*-butyl systems discussed above, similar to those of BPEB at room temperature with intramolecular rotation about the acetylenic bond possible in solution.

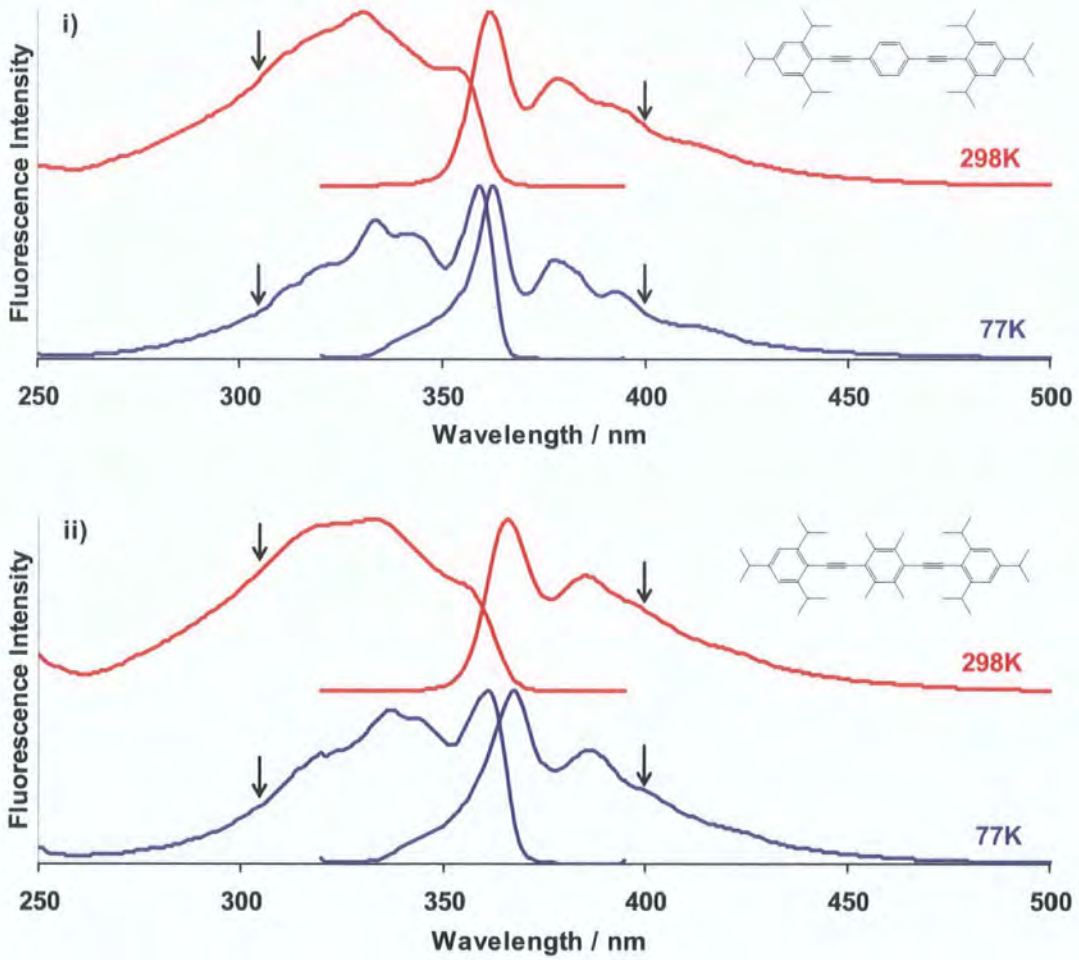

Figure 4.19: Normalised fluorescence emission-excitation spectra of i) **201** and ii) **202** at 298 K and 77 K in EPA. (λ_{ex} = 305 nm, λ_{em} = 400 nm, denoted by arrows on spectra).

	Excitation Features (nm)		Emission Features (nm)	
	298K	77K	298K	77K
201	335, 353	333, 359	362, 380, 393	341, 362, 378, 392
202	336, 356	337, 361	366, 385	342, 368, 387

Table 4.4: Summary of features on emission-excitation spectra of **201** and **202**.

Again the low temperature excitation spectra behave in a similar way to BPEB with an increased intensity at the red edge. In the low temperature emission spectra there is a slight shoulder observed to the blue end of the fluorescence profile at low temperature at around 342 nm, which again is likely to be emission from some twisted species, although this feature is nowhere near as prominent as for **189**.

This data shows that despite the crystal structure showing a planar conformation, at low temperature there is still enough bulk present to have an effect on the blue edge of the emission profile of these compounds. The shoulder observed is independent of whether the central ring is benzene or durene, and possibly occurs because of rotation of the *iso*-propyl groups in the viscous medium leading to the hindrance of the rotation about the acetylenic bond.

As *tert*-butyl groups are not able to rotate out of the way like the *iso*-propyl groups, as well as **208** and **209** showing twisted structures in the solid state, it was expected that the photophysical behaviour would show a greater departure from than that of BPEB than the previously studied derivatives, and this was indeed the case.

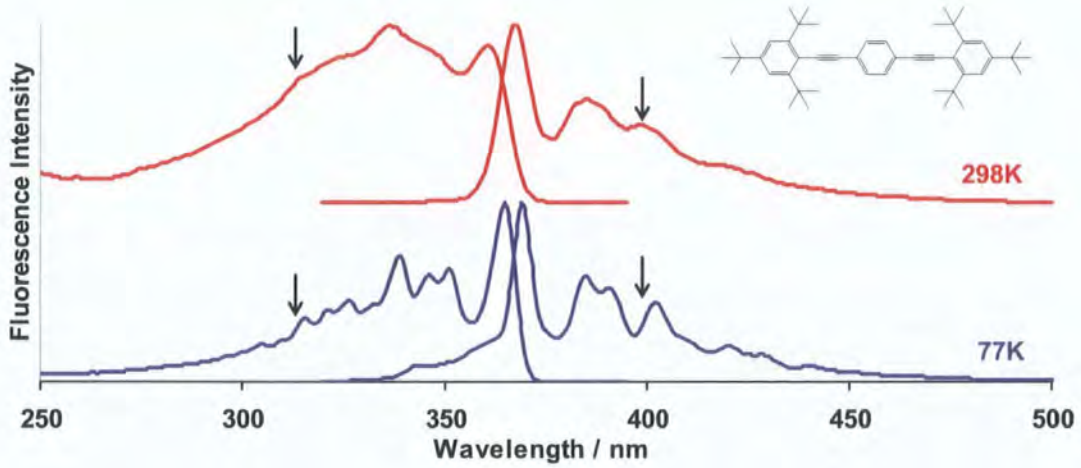

Figure 4.20: Normalised Fluorescence emission-excitation spectra of **208** at 298 K and 77 K in EPA. (λ_{ex} = 315 nm, λ_{em} = 400 nm, denoted by arrows on spectra).

	Excitation Features (nm)		Emission Features (nm)	
	298K	77K	298K	77K
208	340, 361	339, 351, 365	368, 385, 399	346, 369, 385, 391, 403

Table 4.5: Summary of features on emission-excitation spectra of **208.**

The hexa-*tert*-butyl-BPEB, **208**, has room temperature emission and excitation spectra that are similar to those of BPEB. However, as can be seen from Figure 4.20, dropping the temperature to 77 K leads to a greater change in the spectra than previously observed for compounds **188**, **189**, **201** and **202**. As well as seeing the extra feature on the blue edge of the emission spectrum (which has also been observed for the other compounds), the spectra display an increased amount of fine structure. This points to a greater restriction of intramolecular rotation caused by the addition of the *tert*-butyl groups adjacent to the acetylene bond. This causes less averaging of conformations and hence more discrete conformations are seen absorbing and emitting.

The hexa-*tert*-butyl-BPED, **209**, shows a much more marked difference in behaviour compared to BPEB than the other derivatives studied, as can be seen in Figure 4.21.

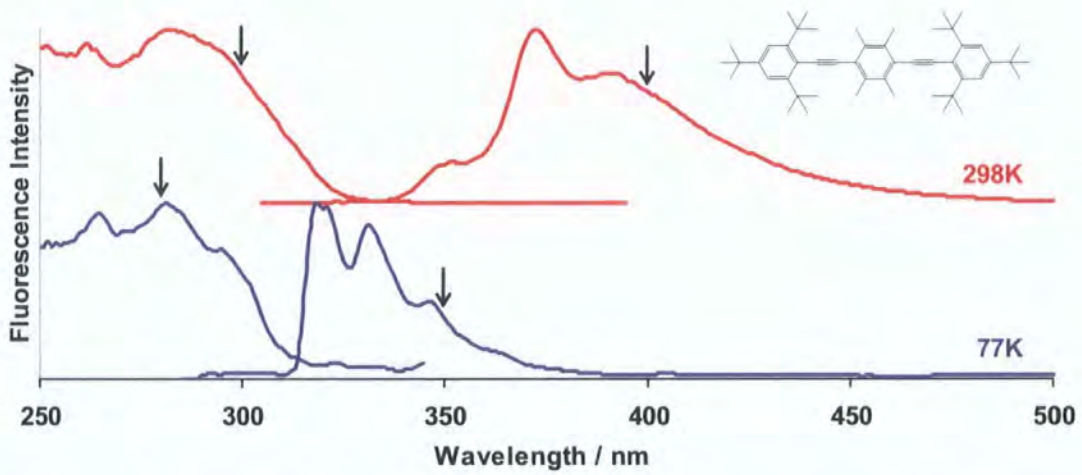

Figure 4.21: Normalised Fluorescence emission-excitation spectra of **209** at 298 K (λ_{ex} = 300 nm, λ_{em} = 400 nm) and 77 K (λ_{ex} = 280 nm, λ_{em} = 350 nm) in EPA (Arrows on spectra denote emission and excitation wavelengths).

	Excitation Features (nm)		Emission Features (nm)	
	298K	77K	298K	77K
209	262, 286	265, 281, 295	352, 373, 391	318, 331, 346

Table 4.6: Summary of features on emission-excitation spectra of **209.**

At 298 K the excitation spectrum is blue shifted by around 50nm compared to that of BPEB, with the emission profile similar to that of BPEB and the other analogues. There is however a shoulder present at ca. 352 nm, which resembles the extra feature seen in the spectra of eg. **189** at low temperature. The effect of the shift in position of the absorption band with the emission staying relatively in the same place is to give a large

Stokes shift. This suggests that on excitation the molecule undergoes a conformational change, presumably to a more planarised form.

Upon cooling to 77 K there is little change in the excitation profile apart from a very slight sharpening of structure. There is however a significant change at low temperature in the emission spectrum, with a pronounced blue shift in the emission again by the order of about 50nm. Vibronic structure also appears with a $\Delta\bar{\nu}$ of 1270 ± 60 cm^{-1}, which correlates with an aryl vibration as opposed to an acetylenic or cumulenic one. The lack of a large Stokes shift suggests that there is no reorientation of the molecule on the fluorescence timescale, leading to emission from the twisted form.

With the extra feature observed on the blue edge at room temperature, an EEM was obtained to test the homogeneity of the fluorescence response. Emission spectra were collected over the range of excitation wavelengths 250 - 360 nm. As can be seen in Figure 4.22, the shape of the emission is homogenous with the profile of the emitted light being independent of the excitation wavelength. This suggests that there is only a single emitting species present.

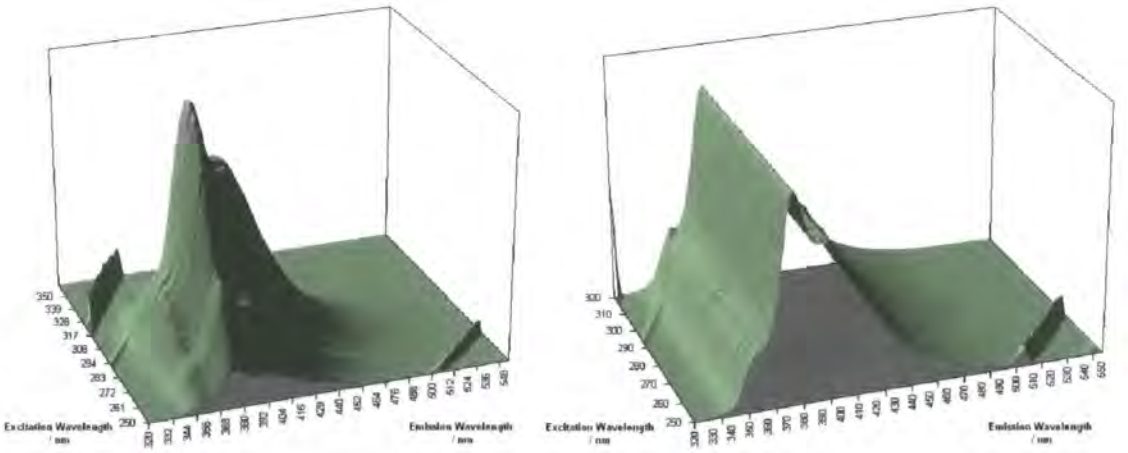

Figure 4.22: Fluorescence EEM of **209** in cyclohexane at 298 K. The observed spectrum is on the left, with the normalised matrix (for the excitation wavelength range of 250-320 nm) shown on the right. The diagonal rows of peaks arise from the first and second order scatter of the incident light.

This behaviour observed for **209** is significantly different compared to BPEB. This can most likely be attributed to the 90° twist in the compound seen in the crystal structure also being present in solution.

Theoretical calculations were undertaken in CAChe to help gain a better understanding on what processes were occurring. Firstly semi-empirical calculations (MOPAC, PM5) were carried out to optimise the structure of **209**, before the electronic transitions were calculated using ZINDO INDO-S. These calculations revealed that the first excited state results from a LUMO ← HOMO transition which is observed at 294 nm. They also allowed the visualisation of the frontier orbitals - these are shown in Figure 4.23. From this, it can be seen that the twisting of the central ring out of the molecular plane in **209** causes the orbitals to be located on the central ring and acetylene groups only and not the two external rings as seen for **2**.

TD-DFT calculations using a B3LYP/6-31g basis set gave a slightly different picture on the electronic processes occurring in **209**. These still show that the first excited state arises from a LUMO ← (HOMO-1) transition (Visualisation of the HOMO-1 orbital is shown in Figure 4.24), although this has a very low oscillator strength (0.0018). It is the fifth excited state which arises from the LUMO ← HOMO transition, with an oscillator strength of 1.51. This fifth excited state is the first to have a major contribution to the electronic processes occurring and hence it is still relevant to just consider the HOMO and LUMO to help interpret the photophysical results.

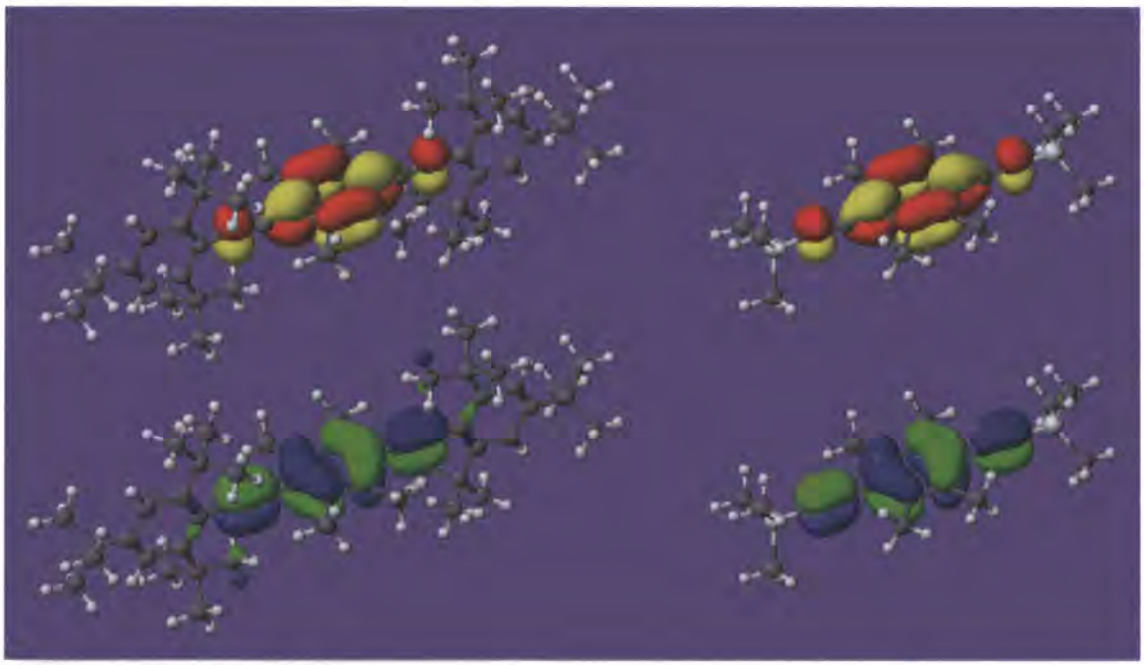

209 **216**

Figure 4.23: HOMOs (blue/green) and LUMOs (red/yellow) for compounds **209** and **216**, calculated using CAChe.

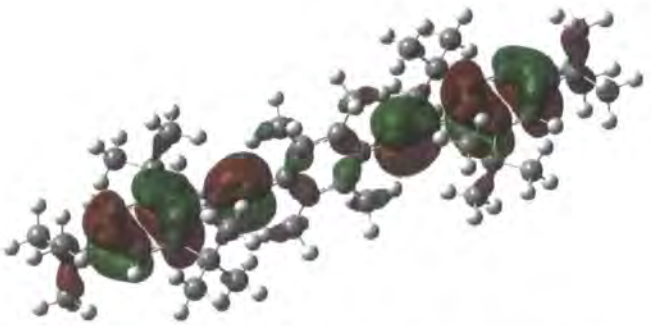

Figure 4.24: HOMO-1 of **209**, visualised using a TD-DFT calculation with a B3LYP/6-31g level of theory (Gaussian 03W)[10].

Further calculations showed that the frontier orbitals of **209** are very similar to those seen for 3,6-bis(trimethylsilylethynyl) durene, **216**, which was shown to also have a first excited state resulting from a transition between these orbitals - although at a lower wavelength (278 nm). This result warranted further investigation and so the emission-excitation spectra were obtained of **216**, and then compared with the low temperature spectra of **209** . This comparison can be seen in Figure 4.25.

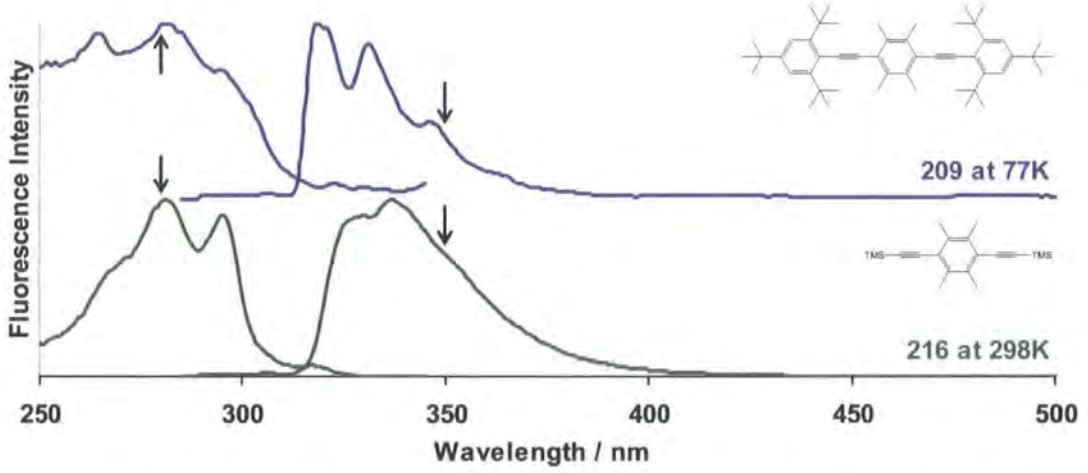

Figure 4.25: Comparison of the normalised Fluorescence emission-excitation profiles of **209** at 77 K and **216** at 298K in EPA. (λ_{ex} = 280 nm, λ_{em} = 350 nm, denoted by arrows on spectra)

It can be seen that the profiles are much more similar than when comparing **209** with BPEB, this also provides further evidence to suggest that in the low temperature sample both emission and excitation occurs from the twisted conformation, with the orbitals involved lying at the centre of the molecule.

To see where the transition between the two emission profiles seen for **209** occurs a variable temperature study of the fluorescence (Figure 4.26) was carried out.

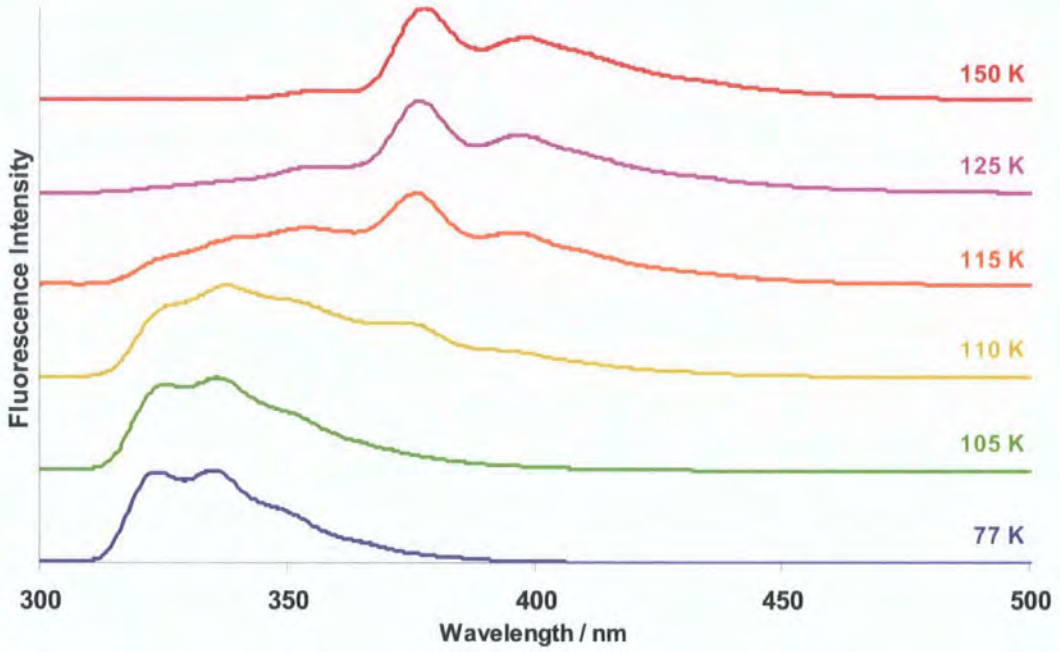

Figure 4.26: Normalised variable temperature emission of **209** in EPA (λ_{ex} = 275 nm).

This study showed that the change in the emission starts to occur around the glass transition temperature of EPA (T_g ~ 140 K)[24]. The high viscosity of the EPA glass below T_g will increase the time it takes for the for the compound to planarise. This means that planarisation now is a longer process than emission, and hence the twisted form is the emitting species.

The TMS substituted derivatives of BPEB were only studied at room temperature, and their emission-excitation profiles can be seen in Figure 4.27. The emission profiles of both compounds and the excitation profile of **224** resemble those of the BPEB parent.

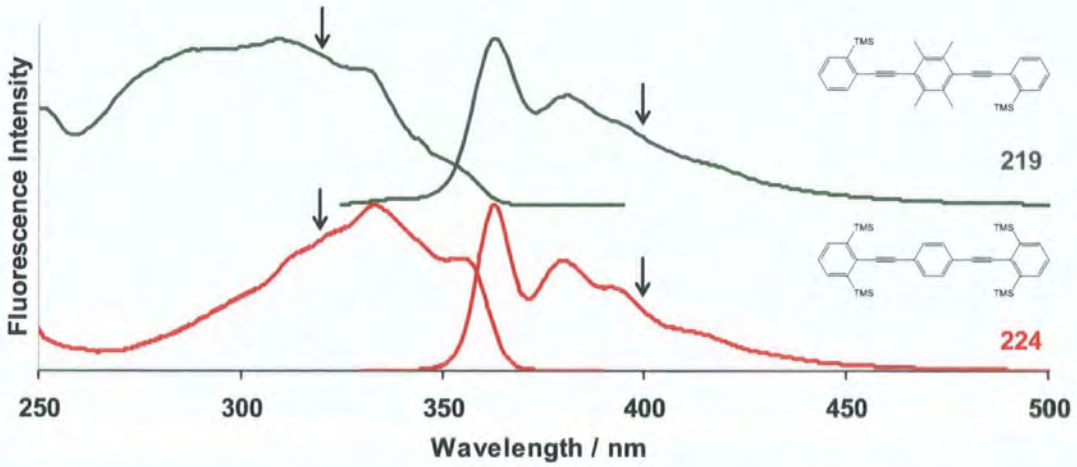

Figure 4.27: Comparison of the normalised Fluorescence emission-excitation profiles of **219** and **224** at 298K in cyclohexane. (λ_{ex} = 320 nm, λ_{em} = 4000 nm, denoted by arrows on spectra)

The excitation profile of **219** appears to have a broader absorption band than BPEB, the significance of which is unclear, and further studies of these systems would be of interest in the future.

Further information was gathered about the behaviour of the substituted BPEB derivatives by looking into their extinction coefficients, fluorescence lifetimes and photoluminescence quantum yields. This data can give an insight into the nature and efficiency of the fluorescence processes observed. A summary of this data obtained can be seen in Table 4.7.

Compound	ε / 10^3 $dm^3mol^{-1}cm^{-1}$ (λ / nm)	$\Phi_f \pm 0.05$	τ_f / ns	k_f / ns^{-1}
2	58.0 (320)[23]	0.79[25]	0.68[25]	1.16
188	73.8 (323)	0.76	0.63	1.20
189	45.0 (330)	0.79	0.72	1.10
201	51.0 (335)	0.87	0.68	1.29
202	40.4 (336)	0.85	0.69	1.23
208	65.9 (340)	0.81	0.70	1.16
209	66.1 (286)	0.59	0.69	0.86
219	33.5 (313)	0.88	0.72	1.22
224	61.1 (334)	0.86	0.73	1.18

Table 4.7. Photophysical data for BPEB as well as synthesised derivatives thereof. Lifetimes obtained by TCSPC. All measurements carried out in cyclohexane solution at 298K. ($k_f = \Phi_f / \tau_f$)

Upon comparing the different compounds, it can be seen that the addition of the various alkyl groups to the compounds has no significant effect on the fluorescence lifetime. This suggests that all the compounds emit from a similar electronic state, which is most likely to be the planarised form. Indeed, even the restriction of rotation observed in **209** does not have an adverse effect on the lifetime of the observed fluorescence at room temperature. This coupled with its emission profile at 298 K shows that whereas in the ground state the compound adopts a twisted conformation, upon excitation it is likely to planarise before emission.

Where the steric bulk does have an effect, however, is on the quantum yield of **209**, which is around 20 % lower than the other compounds studied. This extra loss in energy from the incident light can be attributed to an increase in non-radiative decay processes. These are occurring, in part at least, due to the increased energy gap arising from the increased barrier to rotation which must be overcome in order for the molecule to planarise before emitting.

The fluorescence profile of **209** undergoes a significant change at low temperature, thus it was of interest to study the effect the change in temperature has on its other photophysical properties. It was not possible to record quantum yields at low temperature with sufficient precision. Instead estimated values for the quantum yield at 77 K were obtained by comparing the non-normalised emission intensities of a specific compound at both 298 and 77 K. Due to refractive index changes at low temperature this does not give a totally accurate value and the actual value is likely to be higher.

Compound	τ_f / ns 298 K	τ_f / ns 77 K	Φ_f 298 K	Φ_f 77 K	k_f / ns^{-1} 298 K	k_f / ns^{-1} 77 K
208	0.70	0.77	0.81	> 0.70*	1.16	> 0.91
209	0.69	13.9	0.59	> 0.49*	0.86	> 0.035
216	12.9	-	-	-	-	-

Table 4.8: Effect of temperature on fluorescence lifetime and quantum yields of the hexa-*tert*-butyl-BPEB derivatives **208** & **209** in EPA. * Estimated value. ($k_f = \Phi_f / \tau_f$)

As shown in Table 4.8, in the EPA glass at 77 K there is a negligible difference on the photophysical properties of **208** at low temperature. The quantum yield of compound **209** is not particularly different in the low temperature glass, however there is a significant increase in the fluorescence lifetime. Indeed, this lifetime is similar to that of **216**, a result which agrees with the hypothesis that **209** emits from the twisted conformation with the chromophore located on the central ring.

4.3.1.2 - BPEA Derivatives

At room temperature the emission and excitation spectra of **211** are very similar to those of BPEA, as can be seen in Figure 4.28. The excitation spectra feature a broad, relatively featureless, band between approximately 350 and 480 nm. The emission of

light from these compounds occurs between around 450 and 550 nm, unlike the excitation spectra the emission spectra do display some vibrational fine structure.

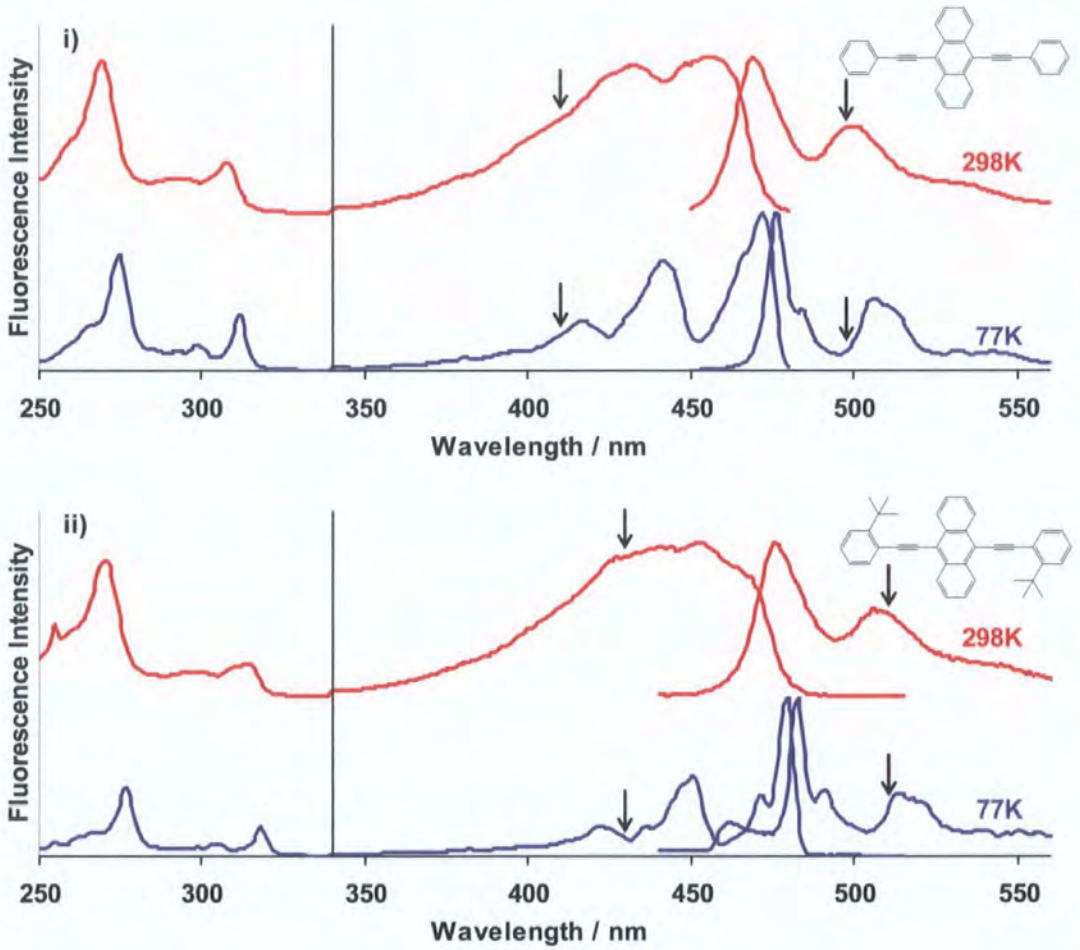

Figure 4.28: Normalised Fluorescence emission-excitation spectra of i) **31** (λ_{ex} = 410 nm, λ_{em} = 498 nm) and ii) **211** (λ_{ex} = 430 nm, λ_{em} = 511 nm) at 298 K and 77 K in EPA. (Arrows on spectra denote emission and excitation wavelengths). The excitation spectra have been scaled down by a factor of 4 for $\lambda < 340$ nm

At low temperature the vibrational structure in the emission spectrum of BPEA becomes more pronounced. The excitation spectrum starts to exhibit vibrational fine structure as well as a strengthening of the signal at the red edge and the profile is closer to being a mirror image of that of the emission. The low temperature spectra are also red shifted by around 300 cm^{-1} compared to the those observed at room temperature.

In general the observed photophysical behaviour of **211** at 77 K is fairly similar to that of BPEA. Also more significantly there is the appearance of an extra band at 464 nm in the spectrum. There are differences between the two, for example there is a greater amount of vibrational fine structure in **211**. The observed fine structure (similarly to

that for BPEA) has spacings characteristic to the presence of an anthracene chromophore, of the order of 1400 and 400 cm^{-1}.

The extra band seen for **211** is analogous to that seen in the emission spectrum of **189**, and is likely to occur from the presence of a small amount of a twisted conformation, with the majority of the emitting species being planar. With the crystal structure showing a twisted conformation, this result highlights how the solid state structure obtained for a compound cannot be relied upon to give information on its conformation in solution.

Compound **214** displays similar behaviour to that of **211** (Figure 4.29). At room temperature the emission and excitation spectra resemble those of BPEA, and in the viscous EPA glass at 77 K there is the emergence of increased vibrational structure, plus a new band on the blue edge of the emission spectrum at *ca.* 460 nm. This extra feature again shows that there is a small degree of restricted rotation in the molecule, with the single *tert*-butyl substituent being enough to affect the planarisation of the molecule in the EPA glass.

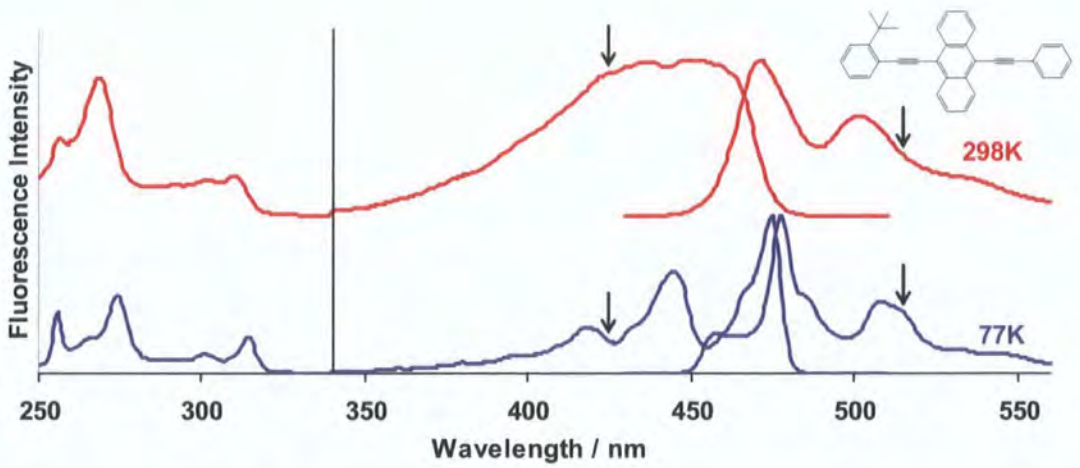

Figure 4.29: Normalised Fluorescence emission-excitation spectra of **214** at 298 K and 77 K in EPA. (λ_{ex} = 425 nm, λ_{em} = 515 nm, denoted by arrows on spectra). The excitation spectra have been scaled down by a factor of 4 for λ < 340 nm.

The room temperature spectra of **212** are again similar to those of BPEA and are given in Figure 4.30, however no low temperature spectra were recorded.

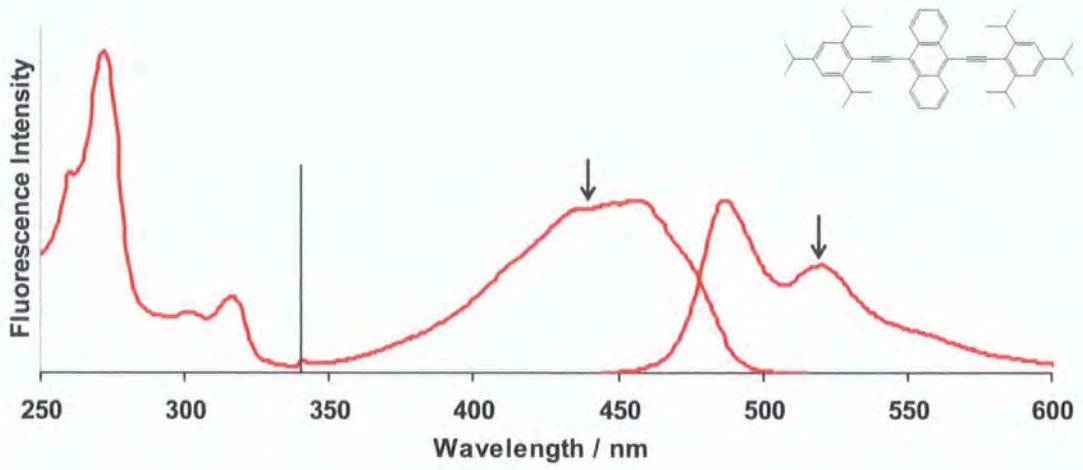

Figure 4.30: Normalised Fluorescence emission-excitation spectra of **212** at 298 K in cyclohexane. (λ_{ex} = 440 nm, λ_{em} = 520 nm, denoted by arrows on spectra). The excitation spectrum has been scaled down by a factor of 2 for $\lambda < 340$ nm.

Hexa-*tert*-butyl-BPEA, **213**, as with its BPEB analogue, **209**, shows significantly different behaviour compared to that of the BPEA parent (Figure 4.31). The room temperature excitation spectrum of **213** shows vibronic structure, the progression of which has an anthracene characteristic spacing of 1380 cm^{-1}. This absorption band lies between about 350 and 455 nm, and is slightly blue shifted in relation to the first absorption band of BPEA. The room temperature emission spectrum has a broad emission band with a larger Stokes shift than seen for BPEA. This Stokes shift is of the order of 2500 cm^{-1} and suggests that, like in **209**, there is a conformational change on excitation, with the twisted molecule reorientating to a more planar form before emission can occur.

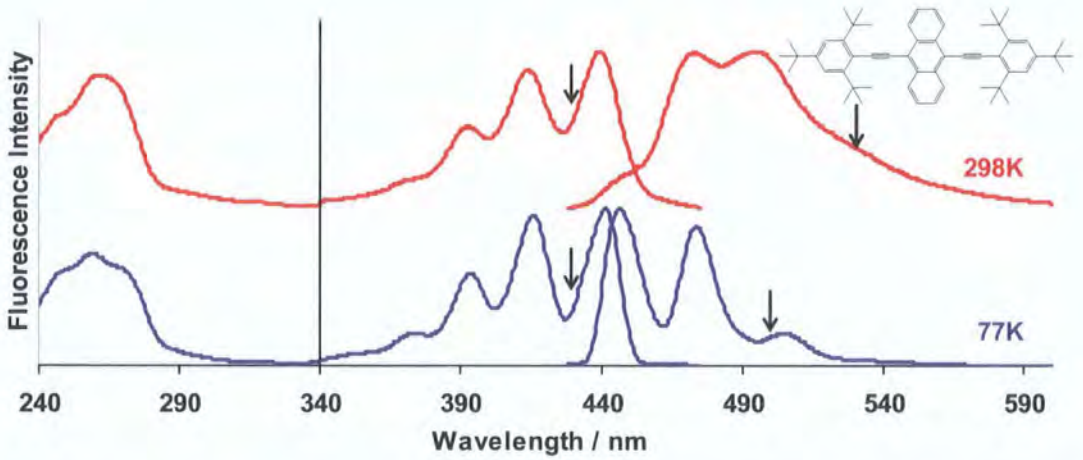

Figure 4.31: Normalised Fluorescence emission-excitation spectra of **213** at 298 K (λ_{ex} = 430 nm, λ_{em} = 530 nm) and 77 K (λ_{ex} = 430 nm, λ_{em} = 500 nm) in EPA (Arrows on spectra denote emission and excitation wavelengths). The excitation spectra have been scaled down by a factor of 2 for $\lambda < 340$ nm.

In the EPA glass at 77 K there is no significant change to the excitation profile of **213** from that seen at room temperature, however the emission spectrum does exhibit a change. At 77 K it undergoes a significant blue shift and develops vibronic structure, becoming a mirror image of the low energy absorption band. As seen for the BPEB analogue, this low temperature fluorescence spectrum only has a small Stokes shift compared to the room temperature spectrum. From this it can be concluded that emission is most likely occurring from a twisted conformation, with reorientation of the molecule not being possible on a fluorescence timescale. Indeed, the emission and excitation observed at 77 K are very similar to those seen for 9,10-bis(trimethylsilylethynyl)anthracene, **226**, at room temperature - which has a similar chromophore to that expected for the twisted form.

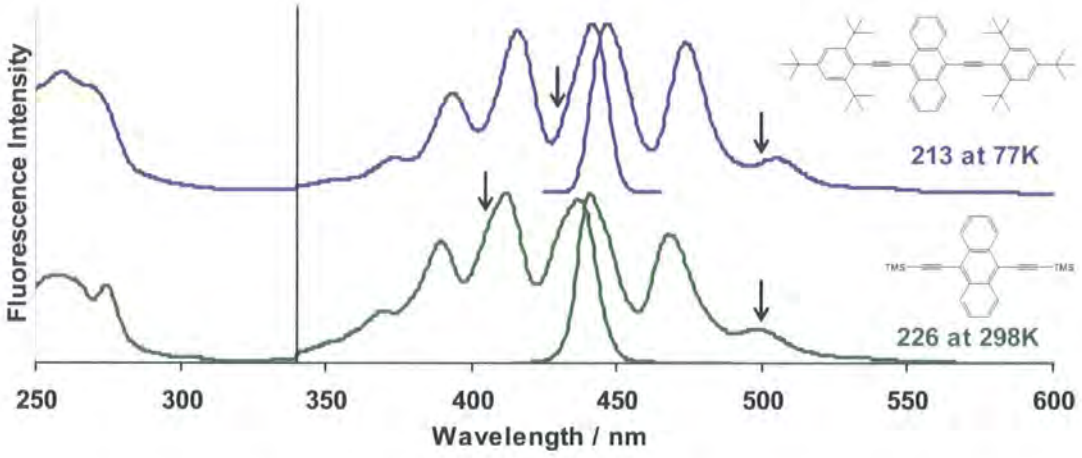

Figure 4.32: Comparison of the normalised Fluorescence emission-excitation profiles of **213** at 77 K (λ_{ex} = 280 nm, λ_{em} = 350 nm) and **226** at 298K (λ_{ex} = 405 nm, λ_{em} = 500 nm) in EPA. (Arrows on spectra denote emission and excitation wavelengths). The excitation spectra have been scaled down by a factor of 2 for $\lambda < 340$ nm.

As for the BPEB derivative **209**, theoretical calculations were carried out in CAChe to look at the nature of the excited state of **213** and to compare it with those of **31** and **226**. The structures were optimised using a semi-empirical calculations (MOPAC, PM5) before calculation of the electronic transitions using ZINDO INDO-S. As with the BPEB systems the calculations showed that the first excited state arises from a LUMO ← HOMO transition, although the energies calculated for these were overestimated. The calculated wavelengths for the transitions were 400 (**213**), 407 (**31**) and 375 nm (**226**).

The calculation of the transitions also allowed the visualisation of the frontier orbitals of these compounds. These showed that the twist in the structure of **213** has the same effect on these orbitals as seen for **209**, with them being located on the anthracene and acetylene groups and not on the outer, orthogonal rings. These orbitals resemble those of **226** and not those seen for **31**, supporting the theory that the emission at low temperature is seen from the twisted conformation as opposed to a planar one.

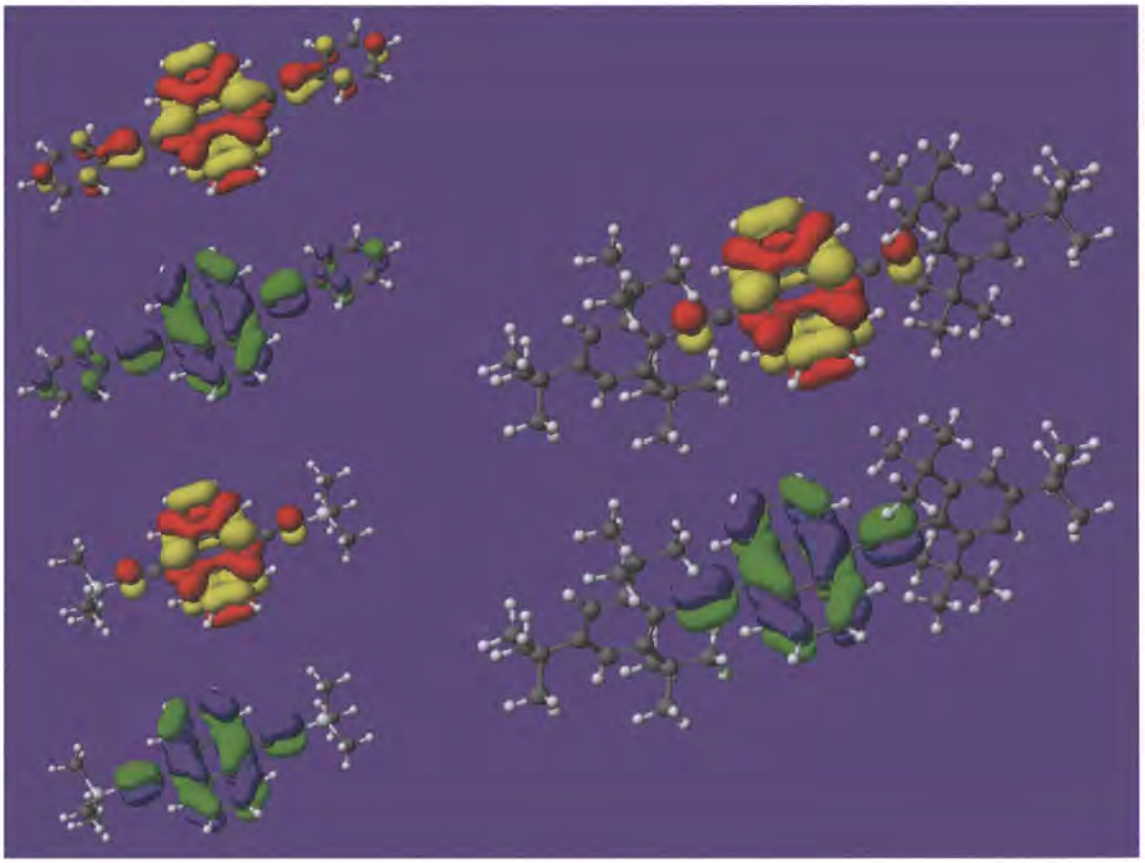

31 **213**

226

Figure 4.33: HOMOs (blue/green) and LUMOs (red/yellow) for compounds **31**. **226** and **213**, calculated using CAChe.

The result from these theoretical calculations correlates with those seen for **209**. In both cases the *tert*-butyl substituents on the external rings prevent planarisation in the ground state and therefore restrict the orbitals involved in fluorescence to the central part of the molecule.

The photophysical parameters for the BPEA derivatives are of interest. These allow a more detailed insight into the nature of the processes occurring. A summary of the

extinction coefficients, fluorescence quantum yields and lifetimes recorded are shown in Table 4.9.

Compound	ε / 10^3 $dm^3mol^{-1}cm^{-1}$ (λ / nm)	Φ_f Error ± 0.1	τ_f / ns	k_f / ns^{-1}
211	31.6 (454)	0.98	3.00	0.33
214	32.6 (452)	0.98	3.02	0.32
212	37.3 (454)	0.97	2.80	0.35
213	44.9 (441)	0.84	3.07	0.27

Table 4.9: Photophysical data for compounds **211** - **214**. Lifetimes obtained by TCSPC. All measurements carried out in cyclohexane solution at 298K. ($k_f = \Phi_f / \tau_f$)

In general all four compounds display similar photophysical behaviour, the very high quantum yields obtained for **211**, **212** and **214** showing that virtually none of the excited state deactivation occurs via non-radiative pathways. Compound **213** however has a slightly lower quantum yield, closer to that of **226**, indicating a greater amount of non-radiative decay for these two compounds.

Compound	τ_f / ns 298 K	τ_f / ns 77 K	Φ_f 298 K	Φ_f 77 K	k_f / ns^{-1} 298 K	k_f / ns^{-1} 77 K
31	3.40	3.17	0.98	-	0.29	-
211	3.55	3.32	0.98	-	0.28	-
213	3.46	4.02	0.84	> 0.77*	0.24	> 5.22*
226	5.69	5.30	0.80	-	0.14	-

Table 4.10: Effect of temperature on photophysical data of compounds **31**, **211**, **213** and **226** in EPA. ($k_f = \Phi_f / \tau_f$). * Estimated value.

In EPA BPEA and its derivative **211** see an unusual slight decrease in their fluorescence lifetime on going from 298 to 77 K. More commonly the reduction of non-radiative processes at low temperature results in an increased lifetime. However, these systems have quantum yields that are close to unity and as such see almost no deactivation of the S_1 state via non-radiative decay. The refractive index of the solution increases on cooling, leading to an increase in the rate of the radiative decay processes and hence a shortening of the lifetime of **31** and **211** is observed.[26] Compound **213** however shows the opposite behaviour, with its lifetime increasing as the temperature decreases. As with compound **209**, the low temperature quantum yield could only be estimated, with a

value being determined by comparing the emission intensities at the two temperatures and using the ratio of the two to determine a value from the 298 K figure. The value obtained is not significantly different, and the difference in lifetime is likely to be down to the nature of the planar and twisted emitting states.

4.4 - Conclusions

The work in this chapter has shown that it is possible to use steric bulk to restrict the rotation about the acetylenic bond in aryleneethynylenes with a noticeable effect on the behaviour of the compounds' behaviour. The initial approach of adding a single *tert*-butyl group adjacent to the acetylene moiety proved unsuccessful in substantially restricting the molecule. A small degree of rotation was observed in the solid state for compounds **188** and **189**, but the steric interactions between the *tert*-butyl group and the substituents on the central ring were minimised mainly through the bending of the acetylene bond. The observed photophysics were similar to those of BPEB, with the only evidence of any effect from the added bulk coming from a small extra band at the blue edge of the low temperature emission spectrum. This band resulted from a small number of molecules that were not able to fully planarise on the fluorescence timescale.

211 has a twisted structure in the solid state, although this is most likely due to packing effects, with the similar asymmetric compound **214** having a planar structure. Once again in solution state these compounds were similar to the parent compound (BPEA), with the only evidence of the added bulk again coming from the appearance of an extra band at the blue edge of the emission at low temperature.

The next approach of using two *iso*-propyl groups adjacent to the acetylene bond proved less successful than the single *tert*-butyl group. The *iso*-propyl groups are able to rotate to minimise steric strain, with the lone hydrogen atom facing towards the centre of the molecule. There was still some effect on the rotation of the molecule seen in the low temperature photophysics of compounds **201** and **202** where a shoulder was observed at the blue edge of the emission spectra.

Increasing the bulk further to two *tert*-butyl groups adjacent to the acetylene did result in conformational restriction. With just a central phenyl ring, compound **208** showed the least effect of this extra bulk. In the solid state the central ring is twisted *ca.* 35° out

of the plane of the external rings, and shows a greater amount of vibronic structure in both the emission and excitation spectra at low temperature, as well as the extra band at the blue edge of the emission.

Compound **209** has the central durene moiety orthogonal to the outer two rings in the solid state with crystals of **213** proving not possible to obtain in sufficient quality for X-ray crystallographic analysis. Both these compounds display a large Stokes shift in their room temperature spectra, with the excitation blue shifted relative to that of their respective parent molecules, and the excitation of **213** showing vibronic structure. The room temperature emission spectra were similar to the parents, albeit with the extra band at the blue edge that was previously visible in other compounds at low temperature.

At low temperature **209** and **213** have relatively unchanged excitation spectra, and blue shifted emission spectra relative to the room temperature observations, and thus a lowered Stokes shift. These low temperature spectra, as well as the theoretically obtained HOMO and LUMOs are very similar to those obtained for compounds **216** and **226**, with the molecules' chromophores located on the central rings and acetylene groups. Thus the steric bulk in these systems is affecting the conformation of the compounds and restricting rotation about the long axis of the molecule.

4.5 - References

1. G. Brizius and U. H. F. Bunz, *Org. Lett.*, 2002, ***4***, 2829-2831.
2. G. Brizius, K. Billingsley, M. D. Smith and U. H. F. Bunz, *Org. Lett.*, 2003, ***5***, 3951-3954.
3. G. T. Crisp and T. P. Bubner, *Tetrahedron*, 1997, ***53***, 11881-11898.
4. S. A. McFarland and N. S. Finney, *J. Am. Chem. Soc.*, 2002, ***124***, 1178-1179.
5. G. T. Crisp and T. P. Bubner, *Tetrahedron*, 1997, ***53***, 11899-11912.
6. A. Mortreux and M. Blanchard, *J. Chem. Soc.-Chem. Commun.*, 1974, 786-787.
7. P. Y. Bruice, *Organic Chemistry*, Second ed.; Prentice-Hall International: London, 1998.
8. O. Mitsunobu, *Synthesis*, 1981, 1-28.
9. O. F. Koentjoro. *Synthetic and Computational Studies of Conjugated Acetylenic Systems*, University of Durham 2003.
10. Gaussian 03, Revision C.02, M. J. Frisch, G. W. Trucks, H. B. Schlegel, G. E. Scuseria, M. A. Robb, J. R. Cheeseman, J. A. M. Jr., T. Vreven, K. N. Kudin, J. C. Burant, J. M. Millam, S. S. Iyengar, J. Tomasi, V. Barone, B. Mennucci, M. Cossi, G. Scalmani, N. Rega, G. A. Petersson, H. Nakatsuji, M. Hada, M. Ehara, K. Toyota, R. Fukuda, J. Hasegawa, M. Ishida, T. Nakajima, Y. Honda, O. Kitao, H. Nakai, M. Klene, X. Li, J. E. Knox, H. P. Hratchian, J. B. Cross, C. Adamo, J. Jaramillo, R. Gomperts, R. E. Stratmann, O. Yazyev, A. J. Austin, R. Cammi, C. Pomelli, J. W. Ochterski, P. Y. Ayala, K. Morokuma, G. A. Voth, P. Salvador, J. J. Dannenberg, V. G. Zakrzewski, S. Dapprich, A. D. Daniels, M. C. Strain, O. Farkas, D. K. Malick, A. D. Rabuck, K. Raghavachari, J. B. Foresman, J. V. Ortiz, Q. Cui, A. G. Baboul, S. Clifford, J. Cioslowski, B. B. Stefanov, G. Liu, A. Liashenko, P. Piskorz, I. Komaromi, R. L. Martin, D. J. Fox, T. Keith, M. A. Al-Laham, C. Y. Peng, A. Nanayakkara, M. Challacombe, P. M. W. Gill, B. Johnson, W. Chen, M. W. Wong, C. Gonzalez and J. A. Pople, Gaussian, Inc., Wallingford CT, 2004,
11. M. S. Lesslie and U. J. H. Mayer, *J. Chem. Soc.*, 1961, 611-618.
12. K. Sonogashira, Y. Tohda and N. Hagihara, *Tetrahedron Lett.*, 1975, 4467-4470.
13. L. Fogel, R. P. Hsung, W. D. Wulff, R. D. Sommer and A. L. Reingold, *J. Am. Chem. Soc.*, 2001, ***123***, 5580-5581.
14. P. Delair, A. M. Kanazawa, M. B. M. deAzevedo and A. E. Greene, *Tetrahedron: Asymmetry*, 1996, *7*, 2707-2710.
15. R. Knorr, J. Ruhdorfer, P. Böhrer, H. Bronberger and E. Räpple, *Liebigs Ann. Chem.*, 1994, 433-438.
16. H. E. Zimmerman and J. R. Dodd, *J. Am. Chem. Soc.*, 1970, ***92***, 6507-6515.
17. P. G. Urben, *Bretherick's Handbook of Reactive Chemical Hazards Vol 1*, 5th ed.; Butterworth-Heinemann Ltd: Oxford, 1995.
18. P. Nguyen, S. Todd, D. Vandenbiggelaar, N. J. Taylor, T. B. Marder, F. Wittmann and R. H. Friend, *Synlett*, 1994, 299-301.
19. Data extracted from Cambridge Structural Database V 5.27, Nov. 2005, LEPPIF, F. H. Allen, *Acta Crystallogr.*, 2002, **B58**, 380.
20. M. Yamaguchi, Y. Tsukamoto, C. Ikeura, S. Nakamura and T. Minami, *Chem. Lett.*, 1991, 1259-1262.
21. M. Levitus and M. A. Garcia-Garibay, *J. Phys. Chem. A*, 2000, ***104***, 8632-8637.
22. M. Levitus, K. Schmieder, H. Ricks, K. D. Shimizu, U. H. F. Bunz and M. A. Garcia-Garibay, *J. Am. Chem. Soc.*, 2001, ***123***, 4259-4265.
23. A. Beeby, K. Findlay, P. J. Low and T. B. Marder, *J. Am. Chem. Soc.*, 2002, ***124***, 8280-8284.

24. C. F. Stanley. *Photophysical evaluation of substituted zinc phthalocyanines as sensitisers for photodynamic therapy*, University of Durham 1997.
25. U. W. Grummt, E. Birckner, E. Klemm, D. A. M. Egbe and B. Heise, *J. Phys. Org. Chem.*, 2000, ***13***, 112-126.
26. R. A. Lampert, S. R. Meech, J. Metcalfe, D. Phillips and A. P. Schaap, *Chem. Phys. Lett.*, 1983, ***94***, 137-140.

CHAPTER 5

CONCLUSIONS AND FURTHER WORK

5.1 - Study of Aryleneethynylene Series

The initial studies into BPEB analogues showed that superficially the choice of aromatic rings does not have a large effect on the photophysical behaviour observed. The emission and excitation profiles of the compounds tested are all similar with broad featureless excitation spectra and emission spectra showing vibronic structure at room temperature. The wavelengths the profiles are observed at is the most obvious difference between compounds, all of which were found to be red shifted in relation to the BPEB parent. The choice of central ring was observed to lead to the greatest change in photophysical behaviour, due to the greater contribution to the molecular orbitals involved in the transitions coming from the centre of the molecules.

Where investigated, the low temperature spectra of the compounds in an EPA glass also behaved in a similar way to BPEB, with the appearance of fine structure and enhancement of the red edge of the spectrum observed in the excitation spectra. This is accompanied by a sharpening of the fine structure in the emission spectrum. At low temperature there is more of a mirror-image relationship between the emission and excitation profiles, showing that the absorbing and emitting states have more similar structures. This is due the lower energy of the system at low temperature leading to a decreased population of molecules that show rotation about the acetylenic axis and thus an increase in the population of the planar conformation.

Closer examination of the compounds by observing their photophysical parameters showed greater differences in behaviour between the different series studied. The naphthalene based systems were the most BPEB-like, with the quantum yields and fluorescence lifetimes observed being fairly similar. The incorporation of the five ring, heteroaromatic, thiophene moiety resulted in compounds that show a poorer photophysical behaviour. The observed parameters are vastly reduced, especially in compounds **113** and **159**.

5.2 - Twisting a Molecular Wire

The studies into the use of steric bulk to restrict rotation about the acetylenic groups proved successful. The inclusion of a single *tert*-butyl group or two *iso*-propyl groups on the outer rings, adjacent to the acetylenic bond, showed some evidence of rotational restriction at low temperature, with the appearance of an extra band at the blue edge of the emission profiles observed. The *iso*-propyl approach was the least successful, due to the steric bulk rotating away from the centre of the molecule to reduce strain. In the solid state structure of the BPEB analogues **188** and **189** it could be seen that the single *tert*-butyl group causes a small degree of rotation about the long axis, although most of the steric strain appears to be reduced by a bending of the acetylenic group.

The incorporation of a second *tert*-butyl group adjacent to the acetylene prevented the resultant compounds from bending to relieve strain, leaving rotation about the acetylene group as the only route to a lower energy conformation. Of compounds **208, 209** and **213**, **208** showed the least effect from this, due to the lack of substituents on the central benzene ring. **209** and **213**, with their central durene and anthracene ring systems showed the most dramatic effect, with the excitation spectra shifted to higher energy at room temperature (relative to the BPEB and BPEA parents). At low temperature the observed emission spectra were also seen to be blue shifted.

Schematic diagrams of the energy processes involved are shown in Figure 5.1. In BPEB the lowest energy conformation is the planar form, although at room temperature the difference in energy between the planar and twisted forms is of the same order as kT. Excitation of the molecule from S_0 to S_1 occurs from all possible conformations followed by the molecule relaxing into to the planar form in the excited state before emission occurs. At low temperature, kT is reduced, leading to a greater population of the planar conformation in the S_0 state, hence the observed emphasis of the red-edge (low energy) of the spectrum. Relaxation to the planar form in the S_1 state for any non-planar molecules present is slower at low temperature, but is still fast on the fluorescence timescale, and so the emission is relatively unchanged (Figure 5.1(i)).

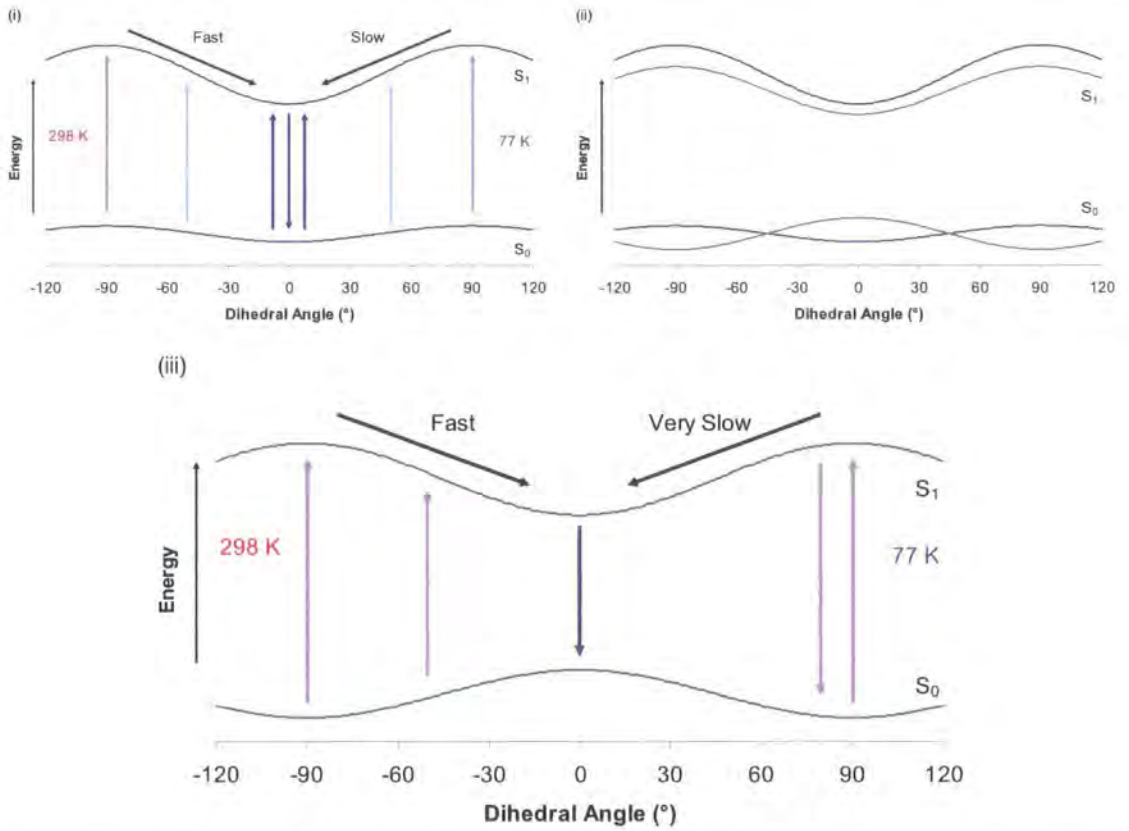

Figure 5.1: Schematic diagrams showing the effect of rotation on the energy levels (and hence the photophysical transitions) of BPEB (—) and **209** (—) at both low and high temperature. (i) photophysical processes for BPEB, (ii) comparison between rotational profiles of BPEB and **209**, (iii) probable photophysical processes for **209**.

A probable comparison between the rotational profiles for BPEB and **209** is shown in Figure 5.1(ii). The ground state of **209** is at the lowest energy at an angle of 90°, with a greater potential well than seen for BPEB. In the S_1 state the planar conformation is still the lowest energy, albeit with a reduced potential well compared to that of **2**. At room temperature this leads to the majority of the excitation occurring from the twisted conformation with the molecule relaxing down to the planar conformation in the excited state before emission can occur. At low temperature the molecule absorbs purely from the twisted conformation, and in the excited state the relaxation to the planar form is slower than the rate of fluorescence, probably due to solvent viscosity, with emission observed from the twisted conformation (Figure 5.1(iii)).

This is supported by the theoretical calculation of the molecular orbitals involved. The twist in the molecule seen for **209** means that the HOMO and LUMO are located on the acetylene groups and the central ring, and not on the outer rings as seen for BPEB. The emission and excitation spectra observed for **209** at low temperature are similar to those of the room temperature spectrum of **216** which has similar frontier orbitals.

5.3 - Further Work

It would be of interest in the future to expand the study of the aryleneethynylene series described in Chapter 3. One series that would be of interest to synthesise would be one incorporating the thiophene-1,1-dioxide unit in the BPEB-type compound. The theoretical calculation of the electronic transitions for **162** carried out in this work indicate that the first excited state occurs via a LUMO ← HOMO transition as well as a second (LUMO+1) ← (HOMO-2) transition. It would be interesting to observe the photophysics of this compound to see what difference, if any, this second transition would have on the compounds' behaviour, compared to the other systems studied, which just display a LUMO ← HOMO transition. Therefore the series of compounds shown in Figure 5.2 could be synthesised.

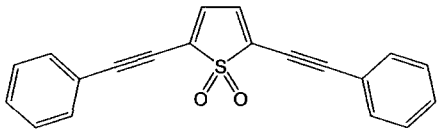

162

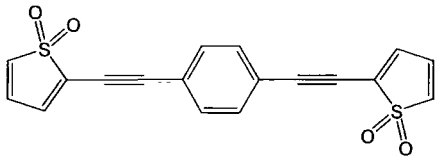

227

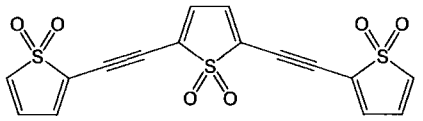

228

Figure 5.2: Potential series of aryleneethynylenes containing the 2,5-dibromothiophene-1,1-dioxide moiety.

This series could be synthesised using the Sonogashira coupling approach used to make the thiophene series described in chapter 3. This method would initially require the preparation of both mono and dibromo substituted thiophene-1,1-dioxide.

The synthesis (shown in Chapter 3) of 2,5-dibromothiophene-1,1-dioxide, **153**, used by Yamamoto *et al.*[1] was first reported by Miyahara and Inazu in 1990.[2] They prepared a solution of dimethyldioxirane by the oxidation of acetone with potassium monopersulfuric acid. A cold solution of 2,5-dibromothiophene, **114**, in methylene chloride was added to the dimethyldioxirane to yield 27 % product.[2]

This approach however would not be a viable approach for the synthesis of 2-bromothiophene-1,1-dioxide, **229**. Miyahara and Inazu found that in the oxidation of thiophenes with a substituent merely in the 2-position the product could not be isolated due to Diels-Alder dimerisation as well as further side reactions.[2]

A more useful approach could be that of Nenajdenko *et al.* who oxidised the thiophene system *via* the use of trifluoroperacetic acid in acetonitrile, Scheme 5.1. The reagent was prepared by the cautious addition of trifluoroacetic anhydride to an ice cold mixture of acetonitrile and hydrogen peroxide. The oxidation reaction proceeded via the addition of a solution of a substituted thiophene to this mixture.[3]

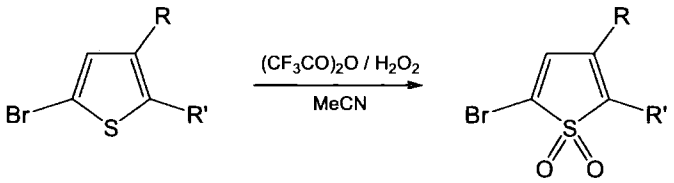

114	R = H, R' = Br	**153**
230	R = Br, R' = H	**232**
231	R= Br, R' = Br	**233**

Scheme 5.1: Nenajdenko *et al.*'s synthetic route to bromo-substituted thiophene-1,1-dioxides.[3]

They carried out this reaction on three bromo-substituted thiophene starting materials, obtaining the oxidised compounds **153**, **232** and **233** in 82, 42 and 85 % yields respectively. No synthesis was reported of 2-bromothiophene-1,1-dioxide and the synthesis would be worth investigating to see if it is a viable route. If side reactions do occur then a sigma-bonded 5-substituent such as a methyl group could be used to protect the system from unwanted reactions.

The work on conformational restriction of aryleneethynylenes could be furthered in several different ways. Firstly the synthesis of 1,4-bis(2,6-bis(trimethylsilyl) phenylethynyl)durene, **225**, needs to be optimised. Attempts at coupling 2-ethynyl-1,3-bis(trimethylsilyl)benzene, **220**, to 1,4-diiododurene, **193** during this research proved unsuccessful with no optimisation of the conditions possible. Therefore the reaction should be looked at again, varying the solvent mixture, concentration of catalyst and reaction temperature used to allow the product to be formed in sufficient yield.

A second approach could be to produce a 'half-twisted' system such as compound **230**. Retrosynthesis of this compound is shown in Scheme 5.2. The photophysical behaviour of such a system would be of interest. From the results described in Chapter 4, it would be expected that the tri(*tert*-butyl)benzene ring would be rotated out of the plane of the molecules, with only the other two phenyl rings involved in the frontier orbitals and hence the behaviour of the transitions to/from the first excited state.

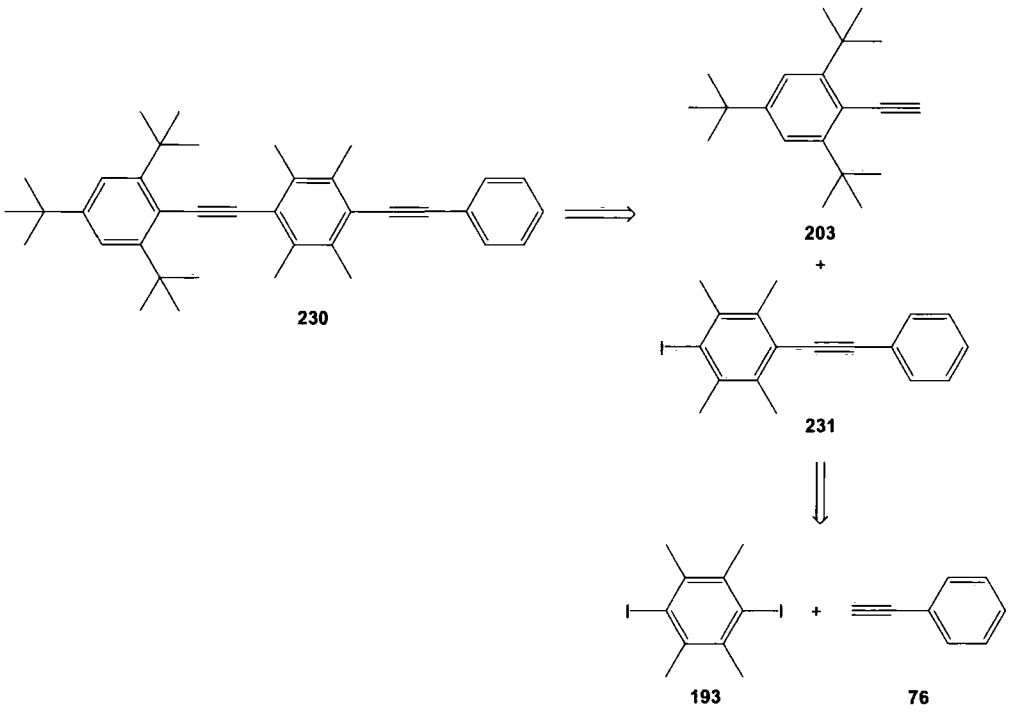

Scheme 5.2: Retrosynthetic study of a potential 'half-twisted' derivative of BPEB.

Another approach into a conformationally restricted system would be to make tethered systems similar to those of Crisp and Bunz,[4-6] albeit with the tethers attached by silicon atoms instead of oxygen. Initially the synthesis of a tethered tolan system should be attempted to determine the best synthetic approach.

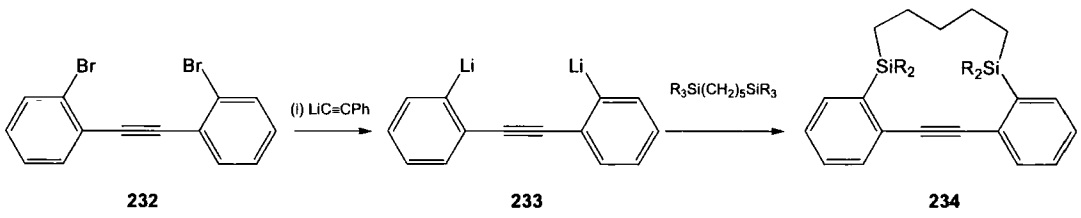

Scheme 5.3: Proposed route into a silane-tethered tolan system.

A proposed potential route into a two ring tethered system, **234**, is shown in Scheme 5.3. This approach involves the lithiation of di(2-bromophenyl)acetylene, **232**,

followed by the subsequent addition of a dilute solution of disilylalkane. The dilute solution should help prevent the substitution of one molecule with more than one disilylalkane group. If successful this could then be extended to longer phenylethynyl systems.

5.4 - References

1. T. Yamamoto, I. Nurulla, H. Hayashi and H. Koinuma, *Synth. Met.*, 1999, ***107***, 137-141.
2. Y. Miyahara and T. Inazu, *Tetrahedron Lett.*, 1990, ***31***, 5955-5958.
3. V. G. Nenajdenko, A. E. Gavryushin and E. S. Balenkova, *Tetrahedron Lett.*, 2001, ***42***, 4397-4399.
4. G. Brizius and U. H. F. Bunz, *Org. Lett.*, 2002, ***4***, 2829-2831.
5. G. Brizius, K. Billingsley, M. D. Smith and U. H. F. Bunz, *Org. Lett.*, 2003, ***5***, 3951-3954.
6. G. T. Crisp and T. P. Bubner, *Tetrahedron*, 1997, ***53***, 11881-11898.

CHAPTER 6

SYNTHESIS

6.1 - General Considerations

All experiments were conducted in standard Quickfit glassware. Where necessary, reactions were performed under an atmosphere of dry nitrogen using standard Schlenk techniques. Dry solvents were freshly distilled under nitrogen from sodium / benzophenone (diethyl ether, THF), potassium hydroxide (triethylamine) or obtained dry from an Innovative Technologies Solvent Purification System and deoxygenated prior to use. Starting materials were obtained from Sigma Aldrich, Avocado and Lancaster and used without further purification, with the exception of 1-ethynyl naphthalene, bis(triphenylphosphine)palladium (II) dichloride and tetrakis(triphenyl phosphine) palladium (0) which were kindly provided by the research group of Dr P. J. Low.

Laboratory coat, safety spectacles and gloves were worn at all times and all experiments conducted in an efficient fume-hood, following completion of appropriate COSHH assessments. Waste products and residues were treated appropriately and returned for disposal following separation.

Routine NMR spectra were collected at ambient temperature using Varian Mercury 200, Varian Unity 300, Varian Mercury 400, Bruker Advance 400 and Varian Inova 500 machines. Chemical shifts were referenced to either the residual protio impurities in the deuterated chloroform solvent (^{1}H, δ7.27, singlet) or the ^{13}C shift of the solvent (^{13}C, δ77.2, triplet).

Both regular and high resolution EI mass spectra were recorded on a Micromass Autospec instrument and are reported in (m/z). GC-MS analyses were performed using a Thermo Finnegan TRACE MS machine. MALDI MS was carried out on an Applied Biosystems Voyager-DE STR machine. Elemental analyses were carried out using an Exeter Analytical Inc. CE-440 Elemental Analyser (C, H, N) and a Dionex DX-120 Ion Chromatograph (S).

6.2 - Experimental Details

1,4-Dibromonaphthalene (107)

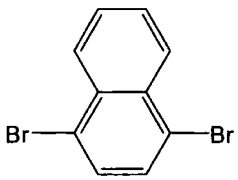

The method described by Cakmak et al.[1] was followed with slight adaptation. Naphthalene (5.13 g, 40 mmol) was dissolved in dichloromethane (DCM) (40 mL) and cooled to -10 °C. Bromine (4.4 mL, 85.9 mmol) was then added and the reaction stirred at -10 °C for two hours after which time the mixture was left to stand for 3 days at the same temperature. The solvent was removed under reduced pressure and the crude product passed through a silica plug with hexane as the eluent to remove baseline impurities. The solvent was then removed and the product recrystallised from hexane to give **107** (7.92 g, 69 %) as white needle shaped crystals.

M.P.: 81 °C. ^{1}H NMR (300MHz, $CDCl_3$): δ_H 8.29-8.23 (m, 2H, Np-H), 7.68-7.63 (m, 2H, Np-H), 7.64 (s, 2H, Np-H). $^{13}C\{^1H\}$ NMR (75.4MHz, $CDCl_3$) δ_c 133.2, 130.3, 128.4, 128.0, 122.8

1,4-Bis(phenylethynyl)naphthalene (60)

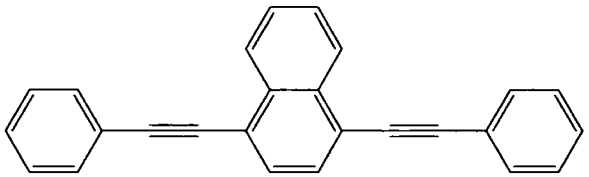

1,4-Dibromonaphthalene (0.5 g, 1.75 mmol) and phenylacetylene (0.58 mL, 5.24 mmol) were dissolved in dry triethylamine (20 mL). The solution was then degassed by three freeze-pump-thaw cycles. To this was added CuI (0.010 g, 0.052 mmol) and $Pd(PPh_3)_2Cl_2$ (0.037 g, 0.052 mmol) and the resultant mixture was refluxed for 16 h under nitrogen. After this time the solvent was removed and the product chromatographed on silica with a 1:1 DCM/hexane mixture. After solvent removal the product was recrystallised from cyclohexane to give **60** (0.49 g, 85 %) as white platelike crystals.

M.P.: 156 °C. ^{1}H NMR (500MHz, $CDCl_3$): δ_H 8.50-8.46 (m, 2H, Np-H), 7.75 (s, 2H, Np-H), 7.68-7.64 (m, 6H, Ar-H), 7.44-7.37 (m, 6H, Ph-H). $^{13}C\{^1H\}$ NMR (125MHz, $CDCl_3$) δ_c 133.3, 131.9, 129.9, 128.9, 128.7, 127.5, 126.9, 123.4, 121.8, 96.2, 87.8. MS (EI): (*m/z*) 328 $[M]^+$, 164 $[M]^{2+}$. Anal. Calcd. for $C_{26}H_{16}$: C, 95.09 %; H, 4.91 %. Found: C, 94.67%, H 4.72%

1,4-Bis(naphthalene-1-ylethynyl)benzene (83)

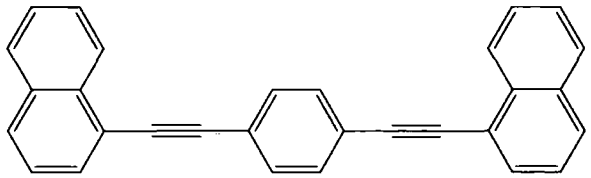

1,4-Diiodobenzene (0.43 g, 1.31 mmol) and 1-ethynylnaphthalene (0.47 mL, 3.29 mmol) were dissolved in dry triethylamine (20 mL). The solution was then degassed by three freeze-pump-thaw cycles. To this was added CuI (7.5 mg, 0.039 mmol) and $Pd(PPh_3)_2Cl_2$ (27.7 mg, 0.039 mmol) and the resultant mixture was stirred under nitrogen for one hour at 25 °C. After this time the solvent was removed and the product chromatographed on silica with DCM. After solvent removal the product was recrystallised twice from DCM/Hexane (1:1) to give **83** (0.27 g, 54 %) as white platelike crystals.

M.P.: 160 °C. ^{1}H NMR (500MHz, $CDCl_3$): δ_H 8.45 (d, 2H, Np-H, J_{HH}=8.0), 7.88 (t, 4H, Np-H, J_{HH}=8.0), 7.79 (d, 2H, Np-H, J_{HH}=7.0), 7.68 (s, 4H, Ph-H), 7.63 (t, 2H, Np-H, J_{HH}=7.5) , 7.56 (t, 2H, Np-H, J_{HH}=7.5), 7.49 (t, 2H, Np-H, J_{HH}=8.0). $^{13}C\{^1H\}$ NMR (125MHz, $CDCl_3$) δ_c 133.5, 131.9, 130.8, 129.3, 128.6, 127.1, 126.8, 126.4, 125.6, 123.6, 120.9, 94.3, 89.8. MS (EI): (*m/z*) 378 $[M]^+$, 189 $[M]^{2+}$. Anal. Calcd. for $C_{26}H_{16}$: C, 95.21 %; H, 4.79 %. Found: C, 95.06%, H 4.68%

1,4-Bis(naphthalene-1-ylethynyl)naphthalene (84)

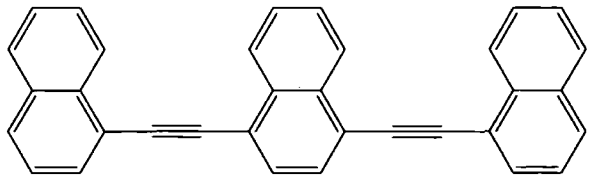

1,4-Dibromonaphthalene (0.38 g, 1.31 mmol) and 1-ethynyl-naphthalene (0.47 mL, 3.29 mmol) were dissolved in dry triethylamine (20 mL). The solution was then degassed by three freeze-pump-thaw cycles. To this was added CuI (7.5 mg, 0.039 mmol) and $Pd(PPh_3)_2Cl_2$ (27.7 mg, 0.039 mmol) and the resultant mixture was refluxed under nitrogen for 16 h. After this time the solvent was removed and the product chromatographed on silica with DCM. After solvent removal the product was recrystallised from layered DCM/Hexane to give **84** (0.16 g, 29 %) as white platelike crystals.

M.P.: 213 °C. ^{1}H NMR (500MHz, $CDCl_3$): δ_H 8.66-8.62 (m, 2H, Np-H), 8.58 (d, 2H, Np-H, J_{HH}= 8.0), 7.93-7.90 (m, 8H, Np-H) , 7.74-7.71 (m, 2H, Np-H), 7.69-65 (m, 2H, Np-H), 7.60-7.57 (m, 2H, Np-H), 7.55-7.52 (m, 2H, Np-H). $^{13}C\{^1H\}$ NMR (125.7MHz, $CDCl_3$) δ_c 133.5, 133.5, 133.4, 131.0, 130.2, 129.4, 128.7, 127.7, 127.3, 127.0, 126.8,

126.5, 125.6, 122.0, 121.1, 94.5, 92.6. MS (EI): (m/z) 428 $[M]^+$, 214 $[M]^{2+}$. Anal. Calcd. for $C_{26}H_{16}$: C, 95.30 %; H, 4.70 %. Found: C, 95.47%, H 4.56%

2,5-Bis(phenylethynyl)thiophene (111)

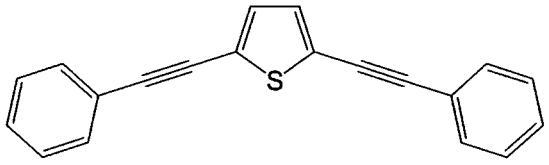

2,5-Dibromothiophene (1.5 g, 6.2 mmol) and phenylacetylene (2.15 mL, 19.5 mmol) were dissolved in dry triethylamine (30 mL). This solution was then degassed via the use of three freeze-pump-thaw cycles. To this was added CuI (0.059 g, 0.31 mmol) and $Pd(PPh_3)Cl_2$ (0.218 g, 0.22 mmol) and the mixture was then stirred under nitrogen at 70 °C for 16 h. After this time the solvent was removed and the product chromatographed on silica with DCM:40/60 Petrol (1:9) to obtain pure **111** (1.21 g, 81 %). The product was then recrystallised from toluene to obtain yellow platelike crystals.

M.P.: 84 °C. ^1H NMR (300MHz, $CDCl_3$): δ_H 7.50-7.45 (m, 4H, Ph-H), 7.33-7.38 (m, 6H, Ph-H), 7.16 (s, 2H, Th-H). $^{13}C\{^1H\}$ NMR (100.6MHz, $CDCl_3$) δ_c 82.3, 94.1, 122.6, 124.6, 128.4, 128.7, 131.5, 131.8. MS (EI): (*m/z*) 284, $[M]^+$; 142, $[M]^{2+}$. Anal. Calcd. for $C_{20}H_{12}S$: C, 84.47 %; H, 4.25 %; S, 11.28 %. Found: C, 84.28 %; H, 4.25 %; S, 11.16 %.

1,4-Bis(thiophen-2ylethynyl)benzene (112)

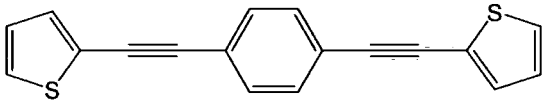

2-Bromothiophene (0.9 mL, 9.3 mmol) and 1,4-bisethynylbenzene (0.5 g, 3.9 mmol) were dissolved in dry triethylamine (20 mL). This solution was then degassed via the use of three freeze-pump-thaw cycles. To this was added CuI (0.038 g, 0.20 mmol) and $Pd(PPh_3)Cl_2$ (0.139 g, 0.20 mmol) and the mixture was then stirred under nitrogen at 70 °C for 16 h. After this time the solvent was removed and the product chromatographed on silica with hexane to obtain pure **112** (1.01 g, 89 %) which was then recrystallised from cyclohexane giving yellow plate-like crystals.

M.P.: 206 °C. ^1H NMR (300MHz, $CDCl_3$): δ_H 7.49 (s, 4H, Ph-H), 7.33-7.28 (m, 4H, Th-H), 7.04-7.00 (m, 2H, Th-H). $^{13}C\{^1H\}$ NMR (125.7MHz, $CDCl_3$) δ_c 84.9, 93.0,

123.1, 123.3, 127.4, 127.9, 131.5, 132.4. Anal. Calcd. for $C_{18}H_{10}S_2$: C, 74.45 %; H, 3.47 %; S, 22.08 %. Found: C, 74.47 %; H, 3.41 %; S, 21.08 %.

Trimethyl(thiophen-2-ylethynyl)silane (154)

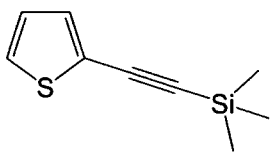

2-Bromothiophene (2.96 mL, 30.7 mmol), and trimethylsilyl acetylene (TMSA) (8.68 mL, 61.4 mmol) were dissolved in dry toluene/triethylamine (1:1, 30 mL). The solution was then freeze-pump-thaw degassed three times. CuI (0.175 g, 0.92 mmol) and $Pd(PPh_3)Cl_2$ (0.646 g, 0.92 mmol) were then added and the reaction mixture heated at 70 °C overnight. After this time the solvent was removed and the product chromatographed on silica with hexane to obtain **154** (4.26 g, 77 %) as a yellow oil.

^{1}H NMR (300MHz, $CDCl_3$): δ_H 7.25-7.22 (m, 2H, Th-H), 6.97-6.93 (m, 1H, Th-H), 0.25 (s, 9H, Me-H). $^{13}C\{^1H\}$ NMR (100.6MHz, $CDCl_3$) δ_c 132.9, 127.5, 127.1, 123.4, 98.9, 97.8, 0.1

2-Ethynylthiophene (134)

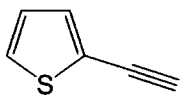

Trimethyl(thiophen-2-ylethynyl)silane (4.26 g, 23.6 mmol) was dissolved in methanol (20 mL) and potassium carbonate (2g, 15 mmol) was then added. The mixture was left stirring for one hour after which time the solvent was removed and the product separated by partition between water and DCM. The organic layer was dried and evaporated to give **134** (2.51g, 98 %) as a yellow oil.

^{1}H NMR (300MHz, $CDCl_3$): δ_H 7.31-7.26 (m, 2H, Th-H), 7.00-6.97 (m, 1H, Th-H), 3.35 (s, 1H, CC-H). $^{13}C\{^1H\}$ NMR (100.6MHz, $CDCl_3$) δ_c 133.3, 127.8, 127.1, 122.3, 81.5, 75.0

2,5-Bis(thiophen-2ylethynyl)thiophene (113)

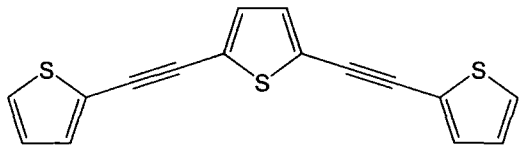

2-Ethynylthiophene (1.1 g, 10.2 mmol) and 2,5-dibromothiophene (1.07 g, 0.5 mL, 3.9 mmol) were dissolved in dry triethylamine (20 mL). The solution was then degassed via the use of three freeze-pump-thaw cycles. To this was added CuI (0.044 g, 0.23

mmol) and $Pd(PPh_3)Cl_2$ (0.162g, 0.23mmol) and the mixture was stirred under nitrogen for 16 h at 70 °C overnight. The solvent was then removed and the product chromatographed on silica with hexane to obtain pure **113** (1.13 g, 86 %) which was then recrystallised from cyclohexane giving yellow platelike crystals.

M.P.: 117 °C. ^1H NMR (400MHz, $CDCl_3$): δ_H 7.34-7.30 (m, 4H, Th-H), 7.15 (s, 2H, Th-H), 7.04-7.01 (m, 2H, Th-H). $^{13}C\{^1H\}$ NMR (100.6MHz, $CDCl_3$) δ_c 86.0, 87.7, 122.7, 124.7, 127.5, 128.3, 132.2, 132.8. Anal. Calcd. for $C_{16}H_8S_3$: C, 64.83 %; H, 2.72 %; S, 32.45 %. Found: C, 65.32 %; H, 2.85 %; S, 31.78 %

1-Bromo-4-phenylethynylbenzene (156)

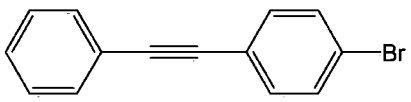

1-Bromo-4-iodobenzene (10 g, 35.3 mmol) and phenylacetylene (3.9 mL, 35.3 mmol) were dissolved in dry of triethylamine (70 mL). This solution was then degassed via the use of three freeze-pump-thaw cycles. To this was added CuI (0.113 g, 0.69 mmol) and $Pd(PPh_3)Cl_2$ (0.248 g, 0.353 mmol) and the resultant solution stirred under nitrogen for two hours. The solvent was then removed and the product chromatographed on silica with hexane. After removal of solvent the resultant solid was recrystallised from cyclohexane to obtain **156** (7.91 g, 87 %) as pale brown crystals.

M.P.: 84 °C. ^1H NMR (300MHz, $CDCl_3$): δ_H 7.54-7.47 (m, 4H, Ph-H), 7.40-7.34 (m, 5H, Ph-H). $^{13}C\{^1H\}$ NMR (125.7MHz, $CDCl_3$) δ_c 133.3, 131.9, 131.8, 128.8, 128.6, 123.1, 122.7, 122.5, 90.7, 88.5. MS (EI): (*m/z*) 258, 256, $[M]^+$; 177, $[M\text{-}Br]^+$. Anal. Calcd. for $C_{20}H_{12}S$: C, 65.40 %; H, 3.53 %. Found: C, 65.28 %; H, 3.51 %.

1-(Thiophen-2ylethynyl)-4-(phenylethynyl)benzene (155)

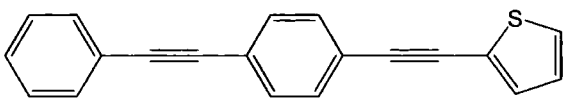

1-Bromo-4-phenylethynylbenzene (1.2 g, 4.67 mmol) and 2-ethynylthiophene (1.0 g, 9.2 mmol) were dissolved in dry triethylamine (30 mL). The solution was then degassed by three freeze-pump-thaw cycles. To this was added CuI (0.018 g, 0.093 mmol) and $Pd(PPh_3)_2Cl_2$ (0.033 g, 0.047 mmol) and the mixture refluxed under nitrogen for 16 h. After this time the solvent was removed and the product chromatographed on silica with hexane to give **155** (0.96g, 72

%) which was then recrystallised from cyclohexane giving light brown, plate-like crystals.

M.P.: 173 °C. ^{1}H NMR (300MHz, $CDCl_3$): δ 7.55-7.48 (m, 6H, Ar-H), 7.39-7.34 (m, 3H, Ar-H), 7.32-7.29 (m, 2H, Ar-H), 7.03 (t, 1H, Ar-H, J_{HH}=4.5). $^{13}C\{^{1}H\}$ NMR (126MHz, $CDCl_3$): δ 132.4, 131.9, 131.8, 131.5, 128.7, 128.7, 127.9, 127.4, 123.5, 123.3, 123.3, 123.0, 93.0, 91.6, 89.3, 84.7. MS (EI): (*m/z*) 284 $[M]^+$, 142 $[M]^{2+}$. Anal. Calcd. for $C_{20}H_{12}S$: C, 84.47 %; H, 4.25 %; S, 11.28 %. Found: C, 83.85 %; H, 4.18 %; S, 10.95 %

3,4-Ethylenedioxy-2-iodothiophene (143)

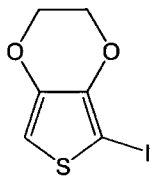

The method of Zotti et al.[2] was followed. *N*-Iodosuccinimide (2.25 g, 10 mmol) was added portionwise to a solution of 3,4-ethylenedioxythiophene (1.42 g, 10 mmol) in DMF (40 mL). The mixture was stirred for three hours and then poured into water and extracted several times with diethylether. The product was chromatographed on silica with hexane to obtain **143** (1.30 g, 48.6 %) as a white solid.

^{1}H NMR (300MHz, $CDCl_3$): δ 6.55 (s, 1H, Th-H), 4.30-4.25 (m, 2H, CH_2), 4.21-4.16 (m, 2H, CH_2).

2,5-Diiodo-3,4-ethylenedioxythiophene (160)

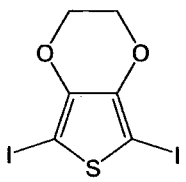

The method of Zotti et al.[2] was followed with slight modification. *N*-Iodosuccinimide (4.50 g, 20 mmol) was added portionwise to a solution of 3,4-ethylenedioxythiophene (1.42 g, 10 mmol) in DMF (60 mL). The reaction mixture was stirred for three hours before being poured into water and extracted several times with diethylether. The crude product was washed with cold diethylether to remove residual DMF and the product then recrystallised from diethylether to obtain **160** (2.20 g, 55.9 %) as a white solid.

M.P.: 186 °C. ^{1}H NMR (300MHz, $CDCl_3$): δ 4.27 (s, 4H, CH_2). MS (EI): (*m/z*) 394 $[M]^+$, 267 $[M\text{-}I]^+$.

Trimethyl(3,4-ethylenedioxythiophen-2-ylethynyl)silane

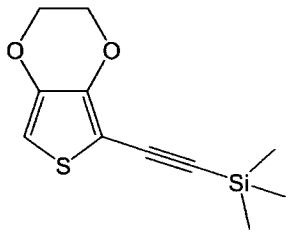

3,4-Ethylenedioxy-2-iodothiophene (1.25 g, 4.7 mmol) and TMSA (2.12 mL, 15.0 mmol) were dissolved in dry triethylamine (25 mL). The solution was then degassed by three freeze-pump-thaw cycles. To this was added CuI (0.018 g, 0.094 mmol) and $Pd(PPh_3)_2Cl_2$ (0.047 g, 0.033 mmol) and the mixture stirred under nitrogen for 16 h at 25 °C. After this time the solvent was removed and the product chromatographed on silica with DCM/hexane (1:1) to give the product (1.0 g, 90 %) as a pale yellow solid.

^{1}H NMR (300MHz, $CDCl_3$): δ 6.26 (s, 1H, Th-H), 4.31-4.26 (m, 2H, CH_2), 4.21-4.15 (m, 2H, CH_2) , 0.24 (s, 9H, Me-H).

3,4-Ethylenedioxy-2-ethynylthiophene (161)

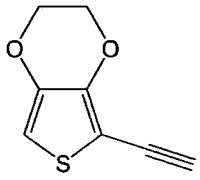

Trimethyl(3,4-ethylenedioxythiophen-2-ylethynyl)silane (1.0 g, 4.2 mmol) was dissolved in methanol (10 mL) and potassium carbonate (1g, 7.2 mmol) was added. The mixture was left stirring for one hour after which time the solvent was removed and the product separated by partition between water and DCM. The organic layer was dried and evaporated to give **161** (2.51g, 98 %) as a pale yellow solid.

^{1}H NMR (300MHz, $CDCl_3$): δ 6.29 (s, 1H, Th-H), 4.32-4.27 (m, 2H, CH_2), 4.23-4.18 (m, 2H, CH_2) , 3.48 (s, 1H, C≡CH).

3,4-Ethylenedioxy-2,5-bis(phenylethynyl)thiophene (157)

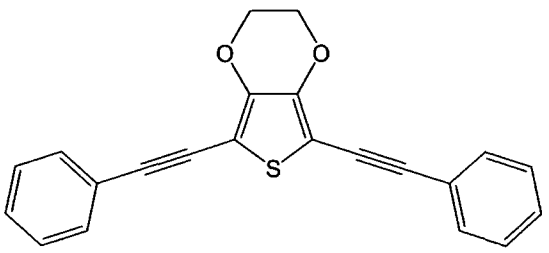

2,5-Diiodo-3,4-ethylenedioxythiophene (1.0 g, 2.54 mmol) and phenylacetylene (0.84 mL, 7.61 mmol) were dissolved in dry triethylamine (20 mL). The solution was then degassed by three freeze-pump-thaw cycles. To this was added CuI (0.024 g , 0.127 mmol) and $Pd(PPh_3)_2Cl_2$ (0.036 g, 0.051 mmol) and the mixture was stirred under nitrogen at 25 °C for 16h. The solvent was then removed and the product

chromatographed on silica with DCM/hexane (1:1) to give **157** (0.54 g, 62 %) which was recrystallised from DCM/Cyclohexane (1:1) to give pale yellow crystals.

M.P.: 152 °C. ^{1}H NMR (400 MHz, $CDCl_3$): δ 7.55-7.49 (m, 4H, Ph-H), 7.36-7.30 (m, 6H, Ph-H), 4.33 (s, 4H, CH_2). $^{13}C\{^1H\}$ NMR (101 MHz, $CDCl_3$): δ 143.2, 131.5, 128.5, 128.3, 122.8, 99.8, 96.8, 79.7, 64.9. MS (EI): (*m/z*) 342 $[M]^+$, 171 $[M]^{2+}$.

1,4-Bis(3,4-ethylenedioxythiophen-2-ylethynyl)benzene (158)

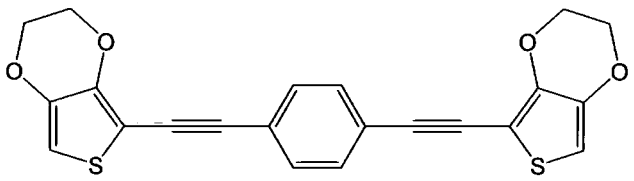

1,4-Bisethynylbenzene (0.39 g, 3.09 mmol) and 3,4-ethylenedioxy-2-iodo-thiophene (1.65 g, 6.17 mmol) were dissolved in dry triethylamine (25 mL). The solution was then degassed by three freeze-pump-thaw cycles. To this was added CuI (0.024 g, 0.123 mmol) and $Pd(PPh_3)_2Cl_2$ (0.047 g, 0.062 mmol) and the resultant mixture was stirred under nitrogen for 16 h at 25 °C. After this time the solvent was removed and the product chromatographed on silica with DCM/hexane (2:1) to give **158** (0.68 g, 54%) which was recrystallised from DCM/cyclohexane (1:1) to give pale yellow crystals.

M.P.: 145 °C. ^{1}H NMR (400 MHz, $CDCl_3$): δ 7.46 (s, 4H, Ph-H), 6.33 (s, 2H, Th-H), 4.33-4.28 (m, 4H, CH_2), 4.23-4.19 (m, 4H, CH_2). $^{13}C\{^1H\}$ NMR (101 MHz, $CDCl_3$): δ 144.4, 140.9, 131.2, 122.8, 101.6, 98.6, 95.5, 82.0, 65.1, 64.4. MS (EI): (*m/z*) 406 $[M]^+$, 203 $[M]^{2+}$.

2,5-Bis(3,4-ethylenedioxythiophen-2-ylethynyl)-3,4-ethylenedioxythiophene (159)

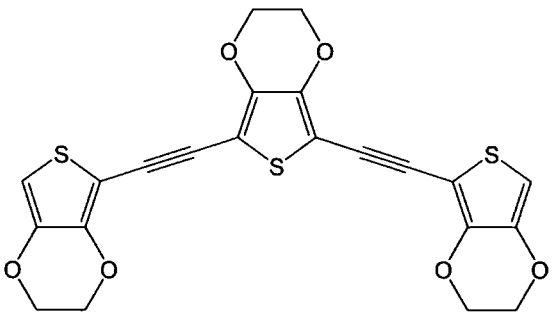

3,4-Ethylenedioxy-2-ethynylthiophene (0.55 g, 3.32 mmol) and 2,5-Diiodo-3,4-ethylenedioxy-thiophene (0.65 g, 1.66 mmol) were dissolved in dry triethylamine (20 mL). The solution was then degassed by three freeze-pump-thaw cycles. To this was added CuI (0.024 g, 0.123 mmol) and $Pd(PPh_3)_2Cl_2$ (0.047 g, 0.062 mmol) and the resultant mixture was stirred under nitrogen for 16 h at 25 °C. After this time the solvent was removed and

the product chromatographed on silica with DCM to give **159** (0.36 g, 46 %) which was recrystallised from DCM/Cyclohexane (1:1) to give pale yellow crystals.
M.P.: 220 °C (decomposed). ^{1}H NMR (400 MHz, $CDCl_3$): δ 6.33 (s, 2H, Th-H), 4.31-4.26 (m, 4H, CH_2), 4.28 (s, 4H, CH_2), 4.21-4.17 (m, 4H, CH_2). $^{13}C\{^1H\}$ NMR (101 MHz, $CDCl_3$): δ 144.8, 143.3, 140.8, 102.1, 100.1, 98.4, 87.3, 85.6, 65.1, 64.8, 64.4. MS (EI): (*m/z*) 470 $[M]^+$, 235 $[M]^{2+}$.

1-*tert*-Butyl-2-iodobenzene (192)

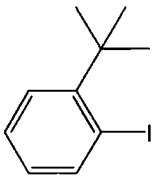

The method described by Lesslie and Mayer was followed with slight adaptation.[3] 2-*tert*-Butylaniline (5 g, 35 mmol) was dissolved in sulphuric acid (30 mL, 3.43 M, d = 1.2). This was cooled to -35 °C using a dry-ice / ethanol bath. Then a concentrated aqueous solution of of sodium nitrite (2.39 g, 35 mmol) was added and the mixture allowed to warm up to -10 °C before an aqueous solution of potassium iodide (17.05 g, 103 mmol) was added. The resultant gelatinous suspension was made basic by the addition of NaOH solution. The product was then extracted into hexane, concentrated in vacuo and the product chromatographed on silica with hexane to give **192** (3.97 g, 53 %) as an orange oil.
^{1}H NMR (300MHz, $CDCl_3$): δ 8.00 (dd, 1H, Ph-H, J_{HH}=8.0, 1.5), 7.44 (dd, 1H, Ph-H, J_{HH}=8.0, 2.0), 7.28 (td, 1H, Ph-H, J_{HH}=7.5, 1.5), 6.83 (td, 1H, Ph-H, J_{HH}=7.5, 1.5), 1.54 (s, 9H, Me-H). MS (EI): (*m/z*) 260 $[M]^+$, 245 $[M\text{-}CH_3]^+$.

(2-*tert*-Butylphenylethynyl)trimethylsilane

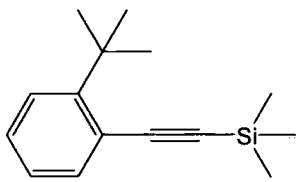

2-*tert*-Butyliodobenzene (3.97 g, 19.2 mmol) and of TMSA (8.15 mL, 57.7 mmol) were dissolved in dry triethylamine (50mL). The solution was then degassed by three freeze-pump-thaw cycles. To this was added CuI (0.040 g, 0.21 mmol) and $Pd(PPh_3)_2Cl_2$ (0.15 g, 0.21 mmol) and the mixture stirred under nitrogen for 16 h at 25 °C. After this time the solvent was removed and the product was chromatographed on silica with hexane to give the product (1.83 g, 52 %) as an orange oil.
^{1}H NMR (300MHz, $CDCl_3$): δ 7.54 (dd, 1H, Ph-H, J_{HH}=7.5, 1.5), 7.39 (dd, 1H, Ph-H, J_{HH}=8.0, 1.0), 7.28 (td, 1H, Ph-H, J_{HH}=7.5, 1.5), 7.15 (td, 1H, Ph-H, J_{HH}=7.5, 1.0), 1.56

(s, 9H, Me-H), 0.31 (s, 9H, TMS-H). MS (EI): (*m/z*) 230 $[M]^+$, 215 $[M\text{-}CH_3]^+$, 115 $[M]^{2+}$.

2-*tert*-Butylphenylacetylene (190)

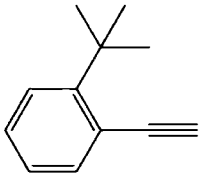

(2-*tert*-Butylphenylethynyl)trimethylsilane (1.83 g, 7.95 mmol) was dissolved in THF (100 mL). To this solution was added 10mL of methanol and TBAF (1.0M in THF, 10mL) and the solution stirred for two hours. After this time the solvent was removed and the product separated by partition between water and DCM. The organic layer was dried and evaporated to give **190** (1.06g, 84%).

^1H NMR (300MHz, $CDCl_3$): δ 7.53 (dd, 1H, Ph-H, J_{HH}=7.5, 1.5), 7.38 (dd, 1H, Ph-H, J_{HH}=8.0, 1.0), 7.28 (td, 1H, Ph-H, J_{HH}=7.5, 1.5) , 7.14 (td, 1H, Ph-H, J_{HH}=7.5, 1.0), 3.41 (s, 1H, C≡CH), 1.52 (s, 9H, Me-H). MS (EI): (*m/z*) 158 ($[M]^+$), 143 ($[M\text{-}(CH_3)]^+$) , 128 ($[M\text{-}(2CH_3)]^+$).

1,4-Bis(2-*tert*-butylphenylethynyl)benzene (188)

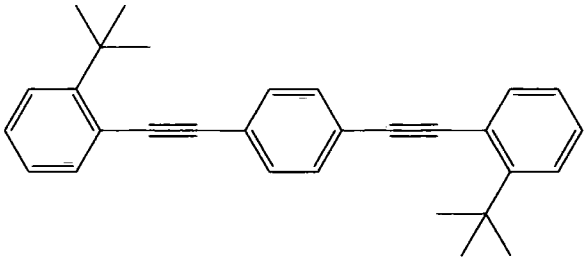

2-*tert*-Butyl-phenylacetylene (1.40 g, 8.85 mmol) and 1,4-diiodobenzene (0.73 g, 2.21 mmol) were dissolved in dry triethylamine (30 mL). The solution was then degassed by three freeze-pump-thaw cycles. To this was added CuI (6.3 mg, 0.033 mmol) and $Pd(PPh_3)_2Cl_2$ (23 mg, 0.033 mmol) and the resultant mixture was stirred under nitrogen for four hours. After this time the solvent was removed and the product chromatographed on silica with hexane. After removal of solvent the resultant solid was recrystallised from DCM to give **188** (0.59g, 68 %) as white crystals.

M.P.: 114 °C. ^1H NMR (500 MHz, $CDCl_3$): δ 7.58 (d, 2H, Ph-H, J_{HH}=8.0), 7.53 (s, 4H, Ph-H), 7.42 (d, 2H, Ph-H, J_{HH}=8.0), 7.29 (t, 2H, Ph-H, J_{HH}=7.5), 7.20 (t, 2H, Ph-H, J_{HH}=7.5), 1.58 (s, 18H, CH_3). $^{13}C\{^1H\}$ NMR (126 MHz, $CDCl_3$): δ 151.9, 135.3, 131.2, 128.8, 125.9, 123.8, 121.5, 94.8, 93.2, 36.2, 30.3. MS (EI): (*m/z*) 390 $[M]^+$, 375 $[M\text{-}Me]^+$. Acc MS (EI): (*m/z*) Calcd. For $C_{30}H_{30}$: 390.234751. Found 390.234826. Anal. Calcd. for $C_{30}H_{30}$: C, 92.26%; H, 7.74%. Found: C, 91.85%, H 7.76%

1,4-Diiodo-2,3,5,6-tetramethylbenzene (1,4-diiododurene) (193)

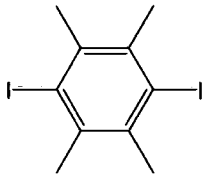

The method described by Suzuki was used with slight modification.[4,5] Durene (6.95 g 51.8 mmol), periodic acid (6.77 g, 29.7 mmol) and iodine (15.2 g, 60.0 mmol) were dissolved in a solution of conc. sulphuric acid (5 mL), water (25 mL) and glacial acetic acid (150mL). The resultant purple solution was heated at 70 °C for 24 hours after which time the reaction mixture was diluted with water (300 mL). The resultant precipitate was filtered off and washed well with water. The solid was then dissolved in DCM and washed with aqueous sodium thiosulfate solution to remove any residual iodine. The DCM layer was partitioned off, dried and evaporated and the resultant solid was recrystallised from acetone to give **193** (16.54 g, 83 %) as white crystals.

M.P.: 143 °C. ^{1}H NMR (300 MHz, $CDCl_3$): δ 2.63 (s, 12H, Me-H)

1,4-Bis(2-*tert*-butylphenylethynyl)durene (189)

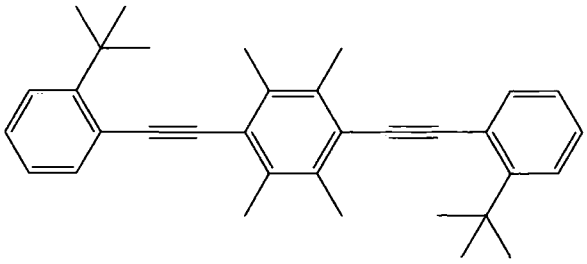

2-*tert*-Butyl-phenylacetylene (1.00 g, 6.32 mmol) and 1,4-diiododurene (0.813 g, 2.11 mmol) were dissolved in dry triethylamine (30 mL). The solution was then degassed by three freeze-pump-thaw cycles. To this was added CuI (0.060 g, 0.32 mmol) and $Pd(PPh_3)_2Cl_2$ (0.133 g, 0.19 mmol) and the resultant solution stirred under nitrogen for 16 h at 60 °C. The solvent was then removed and the product chromatographed on silica with hexane. After removal of solvent the resultant solid was recrystallised from DCM/cyclohexane (1:1) to give **189** (0.42g, 45%) of white crystals (yield 45%).

M.P.: 208 °C. ^{1}H NMR (500 MHz, $CDCl_3$): δ 7.63 (dd, 2H, Ph-H, J_{HH}=7.5, 1.5), 7.42 (d, 2H, Ph-H, J_{HH}=7.5), 7.28 (td, 2H, Ph-H, J_{HH}=8.0, 1.5), 7.20 (td, 2H, Ph-H, J_{HH}=7.5, 1.0), 2.54 (s, 12H, Me-H), 1.58 (s, 18H, CH_3). $^{13}C\{^1H\}$ NMR (126 MHz, $CDCl_3$): δ 151.1, 136.1, 135.7, 128.4, 125.9, 125.9, 124.1, 122.4, 99.6, 95.0, 36.2, 30.4, 18.8. MS (EI): (*m/z*) 446 $[M]^+$, 416 $[M\text{-}2Me]^+$, 386 $[M\text{-}3Me]^+$. Acc MS (EI): (*m/z*) Calcd. For $C_{34}H_{38}$: 446.297352. Found 446.298071. Anal. Calcd. for $C_{34}H_{38}$: C, 91.42%; H, 8.58%. Found: C, 91.15%, H 8.49%

1-(2,4,6-Triisopropylphenyl)ethanol (196)

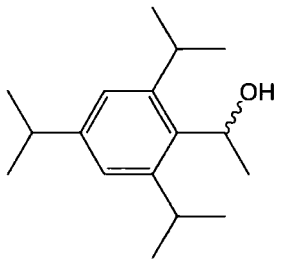

The procedure of Delair et al.[6] was followed at a reduced scale. 2,4,6-Triisopropyl acetophenone (7.5 g, 0.30 mmol) dissolved in dry diethylether (60 mL) was added portionwise with stirring to lithium aluminium hydride (1.2 g, 0.32 mmol) under nitrogen. The mixture was then refluxed for two hours before being cooled to 0 °C and hydrolysed, initially with water and then 5 M sodium hydroxide. The resultant precipitate was filtered off and rinsed well with Et_2O. The ether filtrates were combined, dried and evaporated to give **196** (7.01 g, 93 %) as a white solid.

M.P.: 91 °C. ^{1}H NMR (300 MHz, $CDCl_3$): δ 7.03 (s, 2H, Ph-H), 5.53 (qd, 1H, CH, J_{HH}= 7.0, 2.5), 3.59 (broad s, 2H, CH), 2.87 (sep, 1H, CH, J_{HH}=7.0), 1.76 (d, 1H, OH, J_{HH}= 2.0), 1.61 (d, 3H, CH_3, J_{HH}= 7.0), 1.26 (m, 18H, CH_3).

2,4,6-Triisopropylstyrene (197)

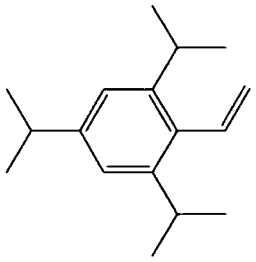

Synthesis adapted from procedure used by Knorr et al.[7] 1-(2,4,6-Triisopropylphenyl)ethanol (8.93 g, 35.9 mmol) and of $KHSO_4$ (0.95 g, 7 mmol) were slowly heated in a round bottomed flask to 180 °C at which temperature the mixture was stirred for 2 hours. The mixture was then left to cool and the crude product chromatographed on silica with hexane to obtain **197** (6.81 g, 82 %) as a yellow solid.

M.P.: °C. ^{1}H NMR (300 MHz, $CDCl_3$): δ 7.04 (s, 2H, Ph-H), 6.81 (dd, 1H, CH=C, J_{HH}=6.5, 11.5), 5.98 (dd, 1H, C=CH_2, J_{HH}= 2.5, 9.0), 5.98 (dd, 1H, C=CH_2, J_{HH}=2.5, 15.5), 3.28 (sep, 1H, CH, J_{HH}= 7.0), 2.92 (sep, 1H, CH, J_{HH}= 7.0), 1.30 (d, 6H, CH_3, J_{HH}= 7.0), 1.22 (d, 12H, CH_3, J_{HH}= 6.5). MS (EI): (*m/z*) 230 $[M]^+$, 215 $[M\text{-}Me]^+$, 187 $[M\text{-}^iPr]^+$, 115 $[M]^{2+}$.

1,2-Dibromo-1-(2,4,6-triisopropylphenyl)ethane (198)

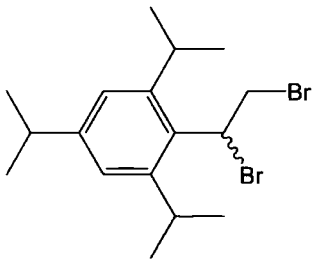

Synthesis adapted from procedure used by Knorr et al.[7] 2,4,6-Triisopropylstyrene (6.81 g, 29.6 mmol) was dissolved in chloroform (60 mL) and stirred. Bromine was then pipetted in until the solution stayed an orange/brown colour. This was stirred for five minutes and the reaction quenched by the addition of sodium thiosulfate solution (2M, 75 mL). The organic layer was separated off and the aqueous layer washed successively with chloroform. The organic layers were combined, dried and evaporated to leave **198** (11.40 g, 98.9 %) as a pale yellow oil.

^{1}H NMR (300 MHz, $CDCl_3$): δ 7.05 (d, 1H, Ph-H, J_{HH}=2.), 6.96 (d, 1H, Ph-H, J_{HH}=2.0), 5.87 (t, 1H, CHBr, J_{HH}=7.0), 4.15 (m, 2H, CH_2Br), 3.66 (sep, 1H, CH, J_{HH}=7.0), 3.24 (sep, 1H, CH, J_{HH}=7.0), 2.87 (sep, 1H, CH, J_{HH}=7.0),1.28 (m, 18H, CH_3). MS (EI): (*m/z*) 390 [M^+], 309 [M-Br]$^+$, 231 [M-2Br]$^+$

(E)-β-Bromo-2,4,6-triisopropylstyrene (199)

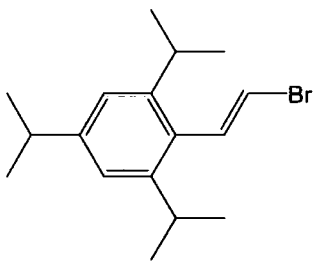

1,2-Dibromo-1-(2,4,6-triisopropylphenyl)ethane (11.40 g, 29.2 mmol) in ethanol (100 mL) was poured into a warm (45 °C) solution of KOH (3 g) in ethanol (60 mL). This solution was then stirred for 10 minutes before being poured into 150 mL of distilled water. The product was extracted into chloroform, washed with distilled water, dried and evaporated to give isomerically pure **199** (8.17g, 89.7%) as a pale yellow solid.

M.P.: 115 °C. ^{1}H NMR (300 MHz, $CDCl_3$): δ 7.18 (d, 1H, CH=C, J_{HH}=14.5), 7.00 (s, 2H, Ph-H), 6.16 (d, 1H, CH=C, J_{HH}=14.0), 3.14 (sep, 1H, CH, J_{HH}=7.0), 2.88 (sep, 1H, CH, J_{HH}=7.0), 1.25 (d, 6H, CH_3, J_{HH}= 7.0), 1.19 (d, 12H, CH_3, J_{HH}=7.0). MS (EI): (*m/z*) 310 [M(^{81}Br)]$^+$, 308 [M(^{79}Br)]$^+$, 229 [M-Br]$^+$, 187 [229-^{i}Pr]$^+$, 145 [197-^{i}Pr]$^+$.

2,4,6-Triisopropylphenylacetylene (200)

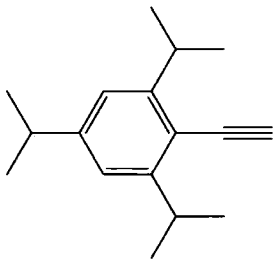

β-Bromo-2,4,6-triisopropylstyrene (8.17 g, 35.8 mmol) was dissolved in dry THF (50 mL) under nitrogen. To this was added potassium *tert*-butoxide (4 g, 35.8 mmol) and the mixture refluxed for 2 hours. The solvent was then removed under vacuum and the product separated by partition between distilled water and DCM. The organic layer was dried and evaporated to leave a brown oil which was then chromatographed on silica with hexane to give **200** (4.74 g, 78.6 %) as a pale yellow oil.

^{1}H NMR (300MHz, $CDCl_3$): δ 7.00 (s, 2H, Ph-H), 3.56 (sep, 2H, CH, J_{HH}=7.0), 3.43 (s, 1H, C≡CH), 2.91 (sep, 1H, CH, J_{HH}= 7.0), 1.28 (m, 18H, CH_3). $^{13}C\{^1H\}$ NMR (75 MHz, $CDCl_3$) 23.5, 24.2, 31.9, 34.8, 81.1, 84.5, 117.6, 120.5, 149.8, 151.6. MS (EI): (*m/z*) 228 $[M]^+$, 213 $[M\text{-}Me]^+$, 185 $[M\text{-}^iPr]^+$

1,4-Bis(2,4,6-triisopropylphenylethynyl)benzene (201)

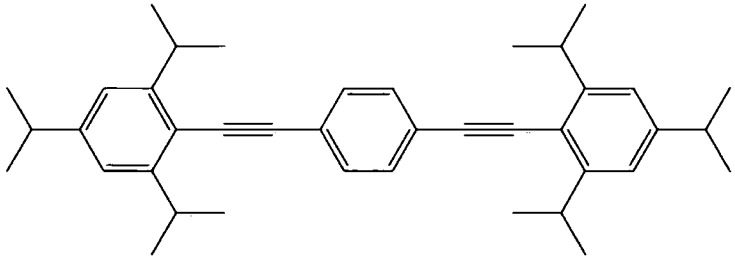

2,4,6-Triisopropylphenyl acetylene (0.90 g, 3.94 mmol) and 1,4-diiodo benzene (0.59 g, 1.8 mmol) were dissolved in dry triethylamine/THF (1:1, 20mL). The solution was then degassed by three freeze-pump-thaw cycles. To this was added CuI (0.015 g, 0.078 mmol) and $Pd(PPh_3)_2Cl_2$ (0.028 g, 0.039 mmol) and the solution stirred under nitrogen for 16 h at 25 °C. After this time the solvent was removed and the product chromatographed on silica with hexane to give **201** (0.58 g, 61 %) as a white solid, which was then recrystallised from toluene needle-like crystals.

M.P.: 229 °C. ^{1}H NMR (500 MHz, $CDCl_3$): δ 7.49 (s, 4H, Ph-H), 7.00 (s, 4H, Ph-H), 3.58 (sep, 4H, CH, J_{HH}=7.0), 2.91 (sep, 2H, CH, J_{HH}=7.0), 1.32 (d, 24H, CH_3, J_{HH}=7.0), 1.27 (d, 12H, CH_3, J_{HH}=7.0). $^{13}C\{^1H\}$ NMR (126 MHz, $CDCl_3$): δ 23.5, 24.2, 32.2, 34.8, 89.1, 96.8, 118.5, 120.7, 123.8, 131.4, 149.7, 151.0. MS (EI): (*m/z*) 530 $[M]^+$, 515 $[M\text{-}Me]^+$, 487 $[M\text{-}iPr]^+$. Anal. Calcd. for $C_{40}H_{50}$: C, 90.51%; H, 9.49%. Found: C, 90.50%; H, 9.57%

1,4-Bis(2,4,6-triisopropylphenylethynyl)durene (202)

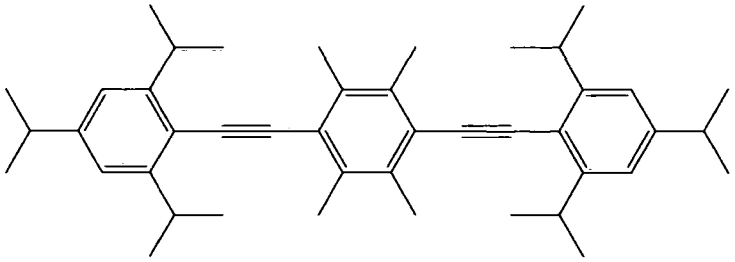

2,4,6-Triisopropylphenyl acetylene (1.58 g, 6.9 mmol) and 1,4-diiodo durene (1.24 g, 3.2 mmol) were dissolved in dry triethylamine/THF (1:1, 20mL). The solution was then degassed by three freeze-pump-thaw cycles. To this was added CuI (0.012 g, 0.064 mmol) and $Pd(PPh_3)_2Cl_2$ (0.022 g, 0.032 mmol) and the mixture stirred under nitrogen for 16 h at 45 °C. After this time the solvent was removed and the product chromatographed on silica with hexane to give a white powder. This was then recrystallised from toluene to give **202** (0.33g, 17%) as needle-like crystals.

M.P.: 203 °C. ^{1}H NMR (500 MHz, $CDCl_3$): δ 7.04 (s, 4H, Ph-H), 3.70 (sep, 4H, CH, J_{HH}=7.0), 2.92 (sep, 2H, CH, J_{HH}=7.0), 2.54 (s, 12H, Me-H), 1.31 (d, 24H, CH_3, J_{HH}=7.0), 1.28 (d, 12H, CH_3, J_{HH}=6.5). ^{13}C{^{1}H} NMR (126 MHz, $CDCl_3$): δ 18.7, 23.8, 24.2, 32.1, 34.8, 95.8, 96.1, 119.4, 120.6, 124.3, 135.8, 149.4, 150.8. MS (EI): (*m/z*) 586 $[M]^+$, 571 $[M\text{-}Me]^+$, 543 $[M\text{-}iPr]^+$. Anal. Calcd. for $C_{44}H_{58}$: C, 90.04%; H, 9.96%. Found: C, 89.92%; H, 10.00%

2-Iodo-1,3,5-*tert*-butylbenzene (205)

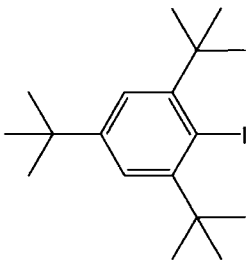

The procedure of Zimmerman and Dodd was followed.[8] 2-Bromo-1,3,5-*tert*-butylbenzene (4.92 g, 15.1 mmol) was dissolved in dry diethylether (90 mL) under nitrogen. *n*-BuLi (1.6 M in hexanes, 12.8 mL, 20.5 mmol) was added at 25 °C. The solution was then refluxed under nitrogen for one hour after which time it was cooled to 0 °C and iodine (5.20 g, 20.5 mmol) dissolved dry diethylether (40 mL) was added slowly. The resultant dark brown solution was stirred for two further hours at 25 °C before being quenched by the addition of aqueous sodium sulfite solution. The organic layer was separated off, dried and evaporated to give 5.11 g of a pale yellow solid determined to be a majority of 2-iodo-1,3,5-*tert*-butylbenzene with approx 20% 1,3,5-*tert*-butylbenzene impurity. The impurity could not be easily separated so the product was reacted on in crude form.

^{1}H NMR (300 MHz, $CDCl_3$): δ 7.41 (s, 2H, Ar-H), 1.66 (s, 18H, *o*-^{t}Bu), 1.34 (s, "8H", ^{t}Bu, impurity), 1.32 (s, 9H, *p*-^{t}Bu). GCMS (EI) (product): (*m/z*) 372 $[M]^+$, 357 $[M\text{-}Me]^+$, 245 $[M\text{-}I]^+$, GCMS (EI) (impurity): (*m/z*) 246 $[M]^+$, 231 $[M\text{-}Me]^+$

Ethyl 3-(2,4,6-tri-*tert*-butylphenyl)propiolate (206)

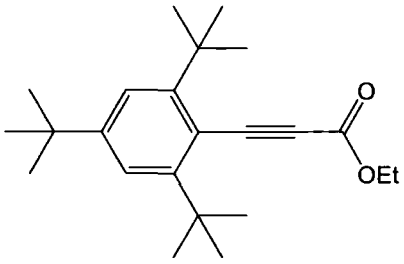

The procedure of Zimmerman and Dodd was followed.[8] Copper (I) chloride (9.35 g, 95 mmol) was dissolved in ammonia (75 mL) and then diluted to 300 mL with water. This solution was brought to a pH of about 7.5 by the addition of conc. HCl (*ca.* 110 mL) and was further diluted to 500 mL with water. This solution was added to a stirred solution of ethyl propiolate (9.24 g, 94.2 mmol) in water (200 mL). The resultant yellow precipitate was washed sparingly with ammonia, water and then NMP successively (100 mL each). The wet precipitate was then placed in NMP (150 mL) under nitrogen. To this solution was then added the crude 2-iodo-1,3,5-*tert*-butylbenzene, **205**, (5 g, which was assumed to be pure, 13.4 mmol). This solution was then heated with stirring for 24 hours at 86 °C. After which time the reaction mixture was allowed to cool and then diluted with water, acidified with HCl before being extracted into toluene. The organic layer was dried and evaporated to obtain crude product as a dark brown oil. This crude material was chromatographed on silica with DCM/Hexane (1:3) mixture to obtain **206** (1.4 g, 30 %) as a brown solid.
^{1}H NMR (500 MHz, $CDCl_3$): δ 7.36 (s, 2H, Ar-H), 4.30 (q, 2H, CH_2, J_{HH}=7.0), 1.56 (s, 18H, *o*-^{t}Bu), 1.35 (t, 3H, CH_3, J_{HH}=7.5), 1.32 (s, 9H, *p*-^{t}Bu). $^{13}C\{^1H\}$ NMR (126 MHz, $CDCl_3$): δ 14.4, 30.9, 31.4, 35.7, 36.9, 61.9, 89.3, 94.3, 113.8, 121.3, 153.0, 155.0, 156.2. MS (EI): (*m/z*) 342 $[M]^+$, 327 $[M\text{-}Me]^+$, 297 $[M\text{-}OEt]^+$.

2,4,6-Tri-*tert*-butylphenylpropiolic acid (207)

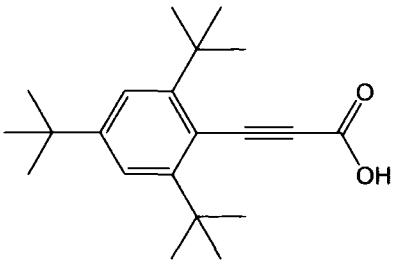

The procedure of Zimmerman and Dodd was followed.[8] Ethyl 2,4,6-tri-*tert*-butylphenylpropiolate (1.4 g, 4.1 mmol) and potassium hydroxide (0.45 g, 8.2 mmol) were dissolved in ethanol (15 mL) and refluxed for an hour. The mixture was then cooled and water added a pale yellow solid precipitated out of solution and was filtered off and dried to give **207** (1.17 g, 91.4 %).

M.P.: 201 °C (decomposed). ^{1}H NMR (500 MHz, $CDCl_3$): δ 7.38 (s, 2H, Ar-H), 1.57 (s, 18H, *o*-^{t}Bu) , 1.33 (s, 9H, *p*-^{t}Bu), The OH peak does not show up in the spectrum. $^{13}C\{^1H\}$ NMR (126 MHz, $CDCl_3$): δ 158.9, 156.8, 153.7, 121.4, 113.2, 93.5, 92.3, 37.0, 35.8, 31.4, 30.9. MS (EI): (*m/z*) 314 $[M]^+$, 299 $[M\text{-}Me]^+$, 157 $[M]^{2+}$.

2,4,6-Tri-*tert*-butylphenylacetylene (203)

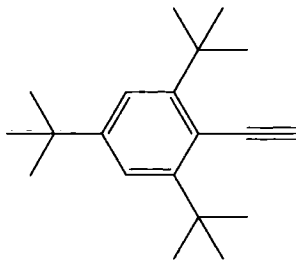

2,4,6-Tri-*tert*-butylphenylpropiolic acid (1.06 g, 3.37 mmol) was heated to 210°C and left for ten minutes once melted. After this time the material was allowed to cool before the product was chromatographed on silica with hexane to remove polar baseline impurities to give **203** (0.56g, 65 %) as a white solid.

M.P.: 112 °C. ^{1}H NMR (500 MHz, $CDCl_3$): δ 7.33 (s, 2H, Ar-H), 3.77 (s, 1H, C≡CH), 1.57 (s, 18H, *o*-^{t}Bu), 1.32 (s, 9H, *p*-^{t}Bu). $^{13}C\{^1H\}$ NMR (126 MHz, $CDCl_3$): δ 154.1, 150.5, 121.0, 116.6, 91.9, 86.4, 36.8, 35.5, 31.5, 30.6. MS (EI): (*m/z*) 270 $[M]^+$, 255 $[M\text{-}Me]^+$, 213 $[M\text{-}^tBu]^+$.

1,4-Bis(2,4,6-tritertbutylphenylethynyl)benzene (208)

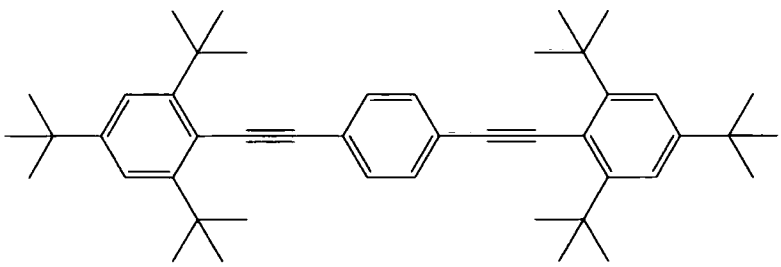

2,4,6-Tri-*tert*-butylphenyl acetylene (0.40 g, 1.48 mmol) and 1,4-diiodo benzene (0.20 g, 0.6 mmol) were dissolved in dry triethylamine (20 mL). The solution was then degassed by three freeze-pump-thaw cycles. To this was added CuI (0.0056 g, 0.029 mmol) and $Pd(PPh_3)_2Cl_2$ (0.010 g, 0.014 mmol) and the mixture stirred under nitrogen for two hours. After this time the solvent was removed and the product chromatographed on silica with hexane to give a white solid. This was then recrystallised from toluene to give **208** (0.164 g, 44 %) as needle-like crystals.

M.P.: 312 °C. ^{1}H NMR (500 MHz, $CDCl_3$): δ 7.53 (s, 4H, Ph-H), 7.38 (s, 4H, Ph-H), 1.63 (s, 36H, *o*-^{t}Bu), 1.34 (s, 18H, *p*-^{t}Bu). $^{13}C\{^1H\}$ NMR (126 MHz, $CDCl_3$): δ 30.8, 31.6, 35.5, 37.00, 95.0, 101.9, 117.2, 121.1, 124.3, 130.4, 150.5, 153.2. MS (EI): (*m/z*)

614 $[M]^+$, 599 $[M\text{-}Me]^+$, 487 $[M\text{-}iPr]^+$. Anal. Calcd. for $C_{46}H_{62}$: C, 89.84%; H, 10.16%. Found: C, 89.83%; H, 10.13%

1,4-Bis(2,4,6-tritertbutylphenylethynyl)durene (209)

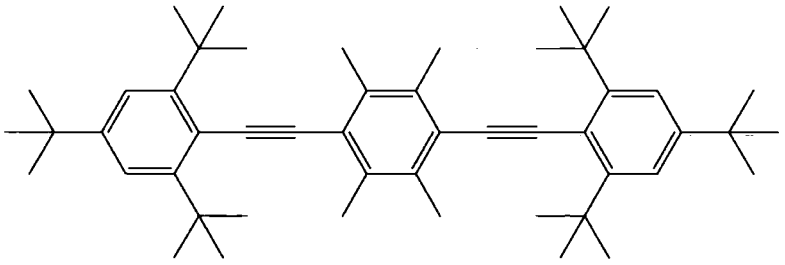

2,4,6-Tri-*tert*-butylphenyl acetylene (0.49 g, 1.8 mmol) and 1,4-diiodo durene (0.60 g, 0.9 mmol) were dissolved in dry triethylamine (10 mL). The solution was then degassed by three freeze-pump-thaw cycles. To this was added CuI (0.013 g, 0.072 mmol) and $Pd(PPh_3)_4$ (0.042 g, 0.036 mmol) and the mixture heated in a sealed Schlenk tube at 70 °C for 60 h. After this time the solvent was removed and the product chromatographed on silica with hexane giving **209** (0.39g, 65 %) as a white solid which was then recrystallised from toluene to give needle-like crystals.

M.P.: 340 °C (decomposed). ^1H NMR (500 MHz, $CDCl_3$): δ 7.42 (s, 4H, Ph-H), 2.50 (s, 12H, Me-H), 1.59 (s, 36H, CH_3), 1.35 (s, 18H, CH_3). $^{13}C\{^1H\}$ NMR (126 MHz, $CDCl_3$): δ 18.5, 30.9, 31.6, 35.5, 37.0, 99.5, 101.7, 117.7, 121.2, 124.1, 136.0, 150.1, 153.2. MS (EI): (*m/z*) 670 $[M]^+$, 655 $[M\text{-}Me]^+$. Anal. Calcd. for $C_{50}H_{70}$: C, 89.49 %; H, 10.51 %. Found: C, 89.39 %; H, 10.51 %

9,10-Bis(2-*tert*-butylphenylethynyl)anthracene (211)

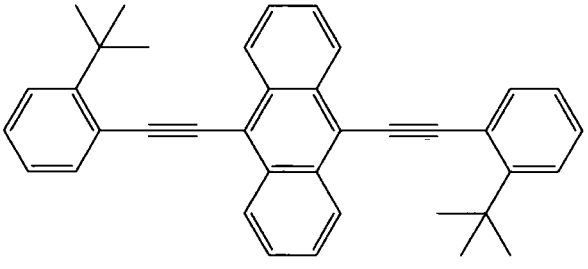

9,10-Dibromoanthracene (0.708 g, 2.11 mmol) and 2-*tert*-butyl-phenyl acetylene (1.0 g, 6.32 mmol) were dissolved in 30 mL dry triethylamine. The solution was then degassed by three freeze-pump-thaw cycles. To this was added CuI (0.060 g, 0.32 mmol) and $Pd(PPh_3)_2Cl_2$ (0.133 g, 0.19 mmol) and the resultant solution stirred under nitrogen at 60 °C for 16 hours. The solvent was then removed and the product chromatographed on silica with hexane. Removal of solvent yielding an orangepowder, which was then recrystallised from DCM/cyclohexane (1:1) giving **211** (0.62 g, 60 %) as needle-like crystals.

M.P.: 213 °C. ^{1}H NMR (500MHz, $CDCl_3$): δ_H 8.76-8.72 (m, 4H, Ant-H), 7.88 (dd, 2H, J_{HH}=7.5, 1.5), 7.65-7.61 (m, 4H, Ant-H), 7.51 (d, 2H, Ph-H, J_{HH}=8.0), 7.37 (td, 2H, Ph-H, J_{HH}=7.5, 1.0), 7.31 (td, 2H, Ph-H, J_{HH}=7.5, 1.0), 1.71 (s, 18H, Me-H). $^{13}C\{^1H\}$ NMR (126MHz, $CDCl_3$): δ_C 149.7, 134.1, 130.7, 127.1, 125.6, 125.0, 124.1, 120.0, 117.3, 101.9, 91.0, 34.4, 28.7. MS (EI): (*m/z*) 490 $[M]^+$, 430 $[M-(4CH_3)]^+$. Acc MS (EI): (*m/z*) Calcd. For $C_{38}H_{34}$: 490.266051. Found 490.267329

9,10-Bis(2,4,6-triisopropylphenylethynyl)anthracene (212)

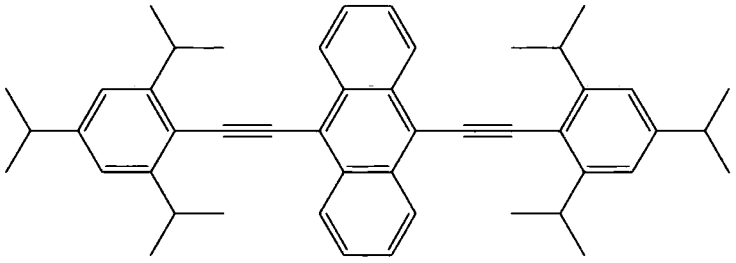

2,4,6-Triisopropyl-phenyl acetylene (1.58 g, 6.92 mmol) and 9,10-dibromo anthracene (1.08 g, 3.2 mmol) were dissolved in dry triethylamine/THF (1:3, 40mL). The solution was then degassed by three freeze-pump-thaw cycles. To this was added CuI (0.012g, 0.064mmol) and $Pd(PPh_3)_2Cl_2$ (0.022g, 0.031 mmol) and the mixture stirred at 70°C for 16h. After cooling the solvent was removed and the the product then chromatographed on silica with hexane to give **212** (0.561g, 28%) as an orange powder, which was recrystallised from methanol giving needle-like crystals.

M.P.: 259 °C. ^{1}H NMR (500 MHz, $CDCl_3$): δ 8.72-8.76 (m, 4H, Ant-H), 7.60-7.64 (m, 4H, Ant-H), 7.12 (s, 4H, Ph-H), 3.92 (sep, 4H, CH, J_{HH}=7.0), 2.97 (sep, 2H, CH, J_{HH}=7.0), 1.43 (d, 24H, CH_3, J_{HH}=7.0), 1.32 (d, 12H, CH_3, J_{HH}=6.5). $^{13}C\{^1H\}$ NMR (126 MHz, $CDCl_3$): δ 23.9, 24.2, 32.5, 34.9, 94.1, 100.1, 119.0, 119.4, 120.8, 126.8, 127.6, 132.5, 150.1, 151.1. MS (EI): (*m/z*) 630 $[M]^+$, 315 $[M]^{2+}$. Anal. Calc: C 91.37 %, H 8.63 %. Found. C, 91.30 %; H 8.63 %

9,10-Bis(2,4,6-tritertbutylphenylethynyl)anthracene (213)

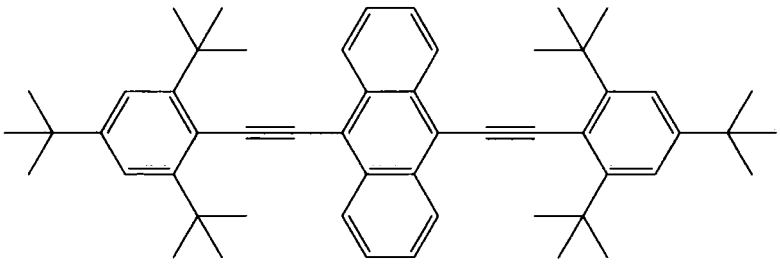

9,10-Dibromoanthracene (0.084 g 0.25 mmol) and 2,4,6-tri-*tert*-butylphenyl acetylene (0.17 g, 0.63 mmol) were dissolved in dry triethylamine (10 mL). The solution was then degassed by three freeze-pump-thaw

cycles. To this was added CuI (0.0024 g, 0.00126 mmol) and $Pd(PPh_3)_4$ (0.0044 g, 0.00063 mmol) and the mixture heated in a sealed Schlenk tube at 70 °C for 60 h. After this time the solvent was removed and the product chromatographed on silica with hexane to give **213** (0.056g, 31 %) as a yellow solid, which was then recrystallised from toluene to give small needle-like crystals.

M.P.: 365 °C (decomposed). ^{1}H NMR (500 MHz, $CDCl_3$): δ 8.72-8.69 (m, 4H, Ant-H), 7.55-7.51 (m, 4H, Ant-H), 7.49 (s, 4H, Ph-H), 1.63 (s, 36H, Me-H), 1.39 (s, 18H, Me-H). $^{13}C\{^1H\}$ NMR (126 MHz, $CDCl_3$): δ 153.7, 150.9, 132.4, 127.5, 127.0, 121.3, 119.2, 117.1, 104.3, 99.6, 37.1, 35.6, 31.6, 31.0. HR:MALDI-MS: (*m/z*) calcd. for $C_{54}H_{66}$: 714.51590. Found: 714.51565. Anal. calcd. for $C_{54}H_{66}$: C, 90.70 %; H, 9.30 %. Found: C, 90.22 %; H, 9.21 %.

9-Bromo-10-(phenylethynyl)anthracene (215)

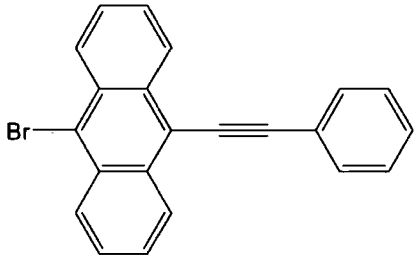

9,10-Dibromoanthracene (2.0 g, 5.95 mmol) and phenylacetylene (0.52 mL, 4.76 mmol) were dissolved in dry triethylamine/THF (1:1, 80mL). The solution was then degassed by three freeze-pump-thaw cycles. To this was added CuI (0.060 g, 0.32 mmol) and $Pd(PPh_3)_2Cl_2$ (0.133 g, 0.19 mmol) and the resultant solution refluxed under nitrogen overnight. The solvent was then removed and the product chromatographed on silica with hexane to give **215** (1.43g, 84%) as a yellow solid.

M.P.: 174 °C. ^{1}H NMR (300MHz, $CDCl_3$): δ_H 8.73-8.68 (m, 2H, Ar-H), 8.61-8.55 (m, 2H, Ar-H), 7.80-7.75 (m, 2H, Ar-H), 7.68-7.60 (m, 4H, Ar-H), 7.49-7.43 (m, 3H, Ar-H)

10-(2-*tert*-Butylphenylethynyl)-9-(phenylethynyl)anthracene (214)

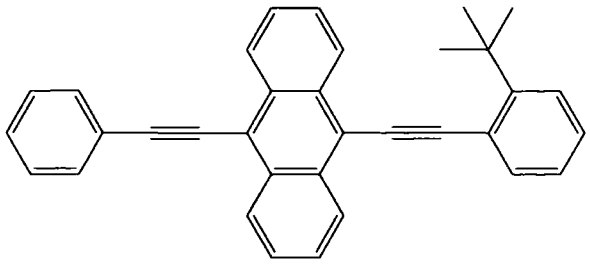

9-Bromo-10-(phenylethynyl)anthracene (0.109 g, 0.31 mmol) and 2-tertbutyl-phenylacetylene (0.145 g, 0.916 mmol) were dissolved in triethylamine/THF (1:1, 10mL). The solution was then degassed by three freeze-pump-thaw cycles. To this was added CuI (1.7 mg, 0.009 mmol) and $Pd(PPh_3)_2Cl_2$ (2.1 mg, 0.003

mmol) and the resultant solution refluxed under nitrogen for 16 h. The solvent was then removed and the product chromatographed on silica with hexane to give **214** (0.085g, 64%) which was then recrystallised from methanol to give orange needle-like crystals.
M.P.: 160 °C. ^{1}H NMR (300MHz, $CDCl_3$): δ_H 8.75-8.70 (m, 4H, Ant-H), 7.88 (d, 1H, Ph-H, J_{HH}=7.5), 7.79 (d, 2H, Ph-H, J_{HH}=7.0), 7.67-7.62 (m, 4H, Ant-H), 7.52-7.41 (m, 4H Ph-H), 7.38 (t, 1H, Ph-H, J_{HH}=8.0), 7.31 (t, 1H, Ph-H, J_{HH}=7.5), 1.71 (s, 9H, Me-H). ^{13}C{^{1}H} NMR (126MHz, $CDCl_3$): δ_C 151.6, 136.0, 132.5, 132.4, 132.0, 129.1, 129.0, 128.8, 127.6, 127.5, 127.0, 127.0, 126.1, 123.7, 122.0, 119.4, 118.6, 104.0, 102.6, 92.9, 86.8, 53.7, 36.4, 30.7. MS (EI): (*m/z*) 434 $[M]^+$, 419 $[M-(CH_3)]^+$, 217 $[M]^{2+}$

1,4-Bis(trimethylsilylethynyl)durene (216)

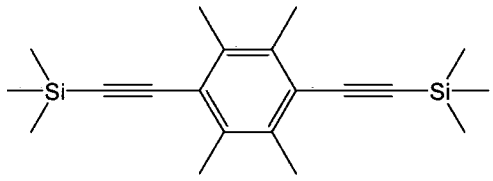

1,4-Diiododurene (7.0 g, 18.13 mmol) and TMSA (6 mL, 42.5 mmol) were dissolved in dry triethylamine/THF (2:3, 50 mL). The solution was then degassed by three freeze-pump-thaw cycles. To this was added CuI (0.14 g, 0.73 mmol) and $Pd(PPh_3)_2Cl_2$ (0.25 g, 0.36 mmol) and the resultant solution stirred under nitrogen for two hours at 20 °C. The solvent was then removed and the the product then chromatographed on silica with hexane to give **216** (3.54 g, 72 %) product as a white solid.
M.P.: 172 °C. ^{1}H NMR (300MHz, $CDCl_3$): δ_H 2.48 (s, 12H, Me-H), 0.27 (s, 18H, TMS-H)..

1,4-Bisethynyldurene (217)

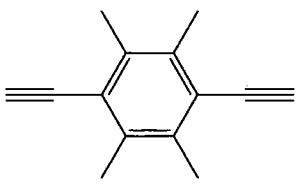

1,4-Bis(trimethylsilylethynyl)durene (1.31 g, 4.0 mmol) was dissolved in methanol (15 mL) and potassium carbonate (1g, 7.2 mmol) was added. The mixture was left stirring for one hour after which time the solvent was removed and the product separated by partition between water and DCM. The organic layer was dried and evaporated to give **217** (0.71g, 97 %) of product as white solid.
^{1}H NMR (300MHz, $CDCl_3$): δ_H 3.54 (s, 2H, C≡CH), 2.42 (s, 12H, Me-H)

1,4-Bis(2-bromophenylethynyl)durene (218)

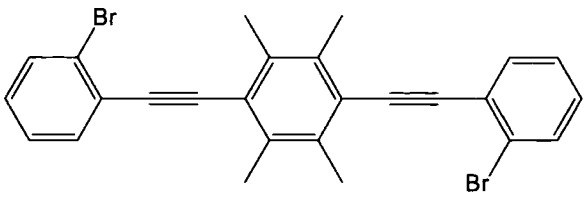

1,4-Bisethynyldurene (0.71 g, 3.88 mmol) and 2-iodobromobenzene (1.5 mL, 11.7 mmol) were dissolved in dry triethylamine/THF (1:1, 40 mL). The solution was then degassed by three freeze-pump-thaw cycles. To this was added CuI (0.015 g, 0.08 mmol) and $Pd(PPh_3)_2Cl_2$ (0.028 g, 0.04 mmol) and the resultant solution stirred under nitrogen at for two hours at 25 °C. The solvent was then removed and the the product then chromatographed on silica with DCM/hexane (3:5) to give **218** (0.71 g, 36 %) as a white solid.

M.P.: 207 °C. ^{1}H NMR (300MHz, $CDCl_3$): δ_H 7.63 (dd, 2H, Ph-H, J_{HH} = 8.0, 1.5), 7.60 (dd, 2H, Ph-H, J_{HH} = 8.0, 1.5), 7.31 (td, 2H, Ph-H, J_{HH} = 8.0, 1.00), 7.18 (td, 2H, Ph-H, J_{HH} = 8.0, 1.5), 2.56 (s, 12H, Me-H)

1,4-Bis((2-trimethylsilyl)phenylethynyl)durene (219)

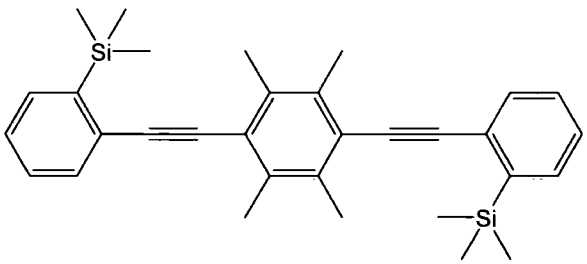

1,4-Bis(2-bromophenylethynyl)durene (0.25 g, 0.51 mmol) was dissolved in dry, degassed THF (10 mL) under nitrogen. This solution was cooled to -78 °C and *n*-BuLi (0.96 mL, 1.53 mmol, 1.6M in hexanes) was added dropwise. The resultant dark green solution was stirred for 20 minutes after which time chloro trimethylsilane (TMSCl) (0.33 mL, 2.55 mmol) was added. The solution was then allowed to warm up to 25 °C, during which time it became pale yellow in colour. The reaction was quenched by the addition of water (10 mL). The organic solvent was removed and the product separated by partition between water and DCM. The organic layer was dried and evaporated to give a yellow powder. The product was then chromatographed on silica with hexane to give **219** (0.13 g, 53 %) as a white solid which was then recrystallised from cyclohexane.

M.P.: 171 °C. ^{1}H NMR (500MHz, $CDCl_3$): δ_H 7.61 (d, 2H, Ph-H, J_{HH}= 8.0), 7.55 (d, 2H, Ph-H, J_{HH}= 7.5), 7.37 (t, 2H, Ph-H, J_{HH}= 7.5), 7.32 (t, 2H, Ph-H, J_{HH}=7.5), 2.51 (s,

12H, Me-H), 0.41 (s, 18H, TMS-H). $^{13}C\{^1H\}$ NMR (126MHz, $CDCl_3$): δ_C 141.9, 136.2, 134.3, 133.3, 129.2, 129.0, 127.6, 123.8, 99.5, 91.7, 18.9, -0.5

Trimethyl(phenylethynyl)silane (221)

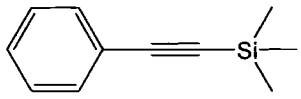

Phenylacetylene (5.37 mL, 49 mmol) was dissolved in THF (15 mL) and the resultant solution cooled to -78 °C before the dropwise addition of *n*-Buli (33.7 mL, 53.9 mmol, 1.6M in hexanes). The solution was stirred for ten minutes then TMSCl (12.6 mL, 99 mmol) was added portionwise. The solution was then allowed to warm to 25 °C and the reaction quenched by the addition of water (30mL). The product was then extracted into DCM and removal of organic solvent gave **221** (8.26 g, 96.7 %) as a yellow oil.

^1H NMR (300MHz, $CDCl_3$): δ_H 7.51-7.46 (m, 2H, Ph-H), 7.34-7.28 (m, 3H, Ph-H), 0.27 (s, 9H, TMS-H).

1-Trimethylsilyl-2-(trimethylsilylethynyl)benzene (222)

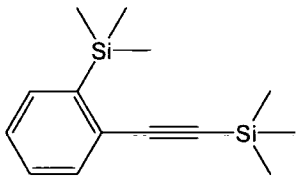

Reaction based on the method of Yamaguchi et al.[9] Trimethyl(phenylethynyl)silane (2.61 g, 15 mmol) was dissolved in dry, degassed THF (15 mL) under nitrogen and the resultant solution cooled to -78 °C. A solution of potassium *tert*-butoxide (6.72 g, 60 mmol) and *n*-butyllithium (41.3 mL, 66 mmol, 1.6M in hexanes) in dry THF (30 mL) was then prepared at -78 °C before being added portionwise to the trimethy(phenylethynyl)silane solution. The resultant deep red solution was stirred at -78 °C for 2 hours after which time TMSCl (15.3 mL, 120 mmol) was added. The solution was allowed to warm to 25 °C and stirred for 16 h. The resultant pale yellow, cloudy solution was then quenced with the addition of water (*ca.* 45 mL). The organic solvent was removed under vacuum and the product extracted into DCM. Evaporation of the solvent gave **222** (2.22 g, 60 %) as a yellow oil.

^1H NMR (300MHz, $CDCl_3$): δ_H 7.50-7.44 (m, 2H, Ph-H), 7.31-7.26 (m, 2H, Ph-H), 0.37 (s, 9H, TMS-H), 0.25 (s, 9H, TMS-H). MS (EI): (*m/z*) 246 $[M]^+$, 231 $[M\text{-}Me]^+$

1,3-Bis(trimethylsilyl)-2-(trimethylsilylethynyl)benzene (223)

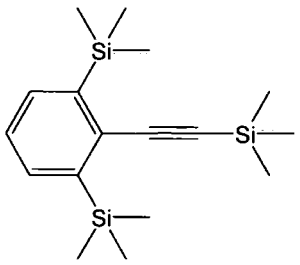

Reaction based on the method of Yamaguchi et al.[9] 1-Trimethylsilyl-2-(trimethylsilylethynyl)benzene (2.22g, 9.0 mmol) was dissolved in dry, degassed THF (15 mL) under nitrogen and the resultant solution cooled to -78 °C. A solution of potassium *tert*-butoxide (6.72 g, 60 mmol) and *n*-butyllithium (41.3 mL, 66 mmol, 1.6M in hexanes) in dry, THF (30 mL) was then prepared at -78 °C before being added portionwise to the solution of **222**. The resultant deep red solution was stirred at -78 °C for 2 hours after which time TMSCl (13 g, 120 mmol) was added. The solution was allowed to warm to 25 °C and stirred for 16 h. The resultant pale yellow, cloudy solution was quenced with the addition of water (*ca.* 45 mL). The organic solvent was then removed under vacuum and the product extracted into DCM. After removal of solvent the product was chromatographed on silica with hexane to give **223** (1.37g, 47 % as a yellow oil).

^{1}H NMR (300MHz, $CDCl_3$): δ_H 7.48 (d, 2H, Ph-H, J_{HH}=7.5), 7.26 (t, 1H, Ph-H, J_{HH}=7.5), 0.38 (s, 18H, TMS-H), 0.25 (s, 9H, TMS-H). MS (EI): (*m/z*) 318 $[M]^+$, 303 $[M\text{-}Me]^+$, 273 $[M\text{-}3Me]^+$

2-Ethynyl-1,3-bis(trimethylsilyl)benzene (220)

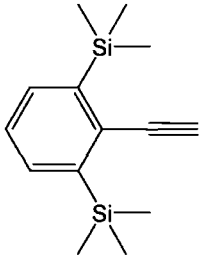

1,3-bis(trimethylsilyl)-2-(trimethylsilylethynyl)benzene (1.37 g, 4.30 mmol) was dissolved in THF (50 mL). To this solution was added 10mL of methanol and TBAF (1.0M in THF, 10mL) and the solution stirred for two hours. After this time the solvent was removed and the product separated by partition between water and DCM. The organic layer was dried and evaporated to give **220** (1.01g, 95%).

^{1}H NMR (300MHz, $CDCl_3$): δ_H 7.50 (d, 2H, Ph-H, J_{HH}=7.0), 7.29 (t, 1H, Ph-H, J_{HH}=7.5), 3.38 (s, 1H, C≡CH), 0.38 (s, 18H, TMS-H). ^{13}C NMR (75 MHz, $CDCl_3$): δ_C 143.5, 134.8, 132.8, 127.2, 86.6, 84.2, -0.7

1,4-Bis(2,6-bis(trimethylsilyl)phenylethynyl)benzene (224)

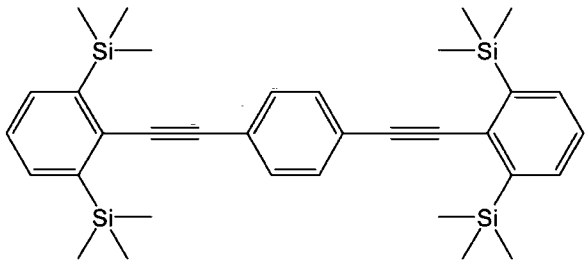

1,4-Diiodobenzene (0.25 g, 0.76 mmol) and 2-ethynyl-1,3-bis (trimethylsilyl)benzene (0.45 g 1.8 mmol) were dissolved in dry triethylamine (25 mL). The solution was then degassed by three freeze-pump-thaw cycles. To this was added CuI (0.0069 g, 0.036 mmol) and $Pd(PPh_3)_4$ (0.021 g, 0.018 mmol) and the mixture heated in a sealed Schlenk tube at 70 °C for 60 h. . After this time the solvent was removed and the product chromatographed on silica with hexane to give **224** (0.243 g, 56.5 %) as a white solid, which was then recrystallised from cyclohexane.

M.P.: 253 °C. ^{1}H NMR (500MHz, $CDCl_3$): δ 7.56 (d, 4H, Ph-H, J_{HH}=7.5), 7.54 (s, 4H, Ph-H), 7.32 (t, 2H, Ph-H, J_{HH}=7.5), 0.45 (s, 36H, TMS-H). $^{13}C\{^1H\}$ NMR (126MHz, $CDCl_3$): δ_C 142.9, 135.0, 133.6, 131.6, 131.2, 127.0, 123.7, 94.9, -0.5.

6.3 - References

1. O. Cakmak, I. Demirtas and H. T. Balaydin, *Tetrahedron*, 2002, ***58***, 5603-5609.
2. G. Zotti, G. Schiavon, S. Zecchin and A. Berlin, *Synth. Met.*, 1998, ***97***, 245-254.
3. M. S. Lesslie and U. J. H. Mayer, *J. Chem. Soc.*, 1961, 611-618.
4. H. Suzuki, *Org. Syn.*, 1971, ***51***, 94-95.
5. O. F. Koentjoro. *Synthetic and Computational Studies of Conjugated Acetylenic Systems*, University of Durham 2003.
6. P. Delair, A. M. Kanazawa, M. B. M. deAzevedo and A. E. Greene, *Tetrahedron: Asymmetry*, 1996, *7*, 2707-2710.
7. R. Knorr, J. Ruhdorfer, P. Böhrer, H. Bronberger and E. Räpple, *Liebigs Ann. Chem.*, 1994, 433-438.
8. H. E. Zimmerman and J. R. Dodd, *J. Am. Chem. Soc.*, 1970, ***92***, 6507-6515.
9. M. Yamaguchi, Y. Tsukamoto, C. Ikeura, S. Nakamura and T. Minami, *Chem. Lett.*, 1991, 1259-1262.

APPENDIX A

CRYSTALLOGRAPHIC DATA

A.1- Introduction

X-ray crystallography was carried out by the Durham University Crystallography Service using a Bruker SMART-1K area detector diffractometer.

A.2 - 1,4-Bis(naphthalene-1-ylethynyl)benzene (83)

Crystal data and structure refinement

Identification code	03srv107	
Empirical formula	C30 H18	
Formula weight	378.44	
Temperature	120(2) K	
Wavelength	0.71073 Å	
Crystal system	Monoclinic	
Space group	P2(1)/c	
Unit cell dimensions	a = 9.758(3) Å	α= 90°.
	b = 8.297(3) Å	β= 100.84(2)°.
	c = 12.477(4) Å	γ = 90°.
Volume	992.2(6) $Å^3$	
Z	2	
Density (calculated)	1.267 Mg/m^3	
Absorption coefficient	0.072 mm^{-1}	
F(000)	396	
Crystal size	0.40 x 0.35 x 0.30 mm^3	
Theta range for data collection	2.13 to 29.06°.	
Index ranges	-12<=h<=13, -6<=k<=11, -7<=l<=16	
Reflections collected	6241	
Independent reflections	2501 [R(int) = 0.0224]	
Completeness to theta = 29.06°	94.1 %	
Absorption correction	Multiscan	
Max. and min. transmission	0.9788 and 0.9718	
Refinement method	Full-matrix least-squares on F^2	
Data / restraints / parameters	2501 / 0 / 172	
Goodness-of-fit on F^2	1.056	
Final R indices [I>2sigma(I)]	R1 = 0.0464, wR2 = 0.1218	
R indices (all data)	R1 = 0.0617, wR2 = 0.1311	
Extinction coefficient	0	
Largest diff. peak and hole	0.326 and -0.206 $e.Å^{-3}$	

Atomic coordinates (x 10^4) and equivalent isotropic displacement parameters ($Å^2$ x 10^3) for 03srv107. U(eq) is defined as one third of the trace of the orthogonalized U^{ij} tensor.

	x	y	z	U(eq)
C(1)	11346(1)	-571(2)	10383(1)	26(1)
C(2)	10799(1)	-599(2)	9271(1)	26(1)
C(3)	9447(1)	-24(2)	8872(1)	24(1)
C(4)	8886(1)	-42(2)	7721(1)	26(1)
C(5)	8441(1)	-52(2)	6753(1)	25(1)
C(6)	7907(1)	-2(2)	5599(1)	23(1)
C(7)	8511(1)	-921(2)	4888(1)	26(1)
C(8)	8009(2)	-841(2)	3746(1)	28(1)
C(9)	6897(2)	128(2)	3337(1)	26(1)
C(10)	6225(1)	1069(2)	4038(1)	22(1)
C(11)	5046(1)	2050(2)	3633(1)	25(1)
C(12)	4411(1)	2945(2)	4325(1)	25(1)
C(13)	4929(1)	2911(2)	5462(1)	24(1)
C(14)	6060(1)	1967(2)	5883(1)	23(1)
C(15)	6734(1)	1016(2)	5189(1)	21(1)

Bond lengths [Å] and angles [°]for 03srv107.

C(1)-C(2)	1.3901(18)	C(8)-H(8)	0.977(18)
C(1)-C(3)#1	1.406(2)	C(9)-C(10)	1.4213(19)
C(1)-H(1)	0.974(16)	C(9)-H(9)	1.011(17)
C(2)-C(3)	1.4031(19)	C(10)-C(11)	1.4224(19)
C(2)-H(2)	0.985(17)	C(10)-C(15)	1.4287(16)
C(3)-C(1)#1	1.406(2)	C(11)-C(12)	1.372(2)
C(3)-C(4)	1.4381(17)	C(11)-H(11)	0.980(15)
C(4)-C(5)	1.2038(18)	C(12)-C(13)	1.4141(18)
C(5)-C(6)	1.4373(17)	C(12)-H(12)	0.998(18)
C(6)-C(7)	1.3830(19)	C(13)-C(14)	1.3744(19)
C(6)-C(15)	1.4368(18)	C(13)-H(13)	0.998(17)
C(7)-C(8)	1.4179(18)	C(14)-C(15)	1.4221(18)
C(7)-H(7)	0.955(17)	C(14)-H(14)	0.982(14)
C(8)-C(9)	1.370(2)		
C(2)-C(1)-C(3)#1	120.64(12)	C(8)-C(9)-H(9)	119.2(10)
C(2)-C(1)-H(1)	118.8(9)	C(10)-C(9)-H(9)	119.7(10)
C(3)#1-C(1)-H(1)	120.6(9)	C(9)-C(10)-C(11)	122.11(11)
C(1)-C(2)-C(3)	120.46(13)	C(9)-C(10)-C(15)	119.21(12)
C(1)-C(2)-H(2)	119.2(9)	C(11)-C(10)-C(15)	118.68(12)
C(3)-C(2)-H(2)	120.4(9)	C(12)-C(11)-C(10)	121.13(11)

C(2)-C(3)-C(1)#1	118.89(11)	C(12)-C(11)-H(11)	119.7(10)
C(2)-C(3)-C(4)	120.41(12)	C(10)-C(11)-H(11)	119.1(10)
C(1)#1-C(3)-C(4)	120.69(12)	C(11)-C(12)-C(13)	120.14(13)
C(5)-C(4)-C(3)	178.81(15)	C(11)-C(12)-H(12)	120.5(9)
C(4)-C(5)-C(6)	177.89(15)	C(13)-C(12)-H(12)	119.2(9)
C(7)-C(6)-C(15)	120.18(11)	C(14)-C(13)-C(12)	120.33(12)
C(7)-C(6)-C(5)	120.58(12)	C(14)-C(13)-H(13)	119.4(9)
C(15)-C(6)-C(5)	119.24(12)	C(12)-C(13)-H(13)	120.2(9)
C(6)-C(7)-C(8)	120.66(13)	C(13)-C(14)-C(15)	120.89(11)
C(6)-C(7)-H(7)	118.7(9)	C(13)-C(14)-H(14)	120.6(9)
C(8)-C(7)-H(7)	120.7(9)	C(15)-C(14)-H(14)	118.5(9)
C(9)-C(8)-C(7)	120.12(13)	C(14)-C(15)-C(10)	118.82(12)
C(9)-C(8)-H(8)	119.6(9)	C(14)-C(15)-C(6)	122.55(11)
C(7)-C(8)-H(8)	120.2(9)	C(10)-C(15)-C(6)	118.62(11)
C(8)-C(9)-C(10)	121.18(12)		

Symmetry transformations used to generate equivalent atoms:

#1 -x+2,-y,-z+2

Anisotropic displacement parameters ($Å^2 x\ 10^3$) for 03srv107. The anisotropic displacement factor exponent takes the form: $-2\pi^2 [h^2 a^{*2} U^{11} + ... + 2 h k a^* b^* U^{12}]$

	U^{11}	U^{22}	U^{33}	U^{23}	U^{13}	U^{12}
C(1)	22(1)	26(1)	26(1)	1(1)	-1(1)	5(1)
C(2)	26(1)	28(1)	24(1)	-1(1)	3(1)	4(1)
C(3)	25(1)	22(1)	23(1)	2(1)	0(1)	0(1)
C(4)	25(1)	25(1)	26(1)	1(1)	1(1)	1(1)
C(5)	23(1)	24(1)	26(1)	1(1)	3(1)	0(1)
C(6)	22(1)	23(1)	22(1)	1(1)	2(1)	-4(1)
C(7)	24(1)	24(1)	29(1)	1(1)	5(1)	-1(1)
C(8)	31(1)	28(1)	27(1)	-5(1)	10(1)	-3(1)
C(9)	31(1)	26(1)	20(1)	-1(1)	5(1)	-5(1)
C(10)	24(1)	20(1)	20(1)	0(1)	3(1)	-6(1)
C(11)	28(1)	25(1)	19(1)	3(1)	1(1)	-4(1)
C(12)	26(1)	23(1)	26(1)	4(1)	3(1)	-1(1)
C(13)	29(1)	21(1)	24(1)	0(1)	7(1)	-1(1)
C(14)	28(1)	22(1)	18(1)	1(1)	4(1)	-4(1)
C(15)	23(1)	20(1)	19(1)	1(1)	3(1)	-5(1)

Hydrogen coordinates (x 10^4) and isotropic displacement parameters ($Å^2$ x 10^3) for 03srv107.

	x	y	z	U(eq)
H(2)	11373(17)	-1030(20)	8765(12)	30(4)
H(1)	12282(17)	-990(20)	10638(12)	29(4)
H(7)	9274(17)	-1610(20)	5181(12)	31(4)
H(8)	8446(17)	-1490(20)	3248(13)	34(4)
H(9)	6560(18)	180(20)	2521(14)	36(4)
H(11)	4670(17)	2060(20)	2847(13)	30(4)
H(12)	3552(18)	3580(20)	4038(13)	33(4)
H(13)	4468(17)	3560(20)	5966(13)	31(4)
H(14)	6407(16)	1918(19)	6674(12)	25(4)
H(2)	11373(17)	-1030(20)	8765(12)	30(4)
H(1)	12282(17)	-990(20)	10638(12)	29(4)
H(7)	9274(17)	-1610(20)	5181(12)	31(4)

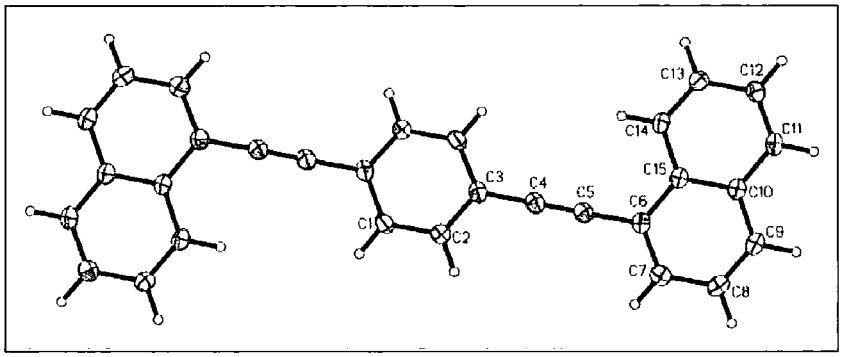

A.3 - 2,5-Bis(phenylethynyl)thiophene (111)

Crystal data and structure refinement

Identification code	02srv307	
Empirical formula	C20 H12 S1	
Formula weight	284.38	
Temperature	120(2) K	
Wavelength	0.71073 Å	
Crystal system	Monoclinic	
Space group	P2(1)/n	
Unit cell dimensions	a = 14.7523(6) Å	α= 90°.
	b = 5.7461(2) Å	β= 90.865(2)°.
	c = 17.3392(7) Å	γ = 90°.
Volume	1469.65(10) $Å^3$	
Z	4	
Density (calculated)	1.285 Mg/m^3	
Absorption coefficient	0.209 mm^{-1}	
F(000)	592	
Crystal size 0.30 x 0.10 x 0.02	mm^3	
Theta range for data collection	1.80 to 27.48°.	
Index ranges	-19<=h<=18, -7<=k<=6, -22<=l<=19	
Reflections collected	9135	
Independent reflections	3368 [R(int) = 0.0674]	
Completeness to theta = 27.48°	99.6 %	
Absorption correction	Semi-empirical from equivalents	
Max. and min. transmission	0.9958 and 0.9398	
Refinement method	Full-matrix least-squares on F^2	
Data / restraints / parameters	3368 / 0 / 190	
Goodness-of-fit on F^2	1.004	
Final R indices [I>2sigma(I)]	R1 = 0.0504, wR2 = 0.1060	
R indices (all data)	R1 = 0.1041, wR2 = 0.1296	
Extinction coefficient	.	
Largest diff. peak and hole	0.333 and -0.350 $e.Å^{-3}$	

Atomic coordinates (x 10^4) and equivalent isotropic displacement parameters ($Å^2$ x 10^3) for 02srv307. U(eq) is defined as one third of the trace of the orthogonalized U^{ij} tensor.

	x	y	z	U(eq)
S(1)	1777(1)	1082(1)	9239(1)	24(1)
C(1)	183(2)	128(5)	8715(2)	28(1)
C(2)	379(2)	-1599(5)	9272(2)	26(1)
C(11)	872(2)	1714(5)	8626(1)	21(1)
C(12)	928(2)	3537(5)	8072(1)	22(1)
C(13)	995(2)	4970(5)	7568(1)	22(1)
C(14)	1083(2)	6619(5)	6946(1)	21(1)
C(15)	660(2)	6186(5)	6229(1)	24(1)
C(16)	744(2)	7776(5)	5632(2)	26(1)
C(17)	1246(2)	9799(5)	5734(2)	26(1)
C(18)	1678(2)	10229(5)	6439(2)	24(1)
C(19)	1600(2)	8650(5)	7041(2)	23(1)
C(21)	1225(2)	-1325(5)	9608(1)	20(1)
C(22)	1666(2)	-2748(5)	10171(1)	21(1)
C(23)	2082(2)	-3925(5)	10624(1)	20(1)
C(24)	2615(2)	-5411(4)	11126(1)	18(1)
C(25)	3498(2)	-4766(5)	11356(1)	20(1)
C(26)	4017(2)	-6241(5)	11817(1)	24(1)
C(27)	3662(2)	-8351(5)	12067(2)	25(1)
C(28)	2789(2)	-8999(5)	11844(1)	23(1)
C(29)	2270(2)	-7554(5)	11375(1)	21(1)

Bond lengths [Å] and angles [°]for 02srv307.

S(1)-C(21)	1.732(3)	C(18)-C(19)	1.389(4)
S(1)-C(11)	1.734(3)	C(18)-H(18A)	0.93
C(1)-C(11)	1.375(4)	C(19)-H(19A)	0.93
C(1)-C(2)	1.411(4)	C(21)-C(22)	1.424(4)
C(1)-H(1A)	0.93	C(22)-C(23)	1.197(4)
C(2)-C(21)	1.378(3)	C(23)-C(24)	1.444(4)
C(2)-H(2A)	0.93	C(24)-C(29)	1.403(4)
C(11)-C(12)	1.425(4)	C(24)-C(25)	1.407(3)
C(12)-C(13)	1.205(4)	C(25)-C(26)	1.387(4)
C(13)-C(14)	1.442(4)	C(25)-H(25A)	0.93
C(14)-C(19)	1.403(4)	C(26)-C(27)	1.393(4)
C(14)-C(15)	1.406(3)	C(26)-H(26A)	0.93
C(15)-C(16)	1.387(4)	C(27)-C(28)	1.389(4)
C(15)-H(15A)	0.93	C(27)-H(27A)	0.93

C(16)-C(17)	1.389(4)	C(28)-C(29)	1.385(3)
C(16)-H(16A)	0.93	C(28)-H(28A)	0.93
C(17)-C(18)	1.392(4)	C(29)-H(29A)	0.93
C(17)-H(17A)	0.93		
C(21)-S(1)-C(11)	91.79(12)	C(18)-C(19)-C(14)	120.4(2)
C(11)-C(1)-C(2)	113.5(2)	C(18)-C(19)-H(19A)	119.8
C(11)-C(1)-H(1A)	123.3	C(14)-C(19)-H(19A)	119.8
C(2)-C(1)-H(1A)	123.3	C(2)-C(21)-C(22)	128.8(2)
C(21)-C(2)-C(1)	112.6(2)	C(2)-C(21)-S(1)	111.3(2)
C(21)-C(2)-H(2A)	123.7	C(22)-C(21)-S(1)	119.94(19)
C(1)-C(2)-H(2A)	123.7	C(23)-C(22)-C(21)	176.3(3)
C(1)-C(11)-C(12)	127.9(2)	C(22)-C(23)-C(24)	176.1(3)
C(1)-C(11)-S(1)	110.9(2)	C(29)-C(24)-C(25)	118.8(2)
C(12)-C(11)-S(1)	121.0(2)	C(29)-C(24)-C(23)	120.5(2)
C(13)-C(12)-C(11)	175.6(3)	C(25)-C(24)-C(23)	120.6(2)
C(12)-C(13)-C(14)	178.0(3)	C(26)-C(25)-C(24)	120.2(2)
C(19)-C(14)-C(15)	119.0(2)	C(26)-C(25)-H(25A)	119.9
C(19)-C(14)-C(13)	120.9(2)	C(24)-C(25)-H(25A)	119.9
C(15)-C(14)-C(13)	120.1(2)	C(25)-C(26)-C(27)	120.3(2)
C(16)-C(15)-C(14)	120.0(3)	C(25)-C(26)-H(26A)	119.9
C(16)-C(15)-H(15A)	120	C(27)-C(26)-H(26A)	119.9
C(14)-C(15)-H(15A)	120	C(28)-C(27)-C(26)	119.8(2)
C(15)-C(16)-C(17)	120.6(2)	C(28)-C(27)-H(27A)	120.1
C(15)-C(16)-H(16A)	119.7	C(26)-C(27)-H(27A)	120.1
C(17)-C(16)-H(16A)	119.7	C(29)-C(28)-C(27)	120.3(3)
C(16)-C(17)-C(18)	119.8(3)	C(29)-C(28)-H(28A)	119.8
C(16)-C(17)-H(17A)	120.1	C(27)-C(28)-H(28A)	119.8
C(18)-C(17)-H(17A)	120.1	C(28)-C(29)-C(24)	120.5(2)
C(19)-C(18)-C(17)	120.1(3)	C(28)-C(29)-H(29A)	119.8
C(19)-C(18)-H(18A)	119.9	C(24)-C(29)-H(29A)	119.8
C(17)-C(18)-H(18A)	119.9		

Anisotropic displacement parameters ($Å^2 x\ 10^3$) for 02srv307. The anisotropic displacement factor exponent takes the form: $-2\pi^2 [h^2 a^{*2} U^{11} + ... + 2 h k a^* b^* U^{12}]$

	U^{11}	U^{22}	U^{33}	U^{23}	U^{13}	U^{12}
S(1)	24(1)	24(1)	23(1)	4(1)	-5(1)	-3(1)
C(1)	21(1)	37(2)	25(1)	8(1)	-3(1)	1(1)
C(2)	23(1)	30(2)	25(1)	6(1)	0(1)	-6(1)
C(11)	23(1)	24(2)	17(1)	0(1)	-1(1)	6(1)
C(12)	20(1)	26(2)	19(1)	0(1)	-1(1)	2(1)

C(13)	22(1)	23(2)	20(1)	-2(1)	-2(1)	3(1)
C(14)	18(1)	22(2)	22(1)	2(1)	0(1)	5(1)
C(15)	23(1)	24(2)	24(1)	0(1)	-1(1)	-2(1)
C(16)	23(1)	32(2)	21(1)	2(1)	-3(1)	4(1)
C(17)	27(1)	27(2)	24(1)	9(1)	6(1)	5(1)
C(18)	25(1)	19(1)	28(2)	-1(1)	4(1)	0(1)
C(19)	20(1)	25(2)	24(1)	-2(1)	-2(1)	5(1)
C(21)	20(1)	20(1)	19(1)	2(1)	1(1)	0(1)
C(22)	23(1)	20(1)	20(1)	-2(1)	2(1)	-1(1)
C(23)	21(1)	19(1)	20(1)	-1(1)	2(1)	-2(1)
C(24)	22(1)	19(1)	14(1)	-2(1)	1(1)	1(1)
C(25)	22(1)	18(1)	20(1)	1(1)	4(1)	-2(1)
C(26)	18(1)	31(2)	21(1)	-1(1)	-2(1)	-1(1)
C(27)	26(1)	28(2)	20(1)	1(1)	1(1)	8(1)
C(28)	29(1)	19(1)	22(1)	5(1)	1(1)	0(1)
C(29)	17(1)	22(1)	23(1)	0(1)	-1(1)	-2(1)

Hydrogen coordinates (x 10^4) and isotropic displacement parameters ($Å^2$ x 10^3) for 02srv307.

	x	y	z	U(eq)
H(1A)	-360	189	8436	33
H(2A)	-18	-2792	9397	31
H(15A)	324	4833	6154	28
H(16A)	461	7484	5159	31
H(17A)	1294	10863	5333	31
H(18A)	2019	11576	6507	29
H(19A)	1894	8941	7510	28
H(25A)	3735	-3347	11199	24
H(26A)	4604	-5819	11959	28
H(27A)	4008	-9324	12383	30
H(28A)	2553	-10410	12010	28
H(29A)	1688	-8008	11224	25

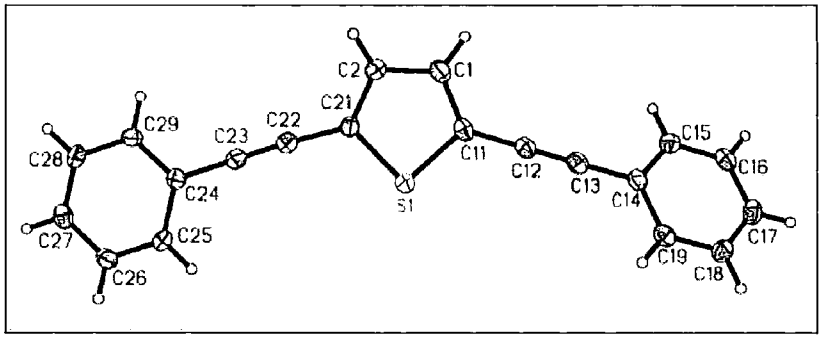

A.4 - 1,4-Bis(thiophen-2-ylethynyl)benzene (112)

Crystal data and structure refinement

Identification code	03srv014	
Empirical formula	C18 H10 S2	
Formula weight	290.38	
Temperature	120(2) K	
Wavelength	0.71073 Å	
Crystal system	Monoclinic	
Space group	P2(1)/c	
Unit cell dimensions	a = 12.564(3) Å	α= 90°.
	b = 5.0422(12) Å	β= 91.311(13)°.
	c = 10.992(3) Å	γ = 90°.
Volume	696.2(3) $Å^3$	
Z	2	
Density (calculated)	1.385 Mg/m^3	
Absorption coefficient	0.367 mm-1	
F(000)	300	
Crystal size	0.30 x 0.25 x 0.05 mm^3	
Theta range for data collection	1.62 to 27.82°.	
Index ranges	-15<=h<=16, -6<=k<=6, -14<=l<=11	
Reflections collected	4250	
Independent reflections	1595 [R(int) = 0.0490]	
Completeness to theta = 27.82°	96.1 %	
Absorption correction	Integration	
Max. and min. transmission	0.9819 and 0.8979	
Refinement method	Full-matrix least-squares on F^2	
Data / restraints / parameters	1595 / 0 / 91	
Goodness-of-fit on F^2	1.042	
Final R indices [I>2sigma(I)]	R1 = 0.0664, wR2 = 0.1765	
R indices (all data)	R1 = 0.0750, wR2 = 0.1867	
Extinction coefficient	0	
Largest diff. peak and hole	0.819 and -1.097 $e.Å^{-3}$	

Atomic coordinates (x 10^4) and equivalent isotropic displacement parameters ($Å^2$ x 10^3) for 03srv014. U(eq) is defined as one third of the trace of the orthogonalized U^{ij} tensor.

	x	y	z	U(eq)
S(1)	6237(1)	1022(1)	5732(1)	22(1)
C(1)	5846(2)	-1123(5)	6855(3)	22(1)
C(2)	6460(2)	-865(5)	7897(2)	21(1)
C(3)	7281(2)	1133(4)	7822(2)	13(1)
C(4)	7258(2)	2334(4)	6648(2)	14(1)
C(5)	7951(2)	4339(4)	6203(2)	15(1)
C(6)	8556(2)	6036(4)	5835(2)	14(1)
C(7)	9281(2)	8042(4)	5413(2)	13(1)
C(8)	10098(2)	9041(4)	6196(2)	15(1)
C(9)	10810(2)	10963(4)	5790(2)	15(1)

Bond lengths [Å] and angles [°]for 03srv014.

S(1)-C(1)	1.721(3)	S(1)-C(1)-H(1)	124
S(1)-C(4)	1.744(2)	C(1)-C(2)-C(3)	114.0(2)
C(1)-C(2)	1.373(4)	C(1)-C(2)-H(2)	123
C(1)-H(1)	0.95	C(3)-C(2)-H(2)	123
C(2)-C(3)	1.445(3)	C(4)-C(3)-C(2)	110.4(2)
C(2)-H(2)	0.95	C(4)-C(3)-H(3)	124.8
C(3)-C(4)	1.425(3)	C(2)-C(3)-H(3)	124.8
C(3)-H(3)	0.95	C(3)-C(4)-C(5)	127.73(19)
C(4)-C(5)	1.427(3)	C(3)-C(4)-S(1)	111.16(16)
C(5)-C(6)	1.220(3)	C(5)-C(4)-S(1)	121.11(16)
C(6)-C(7)	1.445(3)	C(6)-C(5)-C(4)	178.9(2)
C(7)-C(8)	1.417(3)	C(5)-C(6)-C(7)	179.2(2)
C(7)-C(9)#1	1.417(3)	C(8)-C(7)-C(9)#1	118.9(2)
C(8)-C(9)	1.399(3)	C(8)-C(7)-C(6)	120.50(19)
C(8)-H(8)	0.95	C(9)#1-C(7)-C(6)	120.64(19)
C(9)-C(7)#1	1.417(3)	C(9)-C(8)-C(7)	120.8(2)
C(9)-H(9)	0.95	C(9)-C(8)-H(8)	119.6
		C(7)-C(8)-H(8)	119.6
C(1)-S(1)-C(4)	92.43(12)	C(8)-C(9)-C(7)#1	120.3(2)
C(2)-C(1)-S(1)	112.00(18)	C(8)-C(9)-H(9)	119.8
C(2)-C(1)-H(1)	124	C(7)#1-C(9)-H(9)	119.8

Symmetry transformations used to generate equivalent atoms:

#1 -x+2,-y+2,-z+1

Anisotropic displacement parameters ($Å^2 x\ 10^3$) for 03srv014. The anisotropic displacement factor exponent takes the form: $-2\pi^2 [h^2 a^{*2} U^{11} + ... + 2 h k a^* b^* U^{12}]$

	U^{11}	U^{22}	U^{33}	U^{23}	U^{13}	U^{12}
S(1)	28(1)	27(1)	11(1)	1(1)	2(1)	-7(1)
C(1)	24(1)	20(1)	21(1)	-1(1)	8(1)	-5(1)
C(2)	27(1)	22(1)	15(1)	7(1)	11(1)	2(1)
C(3)	19(1)	16(1)	6(1)	3(1)	6(1)	1(1)
C(4)	20(1)	17(1)	6(1)	-1(1)	6(1)	0(1)
C(5)	21(1)	20(1)	4(1)	-1(1)	3(1)	1(1)
C(6)	21(1)	19(1)	3(1)	-1(1)	2(1)	0(1)
C(7)	19(1)	15(1)	5(1)	1(1)	6(1)	1(1)
C(8)	22(1)	20(1)	4(1)	3(1)	4(1)	0(1)
C(9)	21(1)	19(1)	5(1)	-1(1)	2(1)	-3(1)

Hydrogen coordinates ($x\ 10^4$) and isotropic displacement parameters ($Å^2 x\ 10^3$) for 03srv014.

	x	y	z	U(eq)
H(1)	5273	-2342	6765	26
H(2)	6355	-1906	8605	25
H(3)	7767	1582	8464	16
H(8)	10163	8398	7007	18
H(9)	11356	11604	6324	18

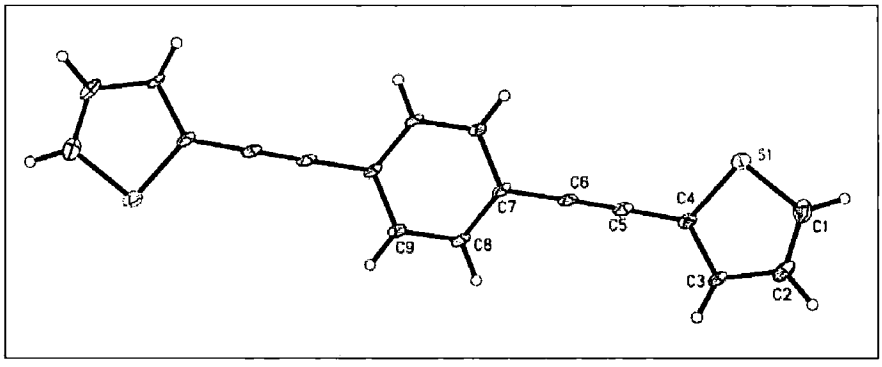

A.5 - 2,5-Bis(thiophen-2-ylethynyl)thiophene (113)

Crystal data and structure refinement

Identification code	03srv023	
Empirical formula	C16 H8 S3	
Formula weight	296.40	
Temperature	120(2) K	
Wavelength	0.71073 Å	
Crystal system	Monoclinic	
Space group	C2/c	
Unit cell dimensions	a = 14.9545(5) Å	α= 90°.
	b = 11.2060(3) Å	β= 93.280(2)°.
	c = 32.9982(11) Å	γ = 90°.
Volume	5520.8(3) $Å^3$	
Z	16	
Density (calculated)	1.426 Mg/m^3	
Absorption coefficient	0.517 mm^{-1}	
F(000)	2432	
Crystal size	0.38 x 0.32 x 0.20 mm^3	
Theta range for data collection	1.24 to 28.33°.	
Index ranges	-19<=h<=19, -14<=k<=14, -43<=l<=44	
Reflections collected	16570	
Independent reflections	6852 [R(int) = 0.0409]	
Completeness to theta = 28.33°	99.6 %	
Absorption correction	Integration	
Max. and min. transmission	0.9036 and 0.8277	
Refinement method	Full-matrix least-squares on F^2	
Data / restraints / parameters	6852 / 0 / 343	
Goodness-of-fit on F^2	1.035	
Final R indices [I>2sigma(I)]	R1 = 0.0568, wR2 = 0.1356	
R indices (all data)	R1 = 0.0851, wR2 = 0.1516	
Extinction coefficient	0	
Largest diff. peak and hole	0.583 and -0.554 e.$Å^{-3}$	

Atomic coordinates (x 10^4) and equivalent isotropic displacement parameters ($Å^2$ x 10^3) for 03srv023. U(eq) is defined as one third of the trace of the orthogonalized U^{ij} tensor.

	x	y	z	U(eq)
C(1)	7984(2)	5787(1)	1081(1)	20(1)
S(10)	-2230(1)	9697(1)	911(1)	28(1)
C(11)	-1551(2)	11552(3)	592(1)	31(1)
C(12)	-829(2)	10946(3)	794(1)	32(1)
S(11)	-5421(1)	11403(1)	-187(1)	41(1)
C(111)	-2354(2)	10991(3)	626(1)	25(1)
C(112)	-3210(2)	11368(3)	464(1)	26(1)
C(113)	-3918(2)	11715(3)	324(1)	27(1)
C(114)	-4747(2)	12184(3)	159(1)	28(1)
C(115)	-5113(2)	13290(3)	236(1)	28(1)
C(116)	-5938(2)	13485(3)	13(1)	31(1)
C(117)	-6183(2)	12542(3)	-226(1)	39(1)
S(12)	1538(1)	7211(1)	1491(1)	44(1)
C(121)	-1087(2)	9908(3)	980(1)	25(1)
C(122)	-537(2)	9069(3)	1198(1)	27(1)
C(123)	-82(2)	8347(3)	1378(1)	28(1)
C(124)	445(2)	7491(3)	1598(1)	28(1)
C(125)	189(3)	6776(4)	1921(1)	49(1)
C(126)	916(3)	6045(4)	2069(1)	51(1)
C(127)	1664(2)	6182(3)	1867(1)	37(1)
S(20)	3841(1)	4343(1)	2188(1)	25(1)
C(21)	2641(2)	4393(3)	2714(1)	30(1)
C(22)	2339(2)	3550(3)	2424(1)	28(1)
S(21)	5983(1)	7509(1)	3261(1)	42(1)
C(211)	3450(2)	4896(3)	2632(1)	24(1)
C(212)	3943(2)	5763(3)	2858(1)	26(1)
C(213)	4358(2)	6510(3)	3049(1)	28(1)
C(214)	4833(2)	7390(3)	3278(1)	28(1)
C(215)	4479(2)	8264(3)	3540(1)	37(1)
C(216)	5189(2)	8991(4)	3706(1)	47(1)
C(217)	6012(2)	8691(3)	3584(1)	43(1)
S(22)	1834(1)	260(1)	1090(1)	33(1)
C(22A)	1834(1)	260(1)	1090(1)	33(1)
C(221)	2922(2)	3415(2)	2117(1)	23(1)
C(222)	2834(2)	2649(2)	1773(1)	21(1)
C(223)	2753(2)	2012(2)	1485(1)	23(1)
C(224)	2651(2)	1240(2)	1145(1)	23(1)

C(225)	3348(1)	1232(1)	780(1)	31(1)
S(22A)	3348(1)	1232(1)	780(1)	31(1)
C(226)	2895(2)	163(3)	537(1)	37(1)
C(227)	2160(2)	-318(3)	691(1)	40(1)

Bond lengths [Å] and angles [°]for 03srv023.

S(10)-C(121)	1.728(3)	S(20)-C(211)	1.723(3)
S(10)-C(111)	1.732(3)	S(20)-C(221)	1.730(3)
C(11)-C(111)	1.366(4)	C(21)-C(211)	1.376(4)
C(11)-C(12)	1.409(4)	C(21)-C(22)	1.399(4)
C(11)-H(11A)	0.95	C(21)-H(21A)	0.95
C(12)-C(121)	1.381(4)	C(22)-C(221)	1.383(4)
C(12)-H(12A)	0.95	C(22)-H(22A)	0.95
S(11)-C(117)	1.712(4)	S(21)-C(217)	1.701(4)
S(11)-C(114)	1.719(3)	S(21)-C(214)	1.729(3)
C(111)-C(112)	1.423(4)	C(211)-C(212)	1.408(4)
C(112)-C(113)	1.195(4)	C(212)-C(213)	1.199(4)
C(113)-C(114)	1.425(4)	C(213)-C(214)	1.410(4)
C(114)-C(115)	1.385(4)	C(214)-C(215)	1.428(4)
C(115)-C(116)	1.417(4)	C(215)-C(216)	1.423(4)
C(115)-H(11B)	0.95	C(215)-H(21B)	0.95
C(116)-C(117)	1.356(5)	C(216)-C(217)	1.358(5)
C(116)-H(11C)	0.95	C(216)-H(21C)	0.95
C(117)-H(11D)	0.95	C(217)-H(21D)	0.95
S(12)-C(127)	1.698(4)	S(22)-C(227)	1.572(4)
S(12)-C(124)	1.722(3)	S(22)-C(224)	1.645(3)
C(121)-C(122)	1.418(4)	C(221)-C(222)	1.422(4)
C(122)-C(123)	1.193(4)	C(222)-C(223)	1.191(4)
C(123)-C(124)	1.415(4)	C(223)-C(224)	1.417(4)
C(124)-C(125)	1.403(4)	C(224)-C(225)	1.638(3)
C(125)-C(126)	1.425(5)	C(225)-C(226)	1.573(4)
C(125)-H(12B)	0.95	C(225)-H(22C)	0.95
C(126)-C(127)	1.342(5)	C(226)-C(227)	1.349(5)
C(126)-H(12C)	0.95	C(226)-H(22D)	0.95
C(127)-H(12D)	0.95	C(227)-H(22E)	0.95
C(121)-S(10)-C(111)	91.78(14)	C(211)-S(20)-C(221)	91.44(14)
C(111)-C(11)-C(12)	113.2(3)	C(211)-C(21)-C(22)	113.3(3)
C(111)-C(11)-H(11A)	123.4	C(211)-C(21)-H(21A)	123.3
C(12)-C(11)-H(11A)	123.4	C(22)-C(21)-H(21A)	123.3

C(121)-C(12)-C(11)	112.9(3)	C(221)-C(22)-C(21)	112.4(3)
C(121)-C(12)-H(12A)	123.5	C(221)-C(22)-H(22A)	123.8
C(11)-C(12)-H(12A)	123.5	C(21)-C(22)-H(22A)	123.8
C(117)-S(11)-C(114)	91.91(16)	C(217)-S(21)-C(214)	91.64(16)
C(11)-C(111)-C(112)	127.6(3)	C(21)-C(211)-C(212)	128.2(3)
C(11)-C(111)-S(10)	111.2(2)	C(21)-C(211)-S(20)	111.4(2)
C(112)-C(111)-S(10)	121.2(2)	C(212)-C(211)-S(20)	120.4(2)
C(113)-C(112)-C(111)	178.1(3)	C(213)-C(212)-C(211)	179.2(4)
C(112)-C(113)-C(114)	177.3(3)	C(212)-C(213)-C(214)	178.9(3)
C(115)-C(114)-C(113)	127.1(3)	C(213)-C(214)-C(215)	127.7(3)
C(115)-C(114)-S(11)	110.8(2)	C(213)-C(214)-S(21)	120.5(2)
C(113)-C(114)-S(11)	122.1(2)	C(215)-C(214)-S(21)	111.8(2)
C(114)-C(115)-C(116)	112.6(3)	C(216)-C(215)-C(214)	109.3(3)
C(114)-C(115)-H(11B)	123.7	C(216)-C(215)-H(21B)	125.3
C(116)-C(115)-H(11B)	123.7	C(214)-C(215)-H(21B)	125.3
C(117)-C(116)-C(115)	112.4(3)	C(217)-C(216)-C(215)	114.4(3)
C(117)-C(116)-H(11C)	123.8	C(217)-C(216)-H(21C)	122.8
C(115)-C(116)-H(11C)	123.8	C(215)-C(216)-H(21C)	122.8
C(116)-C(117)-S(11)	112.4(2)	C(216)-C(217)-S(21)	112.8(3)
C(116)-C(117)-H(11D)	123.8	C(216)-C(217)-H(21D)	123.6
S(11)-C(117)-H(11D)	123.8	S(21)-C(217)-H(21D)	123.6
C(127)-S(12)-C(124)	92.26(15)	C(227)-S(22)-C(224)	95.95(17)
C(12)-C(121)-C(122)	128.0(3)	C(22)-C(221)-C(222)	128.2(3)
C(12)-C(121)-S(10)	110.9(2)	C(22)-C(221)-S(20)	111.4(2)
C(122)-C(121)-S(10)	121.2(2)	C(222)-C(221)-S(20)	120.4(2)
C(123)-C(122)-C(121)	178.8(3)	C(223)-C(222)-C(221)	179.3(3)
C(122)-C(123)-C(124)	178.7(3)	C(222)-C(223)-C(224)	179.1(3)
C(125)-C(124)-C(123)	127.6(3)	C(223)-C(224)-C(225)	122.7(2)
C(125)-C(124)-S(12)	110.8(2)	C(223)-C(224)-S(22)	122.8(2)
C(123)-C(124)-S(12)	121.6(2)	C(225)-C(224)-S(22)	114.52(18)
C(124)-C(125)-C(126)	110.7(3)	C(226)-C(225)-C(224)	96.09(17)
C(124)-C(125)-H(12B)	124.7	C(226)-C(225)-H(22C)	132
C(126)-C(125)-H(12B)	124.7	C(224)-C(225)-H(22C)	132
C(127)-C(126)-C(125)	113.9(3)	C(227)-C(226)-C(225)	116.7(3)
C(127)-C(126)-H(12C)	123.1	C(227)-C(226)-H(22D)	121.7
C(125)-C(126)-H(12C)	123.1	C(225)-C(226)-H(22D)	121.7
C(126)-C(127)-S(12)	112.3(2)	C(226)-C(227)-S(22)	116.7(3)
C(126)-C(127)-H(12D)	123.8	C(226)-C(227)-H(22E)	121.7
S(12)-C(127)-H(12D)	123.8	S(22)-C(227)-H(22E)	121.7

Anisotropic displacement parameters ($Å^2 x\ 10^3$) for 03srv023. The anisotropic displacement factor exponent takes the form: $-2\pi^2 [h^2 a^{*2} U^{11} + ... + 2 h k a^* b^* U^{12}]$

	U^{11}	U^{22}	U^{33}	U^{23}	U^{13}	U^{12}
S(10)	23(1)	26(1)	34(1)	7(1)	-1(1)	2(1)
C(11)	30(2)	29(2)	34(2)	10(1)	5(1)	2(1)
C(12)	25(1)	32(2)	38(2)	3(1)	0(1)	3(1)
S(11)	41(1)	36(1)	45(1)	-2(1)	-14(1)	1(1)
C(111)	26(1)	25(1)	24(1)	0(1)	-1(1)	7(1)
C(112)	32(2)	23(1)	25(1)	-1(1)	2(1)	3(1)
C(113)	28(1)	27(2)	24(1)	1(1)	0(1)	1(1)
C(114)	25(1)	35(2)	24(1)	6(1)	1(1)	-1(1)
C(115)	24(1)	32(2)	27(1)	2(1)	0(1)	6(1)
C(116)	28(1)	37(2)	28(2)	4(1)	-1(1)	12(1)
C(117)	29(2)	50(2)	38(2)	12(2)	-8(1)	4(2)
S(12)	32(1)	51(1)	49(1)	14(1)	7(1)	14(1)
C(121)	22(1)	28(2)	23(1)	-1(1)	1(1)	5(1)
C(122)	25(1)	32(2)	23(1)	1(1)	1(1)	3(1)
C(123)	25(1)	31(2)	26(1)	0(1)	1(1)	2(1)
C(124)	30(1)	28(2)	27(1)	2(1)	-1(1)	8(1)
C(125)	44(2)	56(2)	49(2)	28(2)	15(2)	30(2)
C(126)	52(2)	54(2)	48(2)	23(2)	11(2)	28(2)
C(127)	32(2)	36(2)	43(2)	2(1)	-4(1)	15(1)
S(20)	20(1)	28(1)	28(1)	-6(1)	1(1)	-1(1)
C(21)	34(2)	37(2)	21(1)	-4(1)	5(1)	-6(1)
C(22)	28(1)	29(2)	28(2)	-2(1)	5(1)	-10(1)
S(21)	33(1)	51(1)	42(1)	-11(1)	6(1)	-14(1)
C(211)	26(1)	24(1)	23(1)	-4(1)	-2(1)	0(1)
C(212)	24(1)	28(2)	26(1)	-4(1)	1(1)	-1(1)
C(213)	25(1)	30(2)	28(1)	-3(1)	1(1)	-1(1)
C(214)	25(1)	30(2)	28(1)	-7(1)	0(1)	-5(1)
C(215)	35(2)	33(2)	41(2)	-13(1)	-5(1)	-12(1)
C(216)	48(2)	44(2)	49(2)	-20(2)	6(2)	-16(2)
C(217)	38(2)	50(2)	40(2)	-8(2)	0(2)	-23(2)
S(22)	36(1)	28(1)	35(1)	2(1)	-5(1)	0(1)
C(22A)	36(1)	28(1)	35(1)	2(1)	-5(1)	0(1)
C(221)	23(1)	20(1)	25(1)	0(1)	-2(1)	0(1)
C(222)	18(1)	21(1)	25(1)	3(1)	-1(1)	0(1)
C(223)	22(1)	21(1)	25(1)	2(1)	1(1)	2(1)
C(224)	23(1)	20(1)	25(1)	1(1)	-3(1)	3(1)
C(225)	38(1)	28(1)	27(1)	-2(1)	-2(1)	6(1)

S(22A)	38(1)	28(1)	27(1)	-2(1)	-2(1)	6(1)
C(226)	48(2)	39(2)	25(2)	-2(1)	1(1)	18(2)
C(227)	42(2)	25(2)	51(2)	-2(1)	-23(2)	-3(1)

Hydrogen coordinates (x 10^4) and isotropic displacement parameters ($Å^2$ x 10^3) for 03srv023.

	x	y	z	U(eq)
H(11A)	-1485	12278	448	37
H(12A)	-228	11222	800	38
H(11B)	-4842	13856	419	33
H(11C)	-6281	14196	29	37
H(11D)	-6718	12517	-396	47
H(12B)	-389	6779	2026	59
H(12C)	875	5508	2290	61
H(12D)	2202	5753	1929	44
H(21A)	2319	4597	2944	36
H(22A)	1794	3119	2437	34
H(21B)	3865	8348	3594	44
H(21C)	5095	9632	3887	56
H(21D)	6546	9098	3671	51
H(22B)	1334	98	1247	40
H(22C)	3855	1711	732	38
H(22D)	3128	-128	294	45
H(22E)	1855	-974	563	48

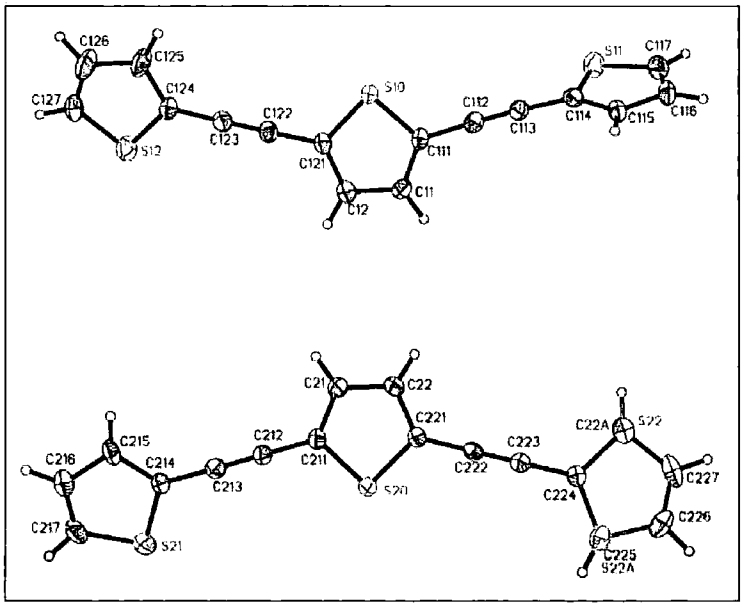

A.6 - 3,4-Ethylenedioxy-2,5-bis(phenylethynyl)thiophene (157)

Crystal data and structure refinement

Identification code	04srv045	
Empirical formula	C22 H14 O2 S	
Formula weight	342.39	
Temperature	120(2) K	
Wavelength	0.71073 Å	
Crystal system	Monoclinic	
Space group	P 21/c	
Unit cell dimensions	a = 13.2880(3) Å	α= 90°.
	b = 5.61860(10) Å	β= 93.0350(10)°.
	c = 22.5335(5) Å	γ = 90°.
Volume	1679.99(6) $Å^3$	
Z	4	
Density (calculated)	1.354 Mg/m^3	
Absorption coefficient	0.204 mm^{-1}	
F(000)	712	
Crystal size	0.50 x 0.16 x 0.10 mm^3	
Theta range for data collection	1.53 to 30.47°.	
Index ranges	-18<=h<=18, -8<=k<=7, -31<=l<=31	
Reflections collected	18746	
Independent reflections	4792 [R(int) = 0.0366]	
Completeness to theta = 30.47°	94.1 %	
Absorption correction	None	
Refinement method	Full-matrix least-squares on F^2	
Data / restraints / parameters	4792 / 0 / 282	
Goodness-of-fit on F^2	1.025	
Final R indices [I>2sigma(I)]	R1 = 0.0413, wR2 = 0.0895	
R indices (all data)	R1 = 0.0612, wR2 = 0.0969	
Largest diff. peak and hole	0.315 and -0.252 $e.Å^{-3}$	

Atomic coordinates (x 10^4) and equivalent isotropic displacement parameters ($Å^2$ x 10^3) for 04srv045. U(eq) is defined as one third of the trace of the orthogonalized U^{ij} tensor.

	x	y	z	U(eq)
S(1)	1288(1)	2586(1)	4004(1)	23(1)
O(1)	760(1)	7092(2)	2717(1)	25(1)
C(1)	731(1)	5043(2)	3652(1)	21(1)
O(2)	2231(1)	3505(2)	2418(1)	27(1)
C(2)	1074(1)	5325(2)	3093(1)	20(1)
C(3)	1051(1)	6647(3)	2115(1)	28(1)
C(4)	2114(1)	5748(3)	2110(1)	28(1)
C(5)	1789(1)	3574(2)	2949(1)	21(1)
C(6)	1990(1)	1953(2)	3395(1)	22(1)
C(11)	-34(1)	6352(2)	3923(1)	22(1)
C(12)	-698(1)	7399(2)	4151(1)	22(1)
C(13)	-1524(1)	8567(2)	4417(1)	21(1)
C(14)	-2476(1)	7497(3)	4389(1)	24(1)
C(15)	-3277(1)	8551(3)	4658(1)	28(1)
C(16)	-3137(1)	10692(3)	4961(1)	29(1)
C(17)	-2200(1)	11789(3)	4983(1)	28(1)
C(18)	-1395(1)	10756(3)	4711(1)	24(1)
C(21)	2719(1)	114(3)	3412(1)	24(1)
C(22)	3364(1)	-1379(3)	3446(1)	25(1)
C(23)	4158(1)	-3109(2)	3504(1)	23(1)
C(24)	4093(1)	-5007(3)	3901(1)	25(1)
C(25)	4865(1)	-6659(3)	3958(1)	27(1)
C(26)	5705(1)	-6455(3)	3622(1)	27(1)
C(27)	5780(1)	-4566(3)	3227(1)	28(1)
C(28)	5012(1)	-2893(3)	3168(1)	26(1)

Bond lengths [Å] and angles [°]for 04srv045.

S(1)-C(6)	1.7372(14)	C(14)-H(14)	0.940(17)
S(1)-C(1)	1.7377(14)	C(15)-C(16)	1.390(2)
O(1) -C(2)	1.3559(16)	C(15)-H(15)	0.958(18)
O(1) -C(3)	1.4531(16)	C(16)-C(17)	1.387(2)
C(1) -C(2)	1.3722(18)	C(16)-H(16)	0.965(18)
C(1) -C(11)	1.4188(19)	C(17)-C(18)	1.389(2)
O(2) -C(5)	1.3608(15)	C(17)-H(17)	0.954(18)
O(2) -C(4)	1.4431(18)	C(18)-H(18)	0.954(17)
C(2) -C(5)	1.4175(19)	C(21)-C(22)	1.199(2)
C(3) -C(4)	1.501(2)	C(22)-C(23)	1.435(2)
C(3) -H(31)	0.994(17)	C(23)-C(24)	1.397(2)
C(3) -H(32)	0.994(17)	C(23)-C(28)	1.404(2)
C(4) -H(42)	0.965(16)	C(24)-C(25)	1.384(2)
C(4) -H(41)	0.993(18)	C(24)-H(24)	0.954(18)
C(5) -C(6)	1.3722(19)	C(25)-C(26)	1.386(2)
C(6) -C(21)	1.4151(19)	C(25)-H(25)	0.938(19)
C(11)-C(12)	1.1977(19)	C(26)-C(27)	1.392(2)
C(12)-C(13)	1.4383(19)	C(26)-H(26)	0.950(18)
C(13)-C(14)	1.399(2)	C(27)-C(28)	1.388(2)
C(13)-C(18)	1.4022(19)	C(27)-H(27)	0.948(17)
C(14)-C(15)	1.385(2)	C(28)-H(28)	0.979(18)
C(6) -S(1)-C(1)	92.01(6)	O(1)-C(3)-H(32)	110.2(10)
C(2) -O(1)-C(3)	111.62(11)	C(4)-C(3)-H(32)	109.7(10)
C(2) -C(1)-C(11)	127.97(13)	H(31)-C(3)-H(32)	111.3(13)
C(2) -C(1)-S(1)	110.95(10)	O(2)-C(4)-C(3)	111.60(12)
C(11)-C(1)-S(1)	120.86(10)	O(2)-C(4)-H(42)	107.3(10)
C(5) -O(2)-C(4)	110.91(11)	C(3)-C(4)-H(42)	109.9(9)
O(1) -C(2)-C(1)	123.50(12)	O(2)-C(4)-H(41)	107.1(10)
O(1) -C(2)-C(5)	123.62(12)	C(3)-C(4)-H(41)	112.0(10)
C(1) -C(2)-C(5)	112.88(12)	H(42)-C(4)-H(41)	108.7(14)
O(1) -C(3)-C(4)	111.20(11)	O(2)-C(5)-C(6)	123.28(12)
O(1) -C(3)-H(31)	104.5(9)	O(2)-C(5)-C(2)	123.14(12)
C(4) -C(3)-H(31)	109.9(9)	C(6)-C(5)-C(2)	113.58(12)
C(5) -C(6)-C(21)	127.61(13)	C(13)-C(18)-H(18)	120.3(10)
C(5) -C(6)-S(1)	110.57(10)	C(22)-C(21)-C(6)	176.74(15)
C(21)-C(6)-S(1)	121.59(11)	C(21)-C(22)-C(23)	177.78(15)
C(12)-C(11)-C(1)	178.03(15)	C(24)-C(23)-C(28)	119.36(13)
C(11)-C(12)-C(13)	177.45(15)	C(24)-C(23)-C(22)	120.34(13)

C(14)-C(13)-C(18)	119.09(13)	C(28)-C(23)-C(22)	120.29(13)
C(14)-C(13)-C(12)	119.57(12)	C(25)-C(24)-C(23)	120.04(14)
C(18)-C(13)-C(12)	121.33(13)	C(25)-C(24)-H(24)	120.9(10)
C(15)-C(14)-C(13)	120.67(14)	C(23)-C(24)-H(24)	119.0(10)
C(15)-C(14)-H(14)	119.2(10)	C(24)-C(25)-C(26)	120.57(14)
C(13)-C(14)-H(14)	120.2(10)	C(24)-C(25)-H(25)	120.3(11)
C(14)-C(15)-C(16)	119.90(14)	C(26)-C(25)-H(25)	119.2(11)
C(14)-C(15)-H(15)	118.4(11)	C(25)-C(26)-C(27)	119.88(14)
C(16)-C(15)-H(15)	121.7(11)	C(25)-C(26)-H(26)	118.8(11)
C(17)-C(16)-C(15)	119.94(14)	C(27)-C(26)-H(26)	121.3(11)
C(17)-C(16)-H(16)	119.6(10)	C(28)-C(27)-C(26)	120.12(14)
C(15)-C(16)-H(16)	120.4(11)	C(28)-C(27)-H(27)	119.1(11)
C(16)-C(17)-C(18)	120.56(14)	C(26)-C(27)-H(27)	120.7(11)
C(16)-C(17)-H(17)	120.5(11)	C(27)-C(28)-C(23)	120.03(14)
C(18)-C(17)-H(17)	118.9(11)	C(27)-C(28)-H(28)	119.1(10)
C(17)-C(18)-C(13)	119.80(14)	C(23)-C(28)-H(28)	120.8(10)
C(17)-C(18)-H(18)	119.9(10)		

Anisotropic displacement parameters ($Å^2 x\ 10^3$) for 04srv045. The anisotropic displacement factor exponent takes the form: $-2\pi^2 [h^2 a^{*2} U^{11} + ... + 2 h k a^* b^* U^{12}]$

	U^{11}	U^{22}	U^{33}	U^{23}	U^{13}	U^{12}
S(1)	25(1)	24(1)	20(1)	2(1)	2(1)	1(1)
O(1)	28(1)	25(1)	20(1)	3(1)	3(1)	6(1)
C(1)	21(1)	21(1)	21(1)	-1(1)	1(1)	0(1)
O(2)	28(1)	33(1)	22(1)	0(1)	7(1)	7(1)
C(2)	19(1)	21(1)	20(1)	0(1)	0(1)	-1(1)
C(3)	31(1)	34(1)	19(1)	3(1)	2(1)	2(1)
C(4)	31(1)	34(1)	19(1)	1(1)	5(1)	-1(1)
C(5)	19(1)	24(1)	19(1)	-3(1)	2(1)	0(1)
C(6)	21(1)	23(1)	22(1)	-2(1)	1(1)	1(1)
C(11)	24(1)	23(1)	18(1)	-1(1)	2(1)	-2(1)
C(12)	26(1)	22(1)	19(1)	1(1)	1(1)	0(1)
C(13)	25(1)	21(1)	16(1)	1(1)	2(1)	3(1)
C(14)	27(1)	23(1)	23(1)	-2(1)	1(1)	2(1)
C(15)	23(1)	33(1)	29(1)	1(1)	3(1)	1(1)
C(16)	28(1)	34(1)	24(1)	-1(1)	4(1)	11(1)
C(17)	38(1)	23(1)	23(1)	-2(1)	0(1)	7(1)
C(18)	28(1)	22(1)	21(1)	2(1)	1(1)	0(1)
C(21)	25(1)	25(1)	22(1)	-2(1)	0(1)	-1(1)
C(22)	26(1)	25(1)	24(1)	-4(1)	-2(1)	2(1)

C(23)	22(1)	23(1)	23(1)	-5(1)	-2(1)	2(1)
C(24)	21(1)	25(1)	29(1)	-3(1)	4(1)	-1(1)
C(25)	28(1)	23(1)	31(1)	2(1)	3(1)	1(1)
C(26)	24(1)	25(1)	32(1)	-3(1)	1(1)	6(1)
C(27)	25(1)	33(1)	25(1)	-3(1)	5(1)	1(1)
C(28)	29(1)	26(1)	23(1)	0(1)	1(1)	1(1)

Hydrogen coordinates (x 10^4) and isotropic displacement parameters ($Å^2$ x 10^3) for 04srv045.

	x	y	z	U(eq)
H(31)	998(12)	8230(30)	1917(7)	26(4)
H(32)	586(13)	5470(30)	1916(7)	32(4)
H(42)	2297(12)	5490(30)	1706(7)	28(4)
H(41)	2602(13)	6880(30)	2305(7)	33(5)
H(14)	-2575(12)	6030(30)	4195(7)	31(4)
H(15)	-3917(13)	7760(30)	4633(8)	34(5)
H(16)	-3693(13)	11450(30)	5145(7)	34(5)
H(17)	-2097(13)	13260(30)	5191(8)	37(5)
H(18)	-755(13)	11530(30)	4727(7)	32(4)
H(24)	3505(13)	-5160(30)	4123(7)	35(5)
H(25)	4818(13)	-7950(30)	4218(8)	40(5)
H(26)	6213(13)	-7640(30)	3660(8)	33(5)
H(27)	6360(13)	-4380(30)	3004(7)	36(5)
H(28)	5083(13)	-1550(30)	2895(8)	37(5)

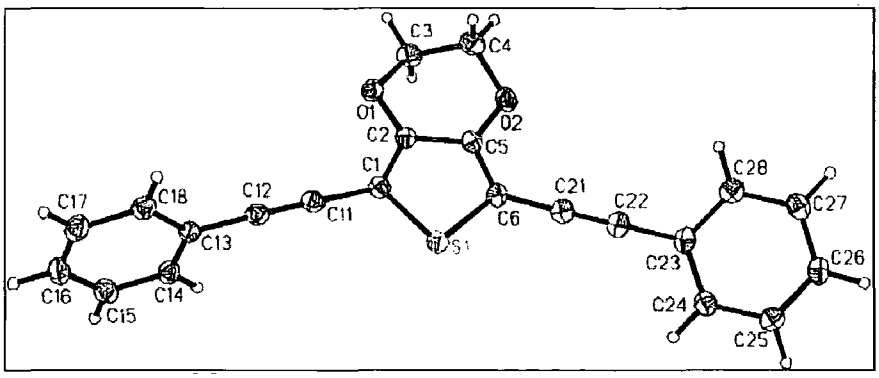

A.7 - 1,4-Bis(2-*tert*-butylphenylethynyl)benzene (188)

Crystal data and structure refinement

Identification code	03srv123	
Empirical formula	C30 H30	
Formula weight	390.54	
Temperature	120(2) K	
Wavelength	0.71073 Å	
Crystal system	Monoclinic	
Space group	P2(1)/c	
Unit cell dimensions	a = 7.0937(6) Å	α= 90°.
	b = 14.4370(13) Å	β= 96.857(2)°.
	c = 11.4020(11) Å	γ = 90°.
Volume	1159.35(18) $Å^3$	
Z	2	
Density (calculated)	1.119 Mg/m^3	
Absorption coefficient	0.063 mm^{-1}	
F(000)	420	
Crystal size	0.24 x 0.10 x 0.10 mm^3	
Theta range for data collection	2.29 to 29.11°.	
Index ranges	-9<=h<=9, -19<=k<=19, -9<=l<=15	
Reflections collected	8189	
Independent reflections	3103 [R(int) = 0.0606]	
Completeness to theta = 29.11°	99.3 %	
Absorption correction	Integration	
Max. and min. transmission	0.9938 and 0.9851	
Refinement method	Full-matrix least-squares on F^2	
Data / restraints / parameters	3103 / 0 / 196	
Goodness-of-fit on F^2	0.998	
Final R indices [I>2sigma(I)]	R1 = 0.0571, wR2 = 0.1087	
R indices (all data)	R1 = 0.1111, wR2 = 0.1257	
Extinction coefficient	0	
Largest diff. peak and hole	0.203 and -0.247 $e.Å^{-3}$	

Atomic coordinates (x 10^4) and equivalent isotropic displacement parameters (Å^2 x 10^3) for 03srv123. U(eq) is defined as one third of the trace of the orthogonalized U^{ij} tensor.

	x	y	z	U(eq)
C(1)	11445(2)	4418(1)	10487(2)	25(1)
C(2)	9736(2)	4048(1)	9999(2)	26(1)
C(3)	8267(2)	4622(1)	9503(1)	23(1)
C(4)	6498(2)	4235(1)	8991(2)	25(1)
C(5)	5041(2)	3871(1)	8587(2)	24(1)
C(6)	3245(2)	3508(1)	8073(1)	22(1)
C(7)	2035(2)	4136(1)	7416(2)	28(1)
C(8)	277(2)	3869(1)	6877(2)	31(1)
C(9)	-308(2)	2965(1)	7001(2)	30(1)
C(10)	864(2)	2337(1)	7653(2)	26(1)
C(11)	2663(2)	2576(1)	8207(1)	22(1)
C(12)	3930(2)	1859(1)	8922(2)	25(1)
C(13)	2951(3)	908(1)	8936(2)	34(1)
C(14)	5788(3)	1719(1)	8373(2)	31(1)
C(15)	4363(3)	2174(1)	10213(2)	29(1)

Bond lengths [Å] and angles [°] for 03srv123.

C(1) -C(2)	1.380(2)	C(2)-C(1)-H(1)	121.7(9)
C(1) -C(3)#1	1.401(2)	C(3)#1-C(1)-H(1)	117.9(9)
C(1) -H(1)	0.989(16)	C(1)-C(2)-C(3)	120.69(14)
C(2) -C(3)	1.397(2)	C(1)-C(2)-H(2)	120.2(10)
C(2) -H(2)	0.947(16)	C(3)-C(2)-H(2)	118.9(10)
C(3) -C(1)#1	1.401(2)	C(2)-C(3)-C(1)#1	118.86(14)
C(3) -C(4)	1.433(2)	C(2)-C(3)-C(4)	120.57(13)
C(4) -C(5)	1.201(2)	C(1)#1-C(3)-C(4)	120.58(14)
C(5) -C(6)	1.437(2)	C(5)-C(4)-C(3)	176.85(17)
C(6) -C(7)	1.402(2)	C(4)-C(5)-C(6)	175.41(16)
C(6) -C(11)	1.422(2)	C(7)-C(6)-C(11)	120.20(14)
C(7) -C(8)	1.378(2)	C(7)-C(6)-C(5)	116.01(14)
C(7) -H(7)	0.985(17)	C(11)-C(6)-C(5)	123.78(14)
C(8) -C(9)	1.381(2)	C(8)-C(7)-C(6)	121.36(15)
C(8) -H(8)	0.988(17)	C(8)-C(7)-H(7)	119.2(10)
C(9) -C(10)	1.385(2)	C(6)-C(7)-H(7)	119.4(10)
C(9) -H(9)	0.985(17)	C(7)-C(8)-C(9)	119.10(16)
C(10)-C(11)	1.398(2)	C(7)-C(8)-H(8)	120.1(10)
C(10)-H(10)	1.006(18)	C(9)-C(8)-H(8)	120.8(10)
C(11)-C(12)	1.539(2)	C(8)-C(9)-C(10)	120.32(16)

C(12)-C(15)	1.537(2)	C(8)-C(9)-H(9)	120.3(10)
C(12)-C(14)	1.538(2)	C(10)-C(9)-H(9)	119.3(10)
C(12)-C(13)	1.540(2)	C(9)-C(10)-C(11)	122.57(15)
C(13)-H(13A)	1.01(2)	C(9)-C(10)-H(10)	119.2(10)
C(13)-H(13B)	0.99(2)	C(11)-C(10)-H(10)	118.2(10)
C(13)-H(13C)	1.020(19)	C(10)-C(11)-C(6)	116.45(14)
C(14)-H(14A)	1.006(19)	C(10)-C(11)-C(12)	121.18(13)
C(14)-H(14B)	1.022(19)	C(6)-C(11)-C(12)	122.36(13)
C(14)-H(14C)	0.986(19)	C(15)-C(12)-C(14)	110.24(14)
C(15)-H(15A)	0.961(17)	C(15)-C(12)-C(11)	110.20(13)
C(15)-H(15B)	1.026(18)	C(14)-C(12)-C(11)	110.32(13)
C(15)-H(15C)	0.997(19)	C(15)-C(12)-C(13)	107.03(15)
		C(14)-C(12)-C(13)	107.27(14)
C(2) -C(1)-C(3)#1	120.45(15)	C(11)-C(12)-C(13)	111.69(14)
C(12)-C(13)-H(13A)	111.7(10)	C(12)-C(14)-H(14C)	112.5(10)
C(12)-C(13)-H(13B)	110.8(11)	H(14A)-C(14)-H(14C)	109.7(14)
H(13A)-C(13)-H(13B)	109.1(15)	H(14B)-C(14) -H(14C)	105.5(15)
C(12)-C(13)-H(13C)	110.4(10)	C(12)-C(15)-H(15A)	112.8(11)
H(13A)-C(13)-H(13C)	108.0(15)	C(12)-C(15)-H(15B)	110.6(10)
H(13B)-C(13)-H(13C)	106.6(14)	H(15A)-C(15)-H(15B)	105.1(13)
C(12)-C(14)-H(14A)	107.7(11)	C(12)-C(15)-H(15C)	109.0(11)
C(12)-C(14)-H(14B)	110.9(10)	H(15A)-C(15)-H(15C)	110.8(14)
H(14A)-C(14)-H(14B)	110.6(14)	H(15B)-C(15) -H(15C)	108.4(15)

Symmetry transformations used to generate equivalent atoms:

#1 -x+2,-y+1,-z+2

Anisotropic displacement parameters ($Å^2 x\ 10^3$) for 03srv123. The anisotropic displacement factor exponent takes the form: $-2p^2 [h^2 a^{*2} U^{11} + ... + 2 h k a^* b^* U^{12}]$

	U^{11}	U^{22}	U^{33}	U^{23}	U^{13}	U^{12}
C(1)	27(1)	21(1)	28(1)	0(1)	1(1)	0(1)
C(2)	32(1)	18(1)	29(1)	-3(1)	2(1)	-4(1)
C(3)	25(1)	22(1)	22(1)	-2(1)	5(1)	-4(1)
C(4)	29(1)	21(1)	25(1)	-1(1)	5(1)	-2(1)
C(5)	28(1)	20(1)	24(1)	0(1)	5(1)	-1(1)
C(6)	21(1)	23(1)	22(1)	-2(1)	2(1)	-1(1)
C(7)	32(1)	23(1)	29(1)	0(1)	5(1)	2(1)
C(8)	29(1)	33(1)	30(1)	2(1)	0(1)	11(1)
C(9)	19(1)	41(1)	30(1)	-5(1)	-3(1)	0(1)
C(10)	24(1)	27(1)	27(1)	-4(1)	3(1)	-5(1)
C(11)	24(1)	22(1)	20(1)	-3(1)	4(1)	-1(1)

C(12)	27(1)	20(1)	26(1)	2(1)	0(1)	-1(1)
C(13)	44(1)	22(1)	34(1)	2(1)	-2(1)	-6(1)
C(14)	32(1)	28(1)	33(1)	1(1)	3(1)	8(1)
C(15)	30(1)	30(1)	24(1)	3(1)	-2(1)	-2(1)

Hydrogen coordinates (x 10^4) and isotropic displacement parameters ($Å^2$ x 10^3) for 03srv123.

	x	y	z	U(eq)
H(1)	12500(20)	4021(11)	10839(14)	24(4)
H(2)	9580(20)	3397(12)	9943(15)	28(4)
H(7)	2450(20)	4781(12)	7333(16)	37(5)
H(8)	-540(20)	4318(12)	6404(16)	34(5)
H(9)	-1570(20)	2764(11)	6640(16)	31(5)
H(10)	410(20)	1684(13)	7742(17)	41(5)
H(13A)	1730(30)	943(12)	9307(18)	40(5)
H(13B)	2680(30)	656(12)	8125(18)	39(5)
H(13C)	3820(20)	441(13)	9405(17)	38(5)
H(14A)	6580(30)	1260(13)	8878(17)	40(5)
H(14B)	5520(20)	1483(11)	7524(17)	30(5)
H(14C)	6500(20)	2301(13)	8322(17)	38(5)
H(15A)	5110(20)	2733(12)	10296(15)	29(4)
H(15B)	5160(20)	1687(12)	10702(17)	37(5)
H(15C)	3140(30)	2254(12)	10554(17)	37(5)

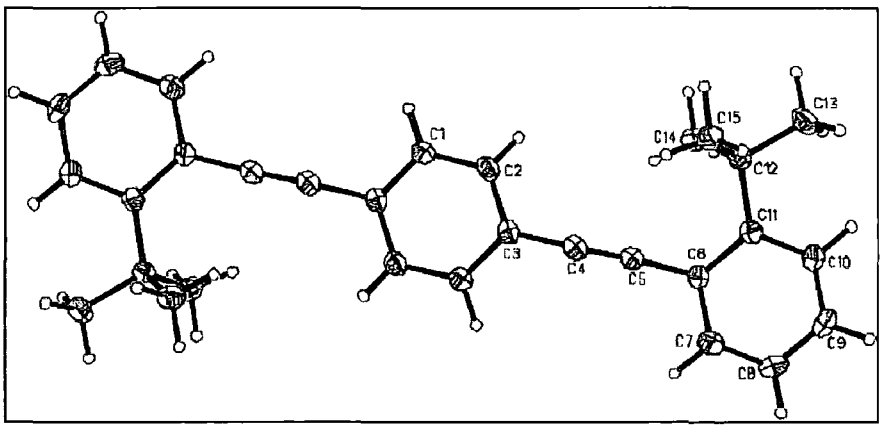

A.8 - 1,4-Bis(2-*tert*-butylphenylethynyl)durene (189)

Crystal data and structure refinement

Identification code	03srv124	
Empirical formula	C34 H38	
Formula weight	446.64	
Temperature	120(2) K	
Wavelength	0.71073 Å	
Crystal system	Triclinic	
Space group	P-1	
Unit cell dimensions	a = 6.0450(6) Å	α= 79.249(2)°.
	b = 7.7895(8) Å	β= 85.080(2)°.
	c = 14.1942(15) Å	γ = 81.676(2)°.
Volume	648.53(12) $Å^3$	
Z	1	
Density (calculated)	1.144 Mg/m^3	
Absorption coefficient	0.064 mm^{-1}	
F(000)	242	
Crystal size	0.28 x 0.16 x 0.06 mm^3	
Theta range for data collection	1.46 to 28.29°.	
Index ranges	-7<=h<=8, -10<=k<=7, -18<=l<=18	
Reflections collected	6722	
Independent reflections	3157 [R(int) = 0.0425]	
Completeness to theta = 28.29°	98.4 %	
Absorption correction	Integration	
Max. and min. transmission	0.9962 and 0.9823	
Refinement method	Full-matrix least-squares on F^2	
Data / restraints / parameters	3157 / 0 / 230	
Goodness-of-fit on F^2	1.081	
Final R indices [I>2sigma(I)]	R1 = 0.0805, wR2 = 0.1707	
R indices (all data)	R1 = 0.1242, wR2 = 0.1903	
Extinction coefficient	0	
Largest diff. peak and hole	0.454 and -0.288 $e.Å^{-3}$	

Atomic coordinates (x 10^4) and equivalent isotropic displacement parameters ($Å^2$ x 10^3) for 03srv124. U(eq) is defined as one third of the trace of the orthogonalized U^{ij} tensor.

	x	y	z	U(eq)
C(1)	1525(4)	-1552(3)	5003(2)	18(1)
C(1A)	3161(5)	-3193(3)	5004(2)	23(1)
C(2)	1762(4)	-409(3)	5626(2)	18(1)
C(2A)	3623(5)	-854(4)	6302(2)	23(1)
C(3)	238(4)	1141(3)	5617(2)	17(1)
C(4)	484(4)	2339(3)	6246(2)	19(1)
C(5)	634(4)	3347(3)	6776(2)	19(1)
C(6)	509(4)	4685(3)	7363(2)	20(1)
C(7)	-1005(5)	6191(3)	7090(2)	24(1)
C(8)	-1352(5)	7540(4)	7625(2)	29(1)
C(9)	-197(5)	7376(4)	8428(2)	29(1)
C(10)	1334(5)	5890(3)	8703(2)	25(1)
C(11)	1743(4)	4510(3)	8185(2)	20(1)
C(12)	3463(5)	2896(3)	8502(2)	24(1)
C(13)	4684(6)	3083(4)	9364(2)	36(1)
C(14)	2232(6)	1256(4)	8784(2)	33(1)
C(15)	5234(5)	2651(4)	7691(2)	30(1)

Bond lengths [Å] and angles [°]for 03srv124.

C(1) -C(2)	1.396(3)	C(14)-H(14A)	1.01(4)
C(1) -C(3)#1	1.403(3)	C(15)-H(15C)	0.95(3)
C(1) -C(1A)	1.498(3)	C(15)-H(15B)	0.99(4)
C(1A)-H(1C)	0.97(3)	C(15)-H(15A)	0.99(4)
C(1A)-H(1B)	0.98(3)		
C(1A)-H(1A)	0.92(4)	C(2)-C(1)-C(3)#1	119.4(2)
C(2) -C(3)	1.407(3)	C(2)-C(1)-C(1A)	119.5(2)
C(2) -C(2A)	1.501(4)	C(3)#1-C(1)-C(1A)	121.1(2)
C(2A)-H(2C)	0.93(4)	C(1)-C(1A)-H(1C)	109.0(18)
C(2A)-H(2B)	0.93(4)	C(1)-C(1A)-H(1B)	111.5(19)
C(2A)-H(2A)	0.98(3)	H(1C)-C(1A)-H(1B)	103(2)
C(3) -C(1)#1	1.403(3)	C(1)-C(1A)-H(1A)	108(2)
C(3) -C(4)	1.436(3)	H(1C)-C(1A)-H(1A)	118(3)
C(4) -C(5)	1.202(3)	H(1B)-C(1A)-H(1A)	107(3)
C(5) -C(6)	1.441(3)	C(1)-C(2)-C(3)	119.4(2)
C(6) -C(7)	1.394(4)	C(1)-C(2)-C(2A)	119.7(2)
C(6) -C(11)	1.414(4)	C(3)-C(2)-C(2A)	120.9(2)

C(7) -C(8)	1.389(4)	C(2)-C(2A)-H(2C)	116(2)
C(7) -H(7)	0.97(3)	C(2)-C(2A)-H(2B)	113(2)
C(8) -C(9)	1.363(4)	H(2C)-C(2A)-H(2B)	100(3)
C(8) -H(8)	0.91(3)	C(2)-C(2A)-H(2A)	111.1(18)
C(9) -C(10)	1.390(4)	H(2C)-C(2A)-H(2A)	106(3)
C(9) -H(9)	0.92(3)	H(2B)-C(2A)-H(2A)	110(3)
C(10)-C(11)	1.394(4)	C(1)#1-C(3)-C(2)	121.2(2)
C(10)-H(10)	0.96(3)	C(1)#1-C(3)-C(4)	118.9(2)
C(11)-C(12)	1.534(4)	C(2)-C(3)-C(4)	119.9(2)
C(12)-C(13)	1.522(4)	C(5)-C(4)-C(3)	178.4(3)
C(12)-C(15)	1.523(4)	C(4)-C(5)-C(6)	171.7(3)
C(12)-C(14)	1.542(4)	C(7)-C(6)-C(11)	120.5(2)
C(13)-H(13B)	1.00(3)	C(7)-C(6)-C(5)	115.5(2)
C(13)-H(13A)	1.05(3)	C(11)-C(6)-C(5)	124.0(2)
C(13)-H(13C)	0.99(4)	C(8)-C(7)-C(6)	120.9(3)
C(14)-H(14C)	0.96(3)	C(8)-C(7)-H(7)	120.4(18)
C(14)-H(14B)	0.95(3)	C(6)-C(7)-H(7)	118.6(18)
C(9) -C(8)-C(7)	119.2(3)	C(12)-C(13)-H(13B)	115.4(18)
C(9) -C(8)-H(8)	122.3(18)	C(12)-C(13)-H(13A)	110.7(16)
C(7) -C(8)-H(8)	118.5(18)	H(13B)-C(13) -H(13A)	112(2)
C(8) -C(9)-C(10)	120.6(3)	C(12)-C(13)-H(13C)	108(2)
C(8) -C(9)-H(9)	124(2)	H(13B)-C(13) -H(13C)	105(3)
C(10)-C(9)-H(9)	116(2)	H(13A)-C(13)-H(13C)	106(3)
C(9) -C(10)-C(11)	122.2(3)	C(12)-C(14)-H(14C)	108.7(17)
C(9) -C(10)-H(10)	117.9(17)	C(12)-C(14)-H(14B)	109(2)
C(11)-C(10)-H(10)	119.9(17)	H(14C)-C(14) -H(14B)	112(3)
C(10)-C(11)-C(6)	116.7(2)	C(12)-C(14)-H(14A)	110(2)
C(10)-C(11)-C(12)	120.9(2)	H(14C)-C(14) -H(14A)	103(3)
C(6) -C(11)-C(12)	122.4(2)	H(14B)-C(14) -H(14A)	114(3)
C(13)-C(12)-C(15)	107.0(3)	C(12)-C(15)-H(15C)	112.0(18)
C(13)-C(12)-C(11)	112.2(2)	C(12)-C(15)-H(15B)	109(2)
C(15)-C(12)-C(11)	110.2(2)	H(15C)-C(15) -H(15B)	117(3)
C(13)-C(12)-C(14)	108.1(2)	C(12)-C(15)-H(15A)	109(2)
C(15)-C(12)-C(14)	110.5(2)	H(15C)-C(15) -H(15A)	105(3)
C(11)-C(12)-C(14)	108.8(2)	H(15B)-C(15) -H(15A)	104(3)

Symmetry transformations used to generate equivalent atoms:

#1 -x,-y,-z+1

Anisotropic displacement parameters ($Å^2 x\ 10^3$) for 03srv124. The anisotropic displacement factor exponent takes the form: $-2\pi^2 [h^2 a^{*2} U^{11} + ... + 2 h k a^* b^* U^{12}]$

	U^{11}	U^{22}	U^{33}	U^{23}	U^{13}	U^{12}
C(1)	19(1)	11(1)	23(1)	-5(1)	0(1)	1(1)
C(1A)	23(2)	16(1)	29(1)	-9(1)	-6(1)	6(1)
C(2)	17(1)	14(1)	22(1)	-5(1)	-2(1)	-1(1)
C(2A)	25(2)	18(1)	29(1)	-9(1)	-6(1)	2(1)
C(3)	19(1)	11(1)	22(1)	-6(1)	-2(1)	0(1)
C(4)	17(1)	16(1)	25(1)	-4(1)	-2(1)	2(1)
C(5)	17(1)	16(1)	25(1)	-5(1)	-3(1)	1(1)
C(6)	22(1)	15(1)	25(1)	-9(1)	1(1)	-4(1)
C(7)	23(2)	19(1)	32(1)	-10(1)	-5(1)	1(1)
C(8)	28(2)	15(1)	44(2)	-10(1)	-3(1)	2(1)
C(9)	35(2)	20(1)	35(1)	-17(1)	2(1)	-4(1)
C(10)	30(2)	21(1)	27(1)	-11(1)	-2(1)	-5(1)
C(11)	21(1)	17(1)	23(1)	-4(1)	2(1)	-8(1)
C(12)	28(2)	19(1)	27(1)	-7(1)	-6(1)	-2(1)
C(13)	42(2)	31(2)	36(2)	-8(1)	-18(1)	1(2)
C(14)	45(2)	22(2)	32(1)	-2(1)	-7(1)	-9(1)
C(15)	22(2)	29(2)	41(2)	-12(1)	-7(1)	-1(1)

Hydrogen coordinates ($x\ 10^4$) and isotropic displacement parameters ($Å^2\ x\ 10^3$) for 03srv124.

	x	y	z	U(eq)
H(1C)	3190(50)	-3870(40)	5650(20)	28(8)
H(1B)	4700(60)	-2920(40)	4870(20)	32(8)
H(1A)	2840(60)	-3750(50)	4520(20)	43(10)
H(2C)	3600(60)	-110(50)	6750(20)	42(9)
H(2B)	3570(60)	-1930(50)	6710(20)	47(10)
H(2A)	5080(60)	-850(40)	5950(20)	37(9)
H(7)	-1780(50)	6300(40)	6510(20)	25(7)
H(8)	-2380(50)	8490(40)	7435(19)	24(7)
H(9)	-430(60)	8180(50)	8840(20)	39(9)
H(10)	2080(50)	5810(40)	9286(19)	18(7)
H(13B)	3730(50)	3120(40)	9970(20)	30(8)
H(13A)	5600(50)	4150(40)	9190(20)	32(8)
H(13C)	5800(60)	2030(50)	9510(20)	44(10)
H(14C)	1260(50)	1390(40)	9341(19)	20(7)
H(14B)	1430(60)	1150(40)	8260(20)	36(9)
H(14A)	3330(60)	190(50)	9010(20)	50(10)

H(15C)	4590(50)	2590(40)	7110(20)	24(7)
H(15B)	6420(60)	1690(50)	7930(20)	49(10)
H(15A)	6020(70)	3710(60)	7540(30)	59(11)

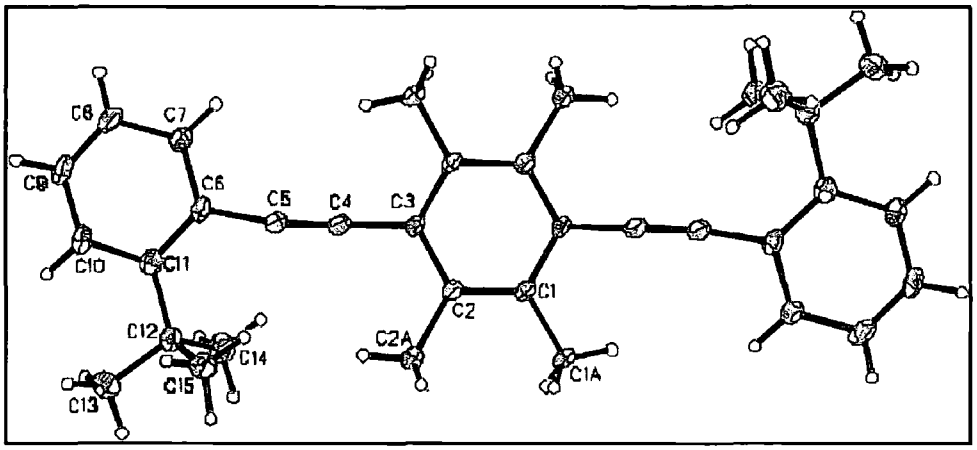

A.9 - 1,4-Bis(2,4,6-triisopropylphenylethynyl)benzene (201)

Crystal data and structure refinement

Identification code	04srv324
Empirical formula	C40 H50
Formula weight	530.80
Temperature	120(2) K
Wavelength	0.71073 Å
Crystal system	Monoclinic
Space group	C2/c
Unit cell dimensions	a = 35.973(5) Å α= 90°.
	b = 8.5080(11) Å β= 107.402(2)°.
	c = 11.2265(14) Å γ = 90°.
Volume	3278.7(7) $Å^3$
Z	4
Density (calculated)	1.075 Mg/m^3
Absorption coefficient	0.060 mm^{-1}
F(000)	1160
Crystal size	0.28 x 0.28 x 0.04 mm^3
Theta range for data collection	2.37 to 25.00°.
Index ranges	-40<=h<=42, -10<=k<=9, -13<=l<=9
Reflections collected	7253
Independent reflections	2857 [R(int) = 0.0938]
Completeness to theta = 25.00°	98.7 %
Absorption correction	Integration
Max. and min. transmission	0.99516 and 0.98210
Refinement method	Full-matrix least-squares on F^2
Data / restraints / parameters	2857 / 0 / 187
Goodness-of-fit on F^2	1.017
Final R indices [I>2sigma(I)]	R1 = 0.1060, wR2 = 0.2495
R indices (all data)	R1 = 0.1269, wR2 = 0.2897
Extinction coefficient	0
Largest diff. peak and hole	0.463 and -0.356 $e.Å^{-3}$

Atomic coordinates (x 10^4) and equivalent isotropic displacement parameters ($Å^2$ x 10^3) for 04srv324. U(eq) is defined as one third of the trace of the orthogonalized U^{ij} tensor.

	x	y	z	U(eq)
C(1)	1581(1)	4430(3)	2068(2)	28(1)
C(2)	1237(1)	5122(3)	2128(2)	29(1)
C(3)	992(1)	4414(3)	2722(2)	29(1)
C(4)	1095(1)	2909(2)	3263(2)	27(1)
C(5)	1444(1)	2178(3)	3210(2)	28(1)
C(6)	1680(1)	2958(2)	2613(2)	29(1)
C(7)	1842(1)	5269(3)	1426(2)	31(1)
C(8)	2220(1)	5825(3)	2372(3)	38(1)
C(9)	1932(1)	4282(3)	411(3)	40(1)
C(10)	630(1)	5268(3)	2779(3)	33(1)
C(11)	367(1)	5657(4)	1485(3)	49(1)
C(12)	735(1)	6747(4)	3588(4)	61(1)
C(13)	1560(1)	552(2)	3769(3)	33(1)
C(14)	1563(1)	-627(3)	2745(3)	52(1)
C(15)	1953(1)	570(3)	4760(3)	45(1)
C(16)	836(1)	2109(2)	3821(2)	28(1)
C(17)	603(1)	1444(3)	4221(2)	32(1)
C(18)	302(1)	701(2)	4627(2)	29(1)
C(19)	-89(1)	1133(3)	4076(2)	35(1)
C(20)	383(1)	-446(3)	5557(3)	34(1)

Bond lengths [Å] and angles [°]for 04srv324.

C(1) -C(2)	1.389(3)	C(14)-H(14B)	0.9800
C(1) -C(6)	1.393(3)	C(14)-H(14C)	0.9800
C(1) -C(7)	1.521(3)	C(15)-H(15A)	0.9800
C(2) -C(3)	1.392(3)	C(15)-H(15B)	0.9800
C(2) -H(2)	0.9500	C(15)-H(15C)	0.9800
C(3) -C(4)	1.418(3)	C(16)-C(17)	1.204(3)
C(3) -C(10)	1.512(3)	C(17)-C(18)	1.442(3)
C(4) -C(5)	1.416(3)	C(18)-C(20)	1.395(4)
C(4) -C(16)	1.441(3)	C(18)-C(19)	1.403(3)
C(5) -C(6)	1.397(3)	C(19)-C(20)#1	1.376(4)
C(5) -C(13)	1.525(3)	C(19)-H(19)	0.9500
C(6) -H(6)	0.9500	C(20)-C(19)#1	1.376(4)
C(7) -C(9)	1.527(4)	C(20)-H(20)	0.9500
C(7) -C(8)	1.529(3)		

C(7) -H(7)	1.0000	C(2)-C(1)-C(6)	118.3(2)
C(8) -H(8A)	0.9800	C(2)-C(1)-C(7)	120.5(2)
C(8) -H(8B)	0.9800	C(6)-C(1)-C(7)	121.2(2)
C(8) -H(8C)	0.9800	C(1)-C(2)-C(3)	122.7(2)
C(9) -H(9A)	0.9800	C(1)-C(2)-H(2)	118.7
C(9) -H(9B)	0.9800	C(3)-C(2)-H(2)	118.7
C(9) -H(9C)	0.9800	C(2)-C(3)-C(4)	118.3(2)
C(10)-C(11)	1.515(4)	C(2)-C(3)-C(10)	119.4(2)
C(10)-C(12)	1.531(4)	C(4)-C(3)-C(10)	122.3(2)
C(10)-H(10)	1.0000	C(5)-C(4)-C(3)	120.0(2)
C(11)-H(11A)	0.9800	C(5)-C(4)-C(16)	120.5(2)
C(11)-H(11B)	0.9800	C(3)-C(4)-C(16)	119.5(2)
C(11)-H(11C)	0.9800	C(6)-C(5)-C(4)	119.0(2)
C(12)-H(12A)	0.9800	C(6)-C(5)-C(13)	119.8(2)
C(12)-H(12B)	0.9800	C(4)-C(5)-C(13)	121.2(2)
C(12)-H(12C)	0.9800	C(1)-C(6)-C(5)	121.7(2)
C(13)-C(15)	1.515(4)	C(1)-C(6)-H(6)	119.1
C(13)-C(14)	1.529(4)	C(5)-C(6)-H(6)	119.1
C(13)-H(13)	1.0000	C(1)-C(7)-C(9)	113.2(2)
C(14)-H(14A)	0.9800	C(1)-C(7)-C(8)	111.3(2)
C(9) -C(7)-C(8)	110.2(2)	H(12A)-C(12)-H(12C)	109.5
C(1) -C(7)-H(7)	107.3	H(12B)-C(12) -H(12C)	109.5
C(9) -C(7)-H(7)	107.3	C(15)-C(13)-C(5)	111.90(19)
C(8) -C(7)-H(7)	107.3	C(15)-C(13)-C(14)	110.1(2)
C(7) -C(8)-H(8A)	109.5	C(5)-C(13)-C(14)	110.4(2)
C(7) -C(8)-H(8B)	109.5	C(15)-C(13)-H(13)	108.1
H(8A)-C(8)-H(8B)	109.5	C(5)-C(13)-H(13)	108.1
C(7) -C(8)-H(8C)	109.5	C(14)-C(13)-H(13)	108.1
H(8A)-C(8)-H(8C)	109.5	C(13)-C(14)-H(14A)	109.5
H(8B)-C(8)-H(8C)	109.5	C(13)-C(14)-H(14B)	109.5
C(7) -C(9)-H(9A)	109.5	H(14A)-C(14)-H(14B)	109.5
C(7) -C(9)-H(9B)	109.5	C(13)-C(14)-H(14C)	109.5
H(9A)-C(9)-H(9B)	109.5	H(14A)-C(14)-H(14C)	109.5
C(7) -C(9)-H(9C)	109.5	H(14B)-C(14) -H(14C)	109.5
H(9A)-C(9)-H(9C)	109.5	C(13)-C(15)-H(15A)	109.5
H(9B)-C(9)-H(9C)	109.5	C(13)-C(15)-H(15B)	109.5
C(3) -C(10)-C(11)	111.3(2)	H(15A)-C(15)-H(15B)	109.5
C(3) -C(10)-C(12)	110.9(2)	C(13)-C(15)-H(15C)	109.5
C(11)-C(10)-C(12)	111.2(2)	H(15A)-C(15)-H(15C)	109.5
C(3) -C(10)-H(10)	107.7	H(15B)-C(15) -H(15C)	109.5

C(11)-C(10)-H(10)	107.7	C(17)-C(16)-C(4)	176.3(3)
C(12)-C(10)-H(10)	107.7	C(16)-C(17)-C(18)	175.7(3)
C(10)-C(11)-H(11A)	109.5	C(20)-C(18)-C(19)	118.1(2)
C(10)-C(11)-H(11B)	109.5	C(20)-C(18)-C(17)	122.3(2)
H(11A)-C(11)-H(11B)	109.5	C(19)-C(18)-C(17)	119.6(2)
C(10)-C(11)-H(11C)	109.5	C(20)#1-C(19)-C(18)	121.0(2)
H(11A)-C(11)-H(11C)	109.5	C(20)#1-C(19)-H(19)	119.5
H(11B)-C(11)-H(11C)	109.5	C(18)-C(19)-H(19)	119.5
C(10)-C(12)-H(12A)	109.5	C(19)#1-C(20)-C(18)	120.9(2)
C(10)-C(12)-H(12B)	109.5	C(19)#1-C(20)-H(20)	119.5
H(12A)-C(12)-H(12B)	109.5	C(18)-C(20)-H(20)	119.5
C(10)-C(12)-H(12C)	109.5		

Symmetry transformations used to generate equivalent atoms:

#1 -x,-y,-z+1

Anisotropic displacement parameters ($Å^2 x\ 10^3$) for 04srv324. The anisotropic displacement factor exponent takes the form: $-2\pi^2 [h^2 a^{*2} U^{11} + ... + 2 h k a^* b^* U^{12}]$

	U^{11}	U^{22}	U^{33}	U^{23}	U^{13}	U^{12}
C(1)	31(1)	25(1)	29(1)	-1(1)	9(1)	-5(1)
C(2)	34(1)	21(1)	31(1)	3(1)	10(1)	0(1)
C(3)	31(1)	24(1)	30(1)	-1(1)	9(1)	-2(1)
C(4)	29(1)	23(1)	30(1)	0(1)	9(1)	-2(1)
C(5)	30(1)	24(1)	31(1)	1(1)	9(1)	-2(1)
C(6)	30(1)	23(1)	37(2)	1(1)	15(1)	1(1)
C(7)	33(1)	25(1)	36(2)	6(1)	12(1)	-1(1)
C(8)	42(2)	34(1)	43(2)	-1(1)	18(1)	-9(1)
C(9)	45(2)	41(2)	39(2)	-2(1)	18(1)	-8(1)
C(10)	29(1)	26(1)	48(2)	3(1)	15(1)	1(1)
C(11)	34(2)	58(2)	56(2)	14(1)	17(1)	9(1)
C(12)	46(2)	52(2)	88(3)	-28(2)	25(2)	3(1)
C(13)	38(2)	22(1)	45(2)	7(1)	21(1)	3(1)
C(14)	74(2)	22(1)	53(2)	-2(1)	8(2)	1(1)
C(15)	57(2)	29(1)	45(2)	7(1)	10(1)	8(1)
C(16)	30(1)	22(1)	35(2)	0(1)	12(1)	1(1)
C(17)	34(1)	25(1)	37(2)	-3(1)	13(1)	1(1)
C(18)	35(1)	21(1)	32(2)	-4(1)	14(1)	-4(1)
C(19)	38(2)	28(1)	40(2)	5(1)	14(1)	-2(1)
C(20)	29(1)	33(1)	41(2)	2(1)	10(1)	1(1)

Hydrogen coordinates (x 10^4) and isotropic displacement parameters ($Å^2$ x 10^3) for 04srv324.

	x	y	z	U(eq)
H(2)	1167	6120	1748	34
H(6)	1914	2471	2579	35
H(7)	1699	6226	1014	37
H(8A)	2159	6520	2984	58
H(8B)	2377	6398	1936	58
H(8C)	2367	4913	2801	58
H(9A)	1688	3894	-169	60
H(9B)	2096	3389	794	60
H(9C)	2069	4929	-45	60
H(10)	483	4550	3182	40
H(11A)	299	4688	995	73
H(11B)	502	6374	1072	73
H(11C)	128	6161	1549	73
H(12A)	882	6449	4442	91
H(12B)	496	7293	3596	91
H(12C)	894	7445	3244	91
H(13)	1360	202	4169	40
H(14A)	1306	-644	2117	78
H(14B)	1624	-1676	3111	78
H(14C)	1761	-316	2349	78
H(15A)	1945	1304	5425	67
H(15B)	2153	906	4386	67
H(15C)	2014	-487	5110	67

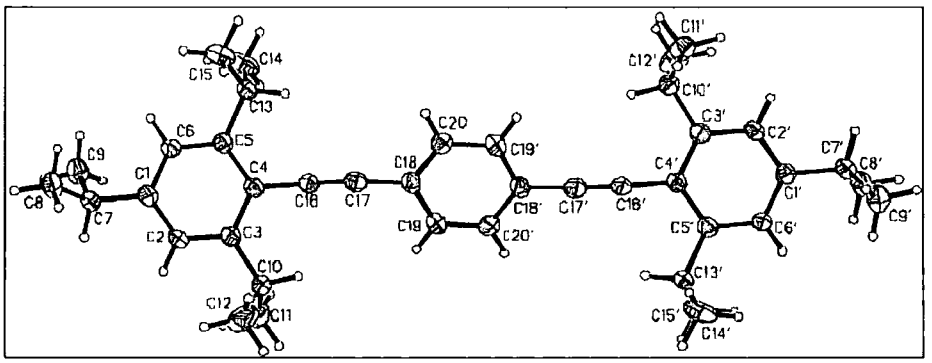

A.10 - 1,4-Bis(2,4,6-triisopropylphenylethynyl)durene (202)

Crystal data and structure refinement

Identification code	04srv325	
Empirical formula	C44 H58	
Formula weight	586.90	
Temperature	120(2) K	
Wavelength	0.71073 Å	
Crystal system	Triclinic	
Space group	P-1	
Unit cell dimensions	a = 6.0219(13) Å	α= 87.924(5)°.
	b = 9.341(2) Å	β= 88.305(5)°.
	c = 16.411(4) Å	γ = 80.947(5)°.
Volume	910.8(3) $Å^3$	
Z	1	
Density (calculated)	1.070 Mg/m^3	
Absorption coefficient	0.060 mm^{-1}	
F(000)	322	
Crystal size	0.46 x 0.18 x 0.16 mm^3	
Theta range for data collection	2.21 to 26.00°.	
Index ranges	-7<=h<=7, -11<=k<=11, -20<=l<=20	
Reflections collected	4807	
Independent reflections	3241 [R(int) = 0.0240]	
Completeness to theta = 26.00°	90.0 %	
Absorption correction	Integration	
Max. and min. transmission	0.9912 and 0.9782	
Refinement method	Full-matrix least-squares on F^2	
Data / restraints / parameters	3241 / 0 / 227	
Goodness-of-fit on F^2	1.024	
Final R indices [I>2sigma(I)]	R1 = 0.0535, wR2 = 0.1275	
R indices (all data)	R1 = 0.0830, wR2 = 0.1415	
Extinction coefficient	0	
Largest diff. peak and hole	0.232 and -0.337 $e.Å^{-3}$	

Atomic coordinates (x 10^4) and equivalent isotropic displacement parameters ($Å^2$ x 10^3) for 04srv325. U(eq) is defined as one third of the trace of the orthogonalized U^{ij} tensor.

	x	y	z	U(eq)
C(1)	1900(3)	2991(2)	1410(1)	23(1)
C(2)	2622(3)	4327(2)	1371(1)	22(1)
C(3)	3867(3)	4776(2)	1981(1)	19(1)
C(4)	4427(3)	3830(2)	2655(1)	22(1)
C(5)	3695(4)	2475(2)	2706(1)	33(1)
C(6)	2442(4)	2092(2)	2081(1)	32(1)
C(7)	592(3)	2515(2)	723(1)	26(1)
C(8)	-1528(4)	1946(3)	1021(2)	37(1)
C(9)	2082(4)	1404(2)	217(1)	30(1)
C(10)	4691(3)	6223(2)	1920(1)	23(1)
C(11)	3106(3)	7412(2)	1481(1)	31(1)
C(12)	7020(4)	6043(2)	1514(1)	34(1)
C(13)	4287(6)	1445(3)	3432(2)	54(1)
C(14)	2683(7)	1552(5)	4048(2)	42(1)
C(15)	5109(8)	-189(4)	3167(3)	43(1)
C(13A)	4287(6)	1445(3)	3432(2)	54(1)
C(14A)	1623(11)	951(7)	3765(4)	33(2)
C(15A)	5774(15)	490(11)	3424(6)	58(3)
C(16)	5803(3)	4219(2)	3278(1)	22(1)
C(17)	7013(3)	4489(2)	3802(1)	23(1)
C(18)	8499(3)	4768(2)	4417(1)	21(1)
C(19)	9896(3)	5818(2)	4265(1)	21(1)
C(20)	8590(3)	3951(2)	5152(1)	21(1)
C(21)	9740(4)	6681(2)	3472(1)	28(1)
C(22)	7056(4)	2843(2)	5298(1)	29(1)

Bond lengths [Å] and angles [°]for 04srv325.

C(1) -C(6)	1.376(3)	C(14)-H(14B)	0.9800
C(1) -C(2)	1.383(3)	C(14)-H(14C)	0.9800
C(1) -C(7)	1.512(3)	C(15)-H(15A)	0.9800
C(2) -C(3)	1.383(3)	C(15)-H(15B)	0.9800
C(2) -H(2A)	0.9500	C(15)-H(15C)	0.9800
C(3) -C(4)	1.405(3)	C(14A)-H(14D)	0.9800
C(3) -C(10)	1.510(3)	C(14A)-H(14E)	0.9800
C(4) -C(5)	1.402(3)	C(14A)-H(14F)	0.9800
C(4)-C(16)	1.427(3)	C(15A)-H(15D)	0.9800

C(5) -C(6)	1.382(3)	C(15A)-H(15E)	0.9800
C(5) -C(13)	1.519(3)	C(15A)-H(15F)	0.9800
C(6) -H(6A)	0.9500	C(16)-C(17)	1.202(3)
C(7) -C(9)	1.516(3)	C(17)-C(18)	1.426(3)
C(7) -C(8)	1.520(3)	C(18)-C(19)	1.401(3)
C(7) -H(7A)	1.0000	C(18)-C(20)	1.402(3)
C(8) -H(8A)	0.9800	C(19)-C(20)#1	1.386(3)
C(8) -H(8B)	0.9800	C(19)-C(21)	1.503(3)
C(8) -H(8C)	0.9800	C(20)-C(19)#1	1.386(3)
C(9) -H(9A)	0.9800	C(20)-C(22)	1.500(3)
C(9) -H(9B)	0.9800	C(21)-H(21A)	0.9800
C(9) -H(9C)	0.9800	C(21)-H(21B)	0.9800
C(10)-C(11)	1.521(3)	C(21)-H(21C)	0.9800
C(10)-C(12)	1.522(3)	C(22)-H(22A)	0.9800
C(10)-H(10A)	1.0000	C(22)-H(22B)	0.9800
C(11)-H(11A)	0.9800	C(22)-H(22C)	0.9800
C(11)-H(11B)	0.9800		
C(11)-H(11C)	0.9800	C(6)-C(1)-C(2)	118.34(18)
C(12)-H(12A)	0.9800	C(6)-C(1)-C(7)	120.70(18)
C(12)-H(12B)	0.9800	C(2)-C(1)-C(7)	120.94(17)
C(12)-H(12C)	0.9800	C(1)-C(2)-C(3)	122.17(18)
C(13)-C(14)	1.373(5)	C(1)-C(2)-H(2A)	118.9
C(13)-C(15)	1.601(5)	C(3)-C(2)-H(2A)	118.9
C(13)-H(13A)	1.0000	C(2)-C(3)-C(4)	118.43(17)
C(14)-H(14A)	0.9800	C(2)-C(3)-C(10)	121.47(17)
C(4) -C(3)-C(10)	120.07(16)	H(11A)-C(11)-H(11B)	109.5
C(5) -C(4)-C(3)	120.15(17)	C(10)-C(11)-H(11C)	109.5
C(5) -C(4)-C(16)	119.53(18)	H(11A)-C(11)-H(11C)	109.5
C(3) -C(4)-C(16)	120.29(17)	H(11B)-C(11) -H(11C)	109.5
C(6) -C(5)-C(4)	118.74(19)	C(10)-C(12)-H(12A)	109.5
C(6) -C(5)-C(13)	120.65(19)	C(10)-C(12)-H(12B)	109.5
C(4) -C(5)-C(13)	120.60(18)	H(12A)-C(12)-H(12B)	109.5
C(1) -C(6)-C(5)	122.16(19)	C(10)-C(12)-H(12C)	109.5
C(1) -C(6)-H(6A)	118.9	H(12A)-C(12)-H(12C)	109.5
C(5) -C(6)-H(6A)	118.9	H(12B)-C(12) -H(12C)	109.5
C(1) -C(7)-C(9)	110.51(16)	C(14)-C(13)-C(5)	114.4(3)
C(1) -C(7)-C(8)	112.84(18)	C(14)-C(13)-C(15)	113.1(3)
C(9) -C(7)-C(8)	110.98(17)	C(5)-C(13)-C(15)	112.5(2)
C(1) -C(7)-H(7A)	107.4	C(14)-C(13)-H(13A)	105.3
C(9) -C(7)-H(7A)	107.4	C(5)-C(13)-H(13A)	105.3

C(8) -C(7)-H(7A)	107.4	C(15)-C(13)-H(13A)	105.3
C(7) -C(8)-H(8A)	109.5	H(14D) -C(14A)-H(14E)	109.5
C(7) -C(8)-H(8B)	109.5	H(14D) -C(14A)-H(14F)	109.5
H(8A)-C(8)-H(8B)	109.5	H(14E)-C(14A)-H(14F)	109.5
C(7) -C(8)-H(8C)	109.5	H(15D) -C(15A)-H(15E)	109.5
H(8A)-C(8)-H(8C)	109.5	H(15D) -C(15A)-H(15F)	109.5
H(8B)-C(8)-H(8C)	109.5	H(15E)-C(15A)-H(15F)	109.5
C(7) -C(9)-H(9A)	109.5	C(17)-C(16)-C(4)	177.2(2)
C(7) -C(9)-H(9B)	109.5	C(16)-C(17)-C(18)	178.1(2)
H(9A)-C(9)-H(9B)	109.5	C(19)-C(18)-C(20)	121.15(17)
C(7) -C(9)-H(9C)	109.5	C(19)-C(18)-C(17)	119.47(17)
H(9A)-C(9)-H(9C)	109.5	C(20)-C(18)-C(17)	119.35(18)
H(9B)-C(9)-H(9C)	109.5	C(20)#1-C(19)-C(18)	119.61(17)
C(3) -C(10)-C(11)	114.06(16)	C(20)#1-C(19)-C(21)	120.75(18)
C(3) -C(10)-C(12)	109.71(16)	C(18)-C(19)-C(21)	119.65(17)
C(11)-C(10)-C(12)	110.46(17)	C(19)#1-C(20)-C(18)	119.25(18)
C(3) -C(10)-H(10A)	107.4	C(19)#1-C(20)-C(22)	120.96(17)
C(11)-C(10)-H(10A)	107.4	C(18)-C(20)-C(22)	119.79(17)
C(12)-C(10)-H(10A)	107.4	C(19)-C(21)-H(21A)	109.5
C(10)-C(11)-H(11A)	109.5	C(19)-C(21)-H(21B)	109.5
C(10)-C(11)-H(11B)	109.5	H(21A)-C(21)-H(21B)	109.5
C(19)-C(21)-H(21C)	109.5	H(22A)-C(22)-H(22B)	109.5
H(21A)-C(21)-H(21C)	109.5	C(20)-C(22)-H(22C)	109.5
H(21B)-C(21)-H(21C)	109.5	H(22A)-C(22)-H(22C)	109.5
C(20)-C(22)-H(22A)	109.5	H(22B)-C(22) -H(22C)	109.5
C(20)-C(22)-H(22B)	109.5		

Symmetry transformations used to generate equivalent atoms:

#1 -x+2,-y+1,-z+1

Anisotropic displacement parameters ($Å^2 x\ 10^3$) for 04srv325. The anisotropic displacement factor exponent takes the form: $-2\pi^2 [h^2 a^{*2} U^{11} + ... + 2 h k a^* b^* U^{12}]$

	U^{11}	U^{22}	U^{33}	U^{23}	U^{13}	U^{12}
C(1)	21(1)	23(1)	26(1)	-5(1)	1(1)	-2(1)
C(2)	19(1)	23(1)	24(1)	1(1)	0(1)	-1(1)
C(3)	17(1)	18(1)	21(1)	-1(1)	4(1)	-2(1)
C(4)	23(1)	21(1)	24(1)	-3(1)	0(1)	-4(1)
C(5)	48(1)	26(1)	28(1)	1(1)	-6(1)	-15(1)
C(6)	42(1)	24(1)	32(1)	-1(1)	-4(1)	-15(1)
C(7)	26(1)	23(1)	31(1)	-3(1)	-6(1)	-4(1)
C(8)	27(1)	42(1)	45(1)	-15(1)	0(1)	-9(1)

C(9)	33(1)	31(1)	27(1)	-5(1)	0(1)	-6(1)
C(10)	23(1)	21(1)	25(1)	1(1)	-2(1)	-5(1)
C(11)	31(1)	23(1)	38(1)	5(1)	-6(1)	-7(1)
C(12)	28(1)	33(1)	43(1)	5(1)	3(1)	-10(1)
C(13)	102(2)	36(2)	34(1)	10(1)	-26(2)	-41(2)
C(14)	36(2)	47(2)	39(2)	5(2)	2(2)	5(2)
C(15)	63(3)	26(2)	37(2)	3(2)	0(2)	3(2)
C(13A)	102(2)	36(2)	34(1)	10(1)	-26(2)	-41(2)
C(14A)	38(4)	28(4)	36(4)	14(3)	2(3)	-11(3)
C(15A)	45(5)	55(6)	61(6)	38(5)	-8(4)	19(5)
C(16)	29(1)	17(1)	21(1)	3(1)	0(1)	-6(1)
C(17)	27(1)	17(1)	24(1)	3(1)	1(1)	-3(1)
C(18)	21(1)	19(1)	21(1)	-3(1)	0(1)	1(1)
C(19)	23(1)	19(1)	20(1)	-1(1)	1(1)	1(1)
C(20)	21(1)	20(1)	22(1)	-2(1)	4(1)	-2(1)
C(21)	31(1)	27(1)	26(1)	4(1)	-3(1)	-6(1)
C(22)	33(1)	31(1)	26(1)	4(1)	-2(1)	-12(1)

Hydrogen coordinates (x 10^4) and isotropic displacement parameters ($Å^2$ x 10^3) for 04srv324.

	x	y	z	U(eq)
H(2A)	2251	4956	911	27
H(6A)	1939	1177	2115	38
H(7A)	119	3386	360	32
H(8A)	-2452	2676	1352	56
H(8B)	-1117	1053	1351	56
H(8C)	-2383	1742	551	56
H(9A)	3413	1806	18	45
H(9B)	1244	1162	-249	45
H(9C)	2551	527	553	45
H(10A)	4843	6541	2488	28
H(11A)	1598	7482	1733	46
H(11B)	3044	7181	905	46
H(11C)	3654	8340	1523	46
H(12A)	8033	5296	1814	51
H(12B)	7602	6965	1516	51
H(12C)	6923	5751	950	51
H(13A)	5633	1760	3672	65
H(14A)	2371	2555	4228	63
H(14B)	3233	907	4508	63

H(14C)	1300	1271	3849	63
H(15A)	6252	-199	2728	65
H(15B)	3826	-597	2973	65
H(15C)	5754	-770	3636	65
H(13B)	4668	2081	3868	65
H(14D)	457	1810	3740	50
H(14E)	1732	562	4328	50
H(14F)	1231	213	3410	50
H(15D)	7199	873	3403	86
H(15E)	5681	-87	2942	86
H(15F)	5696	-123	3918	86
H(21A)	9913	7685	3570	42
H(21B)	8271	6664	3234	42
H(21C)	10933	6256	3094	42
H(22A)	6467	2893	5861	44
H(22B)	7896	1873	5207	44
H(22C)	5805	3041	4921	44

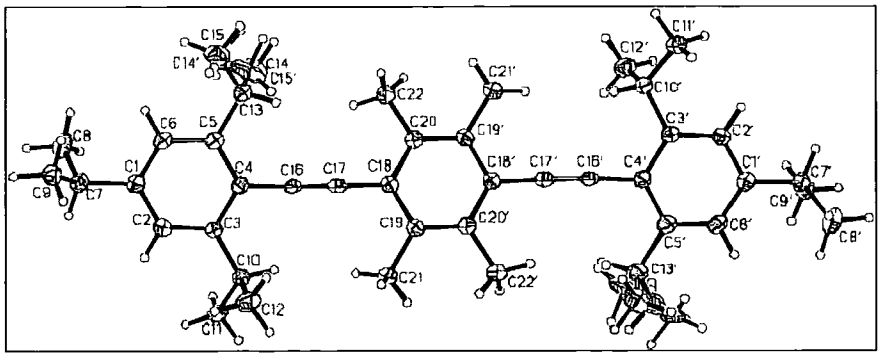

A.11 - 1,4-Bis(2,4,6-tri-*tert*-butylphenylethynyl)benzene (208)

Crystal data and structure refinement

Identification code	04srv359	
Empirical formula	C46 H62	
Formula weight	614.96	
Temperature	120(2) K	
Wavelength	0.71073 Å	
Crystal system	Triclinic	
Space group	P-1	
Unit cell dimensions	a = 5.9686(2) Å	α= 82.1750(10)°.
	b = 10.1769(4) Å	β= 89.0230(10)°.
	c = 17.0324(6) Å	γ = 73.1920(10)°.
Volume	980.89(6) $Å^3$	
Z	1	
Density (calculated)	1.041 Mg/m^3	
Absorption coefficient	0.058 mm^{-1}	
F(000)	338	
Crystal size	0.28 x 0.10 x 0.08 mm^3	
Theta range for data collection	2.11 to 27.00°.	
Index ranges	-7<=h<=7, -12<=k<=12, -21<=l<=21	
Reflections collected	10407	
Independent reflections	4262 [R(int) = 0.0687]	
Completeness to theta = 27.00°	99.8 %	
Absorption correction	Integration	
Max. and min. transmission	0.99577 and 0.98741	
Refinement method	Full-matrix least-squares on F^2	
Data / restraints / parameters	4262 / 0 / 217	
Goodness-of-fit on F^2	0.925	
Final R indices [I>2sigma(I)]	R1 = 0.0431, wR2 = 0.0965	
R indices (all data)	R1 = 0.0726, wR2 = 0.1076	
Extinction coefficient	0	
Largest diff. peak and hole	0.221 and -0.201 $e.Å^{-3}$	

Atomic coordinates (x 10^4) and equivalent isotropic displacement parameters ($Å^2$ x 10^3) for 04srv359. U(eq) is defined as one third of the trace of the orthogonalized U^{ij} tensor.

	x	y	z	U(eq)
C(1)	6725(2)	2587(1)	3440(1)	21(1)
C(2)	6974(2)	1202(1)	3371(1)	22(1)
C(3)	5889(2)	790(1)	2778(1)	21(1)
C(4)	4450(2)	1844(1)	2209(1)	20(1)
C(5)	4179(2)	3262(1)	2257(1)	20(1)
C(6)	5330(2)	3583(1)	2877(1)	22(1)
C(7)	7962(2)	2936(1)	4131(1)	25(1)
C(8)	6988(3)	2418(2)	4914(1)	35(1)
C(9)	10607(2)	2222(2)	4119(1)	34(1)
C(10)	7592(3)	4496(2)	4096(1)	39(1)
C(11)	6223(2)	-771(1)	2760(1)	24(1)
C(12)	7362(2)	-1222(1)	1985(1)	31(1)
C(13)	3862(2)	-1092(1)	2874(1)	30(1)
C(14)	7855(3)	-1677(1)	3437(1)	32(1)
C(15)	2654(2)	4445(1)	1655(1)	23(1)
C(16)	76(2)	4457(2)	1701(1)	30(1)
C(17)	3542(3)	4303(2)	809(1)	31(1)
C(18)	2752(2)	5877(1)	1820(1)	31(1)
C(19)	3250(2)	1450(1)	1596(1)	23(1)
C(20)	2266(2)	1071(1)	1104(1)	25(1)
C(21)	1126(2)	538(1)	539(1)	24(1)
C(22)	2266(3)	-702(2)	258(1)	33(1)
C(23)	-1154(3)	1232(2)	271(1)	34(1)

Bond lengths [Å] and angles [°]for 04srv359.

C(1) -C(6)	1.3847(17)	C(14)-H(14B)	0.9800
C(1) -C(2)	1.3945(17)	C(14)-H(14C)	0.9800
C(1) -C(7)	1.5324(17)	C(15)-C(16)	1.5362(18)
C(2) -C(3)	1.3832(17)	C(15)-C(18)	1.5376(18)
C(2) -H(2)	0.9500	C(15)-C(17)	1.5383(18)
C(3) -C(4)	1.4277(17)	C(16)-H(16A)	0.9800
C(3) -C(11)	1.5463(17)	C(16)-H(16B)	0.9800
C(4) -C(5)	1.4187(17)	C(16)-H(16C)	0.9800
C(4) -C(19)	1.4390(18)	C(17)-H(17A)	0.9800
C(5) -C(6)	1.3928(17)	C(17)-H(17B)	0.9800
C(5) -C(15)	1.5461(17)	C(17)-H(17C)	0.9800

C(6) -H(6)	0.9500	C(18)-H(18A)	0.9800
C(7) -C(10)	1.5315(19)	C(18)-H(18B)	0.9800
C(7) -C(8)	1.5334(19)	C(18)-H(18C)	0.9800
C(7) -C(9)	1.5364(19)	C(19)-C(20)	1.1975(18)
C(8) -H(8A)	0.9800	C(20)-C(21)	1.4348(18)
C(8) -H(8B)	0.9800	C(21)-C(23)	1.3921(19)
C(8) -H(8C)	0.9800	C(21)-C(22)	1.3936(19)
C(9) -H(9A)	0.9800	C(22)-C(23)#1	1.3787(19)
C(9) -H(9B)	0.9800	C(22)-H(22)	0.9500
C(9) -H(9C)	0.9800	C(23)-C(22)#1	1.3787(19)
C(10)-H(10A)	0.9800	C(23)-H(23)	0.9500
C(10)-H(10B)	0.9800		
C(10)-H(10C)	0.9800	C(6)-C(1)-C(2)	117.41(11)
C(11)-C(14)	1.5363(18)	C(6)-C(1)-C(7)	123.33(11)
C(11)-C(12)	1.5390(18)	C(2)-C(1)-C(7)	119.25(11)
C(11)-C(13)	1.5401(18)	C(3)-C(2)-C(1)	123.34(12)
C(12)-H(12A)	0.9800	C(3)-C(2)-H(2)	118.3
C(12)-H(12B)	0.9800	C(1)-C(2)-H(2)	118.3
C(12)-H(12C)	0.9800	C(2)-C(3)-C(4)	117.77(11)
C(13)-H(13A)	0.9800	C(2)-C(3)-C(11)	119.68(11)
C(13)-H(13B)	0.9800	C(4)-C(3)-C(11)	122.54(11)
C(13)-H(13C)	0.9800	C(5)-C(4)-C(3)	120.37(11)
C(14)-H(14A)	0.9800	C(5)-C(4)-C(19)	120.49(11)
C(3) -C(4)-C(19)	119.13(11)	C(13)-C(11)-C(3)	110.16(11)
C(6) -C(5)-C(4)	117.95(11)	C(11)-C(12)-H(12A)	109.5
C(6) -C(5)-C(15)	119.53(11)	C(11)-C(12)-H(12B)	109.5
C(4) -C(5)-C(15)	122.52(11)	H(12A)-C(12)-H(12B)	109.5
C(1) -C(6)-C(5)	123.15(12)	C(11)-C(12)-H(12C)	109.5
C(1) -C(6)-H(6)	118.4	H(12A)-C(12)-H(12C)	109.5
C(5) -C(6)-H(6)	118.4	H(12B)-C(12) -H(12C)	109.5
C(10)-C(7)-C(1)	112.38(11)	C(11)-C(13)-H(13A)	109.5
C(10)-C(7)-C(8)	108.14(12)	C(11)-C(13)-H(13B)	109.5
C(1) -C(7)-C(8)	109.00(11)	H(13A)-C(13)-H(13B)	109.5
C(10)-C(7)-C(9)	108.04(12)	C(11)-C(13)-H(13C)	109.5
C(1) -C(7)-C(9)	110.01(11)	H(13A)-C(13)-H(13C)	109.5
C(8) -C(7)-C(9)	109.20(11)	H(13B)-C(13) -H(13C)	109.5
C(7) -C(8)-H(8A)	109.5	C(11)-C(14)-H(14A)	109.5
C(7) -C(8)-H(8B)	109.5	C(11)-C(14)-H(14B)	109.5
H(8A)-C(8)-H(8B)	109.5	H(14A)-C(14)-H(14B)	109.5
C(7) -C(8)-H(8C)	109.5	C(11)-C(14)-H(14C)	109.5

H(8A)-C(8)-H(8C)	109.5	H(14A)-C(14)-H(14C)	109.5
H(8B)-C(8)-H(8C)	109.5	H(14B)-C(14) -H(14C)	109.5
C(7) -C(9)-H(9A)	109.5	C(16)-C(15)-C(18)	106.97(11)
C(7) -C(9)-H(9B)	109.5	C(16)-C(15)-C(17)	110.49(11)
H(9A)-C(9)-H(9B)	109.5	C(18)-C(15)-C(17)	106.02(11)
C(7) -C(9)-H(9C)	109.5	C(16)-C(15)-C(5)	110.55(10)
H(9A)-C(9)-H(9C)	109.5	C(18)-C(15)-C(5)	111.94(10)
H(9B)-C(9)-H(9C)	109.5	C(17)-C(15)-C(5)	110.71(10)
C(7) -C(10)-H(10A)	109.5	C(15)-C(16)-H(16A)	109.5
C(7) -C(10)-H(10B)	109.5	C(15)-C(16)-H(16B)	109.5
H(10A)-C(10)-H(10B)	109.5	H(16A)-C(16)-H(16B)	109.5
C(7) -C(10)-H(10C)	109.5	C(15)-C(16)-H(16C)	109.5
H(10A)-C(10)-H(10C)	109.5	H(16A)-C(16)-H(16C)	109.5
H(10B)-C(10)-H(10C)	109.5	H(16B)-C(16) -H(16C)	109.5
C(14)-C(11)-C(12)	106.29(11)	C(15)-C(17)-H(17A)	109.5
C(14)-C(11)-C(13)	106.29(11)	C(15)-C(17)-H(17B)	109.5
C(12)-C(11)-C(13)	111.26(11)	H(17A)-C(17)-H(17B)	109.5
C(14)-C(11)-C(3)	111.79(11)	C(15)-C(17)-H(17C)	109.5
C(12)-C(11)-C(3)	110.92(11)	H(17A)-C(17)-H(17C)	109.5
H(17B)-C(17)-H(17C)	109.5	C(23)-C(21)-C(22)	118.45(12)
C(15)-C(18)-H(18A)	109.5	C(23)-C(21)-C(20)	120.91(12)
C(15)-C(18)-H(18B)	109.5	C(22)-C(21)-C(20)	120.63(12)
H(18A)-C(18)-H(18B)	109.5	C(23)#1-C(22)-C(21)	120.70(13)
C(15)-C(18)-H(18C)	109.5	C(23)#1-C(22)-H(22)	119.7
H(18A)-C(18)-H(18C)	109.5	C(21)-C(22)-H(22)	119.7
H(18B)-C(18)-H(18C)	109.5	C(22)#1-C(23)-C(21)	120.85(13)
C(20)-C(19)-C(4)	177.39(14)	C(22)#1-C(23)-H(23)	119.6
C(19)-C(20)-C(21)	176.67(14)	C(21)-C(23)-H(23)	119.6

Symmetry transformations used to generate equivalent atoms:

#1 -x,-y,-z

Anisotropic displacement parameters ($Å^2 x\ 10^3$) for 04srv359. The anisotropic displacement factor exponent takes the form: $-2\pi^2 [h^2 a^{*2} U^{11} + ... + 2 h k a^* b^* U^{12}]$

	U^{11}	U^{22}	U^{33}	U^{23}	U^{13}	U^{12}
C(1)	21(1)	26(1)	20(1)	-5(1)	2(1)	-10(1)
C(2)	23(1)	23(1)	21(1)	0(1)	-2(1)	-7(1)
C(3)	20(1)	22(1)	22(1)	-4(1)	2(1)	-8(1)
C(4)	21(1)	23(1)	18(1)	-5(1)	1(1)	-7(1)
C(5)	18(1)	23(1)	18(1)	-3(1)	3(1)	-6(1)
C(6)	24(1)	20(1)	23(1)	-5(1)	3(1)	-8(1)

C(7)	29(1)	28(1)	21(1)	-7(1)	-2(1)	-12(1)
C(8)	41(1)	49(1)	21(1)	-9(1)	0(1)	-20(1)
C(9)	28(1)	48(1)	31(1)	-11(1)	-4(1)	-15(1)
C(10)	56(1)	34(1)	35(1)	-11(1)	-10(1)	-19(1)
C(11)	26(1)	20(1)	28(1)	-5(1)	-3(1)	-8(1)
C(12)	30(1)	26(1)	37(1)	-11(1)	0(1)	-5(1)
C(13)	32(1)	28(1)	33(1)	-5(1)	-1(1)	-14(1)
C(14)	37(1)	21(1)	38(1)	0(1)	-9(1)	-10(1)
C(15)	22(1)	23(1)	23(1)	-2(1)	0(1)	-3(1)
C(16)	24(1)	31(1)	31(1)	-4(1)	-1(1)	-4(1)
C(17)	32(1)	33(1)	23(1)	1(1)	2(1)	-5(1)
C(18)	31(1)	24(1)	34(1)	-1(1)	-2(1)	-5(1)
C(19)	23(1)	22(1)	22(1)	-3(1)	0(1)	-5(1)
C(20)	26(1)	24(1)	24(1)	-5(1)	-2(1)	-5(1)
C(21)	28(1)	27(1)	19(1)	-4(1)	-3(1)	-10(1)
C(22)	27(1)	34(1)	36(1)	-12(1)	-11(1)	-1(1)
C(23)	32(1)	30(1)	38(1)	-15(1)	-7(1)	0(1)

Hydrogen coordinates (x 10^4) and isotropic displacement parameters ($Å^2$ x 10^3) for 04srv359.

	x	y	z	U(eq)
H(2)	7939	507	3751	27
H(6)	5149	4531	2914	26
H(8A)	5304	2881	4927	52
H(8B)	7783	2629	5358	52
H(8C)	7254	1415	4956	52
H(9A)	10892	1215	4182	51
H(9B)	11389	2468	4555	51
H(9C)	11228	2528	3613	51
H(10A)	5914	4972	4109	59
H(10B)	8237	4844	3605	59
H(10C)	8389	4669	4553	59
H(12A)	6397	-658	1532	46
H(12B)	7485	-2201	1975	46
H(12C)	8928	-1094	1955	46
H(13A)	2772	-563	2441	45
H(13B)	3212	-832	3381	45
H(13C)	4098	-2085	2870	45
H(14A)	9392	-1511	3391	48
H(14B)	8029	-2656	3406	48

H(14C)	7185	-1444	3947	48
H(16A)	-854	5189	1301	44
H(16B)	-503	4633	2229	44
H(16C)	-60	3558	1599	44
H(17A)	2565	5066	438	46
H(17B)	3459	3418	665	46
H(17C)	5168	4335	785	46
H(18A)	1793	6595	1420	46
H(18B)	4376	5911	1795	46
H(18C)	2149	6036	2348	46
H(22)	3826	-1188	432	40
H(23)	-1954	2082	454	41

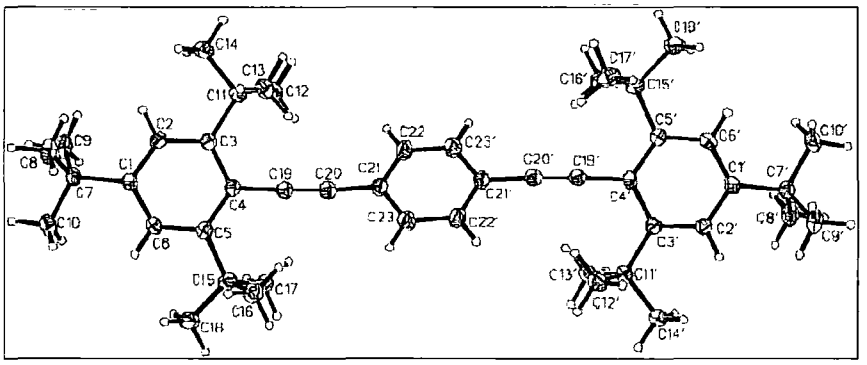

A.12 - 1,4-Bis(2,4,6-tri-*tert*-butylphenylethynyl)durene (209)

Crystal data and structure refinement

Identification code	04srv388	
Empirical formula	C50 H70	
Formula weight	671.06	
Temperature	120(2) K	
Wavelength	0.71073 Å	
Crystal system	Triclinic	
Space group	P -1	
Unit cell dimensions	a = 6.0039(6) Å	α= 80.167(2)°.
	b = 9.7878(9) Å	β= 83.947(2)°.
	c = 18.8607(17) Å	γ = 76.187(2)°.
Volume	1058.06(17) $Å^3$	
Z	1	
Density (calculated)	1.053 Mg/m^3	
Absorption coefficient	0.058 mm^{-1}	
F(000)	370	
Crystal size	0.40 x 0.10 x 0.06 mm^3	
Theta range for data collection	2.57 to 30.52°.	
Index ranges	-8<=h<=8, -13<=k<=13, -26<=l<=26	
Reflections collected	14686	
Independent reflections	6395 [R(int) = 0.0259]	
Completeness to theta = 30.52°	98.7 %	
Absorption correction	None	
Max. and min. transmission	0.9967 and 0.9770	
Refinement method	Full-matrix least-squares on F^2	
Data / restraints / parameters	6395 / 0 / 366	
Goodness-of-fit on F^2	0.973	
Final R indices [I>2sigma(I)]	R1 = 0.0530, wR2 = 0.1372	
R indices (all data)	R1 = 0.0763, wR2 = 0.1540	
Largest diff. peak and hole	0.513 and -0.195 $e.Å^{-3}$	

Atomic coordinates (x 10^4) and equivalent isotropic displacement parameters ($Å^2$ x 10^3) for 04srv388. U(eq) is defined as one third of the trace of the orthogonalized U^{ij} tensor.

	x	y	z	U(eq)
C(1)	8922(2)	2580(1)	186(1)	20(1)
C(2)	6903(2)	3831(1)	89(1)	14(1)
C(3)	4967(2)	3926(1)	586(1)	14(1)
C(4)	3061(2)	5087(1)	498(1)	14(1)
C(5)	1011(2)	5171(1)	1035(1)	20(1)
C(6)	4992(2)	2824(1)	1203(1)	16(1)
C(7)	5214(2)	1902(1)	1717(1)	15(1)
C(8)	5693(2)	800(1)	2334(1)	13(1)
C(9)	5472(2)	-606(1)	2304(1)	14(1)
C(10)	6160(2)	-1655(1)	2886(1)	16(1)
C(11)	7025(2)	-1388(1)	3493(1)	16(1)
C(12)	7141(2)	1(1)	3516(1)	16(1)
C(13)	6498(2)	1116(1)	2954(1)	14(1)
C(20)	4526(2)	-1010(1)	1660(1)	16(1)
C(21)	2075(2)	-126(1)	1545(1)	26(1)
C(22)	4384(3)	-2582(1)	1778(1)	25(1)
C(23)	6106(3)	-801(1)	975(1)	25(1)
C(30)	7873(2)	-2612(1)	4094(1)	19(1)
C(31)	8590(3)	-2100(2)	4739(1)	31(1)
C(32)	9950(2)	-3636(1)	3784(1)	28(1)
C(33)	5961(2)	-3414(1)	4363(1)	25(1)
C(40)	6712(2)	2620(1)	3038(1)	16(1)
C(41)	7572(3)	2648(1)	3772(1)	25(1)
C(42)	8460(2)	3147(1)	2467(1)	22(1)
C(43)	4346(2)	3662(1)	2992(1)	23(1)

Bond lengths [Å] and angles [°]for 04srv388.

C(1) -C(2)	1.5050(15)	C(21)-H(213)	0.98(2)
C(1) -H(11)	0.999(18)	C(22)-H(221)	0.996(17)
C(1) -H(12)	0.984(17)	C(22)-H(222)	0.997(17)
C(1) -H(13)	0.950(19)	C(22)-H(223)	0.981(19)
C(2) -C(4)#1	1.3982(14)	C(23)-H(231)	0.983(16)
C(2) -C(3)	1.4093(15)	C(23)-H(232)	0.991(18)
C(3) -C(4)	1.4086(15)	C(23)-H(233)	0.992(18)
C(3) -C(6)	1.4440(14)	C(30)-C(31)	1.5293(17)
C(4) -C(2)#1	1.3982(14)	C(30)-C(32)	1.5327(19)

C(4) -C(5)	1.5043(16)	C(30)-C(33)	1.5364(18)
C(5) -H(51)	0.954(18)	C(31)-H(311)	0.994(19)
C(5) -H(52)	0.965(19)	C(31)-H(312)	1.020(18)
C(5) -H(53)	0.991(18)	C(31)-H(313)	1.003(18)
C(6) -C(7)	1.2011(15)	C(32)-H(321)	0.985(17)
C(7) -C(8)	1.4460(14)	C(32)-H(322)	1.013(18)
C(8) -C(13)	1.4194(15)	C(32)-H(323)	0.97(2)
C(8) -C(9)	1.4248(15)	C(33)-H(331)	0.981(18)
C(9) -C(10)	1.3923(14)	C(33)-H(332)	1.004(16)
C(9) -C(20)	1.5404(15)	C(33)-H(333)	1.008(17)
C(10)-C(11)	1.3919(15)	C(40)-C(41)	1.5345(17)
C(10)-H(10)	0.978(15)	C(40)-C(42)	1.5359(17)
C(11)-C(12)	1.3869(15)	C(40)-C(43)	1.5394(17)
C(11)-C(30)	1.5315(14)	C(41)-H(411)	0.972(17)
C(12)-C(13)	1.3979(14)	C(41)-H(412)	1.005(16)
C(12)-H(12)	0.953(16)	C(41)-H(413)	1.017(17)
C(13)-C(40)	1.5432(15)	C(42)-H(421)	0.986(17)
C(20)-C(23)	1.5346(17)	C(42)-H(422)	0.990(18)
C(20)-C(21)	1.5347(17)	C(42)-H(423)	0.983(17)
C(20)-C(22)	1.5384(16)	C(43)-H(431)	0.989(16)
C(21)-H(211)	1.020(17)	C(43)-H(432)	1.021(17)
C(21)-H(212)	1.011(17)	C(43)-H(433)	1.00(2)
C(2) -C(1)-H(11)	111.2(11)	H(11)-C(1)-H(12)	106.6(14)
C(2) -C(1)-H(12)	112.0(9)	C(2)-C(1)-H(13)	110.6(11)
H(11)-C(1)-H(13)	106.6(15)	C(8)-C(13)-C(40)	123.52(9)
H(12)-C(1)-H(13)	109.7(14)	C(23)-C(20)-C(21)	110.75(10)
C(4)#1-C(2)-C(3)	119.49(9)	C(23)-C(20)-C(22)	106.13(10)
C(4)#1-C(2)-C(1)	119.89(10)	C(21)-C(20)-C(22)	106.60(10)
C(3) -C(2)-C(1)	120.62(9)	C(23)-C(20)-C(9)	110.68(10)
C(4) -C(3)-C(2)	121.10(9)	C(21)-C(20)-C(9)	110.16(9)
C(4) -C(3)-C(6)	120.16(10)	C(22)-C(20)-C(9)	112.40(9)
C(2) -C(3)-C(6)	118.72(9)	C(20)-C(21)-H(211)	110.1(9)
C(2)#1-C(4)-C(3)	119.41(10)	C(20)-C(21)-H(212)	112.7(10)
C(2)#1-C(4)-C(5)	120.23(10)	H(211)-C(21) -H(212)	108.2(13)
C(3) -C(4)-C(5)	120.36(9)	C(20)-C(21)-H(213)	110.5(11)
C(4) -C(5)-H(51)	112.8(11)	H(211)-C(21) -H(213)	107.6(15)
C(4) -C(5)-H(52)	110.8(11)	H(212)-C(21) -H(213)	107.5(14)
H(51)-C(5)-H(52)	104.2(14)	C(20)-C(22)-H(221)	112.1(10)
C(4) -C(5)-H(53)	111.6(10)	C(20)-C(22)-H(222)	107.9(9)
H(51)-C(5)-H(53)	109.3(14)	H(221)-C(22) -H(222)	106.4(14)

H(52)-C(5)-H(53)	107.7(15)	C(20)-C(22)-H(223)	111.2(11)
C(7) -C(6)-C(3)	174.31(12)	H(221)-C(22) -H(223)	111.1(14)
C(6) -C(7)-C(8)	174.88(12)	H(222)-C(22) -H(223)	107.8(14)
C(13)-C(8)-C(9)	120.33(9)	C(20)-C(23)-H(231)	111.9(10)
C(13)-C(8)-C(7)	119.24(9)	C(20)-C(23)-H(232)	111.1(10)
C(9) -C(8)-C(7)	120.35(9)	H(231)-C(23) -H(232)	106.7(14)
C(10)-C(9)-C(8)	117.90(9)	C(20)-C(23)-H(233)	110.1(10)
C(10)-C(9)-C(20)	119.11(9)	H(231)-C(23) -H(233)	109.5(13)
C(8) -C(9)-C(20)	122.99(9)	H(232)-C(23) -H(233)	107.5(14)
C(11)-C(10)-C(9)	123.12(10)	C(31)-C(30)-C(11)	112.59(10)
C(11)-C(10)-H(10)	118.3(9)	C(31)-C(30)-C(32)	108.77(11)
C(9) -C(10)-H(10)	118.6(9)	C(11)-C(30)-C(32)	108.31(10)
C(12)-C(11)-C(10)	117.58(9)	C(31)-C(30)-C(33)	108.11(11)
C(12)-C(11)-C(30)	122.25(10)	C(11)-C(30)-C(33)	109.85(10)
C(10)-C(11)-C(30)	120.14(10)	C(32)-C(30)-C(33)	109.16(10)
C(11)-C(12)-C(13)	123.00(10)	C(30)-C(31)-H(311)	109.2(11)
C(11)-C(12)-H(12)	119.2(9)	C(30)-C(31)-H(312)	109.6(10)
C(13)-C(12)-H(12)	117.8(9)	H(311)-C(31) -H(312)	106.5(15)
C(12)-C(13)-C(8)	118.00(9)	C(30)-C(31)-H(313)	112.0(10)
C(12)-C(13)-C(40)	118.47(9)	H(311)-C(31) -H(313)	108.8(14)
H(312)-C(31)-H(313)	110.6(14)	C(40)-C(41)-H(411)	110.2(10)
C(30)-C(32)-H(321)	110.8(10)	C(40)-C(41)-H(412)	112.3(9)
C(30)-C(32)-H(322)	112.3(10)	H(411)-C(41) -H(412)	106.1(13)
H(321)-C(32)-H(322)	108.7(14)	C(40)-C(41)-H(413)	112.1(9)
C(30)-C(32)-H(323)	109.3(11)	H(411)-C(41) -H(413)	106.8(13)
H(321)-C(32)-H(323)	107.9(15)	H(412)-C(41) -H(413)	109.1(13)
H(322)-C(32)-H(323)	107.7(15)	C(40)-C(42)-H(421)	110.4(10)
C(30)-C(33)-H(331)	110.7(11)	C(40)-C(42)-H(422)	108.3(11)
C(30)-C(33)-H(332)	111.9(9)	H(421)-C(42) -H(422)	106.9(14)
H(331)-C(33)-H(332)	106.8(13)	C(40)-C(42)-H(423)	111.6(10)
C(30)-C(33)-H(333)	110.7(9)	H(421)-C(42) -H(423)	108.6(14)
H(331)-C(33)-H(333)	107.3(14)	H(422)-C(42) -H(423)	111.0(14)
H(332)-C(33)-H(333)	109.3(13)	C(40)-C(43)-H(431)	114.3(9)
C(41)-C(40)-C(42)	106.10(10)	C(40)-C(43)-H(432)	109.2(10)
C(41)-C(40)-C(43)	106.76(10)	H(431)-C(43) -H(432)	106.9(13)
C(42)-C(40)-C(43)	110.65(10)	C(40)-C(43)-H(433)	109.5(11)
C(41)-C(40)-C(13)	111.94(9)	H(431)-C(43) -H(433)	108.3(14)
C(42)-C(40)-C(13)	111.10(9)	H(432)-C(43) -H(433)	108.5(15)
C(43)-C(40)-C(13)	110.14(9)		

Symmetry transformations used to generate equivalent atoms: #1 -x+1,-y+1,-z

Anisotropic displacement parameters ($Å^2 x\ 10^3$) for 04srv388. The anisotropic displacement factor exponent takes the form: $-2\pi^2 [h^2 a^{*2} U^{11} + ... + 2 h k a^* b^* U^{12}]$

	U^{11}	U^{22}	U^{33}	U^{23}	U^{13}	U^{12}
C(1)	19(1)	17(1)	20(1)	2(1)	-2(1)	1(1)
C(2)	16(1)	13(1)	13(1)	0(1)	-4(1)	-3(1)
C(3)	18(1)	12(1)	13(1)	0(1)	-3(1)	-4(1)
C(4)	15(1)	14(1)	13(1)	0(1)	-2(1)	-4(1)
C(5)	18(1)	20(1)	19(1)	1(1)	1(1)	-5(1)
C(6)	19(1)	15(1)	15(1)	-1(1)	-3(1)	-4(1)
C(7)	18(1)	14(1)	14(1)	-2(1)	-2(1)	-4(1)
C(8)	14(1)	12(1)	13(1)	1(1)	-2(1)	-2(1)
C(9)	16(1)	13(1)	13(1)	-1(1)	-3(1)	-3(1)
C(10)	21(1)	13(1)	16(1)	0(1)	-5(1)	-5(1)
C(11)	19(1)	13(1)	13(1)	2(1)	-4(1)	-3(1)
C(12)	21(1)	15(1)	12(1)	0(1)	-4(1)	-5(1)
C(13)	17(1)	13(1)	13(1)	-1(1)	-1(1)	-4(1)
C(20)	21(1)	14(1)	14(1)	-1(1)	-6(1)	-4(1)
C(21)	23(1)	24(1)	32(1)	-4(1)	-13(1)	-3(1)
C(22)	38(1)	17(1)	23(1)	-1(1)	-12(1)	-10(1)
C(23)	37(1)	25(1)	16(1)	-6(1)	0(1)	-9(1)
C(30)	26(1)	15(1)	17(1)	4(1)	-8(1)	-5(1)
C(31)	51(1)	23(1)	21(1)	6(1)	-19(1)	-12(1)
C(32)	27(1)	23(1)	31(1)	5(1)	-10(1)	0(1)
C(33)	32(1)	23(1)	19(1)	6(1)	-4(1)	-10(1)
C(40)	23(1)	12(1)	15(1)	-1(1)	-2(1)	-7(1)
C(41)	41(1)	19(1)	19(1)	-4(1)	-8(1)	-11(1)
C(42)	25(1)	23(1)	22(1)	-2(1)	0(1)	-13(1)
C(43)	26(1)	17(1)	27(1)	-7(1)	-1(1)	-2(1)

Hydrogen coordinates ($x\ 10^4$) and isotropic displacement parameters ($Å^2\ x\ 10^3$) for 04srv388.

	x	y	z	U(eq)
H(11)	9020(30)	1948(19)	-185(10)	42(5)
H(12)	10390(30)	2878(17)	137(9)	32(4)
H(13)	8770(30)	2013(19)	642(10)	41(5)
H(51)	1130(30)	4343(19)	1391(10)	40(5)
H(52)	-370(30)	5219(19)	801(10)	41(5)
H(53)	750(30)	6024(19)	1277(9)	38(5)
H(10)	6040(30)	-2628(16)	2868(8)	26(4)
H(12)	7720(30)	212(16)	3927(9)	29(4)

H(211)	1460(30)	-385(17)	1115(9)	31(4)
H(212)	1990(30)	933(18)	1456(9)	35(4)
H(213)	1040(30)	-320(20)	1970(11)	49(5)
H(221)	3330(30)	-2813(17)	2202(9)	33(4)
H(222)	3720(30)	-2759(16)	1349(9)	29(4)
H(223)	5920(30)	-3216(19)	1819(10)	44(5)
H(231)	6210(30)	198(17)	836(9)	31(4)
H(232)	7690(30)	-1365(18)	1047(9)	34(4)
H(233)	5540(30)	-1127(18)	571(10)	39(5)
H(311)	9130(30)	-2940(20)	5109(10)	44(5)
H(312)	9950(30)	-1637(18)	4582(9)	35(4)
H(313)	7290(30)	-1423(19)	4962(9)	36(4)
H(321)	10550(30)	-4440(18)	4156(9)	35(4)
H(322)	9570(30)	-4025(18)	3359(10)	37(5)
H(323)	11160(30)	-3130(20)	3619(10)	48(5)
H(331)	6480(30)	-4199(19)	4750(10)	42(5)
H(332)	5500(30)	-3842(16)	3970(9)	27(4)
H(333)	4570(30)	-2760(17)	4566(9)	32(4)
H(411)	7650(30)	3609(18)	3816(9)	30(4)
H(412)	6510(30)	2349(16)	4186(9)	28(4)
H(413)	9180(30)	2026(18)	3837(9)	34(4)
H(421)	9990(30)	2500(18)	2513(9)	32(4)
H(422)	8610(30)	4085(19)	2560(10)	40(5)
H(423)	8000(30)	3208(18)	1976(9)	34(4)
H(431)	3660(30)	3787(16)	2525(9)	26(4)
H(432)	4510(30)	4643(18)	3066(9)	33(4)
H(433)	3250(30)	3320(20)	3384(11)	49(5)

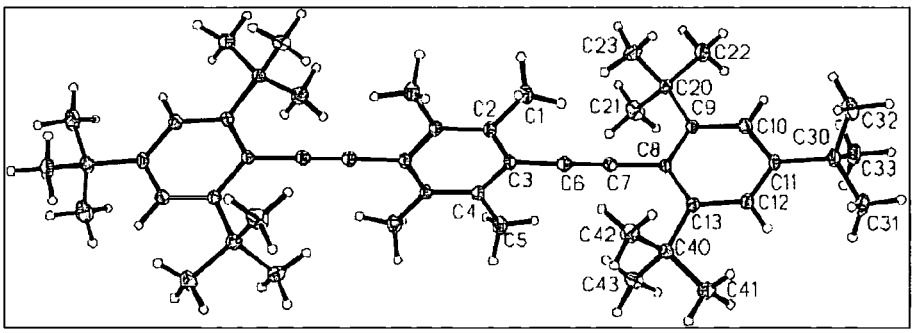

A.13 - 9,10-Bis(2-*tert*-butylphenylethynyl)anthracene (211)

Crystal data and structure refinement

Identification code	03srv127	
Empirical formula	C38 H34	
Formula weight	490.65	
Temperature	120(2) K	
Wavelength	0.71073 Å	
Crystal system	Monoclinic	
Space group	P2(1)/n	
Unit cell dimensions	a = 9.5027(6) Å	α= 90°.
	b = 8.2756(5) Å	β= 98.6420(10)°.
	c = 17.7737(11) Å	γ = 90°.
Volume	1381.86(15) $Å^3$	
Z	2	
Density (calculated)	1.179 Mg/m^3	
Absorption coefficient	0.066 mm^{-1}	
F(000)	524	
Crystal size	0.14 x 0.14 x 0.08 mm^3	
Theta range for data collection	2.30 to 29.13°.	
Index ranges	-12<=h<=12, -11<=k<=11, -24<=l<=23	
Reflections collected	13736	
Independent reflections	3699 [R(int) = 0.0646]	
Completeness to theta = 29.13°	99.6 %	
Absorption correction	Integration	
Max. and min. transmission	0.9947 and 0.9908	
Refinement method	Full-matrix least-squares on F^2	
Data / restraints / parameters	3699 / 0 / 240	
Goodness-of-fit on F^2	1.030	
Final R indices [I>2sigma(I)]	R1 = 0.0538, wR2 = 0.1121	
R indices (all data)	R1 = 0.0959, wR2 = 0.1262	
Extinction coefficient	0	
Largest diff. peak and hole	0.229 and -0.225 $e.Å^{-3}$	

Atomic coordinates (x 10^4) and equivalent isotropic displacement parameters ($Å^2$ x 10^3) for 03srv127. U(eq) is defined as one third of the trace of the orthogonalized U^{ij} tensor.

	x	y	z	U(eq)
C(1)	3550(2)	286(2)	66(1)	18(1)
C(2)	2114(2)	602(2)	160(1)	22(1)
C(3)	1764(2)	1896(2)	567(1)	25(1)
C(4)	2834(2)	2983(2)	902(1)	25(1)
C(5)	4218(2)	2730(2)	826(1)	23(1)
C(6)	4632(2)	1372(2)	414(1)	19(1)
C(7)	6075(2)	1068(2)	346(1)	19(1)
C(8)	7167(2)	2140(2)	701(1)	21(1)
C(9)	8070(2)	2986(2)	1040(1)	21(1)
C(10)	9117(2)	4085(2)	1426(1)	19(1)
C(11)	9421(2)	5449(2)	1015(1)	24(1)
C(12)	10346(2)	6633(2)	1345(1)	26(1)
C(13)	10980(2)	6446(2)	2090(1)	25(1)
C(14)	10711(2)	5078(2)	2499(1)	22(1)
C(15)	9782(2)	3857(2)	2191(1)	19(1)
C(16)	9482(2)	2372(2)	2661(1)	21(1)
C(17)	7902(2)	2345(2)	2759(1)	28(1)
C(18)	10336(2)	2419(2)	3466(1)	28(1)
C(19)	9893(2)	808(2)	2278(1)	26(1)

Bond lengths [Å] and angles [°]for 03srv127.

C(1) -C(7)#1	1.413(2)	C(18)-H(18B)	1.00(2)
C(1) -C(2)	1.424(2)	C(18)-H(18C)	1.011(19)
C(1) -C(6)	1.434(2)	C(19)-H(19A)	1.04(2)
C(2) -C(3)	1.361(2)	C(19)-H(19B)	0.981(19)
C(2) -H(2)	0.960(17)	C(19)-H(19C)	0.966(19)
C(3) -C(4)	1.420(2)		
C(3) -H(3)	0.954(19)	C(7)#1-C(1)-C(2)	121.82(13)
C(4) -C(5)	1.358(2)	C(7)#1-C(1)-C(6)	119.97(13)
C(4) -H(4)	0.963(18)	C(2)-C(1)-C(6)	118.21(13)
C(5) -C(6)	1.429(2)	C(3)-C(2)-C(1)	121.45(15)
C(5) -H(5)	1.005(18)	C(3)-C(2)-H(2)	121.0(10)
C(6) -C(7)	1.416(2)	C(1)-C(2)-H(2)	117.5(10)
C(7) -C(1)#1	1.413(2)	C(2)-C(3)-C(4)	120.28(15)
C(7) -C(8)	1.438(2)	C(2)-C(3)-H(3)	120.0(11)
C(8) -C(9)	1.198(2)	C(4)-C(3)-H(3)	119.8(11)

C(9) -C(10)	1.443(2)	C(5)-C(4)-C(3)	120.25(15)
C(10)-C(11)	1.399(2)	C(5)-C(4)-H(4)	121.1(11)
C(10)-C(15)	1.422(2)	C(3)-C(4)-H(4)	118.6(11)
C(11)-C(12)	1.386(2)	C(4)-C(5)-C(6)	121.20(15)
C(11)-H(11)	0.980(19)	C(4)-C(5)-H(5)	122.4(10)
C(12)-C(13)	1.380(2)	C(6)-C(5)-H(5)	116.3(10)
C(12)-H(12)	0.965(17)	C(7)-C(6)-C(5)	121.89(13)
C(13)-C(14)	1.389(2)	C(7)-C(6)-C(1)	119.50(13)
C(13)-H(13)	0.956(19)	C(5)-C(6)-C(1)	118.60(13)
C(14)-C(15)	1.398(2)	C(1)#1-C(7)-C(6)	120.53(13)
C(14)-H(14)	0.958(17)	C(1)#1-C(7)-C(8)	119.67(13)
C(15)-C(16)	1.537(2)	C(6)-C(7)-C(8)	119.80(13)
C(16)-C(18)	1.536(2)	C(9)-C(8)-C(7)	175.84(17)
C(16)-C(17)	1.537(2)	C(8)-C(9)-C(10)	176.75(17)
C(16)-C(19)	1.540(2)	C(11)-C(10)-C(15)	120.60(14)
C(17)-H(17A)	1.02(2)	C(11)-C(10)-C(9)	116.17(14)
C(17)-H(17B)	0.986(19)	C(15)-C(10)-C(9)	123.20(14)
C(17)-H(17C)	1.001(19)	C(12)-C(11)-C(10)	121.16(15)
C(18)-H(18A)	1.02(2)	C(12)-C(11)-H(11)	118.7(11)
C(10)-C(11)-H(11)	120.2(11)	C(16)-C(17)-H(17A)	109.8(12)
C(13)-C(12)-C(11)	118.96(15)	C(16)-C(17)-H(17B)	109.7(11)
C(13)-C(12)-H(12)	119.9(10)	H(17A)-C(17)-H(17B)	105.7(15)
C(11)-C(12)-H(12)	121.1(10)	C(16)-C(17)-H(17C)	112.8(11)
C(12)-C(13)-C(14)	120.36(15)	H(17A)-C(17)-H(17C)	108.5(16)
C(12)-C(13)-H(13)	120.9(11)	H(17B)-C(17) -H(17C)	110.2(15)
C(14)-C(13)-H(13)	118.7(11)	C(16)-C(18)-H(18A)	108.5(11)
C(13)-C(14)-C(15)	122.64(15)	C(16)-C(18)-H(18B)	111.5(11)
C(13)-C(14)-H(14)	118.7(10)	H(18A)-C(18)-H(18B)	106.8(16)
C(15)-C(14)-H(14)	118.7(10)	C(16)-C(18)-H(18C)	109.2(10)
C(14)-C(15)-C(10)	116.25(14)	H(18A)-C(18)-H(18C)	107.0(16)
C(14)-C(15)-C(16)	121.51(13)	H(18B)-C(18) -H(18C)	113.7(15)
C(10)-C(15)-C(16)	122.23(13)	C(16)-C(19)-H(19A)	110.1(11)
C(18)-C(16)-C(17)	106.48(14)	C(16)-C(19)-H(19B)	112.0(11)
C(18)-C(16)-C(15)	111.81(13)	H(19A)-C(19)-H(19B)	106.9(15)
C(17)-C(16)-C(15)	109.73(12)	C(16)-C(19)-H(19C)	111.4(11)
C(18)-C(16)-C(19)	107.44(13)	H(19A)-C(19)-H(19C)	107.4(16)
C(17)-C(16)-C(19)	110.76(13)	H(19B)-C(19) -H(19C)	108.8(15)
C(15)-C(16)-C(19)	110.54(13)		

Symmetry transformations used to generate equivalent atoms:
#1 -x+1,-y,-z

Anisotropic displacement parameters ($Å^2 x\ 10^3$) for 03srv127. The anisotropic displacement factor exponent takes the form: $-2\pi^2 [h^2 a^{*2} U^{11} + ... + 2 h k a^* b^* U^{12}]$

	U^{11}	U^{22}	U^{33}	U^{23}	U^{13}	U^{12}
C(1)	20(1)	19(1)	15(1)	1(1)	2(1)	0(1)
C(2)	19(1)	26(1)	22(1)	1(1)	1(1)	-1(1)
C(3)	22(1)	30(1)	25(1)	1(1)	6(1)	4(1)
C(4)	28(1)	25(1)	23(1)	-2(1)	4(1)	7(1)
C(5)	26(1)	21(1)	20(1)	-2(1)	-1(1)	0(1)
C(6)	20(1)	19(1)	16(1)	0(1)	0(1)	2(1)
C(7)	21(1)	21(1)	16(1)	1(1)	0(1)	0(1)
C(8)	20(1)	25(1)	18(1)	0(1)	1(1)	3(1)
C(9)	20(1)	23(1)	20(1)	0(1)	4(1)	3(1)
C(10)	16(1)	20(1)	22(1)	-4(1)	4(1)	1(1)
C(11)	23(1)	25(1)	23(1)	0(1)	3(1)	1(1)
C(12)	26(1)	20(1)	33(1)	3(1)	7(1)	-3(1)
C(13)	23(1)	21(1)	33(1)	-5(1)	3(1)	-5(1)
C(14)	20(1)	23(1)	24(1)	-4(1)	1(1)	-1(1)
C(15)	17(1)	19(1)	22(1)	-4(1)	4(1)	1(1)
C(16)	21(1)	20(1)	22(1)	-1(1)	3(1)	-1(1)
C(17)	27(1)	30(1)	30(1)	1(1)	9(1)	-4(1)
C(18)	33(1)	27(1)	24(1)	0(1)	1(1)	1(1)
C(19)	29(1)	21(1)	27(1)	-1(1)	2(1)	1(1)

Hydrogen coordinates ($x\ 10^4$) and isotropic displacement parameters ($Å^2 x\ 10^3$) for 03srv127.

	x	y	z	U(eq)
H(2)	1399(17)	-140(20)	-70(9)	22(4)
H(3)	790(20)	2080(20)	622(10)	36(5)
H(4)	2559(19)	3880(20)	1190(10)	32(5)
H(5)	4997(19)	3500(20)	1032(10)	27(4)
H(11)	8958(19)	5600(20)	488(11)	32(5)
H(12)	10524(18)	7600(20)	1067(10)	23(4)
H(13)	11570(20)	7280(20)	2344(10)	32(5)
H(14)	11178(17)	4969(19)	3012(10)	22(4)
H(17A)	7660(20)	3350(30)	3042(12)	48(6)
H(17B)	7721(19)	1420(20)	3084(10)	35(5)
H(17C)	7250(20)	2290(20)	2262(11)	34(5)
H(18A)	10100(20)	1420(30)	3751(12)	47(6)
H(18B)	11390(20)	2390(20)	3453(11)	37(5)

H(18C)	10022(19)	3380(20)	3749(10)	33(5)
H(19A)	9730(20)	-190(20)	2610(11)	47(6)
H(19B)	9316(19)	640(20)	1778(11)	33(5)
H(19C)	10890(20)	810(20)	2218(10)	35(5)

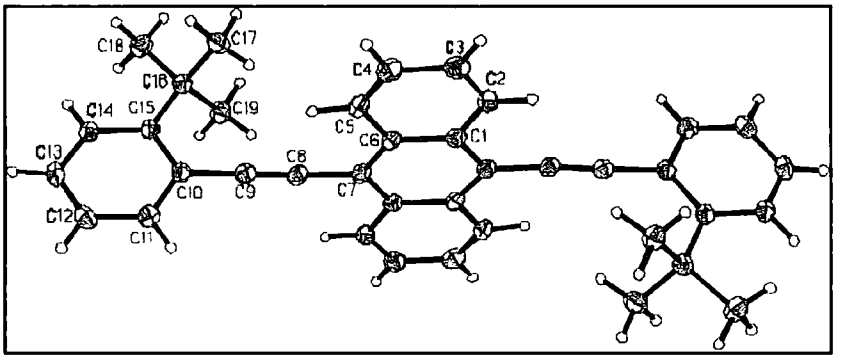

A.14 - 9,10-Bis(2,4,6-triisopropylphenylethynyl)anthracene (212)

Crystal data and structure refinement

Identification code	04srv329	
Empirical formula	C48 H54	
Formula weight	630.91	
Temperature	120(2) K	
Wavelength	0.71073 Å	
Crystal system	Triclinic	
Space group	P-1	
Unit cell dimensions	a = 8.7097(7) Å	α= 75.569(2)°.
	b = 11.2536(9) Å	β= 75.845(2)°.
	c = 20.4061(15) Å	γ = 86.020(2)°.
Volume	1878.1(3) $Å^3$	
Z	2	
Density (calculated)	1.116 Mg/m^3	
Absorption coefficient	0.062 mm^{-1}	
F(000)	684	
Crystal size	0.22 x 0.18 x 0.08 mm^3	
Theta range for data collection	1.87 to 26.00°.	
Index ranges	-10<=h<=10, -13<=k<=13, -25<=l<=25	
Reflections collected	14682	
Independent reflections	7324 [R(int) = 0.0336]	
Completeness to theta = 26.00°	99.3 %	
Absorption correction	Integration	
Max. and min. transmission	0.99497 and 0.97683	
Refinement method	Full-matrix least-squares on F^2	
Data / restraints / parameters	7324 / 0 / 445	
Goodness-of-fit on F^2	0.993	
Final R indices [I>2sigma(I)]	R1 = 0.0480, wR2 = 0.1156	
R indices (all data)	R1 = 0.0833, wR2 = 0.1312	
Extinction coefficient	0	
Largest diff. peak and hole	0.199 and -0.234 $e.Å^{-3}$	

Atomic coordinates (x 10^4) and equivalent isotropic displacement parameters ($Å^2$ x 10^3) for 04srv329. U(eq) is defined as one third of the trace of the orthogonalized U^{ij} tensor.

	x	y	z	U(eq)
C(1)	7984(2)	5787(1)	1081(1)	20(1)
C(2)	9226(2)	6227(1)	1268(1)	20(1)
C(3)	9631(2)	5721(1)	1898(1)	19(1)
C(4)	8715(2)	4734(1)	2366(1)	18(1)
C(5)	7470(2)	4244(1)	2182(1)	19(1)
C(6)	7135(2)	4785(1)	1541(1)	21(1)
C(7)	7541(2)	6430(2)	401(1)	23(1)
C(8)	5878(2)	6986(2)	536(1)	33(1)
C(9)	7692(3)	5610(2)	-101(1)	47(1)
C(10)	11024(2)	6178(1)	2090(1)	21(1)
C(11)	12391(2)	5245(2)	2047(1)	28(1)
C(12)	11622(2)	7438(2)	1641(1)	25(1)
C(13)	6524(2)	3178(1)	2700(1)	21(1)
C(14)	5319(2)	3638(2)	3271(1)	28(1)
C(15)	5708(2)	2403(2)	2371(1)	31(1)
C(16)	9061(2)	4219(1)	3033(1)	18(1)
C(17)	9360(2)	3765(1)	3589(1)	20(1)
C(18)	9710(2)	3210(1)	4249(1)	19(1)
C(19)	10803(2)	3763(1)	4489(1)	19(1)
C(20)	11123(2)	3218(2)	5154(1)	20(1)
C(21)	10331(2)	2124(1)	5571(1)	20(1)
C(22)	9266(2)	1559(1)	5323(1)	19(1)
C(23)	8937(2)	2108(1)	4660(1)	19(1)
C(24)	11574(2)	4883(2)	4094(1)	22(1)
C(25)	12583(2)	5427(2)	4344(1)	24(1)
C(26)	12900(2)	4890(2)	5001(1)	25(1)
C(27)	12200(2)	3813(2)	5392(1)	23(1)
C(28)	8509(2)	433(2)	5715(1)	22(1)
C(29)	7504(2)	-120(2)	5469(1)	25(1)
C(30)	7165(2)	431(2)	4816(1)	26(1)
C(31)	7849(2)	1512(2)	4428(1)	23(1)
C(32)	10600(2)	1606(1)	6248(1)	20(1)
C(33)	10804(2)	1168(1)	6821(1)	20(1)
C(34)	11058(2)	647(1)	7505(1)	19(1)
C(35)	12373(2)	1018(1)	7694(1)	19(1)
C(36)	12575(2)	511(1)	8363(1)	21(1)
C(37)	11532(2)	-352(1)	8843(1)	19(1)

C(38)	10237(2)	-692(1)	8645(1)	20(1)
C(39)	9959(2)	-204(1)	7988(1)	18(1)
C(40)	13530(2)	1937(2)	7164(1)	22(1)
C(41)	14639(2)	1303(2)	6649(1)	34(1)
C(42)	14480(2)	2628(2)	7488(1)	28(1)
C(43)	11794(2)	-977(1)	9561(1)	21(1)
C(44)	12825(2)	-259(2)	9827(1)	28(1)
C(45)	12477(2)	-2265(2)	9554(1)	29(1)
C(46)	8525(2)	-573(2)	7787(1)	20(1)
C(47)	8950(2)	-1668(2)	7457(1)	31(1)
C(48)	7063(2)	-835(2)	8387(1)	30(1)

Bond lengths [Å] and angles [°]for 04srv329.

C(1) -C(2)	1.389(2)	C(14)-H(14B)	0.9800
C(1) -C(6)	1.396(2)	C(14)-H(14C)	0.9800
C(1) -C(7)	1.523(2)	C(15)-H(15A)	0.9800
C(2) -C(3)	1.389(2)	C(15)-H(15B)	0.9800
C(2) -H(2)	0.9500	C(15)-H(15C)	0.9800
C(3) -C(4)	1.416(2)	C(16)-C(17)	1.206(2)
C(3) -C(10)	1.519(2)	C(17)-C(18)	1.432(2)
C(4) -C(5)	1.415(2)	C(18)-C(19)	1.412(2)
C(4) -C(16)	1.437(2)	C(18)-C(23)	1.420(2)
C(5) -C(6)	1.390(2)	C(19)-C(24)	1.427(2)
C(5) -C(13)	1.521(2)	C(19)-C(20)	1.430(2)
C(6) -H(6)	0.9500	C(20)-C(21)	1.423(2)
C(7) -C(9)	1.519(3)	C(20)-C(27)	1.426(2)
C(7) -C(8)	1.527(2)	C(21)-C(22)	1.412(2)
C(7) -H(7)	1.0000	C(21)-C(32)	1.428(2)
C(8) -H(8A)	0.9800	C(22)-C(28)	1.426(2)
C(8) -H(8B)	0.9800	C(22)-C(23)	1.429(2)
C(8) -H(8C)	0.9800	C(23)-C(31)	1.427(2)
C(9) -H(9A)	0.9800	C(24)-C(25)	1.363(2)
C(9) -H(9B)	0.9800	C(24)-H(24)	0.9500
C(9) -H(9C)	0.9800	C(25)-C(26)	1.411(2)
C(10)-C(12)	1.531(2)	C(25)-H(25)	0.9500
C(10)-C(11)	1.533(2)	C(26)-C(27)	1.364(2)
C(10)-H(10)	1.0000	C(26)-H(26)	0.9500
C(11)-H(11A)	0.9800	C(27)-H(27)	0.9500
C(11)-H(11B)	0.9800	C(28)-C(29)	1.362(2)

C(11)-H(11C)	0.9800	C(28)-H(28)	0.9500
C(12)-H(12A)	0.9800	C(29)-C(30)	1.415(2)
C(12)-H(12B)	0.9800	C(29)-H(29)	0.9500
C(12)-H(12C)	0.9800	C(30)-C(31)	1.361(2)
C(13)-C(15)	1.525(2)	C(30)-H(30A)	0.9500
C(13)-C(14)	1.533(2)	C(31)-H(31)	0.9500
C(13)-H(13)	1.0000	C(32)-C(33)	1.202(2)
C(14)-H(14A)	0.9800	C(33)-C(34)	1.438(2)
C(34)-C(35)	1.414(2)	C(48)-H(48B)	0.9800
C(34)-C(39)	1.414(2)	C(48)-H(48C)	0.9800
C(35)-C(36)	1.390(2)		
C(35)-C(40)	1.519(2)	C(2)-C(1)-C(6)	118.36(14)
C(36)-C(37)	1.393(2)	C(2)-C(1)-C(7)	119.83(14)
C(36)-H(36)	0.9500	C(6)-C(1)-C(7)	121.76(14)
C(37)-C(38)	1.393(2)	C(3)-C(2)-C(1)	122.53(15)
C(37)-C(43)	1.523(2)	C(3)-C(2)-H(2)	118.7
C(38)-C(39)	1.390(2)	C(1)-C(2)-H(2)	118.7
C(38)-H(38)	0.9500	C(2)-C(3)-C(4)	117.98(14)
C(39)-C(46)	1.520(2)	C(2)-C(3)-C(10)	122.31(14)
C(40)-C(41)	1.526(2)	C(4)-C(3)-C(10)	119.71(14)
C(40)-C(42)	1.530(2)	C(5)-C(4)-C(3)	120.78(14)
C(40)-H(40)	1.0000	C(5)-C(4)-C(16)	119.71(14)
C(41)-H(41A)	0.9800	C(3)-C(4)-C(16)	119.51(14)
C(41)-H(41B)	0.9800	C(6)-C(5)-C(4)	118.34(14)
C(41)-H(41C)	0.9800	C(6)-C(5)-C(13)	122.67(14)
C(42)-H(42A)	0.9800	C(4)-C(5)-C(13)	118.97(13)
C(42)-H(42B)	0.9800	C(5)-C(6)-C(1)	121.95(15)
C(42)-H(42C)	0.9800	C(5)-C(6)-H(6)	119.0
C(43)-C(44)	1.521(2)	C(1)-C(6)-H(6)	119.0
C(43)-C(45)	1.530(2)	C(9)-C(7)-C(1)	113.41(14)
C(43)-H(43)	1.0000	C(9)-C(7)-C(8)	110.26(16)
C(44)-H(44A)	0.9800	C(1)-C(7)-C(8)	111.14(14)
C(44)-H(44B)	0.9800	C(9)-C(7)-H(7)	107.2
C(44)-H(44C)	0.9800	C(1)-C(7)-H(7)	107.2
C(45)-H(45A)	0.9800	C(8)-C(7)-H(7)	107.2
C(45)-H(45B)	0.9800	C(7)-C(8)-H(8A)	109.5
C(45)-H(45C)	0.9800	C(7)-C(8)-H(8B)	109.5
C(46)-C(48)	1.522(2)	H(8A)-C(8)-H(8B)	109.5
C(46)-C(47)	1.529(2)	C(7)-C(8)-H(8C)	109.5
C(46)-H(46)	1.0000	H(8A)-C(8)-H(8C)	109.5

C(47)-H(47A)	0.9800	H(8B)-C(8)-H(8C)	109.5
C(47)-H(47B)	0.9800	C(7)-C(9)-H(9A)	109.5
C(47)-H(47C)	0.9800	C(7)-C(9)-H(9B)	109.5
C(48)-H(48A)	0.9800	H(9A)-C(9)-H(9B)	109.5
C(7) -C(9)-H(9C)	109.5	C(13)-C(15)-H(15C)	109.5
H(9A)-C(9)-H(9C)	109.5	H(15A)-C(15)-H(15C)	109.5
H(9B)-C(9)-H(9C)	109.5	H(15B)-C(15) -H(15C)	109.5
C(3) -C(10)-C(12)	113.84(13)	C(17)-C(16)-C(4)	178.69(17)
C(3) -C(10)-C(11)	110.07(13)	C(16)-C(17)-C(18)	179.18(17)
C(12)-C(10)-C(11)	109.36(14)	C(19)-C(18)-C(23)	120.58(14)
C(3) -C(10)-H(10)	107.8	C(19)-C(18)-C(17)	120.07(14)
C(12)-C(10)-H(10)	107.8	C(23)-C(18)-C(17)	119.35(14)
C(11)-C(10)-H(10)	107.8	C(18)-C(19)-C(24)	121.86(14)
C(10)-C(11)-H(11A)	109.5	C(18)-C(19)-C(20)	119.86(14)
C(10)-C(11)-H(11B)	109.5	C(24)-C(19)-C(20)	118.25(14)
H(11A)-C(11)-H(11B)	109.5	C(21)-C(20)-C(27)	121.63(14)
C(10)-C(11)-H(11C)	109.5	C(21)-C(20)-C(19)	119.61(14)
H(11A)-C(11)-H(11C)	109.5	C(27)-C(20)-C(19)	118.74(15)
H(11B)-C(11)-H(11C)	109.5	C(22)-C(21)-C(20)	120.34(14)
C(10)-C(12)-H(12A)	109.5	C(22)-C(21)-C(32)	119.90(14)
C(10)-C(12)-H(12B)	109.5	C(20)-C(21)-C(32)	119.76(14)
H(12A)-C(12)-H(12B)	109.5	C(21)-C(22)-C(28)	121.63(14)
C(10)-C(12)-H(12C)	109.5	C(21)-C(22)-C(23)	120.03(14)
H(12A)-C(12)-H(12C)	109.5	C(28)-C(22)-C(23)	118.34(14)
H(12B)-C(12)-H(12C)	109.5	C(18)-C(23)-C(31)	122.03(14)
C(5) -C(13)-C(15)	114.31(13)	C(18)-C(23)-C(22)	119.55(14)
C(5) -C(13)-C(14)	110.44(13)	C(31)-C(23)-C(22)	118.41(14)
C(15)-C(13)-C(14)	110.48(14)	C(25)-C(24)-C(19)	121.07(15)
C(5) -C(13)-H(13)	107.1	C(25)-C(24)-H(24)	119.5
C(15)-C(13)-H(13)	107.1	C(19)-C(24)-H(24)	119.5
C(14)-C(13)-H(13)	107.1	C(24)-C(25)-C(26)	120.68(15)
C(13)-C(14)-H(14A)	109.5	C(24)-C(25)-H(25)	119.7
C(13)-C(14)-H(14B)	109.5	C(26)-C(25)-H(25)	119.7
H(14A)-C(14)-H(14B)	109.5	C(27)-C(26)-C(25)	120.12(16)
C(13)-C(14)-H(14C)	109.5	C(27)-C(26)-H(26)	119.9
H(14A)-C(14)-H(14C)	109.5	C(25)-C(26)-H(26)	119.9
H(14B)-C(14)-H(14C)	109.5	C(26)-C(27)-C(20)	121.14(15)
C(13)-C(15)-H(15A)	109.5	C(26)-C(27)-H(27)	119.4
C(13)-C(15)-H(15B)	109.5	C(20)-C(27)-H(27)	119.4
H(15A)-C(15)-H(15B)	109.5	C(29)-C(28)-C(22)	121.47(15)

C(29)-C(28)-H(28)	119.3	C(42)-C(40)-H(40)	107.3
C(22)-C(28)-H(28)	119.3	C(40)-C(41)-H(41A)	109.5
C(28)-C(29)-C(30)	120.16(15)	C(40)-C(41)-H(41B)	109.5
C(28)-C(29)-H(29)	119.9	H(41A)-C(41)-H(41B)	109.5
C(30)-C(29)-H(29)	119.9	C(40)-C(41)-H(41C)	109.5
C(31)-C(30)-C(29)	120.25(16)	H(41A)-C(41)-H(41C)	109.5
C(31)-C(30)-H(30A)	119.9	H(41B)-C(41) -H(41C)	109.5
C(29)-C(30)-H(30A)	119.9	C(40)-C(42)-H(42A)	109.5
C(30)-C(31)-C(23)	121.35(15)	C(40)-C(42)-H(42B)	109.5
C(30)-C(31)-H(31)	119.3	H(42A)-C(42)-H(42B)	109.5
C(23)-C(31)-H(31)	119.3	C(40)-C(42)-H(42C)	109.5
C(33)-C(32)-C(21)	179.10(18)	H(42A)-C(42)-H(42C)	109.5
C(32)-C(33)-C(34)	179.7(2)	H(42B)-C(42) -H(42C)	109.5
C(35)-C(34)-C(39)	120.81(14)	C(44)-C(43)-C(37)	114.31(13)
C(35)-C(34)-C(33)	119.73(14)	C(44)-C(43)-C(45)	110.77(14)
C(39)-C(34)-C(33)	119.43(14)	C(37)-C(43)-C(45)	109.22(13)
C(36)-C(35)-C(34)	118.42(15)	C(44)-C(43)-H(43)	107.4
C(36)-C(35)-C(40)	122.05(14)	C(37)-C(43)-H(43)	107.4
C(34)-C(35)-C(40)	119.52(14)	C(45)-C(43)-H(43)	107.4
C(35)-C(36)-C(37)	121.96(15)	C(43)-C(44)-H(44A)	109.5
C(35)-C(36)-H(36)	119.0	C(43)-C(44)-H(44B)	109.5
C(37)-C(36)-H(36)	119.0	H(44A)-C(44)-H(44B)	109.5
C(38)-C(37)-C(36)	118.43(14)	C(43)-C(44)-H(44C)	109.5
C(38)-C(37)-C(43)	118.92(14)	H(44A)-C(44)-H(44C)	109.5
C(36)-C(37)-C(43)	122.59(14)	H(44B)-C(44) -H(44C)	109.5
C(39)-C(38)-C(37)	122.29(15)	C(43)-C(45)-H(45A)	109.5
C(39)-C(38)-H(38)	118.9	C(43)-C(45)-H(45B)	109.5
C(37)-C(38)-H(38)	118.9	H(45A)-C(45)-H(45B)	109.5
C(38)-C(39)-C(34)	118.06(14)	C(43)-C(45)-H(45C)	109.5
C(38)-C(39)-C(46)	121.43(14)	H(45A)-C(45)-H(45C)	109.5
C(34)-C(39)-C(46)	120.51(14)	H(45B)-C(45) -H(45C)	109.5
C(35)-C(40)-C(41)	110.21(14)	C(39)-C(46)-C(48)	113.69(13)
C(35)-C(40)-C(42)	113.90(14)	C(39)-C(46)-C(47)	109.74(13)
C(41)-C(40)-C(42)	110.51(15)	C(48)-C(46)-C(47)	111.08(14)
C(35)-C(40)-H(40)	107.3	C(39)-C(46)-H(46)	107.3
C(41)-C(40)-H(40)	107.3	C(48)-C(46)-H(46)	107.3
C(47)-C(46)-H(46)	107.3	C(46)-C(48)-H(48A)	109.5
C(46)-C(47)-H(47A)	109.5	C(46)-C(48)-H(48B)	109.5
C(46)-C(47)-H(47B)	109.5	H(48A)-C(48)-H(48B)	109.5
H(47A)-C(47)-H(47B)	109.5	C(46)-C(48)-H(48C)	109.5

C(46)-C(47)-H(47C)	109.5	H(48A)-C(48)-H(48C)	109.5
H(47A)-C(47)-H(47C)	109.5	H(48B)-C(48) -H(48C)	109.5
H(47B)-C(47)-H(47C)	109.5		

Anisotropic displacement parameters ($Å^2 x\ 10^3$) for 04srv329. The anisotropic displacement factor exponent takes the form: $-2\pi^2 [h^2 a^{*2} U^{11} + ... + 2 h k a^* b^* U^{12}]$

	U^{11}	U^{22}	U^{33}	U^{23}	U^{13}	U^{12}
C(1)	19(1)	23(1)	16(1)	-4(1)	-5(1)	4(1)
C(2)	18(1)	19(1)	18(1)	0(1)	-2(1)	0(1)
C(3)	17(1)	21(1)	18(1)	-5(1)	-4(1)	2(1)
C(4)	18(1)	20(1)	16(1)	-3(1)	-5(1)	2(1)
C(5)	18(1)	19(1)	18(1)	-5(1)	-4(1)	2(1)
C(6)	19(1)	24(1)	22(1)	-6(1)	-8(1)	0(1)
C(7)	23(1)	25(1)	18(1)	0(1)	-8(1)	0(1)
C(8)	30(1)	36(1)	28(1)	5(1)	-11(1)	4(1)
C(9)	80(2)	41(1)	25(1)	-10(1)	-26(1)	19(1)
C(10)	21(1)	23(1)	21(1)	-3(1)	-8(1)	-2(1)
C(11)	21(1)	29(1)	35(1)	-1(1)	-11(1)	-2(1)
C(12)	25(1)	23(1)	28(1)	-4(1)	-9(1)	-3(1)
C(13)	22(1)	21(1)	19(1)	-1(1)	-8(1)	-1(1)
C(14)	25(1)	31(1)	25(1)	-1(1)	-2(1)	-4(1)
C(15)	35(1)	28(1)	28(1)	-1(1)	-10(1)	-11(1)
C(16)	16(1)	19(1)	19(1)	-4(1)	-4(1)	-2(1)
C(17)	18(1)	21(1)	21(1)	-4(1)	-4(1)	-3(1)
C(18)	19(1)	23(1)	16(1)	-5(1)	-5(1)	3(1)
C(19)	16(1)	24(1)	16(1)	-5(1)	-2(1)	3(1)
C(20)	16(1)	24(1)	18(1)	-4(1)	-4(1)	3(1)
C(21)	19(1)	23(1)	16(1)	-3(1)	-6(1)	3(1)
C(22)	17(1)	22(1)	17(1)	-4(1)	-4(1)	3(1)
C(23)	16(1)	23(1)	17(1)	-4(1)	-4(1)	2(1)
C(24)	21(1)	25(1)	18(1)	-4(1)	-4(1)	1(1)
C(25)	21(1)	24(1)	24(1)	-4(1)	0(1)	-3(1)
C(26)	20(1)	30(1)	28(1)	-8(1)	-7(1)	-2(1)
C(27)	20(1)	30(1)	20(1)	-5(1)	-8(1)	2(1)
C(28)	23(1)	24(1)	18(1)	-2(1)	-4(1)	1(1)
C(29)	26(1)	23(1)	21(1)	-2(1)	-1(1)	-3(1)
C(30)	23(1)	31(1)	26(1)	-8(1)	-9(1)	-4(1)
C(31)	22(1)	28(1)	20(1)	-3(1)	-7(1)	-1(1)
C(32)	19(1)	22(1)	20(1)	-4(1)	-5(1)	-1(1)

C(33)	20(1)	21(1)	21(1)	-4(1)	-7(1)	-3(1)
C(34)	20(1)	18(1)	17(1)	-3(1)	-6(1)	0(1)
C(35)	19(1)	20(1)	17(1)	-4(1)	-5(1)	-1(1)
C(36)	20(1)	23(1)	21(1)	-4(1)	-7(1)	-1(1)
C(37)	21(1)	19(1)	17(1)	-4(1)	-6(1)	1(1)
C(38)	21(1)	17(1)	17(1)	-1(1)	-1(1)	-3(1)
C(39)	20(1)	18(1)	19(1)	-5(1)	-5(1)	0(1)
C(40)	23(1)	26(1)	18(1)	-1(1)	-7(1)	-5(1)
C(41)	34(1)	37(1)	28(1)	-9(1)	4(1)	-13(1)
C(42)	28(1)	31(1)	24(1)	-3(1)	-5(1)	-12(1)
C(43)	24(1)	23(1)	15(1)	0(1)	-6(1)	-2(1)
C(44)	37(1)	28(1)	20(1)	-1(1)	-12(1)	-6(1)
C(45)	40(1)	26(1)	23(1)	-3(1)	-14(1)	3(1)
C(46)	18(1)	23(1)	20(1)	-4(1)	-5(1)	-3(1)
C(47)	32(1)	31(1)	35(1)	-12(1)	-13(1)	-2(1)
C(48)	23(1)	39(1)	29(1)	-7(1)	-8(1)	-7(1)

Hydrogen coordinates (x 10^4) and isotropic displacement parameters ($Å^2$ x 10^3) for 04srv329.

	x	y	z	U(eq)
H(2)	9820	6899	953	24
H(6)	6302	4463	1413	25
H(7)	8296	7123	167	27
H(8A)	5678	7488	97	49
H(8B)	5790	7501	867	49
H(8C)	5098	6327	730	49
H(9A)	8780	5294	-203	70
H(9B)	7434	6083	-533	70
H(9C)	6960	4921	111	70
H(10)	10672	6245	2584	25
H(11A)	12040	4459	2371	43
H(11B)	13284	5548	2170	43
H(11C)	12724	5132	1571	43
H(12A)	10722	8006	1611	38
H(12B)	12169	7362	1172	38
H(12C)	12356	7752	1851	38
H(13)	7287	2627	2931	25
H(14A)	4800	2935	3626	42
H(14B)	4522	4156	3066	42
H(14C)	5865	4116	3484	42
H(15A)	6494	2109	2012	46

H(15B)	4906	2902	2161	46
H(15C)	5199	1700	2730	46
H(24)	11381	5256	3649	26
H(25)	13078	6176	4074	29
H(26)	13602	5278	5171	30
H(27)	12434	3452	5830	28
H(28)	8711	61	6158	27
H(29)	7030	-878	5736	30
H(30A)	6456	45	4648	31
H(31)	7599	1878	3994	28
H(36)	13450	761	8496	25
H(38)	9518	-1276	8971	24
H(40)	12896	2559	6895	27
H(41A)	15262	1922	6267	51
H(41B)	14014	838	6460	51
H(41C)	15352	743	6887	51
H(42A)	13753	3000	7832	42
H(42B)	15099	3273	7123	42
H(42C)	15197	2055	7717	42
H(43)	10733	-1073	9895	25
H(44A)	12401	576	9803	42
H(44B)	13909	-225	9538	42
H(44C)	12831	-666	10311	42
H(45A)	12558	-2697	10025	44
H(45B)	13531	-2202	9238	44
H(45C)	11779	-2720	9394	44
H(46)	8256	131	7422	24
H(47A)	8043	-1870	7301	46
H(47B)	9223	-2376	7801	46
H(47C)	9858	-1460	7057	46
H(48A)	6878	-155	8618	45
H(48B)	7229	-1597	8721	45
H(48C)	6142	-923	8207	45

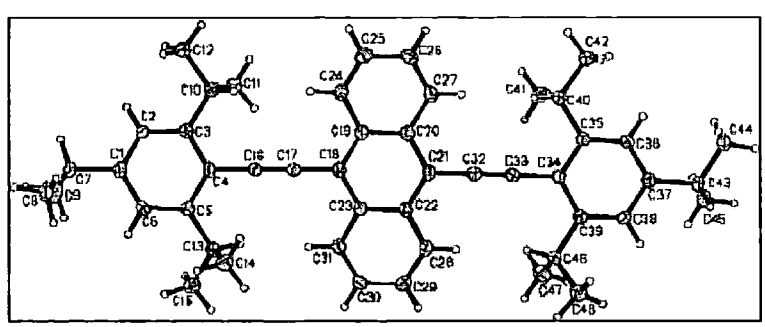

A.15- 10-(2-*tert*-butylphenylethynyl)-9-(phenylethynyl)anthracene (214)

Crystal data and structure refinement

Identification code	04srv281	
Empirical formula	C34 H26	
Formula weight	434.55	
Temperature	120(2) K	
Wavelength	0.71073 Å	
Crystal system	Orthorhombic	
Space group	P b c a	
Unit cell dimensions	a = 8.8619(5) Å	α= 90°.
	b = 17.8452(10) Å	β= 90°.
	c = 30.3744(17) Å	γ = 90°.
Volume	4803.5(5) $Å^3$	
Z	8	
Density (calculated)	1.202 Mg/m^3	
Absorption coefficient	0.068 mm^{-1}	
F(000)	1840	
Crystal size	0.40 x 0.10 x 0.06 mm^3	
Theta range for data collection	1.34 to 30.47°.	
Index ranges	-12<=h<=10, -24<=k<=24, -42<=l<=42	
Reflections collected	42322	
Independent reflections	7004 [R(int) = 0.1472]	
Completeness to theta = 30.47°	95.7 %	
Absorption correction	None	
Max. and min. transmission	0.9959 and 0.9734	
Refinement method	Full-matrix least-squares on F^2	
Data / restraints / parameters	7004 / 0 / 412	
Goodness-of-fit on F^2	1.026	
Final R indices [I>2sigma(I)]	R1 = 0.0726, wR2 = 0.1169	
R indices (all data)	R1 = 0.1861, wR2 = 0.1413	
Extinction coefficient	0.0032(3)	
Largest diff. peak and hole	0.215 and -0.193 $e.Å^{-3}$	

Atomic coordinates (x 10^4) and equivalent isotropic displacement parameters ($Å^2$ x 10^3) for 04srv281. U(eq) is defined as one third of the trace of the orthogonalized U^{ij} tensor.

	x	y	z	U(eq)
C(1)	4220(3)	2515(1)	1805(1)	40(1)
C(2)	4350(3)	1960(2)	2124(1)	48(1)
C(3)	3262(4)	1407(2)	2155(1)	50(1)
C(4)	2045(4)	1405(2)	1874(1)	50(1)
C(5)	1909(3)	1954(1)	1554(1)	43(1)
C(6)	3009(3)	2513(1)	1517(1)	31(1)
C(7)	2887(3)	3057(1)	1172(1)	32(1)
C(8)	2751(2)	3493(1)	871(1)	30(1)
C(9)	2549(2)	4006(1)	514(1)	28(1)
C(10)	1591(2)	3806(1)	159(1)	29(1)
C(11)	805(3)	3109(1)	151(1)	33(1)
C(12)	-136(3)	2934(1)	-185(1)	36(1)
C(13)	-358(3)	3442(1)	-539(1)	35(1)
C(14)	378(3)	4112(1)	-543(1)	32(1)
C(15)	1381(2)	4320(1)	-196(1)	27(1)
C(16)	2142(2)	5015(1)	-195(1)	27(1)
C(17)	3094(2)	5217(1)	160(1)	27(1)
C(18)	3877(2)	5915(1)	168(1)	30(1)
C(19)	4780(3)	6100(1)	513(1)	32(1)
C(20)	4957(3)	5600(1)	871(1)	34(1)
C(21)	4241(3)	4926(1)	874(1)	31(1)
C(22)	3292(2)	4707(1)	518(1)	28(1)
C(23)	1961(2)	5522(1)	-558(1)	30(1)
C(24)	1877(2)	5953(1)	-861(1)	30(1)
C(25)	1872(2)	6539(1)	-1184(1)	30(1)
C(26)	2316(3)	7245(1)	-1029(1)	34(1)
C(27)	2368(3)	7863(1)	-1299(1)	36(1)
C(28)	1969(3)	7781(1)	-1736(1)	40(1)
C(29)	1545(3)	7082(1)	-1897(1)	37(1)
C(30)	1484(2)	6448(1)	-1635(1)	32(1)
C(31)	994(3)	5687(1)	-1823(1)	34(1)
C(32)	2235(3)	5097(2)	-1749(1)	42(1)
C(33)	-473(3)	5437(2)	-1604(1)	41(1)
C(34)	711(4)	5724(2)	-2323(1)	47(1)

Bond lengths [Å] and angles [°]for 04srv281.

C(1) -C(6)	1.384(3)	C(18)-H(18)	1.00(2)
C(1) -C(2)	1.390(3)	C(19)-C(20)	1.416(3)
C(1) -H(1)	0.95(2)	C(19)-H(19)	1.00(2)
C(2) -C(3)	1.383(4)	C(20)-C(21)	1.361(3)
C(2) -H(2)	0.94(3)	C(20)-H(20)	0.95(2)
C(3) -C(4)	1.376(4)	C(21)-C(22)	1.426(3)
C(3) -H(3)	0.97(2)	C(21)-H(21)	0.98(2)
C(4) -C(5)	1.385(3)	C(23)-C(24)	1.202(3)
C(4) -H(4)	1.07(3)	C(24)-C(25)	1.434(3)
C(5) -C(6)	1.399(3)	C(25)-C(26)	1.402(3)
C(5) -H(5)	0.99(3)	C(25)-C(30)	1.421(3)
C(6) -C(7)	1.433(3)	C(26)-C(27)	1.375(3)
C(7) -C(8)	1.206(3)	C(26)-H(26)	0.97(2)
C(8) -C(9)	1.430(3)	C(27)-C(28)	1.382(3)
C(9) -C(22)	1.412(3)	C(27)-H(27)	0.95(2)
C(9) -C(10)	1.419(3)	C(28)-C(29)	1.391(3)
C(10)-C(11)	1.427(3)	C(28)-H(28)	0.96(2)
C(10)-C(15)	1.428(3)	C(29)-C(30)	1.385(3)
C(11)-C(12)	1.354(3)	C(29)-H(29)	0.99(2)
C(11)-H(11)	1.02(2)	C(30)-C(31)	1.536(3)
C(12)-C(13)	1.417(3)	C(31)-C(33)	1.528(3)
C(12)-H(12)	0.99(2)	C(31)-C(32)	1.539(3)
C(13)-C(14)	1.363(3)	C(31)-C(34)	1.540(3)
C(13)-H(13)	1.00(2)	C(32)-H(321)	1.00(3)
C(14)-C(15)	1.427(3)	C(32)-H(322)	1.03(2)
C(14)-H(14)	0.95(2)	C(32)-H(323)	1.05(2)
C(15)-C(16)	1.412(3)	C(33)-H(331)	1.03(3)
C(16)-C(17)	1.417(3)	C(33)-H(332)	0.97(2)
C(16)-C(23)	1.433(3)	C(33)-H(333)	1.01(2)
C(17)-C(18)	1.427(3)	C(34)-H(341)	0.99(2)
C(17)-C(22)	1.427(3)	C(34)-H(342)	1.07(3)
C(18)-C(19)	1.358(3)	C(34)-H(343)	0.94(3)
C(6) -C(1)-C(2)	120.2(3)	C(6)-C(1)-H(1)	119.6(15)
C(2) -C(1)-H(1)	120.2(15)	C(16)-C(15)-C(14)	121.8(2)
C(3) -C(2)-C(1)	119.9(3)	C(16)-C(15)-C(10)	120.02(19)
C(3) -C(2)-H(2)	117.8(17)	C(14)-C(15)-C(10)	118.19(19)
C(1) -C(2)-H(2)	122.2(17)	C(15)-C(16)-C(17)	120.57(19)
C(4) -C(3)-C(2)	120.3(3)	C(15)-C(16)-C(23)	119.99(19)
C(4) -C(3)-H(3)	120.7(14)	C(17)-C(16)-C(23)	119.44(19)

C(2) -C(3)-H(3)	118.8(14)	C(16)-C(17)-C(18)	121.63(19)
C(3) -C(4)-C(5)	120.2(3)	C(16)-C(17)-C(22)	119.40(19)
C(3) -C(4)-H(4)	120.7(15)	C(18)-C(17)-C(22)	118.97(19)
C(5) -C(4)-H(4)	118.7(15)	C(19)-C(18)-C(17)	120.8(2)
C(4) -C(5)-C(6)	120.0(3)	C(19)-C(18)-H(18)	120.1(12)
C(4) -C(5)-H(5)	120.8(16)	C(17)-C(18)-H(18)	119.1(12)
C(6) -C(5)-H(5)	119.1(15)	C(18)-C(19)-C(20)	120.3(2)
C(1) -C(6)-C(5)	119.4(2)	C(18)-C(19)-H(19)	119.8(13)
C(1) -C(6)-C(7)	121.3(2)	C(20)-C(19)-H(19)	119.9(13)
C(5) -C(6)-C(7)	119.3(2)	C(21)-C(20)-C(19)	120.7(2)
C(8) -C(7)-C(6)	177.3(2)	C(21)-C(20)-H(20)	120.3(14)
C(7) -C(8)-C(9)	178.6(2)	C(19)-C(20)-H(20)	118.9(14)
C(22)-C(9)-C(10)	120.44(19)	C(20)-C(21)-C(22)	120.8(2)
C(22)-C(9)-C(8)	120.2(2)	C(20)-C(21)-H(21)	121.9(13)
C(10)-C(9)-C(8)	119.35(19)	C(22)-C(21)-H(21)	117.2(12)
C(9) -C(10)-C(11)	121.7(2)	C(9)-C(22)-C(21)	121.5(2)
C(9) -C(10)-C(15)	119.44(19)	C(9)-C(22)-C(17)	120.11(19)
C(11)-C(10)-C(15)	118.8(2)	C(21)-C(22)-C(17)	118.37(19)
C(12)-C(11)-C(10)	121.0(2)	C(24)-C(23)-C(16)	177.1(2)
C(12)-C(11)-H(11)	121.8(12)	C(23)-C(24)-C(25)	172.2(2)
C(10)-C(11)-H(11)	117.2(12)	C(26)-C(25)-C(30)	119.6(2)
C(11)-C(12)-C(13)	120.6(2)	C(26)-C(25)-C(24)	115.15(19)
C(11)-C(12)-H(12)	119.1(13)	C(30)-C(25)-C(24)	125.24(19)
C(13)-C(12)-H(12)	120.3(13)	C(27)-C(26)-C(25)	122.0(2)
C(14)-C(13)-C(12)	120.1(2)	C(27)-C(26)-H(26)	119.2(13)
C(14)-C(13)-H(13)	117.6(13)	C(25)-C(26)-H(26)	118.9(13)
C(12)-C(13)-H(13)	122.2(13)	C(26)-C(27)-C(28)	118.7(2)
C(13)-C(14)-C(15)	121.3(2)	C(26)-C(27)-H(27)	124.9(14)
C(13)-C(14)-H(14)	117.2(13)	C(28)-C(27)-H(27)	116.4(14)
C(15)-C(14)-H(14)	121.4(13)	C(27)-C(28)-C(29)	120.2(2)
C(27)-C(28)-H(28)	120.6(13)	H(321)-C(32) -H(322)	110.3(19)
C(29)-C(28)-H(28)	118.7(13)	C(31)-C(32)-H(323)	109.0(13)
C(30)-C(29)-C(28)	122.7(2)	H(321)-C(32) -H(323)	105.7(19)
C(30)-C(29)-H(29)	115.5(11)	H(322)-C(32) -H(323)	104.7(18)
C(28)-C(29)-H(29)	121.8(11)	C(31)-C(33)-H(331)	107.8(13)
C(29)-C(30)-C(25)	116.9(2)	C(31)-C(33)-H(332)	113.5(13)
C(29)-C(30)-C(31)	121.2(2)	H(331)-C(33) -H(332)	109.8(19)
C(25)-C(30)-C(31)	121.84(19)	C(31)-C(33)-H(333)	114.0(13)
C(33)-C(31)-C(30)	109.70(18)	H(331)-C(33) -H(333)	105.5(18)
C(33)-C(31)-C(32)	110.2(2)	H(332)-C(33) -H(333)	105.9(18)

C(30)-C(31)-C(32)	110.4(2)	C(31)-C(34)-H(341)	113.5(13)
C(33)-C(31)-C(34)	107.6(2)	C(31)-C(34)-H(342)	112.4(14)
C(30)-C(31)-C(34)	112.0(2)	H(341)-C(34) -H(342)	106.3(19)
C(32)-C(31)-C(34)	106.8(2)	C(31)-C(34)-H(343)	107.9(16)
C(31)-C(32)-H(321)	113.2(14)	H(341)-C(34) -H(343)	108(2)
C(31)-C(32)-H(322)	113.4(12)	H(342)-C(34) -H(343)	109(2)

Anisotropic displacement parameters ($Å^2 x\ 10^3$) for 04srv281. The anisotropic displacement factor exponent takes the form: $-2\pi^2 [h^2 a^{*2} U^{11} + ... + 2 h k a^* b^* U^{12}]$

	U^{11}	U^{22}	U^{33}	U^{23}	U^{13}	U^{12}
C(1)	44(2)	42(2)	33(1)	-1(1)	2(1)	7(1)
C(2)	55(2)	58(2)	32(2)	-1(1)	2(1)	20(2)
C(3)	81(2)	41(2)	27(1)	6(1)	14(2)	17(2)
C(4)	74(2)	43(2)	34(2)	2(1)	13(2)	-3(2)
C(5)	53(2)	43(1)	32(1)	-3(1)	6(1)	-4(1)
C(6)	41(1)	30(1)	24(1)	-2(1)	7(1)	6(1)
C(7)	33(1)	34(1)	29(1)	-6(1)	6(1)	2(1)
C(8)	32(1)	31(1)	27(1)	-6(1)	3(1)	0(1)
C(9)	30(1)	30(1)	25(1)	-4(1)	5(1)	5(1)
C(10)	28(1)	28(1)	30(1)	-7(1)	5(1)	3(1)
C(11)	35(1)	30(1)	33(1)	-4(1)	2(1)	-1(1)
C(12)	35(1)	33(1)	40(2)	-7(1)	5(1)	-4(1)
C(13)	34(1)	38(1)	33(1)	-13(1)	-2(1)	1(1)
C(14)	33(1)	34(1)	29(1)	-6(1)	0(1)	5(1)
C(15)	26(1)	29(1)	25(1)	-5(1)	3(1)	2(1)
C(16)	27(1)	28(1)	25(1)	-4(1)	3(1)	7(1)
C(17)	27(1)	28(1)	26(1)	-5(1)	2(1)	5(1)
C(18)	28(1)	29(1)	32(1)	-2(1)	1(1)	4(1)
C(19)	35(1)	27(1)	35(1)	-4(1)	-3(1)	2(1)
C(20)	33(1)	36(1)	32(1)	-8(1)	-5(1)	1(1)
C(21)	33(1)	32(1)	28(1)	-3(1)	-3(1)	5(1)
C(22)	27(1)	31(1)	25(1)	-2(1)	4(1)	5(1)
C(23)	29(1)	30(1)	33(1)	-7(1)	-1(1)	4(1)
C(24)	29(1)	31(1)	30(1)	-8(1)	-1(1)	3(1)
C(25)	27(1)	30(1)	32(1)	0(1)	-2(1)	6(1)
C(26)	33(1)	35(1)	33(1)	-6(1)	-3(1)	5(1)
C(27)	39(1)	28(1)	42(2)	-1(1)	-2(1)	2(1)
C(28)	44(2)	33(1)	42(2)	4(1)	-6(1)	2(1)
C(29)	42(2)	40(1)	30(1)	-1(1)	-7(1)	5(1)
C(30)	32(1)	32(1)	32(1)	-2(1)	-3(1)	5(1)

C(31)	39(1)	32(1)	31(1)	-4(1)	-2(1)	4(1)
C(32)	47(2)	39(2)	41(2)	-5(1)	1(1)	10(1)
C(33)	42(2)	38(2)	43(2)	-10(1)	-7(1)	-2(1)
C(34)	65(2)	42(2)	35(2)	-9(1)	-14(2)	3(2)

Hydrogen coordinates (x 10^4) and isotropic displacement parameters ($Å^2$ x 10^3) for 04srv281.

	x	y	z	U(eq)
H(1)	4960(30)	2893(13)	1782(8)	46(7)
H(2)	5150(30)	1948(15)	2325(9)	68(9)
H(3)	3400(30)	1004(13)	2367(8)	45(7)
H(4)	1280(30)	945(15)	1869(9)	74(9)
H(5)	1070(30)	1942(14)	1339(9)	70(9)
H(11)	1000(20)	2746(12)	403(7)	39(6)
H(12)	-660(20)	2445(13)	-183(7)	41(6)
H(13)	-1070(30)	3333(13)	-787(8)	54(7)
H(14)	220(20)	4428(11)	-789(7)	32(6)
H(18)	3740(20)	6273(11)	-81(7)	31(6)
H(19)	5290(20)	6602(12)	519(7)	41(6)
H(20)	5580(30)	5746(13)	1113(8)	50(7)
H(21)	4340(20)	4576(12)	1121(7)	38(6)
H(26)	2590(30)	7299(12)	-720(8)	45(7)
H(27)	2700(30)	8348(13)	-1211(7)	45(7)
H(28)	2120(20)	8185(12)	-1942(7)	37(6)
H(29)	1250(20)	7006(10)	-2210(7)	28(6)
H(321)	3200(30)	5220(13)	-1903(8)	53(8)
H(322)	2430(20)	4985(11)	-1423(8)	36(6)
H(323)	1880(30)	4585(14)	-1882(8)	53(7)
H(331)	-1310(30)	5804(14)	-1698(8)	56(8)
H(332)	-410(20)	5417(11)	-1286(8)	32(6)
H(333)	-830(20)	4924(13)	-1701(7)	45(7)
H(341)	-90(30)	6085(13)	-2407(7)	43(7)
H(342)	1700(30)	5884(14)	-2502(9)	65(9)
H(343)	400(30)	5243(15)	-2417(8)	59(8)

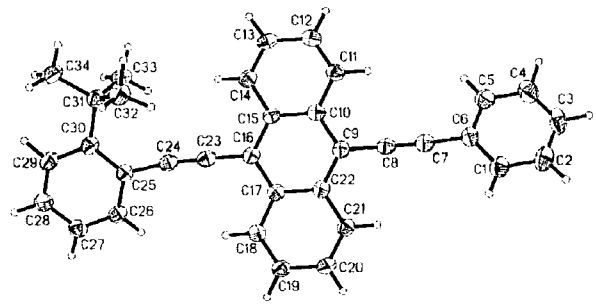

A.16 - 1,4-Bis((2-trimethylsilyl)phenylethynyl)durene (219)

Crystal data and structure refinement

Identification code	05srv084	
Empirical formula	C32 H38 Si2	
Formula weight	478.80	
Temperature	120(2) K	
Wavelength	0.71073 Å	
Crystal system	Triclinic	
Space group	P-1	
Unit cell dimensions	a = 7.0812(2) Å	α= 92.4650(10)°.
	b = 7.9366(2) Å	β= 103.5990(10)°.
	c = 13.8352(3) Å	γ = 110.4600(10)°.
Volume	701.35(3) $Å^3$	
Z	1	
Density (calculated)	1.134 Mg/m^3	
Absorption coefficient	0.144 mm^{-1}	
F(000)	258	
Crystal size	0.55 x 0.16 x 0.07 mm^3	
Theta range for data collection	1.53 to 30.00°.	
Index ranges	-9<=h<=9, -11<=k<=11, -19<=l<=19	
Reflections collected	9998	
Independent reflections	4067 [R(int) = 0.0490]	
Completeness to theta = 30.00°	99.6 %	
Absorption correction	None	
Max. and min. transmission	1.0000 and 0.9342	
Refinement method	Full-matrix least-squares on F^2	
Data / restraints / parameters	4067 / 0 / 164	
Goodness-of-fit on F^2	1.040	
Final R indices [I>2sigma(I)]	R1 = 0.0426, wR2 = 0.1165	
R indices (all data)	R1 = 0.0583, wR2 = 0.1258	
Extinction coefficient	0	
Largest diff. peak and hole	0.405 and -0.239 $e.Å^{-3}$	

Atomic coordinates (x 10^4) and equivalent isotropic displacement parameters ($Å^2$ x 10^3) for 05srv084. U(eq) is defined as one third of the trace of the orthogonalized U^{ij} tensor.

	x	y	z	U(eq)
Si(1)	3508(1)	2334(1)	1196(1)	25(1)
C(1)	9509(2)	5964(2)	2673(1)	31(1)
C(2)	7722(2)	4846(2)	1955(1)	27(1)
C(3)	5890(2)	3803(2)	2205(1)	22(1)
C(4)	5950(2)	3943(2)	3238(1)	22(1)
C(5)	7765(2)	5075(2)	3962(1)	26(1)
C(6)	9533(2)	6082(2)	3677(1)	30(1)
C(7)	4228(3)	2222(2)	-16(1)	34(1)
C(8)	1490(2)	3377(2)	1079(1)	36(1)
C(9)	2499(2)	-42(2)	1492(1)	31(1)
C(10)	4199(2)	2914(2)	3603(1)	23(1)
C(11)	2889(2)	2065(2)	3995(1)	23(1)
C(12)	1405(2)	1010(2)	4500(1)	21(1)
C(13)	-748(2)	278(2)	4003(1)	21(1)
C(14)	-2164(2)	-741(2)	4503(1)	21(1)
C(15)	-1504(2)	559(2)	2932(1)	29(1)
C(16)	-4468(2)	-1572(2)	3977(1)	28(1)
Si(1)	3508(1)	2334(1)	1196(1)	25(1)

Bond lengths [Å] and angles [°]for 05srv084.

C(1) -C(6)	1.376(3)	C(14)-H(14B)	0.9800
Si(1)-C(8)	1.8664(15)	C(8) -H(8B)	0.9800
Si(1)-C(9)	1.8702(15)	C(8) -H(8C)	0.9800
Si(1)-C(7)	1.8712(14)	C(9) -H(9A)	0.9800
Si(1)-C(3)	1.8789(14)	C(9) -H(9B)	0.9800
C(1) -C(6)	1.384(2)	C(9) -H(9C)	0.9800
C(1) -C(2)	1.387(2)	C(10)-C(11)	1.1996(18)
C(1) -H(1)	0.9500	C(11)-C(12)	1.4400(17)
C(2) -C(3)	1.4046(17)	C(12)-C(13)	1.4095(17)
C(2) -H(2)	0.9500	C(12)-C(14)#1	1.4129(17)
C(3) -C(4)	1.4187(18)	C(13)-C(14)	1.3946(17)
C(4) -C(5)	1.4042(18)	C(13)-C(15)	1.5072(17)
C(4) -C(10)	1.4423(17)	C(14)-C(12)#1	1.4129(17)
C(5) -C(6)	1.3856(19)	C(14)-C(16)	1.5086(17)
C(5) -H(5)	0.9500	C(15)-H(15A)	0.9800
C(6) -H(6)	0.9500	C(15)-H(15B)	0.9800

C(7) -H(7A)	0.9800	C(15)-H(15C)	0.9800
C(7) -H(7B)	0.9800	C(16)-H(16A)	0.9800
C(7) -H(7C)	0.9800	C(16)-H(16B)	0.9800
C(8) -H(8A)	0.9800	C(16)-H(16C)	0.9800

C(8) -Si(1)-C(9)	111.14(7)	Si(1)-C(8)-H(8C)	109.5
C(8) -Si(1)-C(7)	110.24(7)	H(8A)-C(8)-H(8C)	109.5
C(9) -Si(1)-C(7)	107.21(7)	H(8B)-C(8)-H(8C)	109.5
C(8) -Si(1)-C(3)	108.03(7)	Si(1)-C(9)-H(9A)	109.5
C(9) -Si(1)-C(3)	111.08(6)	Si(1)-C(9)-H(9B)	109.5
C(7) -Si(1)-C(3)	109.14(6)	H(9A)-C(9)-H(9B)	109.5
C(6) -C(1)-C(2)	120.14(12)	Si(1)-C(9)-H(9C)	109.5
C(6) -C(1)-H(1)	119.9	H(9A)-C(9)-H(9C)	109.5
C(2) -C(1)-H(1)	119.9	H(9B)-C(9)-H(9C)	109.5
C(1) -C(2)-C(3)	122.31(12)	C(11)-C(10)-C(4)	173.35(13)
C(1) -C(2)-H(2)	118.8	C(10)-C(11)-C(12)	176.70(14)
C(3) -C(2)-H(2)	118.8	C(13)-C(12)-C(14)#1	121.43(11)
C(2) -C(3)-C(4)	116.62(12)	C(13)-C(12)-C(11)	120.24(11)
C(2) -C(3)-Si(1)	120.31(10)	C(14)#1-C(12)-C(11)	118.33(11)
C(4) -C(3)-Si(1)	123.07(9)	C(14)-C(13)-C(12)	119.49(11)
C(5) -C(4)-C(3)	120.76(12)	C(14)-C(13)-C(15)	120.34(11)
C(5) -C(4)-C(10)	116.77(11)	C(12)-C(13)-C(15)	120.15(11)
C(3) -C(4)-C(10)	122.46(12)	C(13)-C(14)-C(12)#1	119.08(11)
C(6) -C(5)-C(4)	120.48(12)	C(13)-C(14)-C(16)	120.33(11)
C(6) -C(5)-H(5)	119.8	C(12)#1-C(14)-C(16)	120.58(11)
C(4) -C(5)-H(5)	119.8	C(13)-C(15)-H(15A)	109.5
C(1) -C(6)-C(5)	119.69(13)	C(13)-C(15)-H(15B)	109.5
C(1) -C(6)-H(6)	120.2	H(15A)-C(15)-H(15B)	109.5
C(5) -C(6)-H(6)	120.2	C(13)-C(15)-H(15C)	109.5
Si(1)-C(7)-H(7A)	109.5	H(15A)-C(15)-H(15C)	109.5
Si(1)-C(7)-H(7B)	109.5	H(15B)-C(15)-H(15C)	109.5
H(7A)-C(7)-H(7B)	109.5	C(14)-C(16)-H(16A)	109.5
Si(1)-C(7)-H(7C)	109.5	C(14)-C(16)-H(16B)	109.5
H(7A)-C(7)-H(7C)	109.5	H(16A)-C(16)-H(16B)	109.5
H(7B)-C(7)-H(7C)	109.5	C(14)-C(16)-H(16C)	109.5
Si(1)-C(8)-H(8A)	109.5	H(16A)-C(16)-H(16C)	109.5
Si(1)-C(8)-H(8B)	109.5	H(16B)-C(16)-H(16C)	109.5
H(8A)-C(8)-H(8B)	109.5		

Symmetry transformations used to generate equivalent atoms:

#1 -x,-y,-z+1

Anisotropic displacement parameters ($Å^2 x\ 10^3$) for 05srv084. The anisotropic displacement factor exponent takes the form: $-2\pi^2 [h^2 a^{*2} U^{11} + ... + 2 h k a^* b^* U^{12}]$

	U^{11}	U^{22}	U^{33}	U^{23}	U^{13}	U^{12}
Si(1)	26(1)	30(1)	21(1)	5(1)	8(1)	12(1)
C(1)	25(1)	25(1)	44(1)	11(1)	17(1)	7(1)
C(2)	30(1)	27(1)	31(1)	12(1)	17(1)	13(1)
C(3)	24(1)	22(1)	26(1)	7(1)	11(1)	11(1)
C(4)	23(1)	21(1)	25(1)	6(1)	10(1)	10(1)
C(5)	28(1)	24(1)	26(1)	2(1)	8(1)	9(1)
C(6)	24(1)	23(1)	39(1)	2(1)	8(1)	6(1)
C(7)	43(1)	39(1)	25(1)	6(1)	13(1)	18(1)
C(8)	31(1)	50(1)	32(1)	4(1)	6(1)	22(1)
C(9)	30(1)	29(1)	28(1)	0(1)	8(1)	4(1)
C(10)	24(1)	25(1)	21(1)	3(1)	7(1)	9(1)
C(11)	25(1)	25(1)	21(1)	3(1)	7(1)	10(1)
C(12)	21(1)	21(1)	22(1)	4(1)	9(1)	8(1)
C(13)	22(1)	23(1)	20(1)	4(1)	7(1)	10(1)
C(14)	20(1)	23(1)	22(1)	3(1)	7(1)	8(1)
C(15)	27(1)	38(1)	23(1)	10(1)	8(1)	13(1)
C(16)	20(1)	37(1)	27(1)	8(1)	6(1)	9(1)

Hydrogen coordinates ($x\ 10^4$) and isotropic displacement parameters ($Å^2\ x\ 10^3$) for 05srv084.

	x	y	z	U(eq)
H(1)	10719	6650	2475	37
H(2)	7737	4783	1270	32
H(5)	7782	5151	4651	31
H(6)	10756	6851	4169	36
H(7A)	3037	1347	-526	51
H(7B)	5426	1839	81	51
H(7C)	4599	3424	-238	51
H(8A)	169	2551	624	54
H(8B)	1960	4530	811	54
H(8C)	1281	3598	1742	54
H(9A)	1224	-765	971	46
H(9B)	2183	-29	2145	46
H(9C)	3561	-577	1517	46
H(15A)	-2674	973	2870	43
H(15B)	-1969	-588	2489	43
H(15C)	-362	1476	2740	43

H(16A)	-4672	-2232	3322	43
H(16B)	-5036	-610	3881	43
H(16C)	-5195	-2414	4386	43

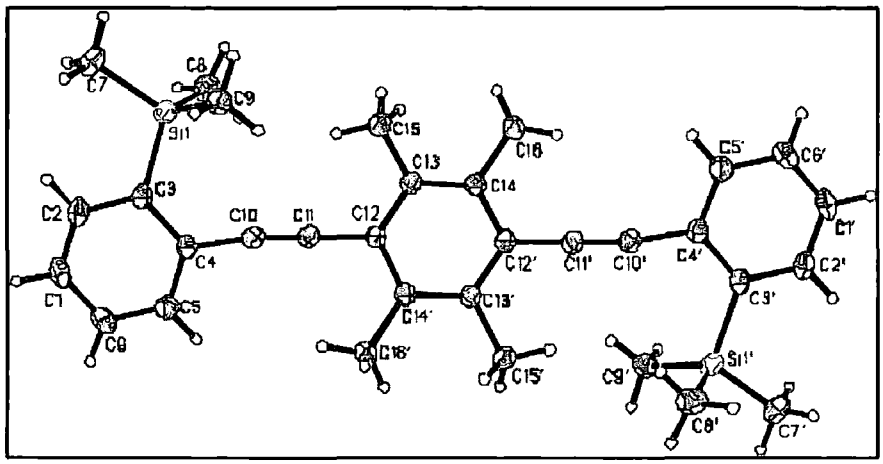

APPENDIX B

ADDITIONAL ACTIVITIES

B.1 - Publications

Studies of the S_1, state in a prototypical molecular wire using picosecond time-resolved spectroscopies.
A. Beeby, K. S. Findlay, P. J. Low, T. B. Marder, P. Matousek, A. W. Parker, S. R. Rutter and M. Towrie, *Chem. Commun.*, 2003, 2406-2407.

Cavity ring-down spectroscopy of the torsional motions of 1,4-bis(phenylethynyl) benzene.
S. J. Greaves, E. L. Flynn, E. L. Futcher, E. Wrede, D. P. Lydon, P. J. Low, S. R. Rutter and A. Beeby, *J. Phys. Chem. A*, 2006, ***110***, 2114-2121.

Engineering a twist in 9,10-diethynylanthracenes by steric interactions.
A. Beeby, K. S. Findlay, A. E. Goeta, L. Porrès, S. R. Rutter and A. L. Thompson, *Photochem. Photobiol. Sci.* In Press.

Synthesis, photophysics and molecular structures of luminescent 2,5-bis(phenylethynyl) thiophenes (BPETs).
J. S. Siddle, R. M. Ward, J. C. Collings, S. R. Rutter, L. Porrès, L. Applegarth, A. Beeby, A. S. Batsanov, A. L. Thompson, J. A. K. Howard, A. Boucekkine, K. Costuas, J-F. Halet and T. B. Marder, *New J. Chem.* Advance Article.

B.2 - Posters Presented

Time-Resolved Spectroscopy of Arylene Ethynylenes
A. Beeby, K. S. Findlay, P. J. Low, T. B. Marder, S. R. Rutter, P. Matousek, A. W. Parker and M. Towrie
FRIS 2003 - Fast Reactions in Solution, RSC Discussion Group Meeting
Martin-Luther-Universität Halle-Wittenberg, Germany, 01/09/03

Twisting A Molecular Wire
A. Beeby, K. S. Findlay, P. J. Low, L. Porrès and S. R. Rutter
Avecia and Rutherford Chemicals Postgraduate Poster Competition
Department of Chemistry, University of Durham, UK, 18/04/05

B.3 - Conferences and Symposia Attended

Biomolecular Probes Mini-Symposium
University of Durham
UK, 16/01/03

FRIS 2003 - Fast Reactions in Solution, RSC Discussion Group Meeting
Martin-Luther-Universität Halle-Wittenberg
Germany, 31/08/03 - 03/09/03

Durham Nanomaterials UIC, Quarterly Review Meeting
University of Durham
UK, 28/06/04

FRIS 2004 - Fast Reactions in Solution, RSC Discussion Group Meeting
Universidad de Burgos
Spain, 05/09/04 - 08/09/04

Photons, Electrons and Inorganic Chemistry
University of York
UK, 24/11/04

B.4- Seminars Attended

09/10/02 Prof Jinqui Qin, Wuhan University, China, "New design approaches for some electroactive materials"

01/11/02 Dr James P. Riehl, University of Minnesota, "Recent theoretical & experimental probes of the solution structure and excited state energetics of Ln(III) complexes."

13/11/02 Prof Geoffrey Lawrence, Newcastle University, Australia, "Designer Ligands: Macrocyclic and alicyclic molecules for metal complexation and biocatalysis"

20/11/02 Dr Mike George, University of Nottingham, "Time resolved IR spectroscopy: from organometallic nobel gas compounds to IR probes of DNA"

29/01/03 Dr Doug Stephan, University of Windsor, Ontario, Canada, "Transition metal phosphinimide complexes: Highly active olefin polymerisation catalysts with unique deactivation pathways."

05/02/03 Dr Rudiger Faust, UCL, "Light, acetylenes and heterocycles - a powerful combination"

12/02/03 Prof Paul Raithby, University of Bath, "Adventures in Organometallic Polymer Chemistry"

19/02/03 Prof Tony Ryan, University of Sheffield, "Introducing Soft Nanotechnology"

26/02/03 Prof Kingsley Cavell, University of Cardiff, "Unique reactions of heterocyclic carbine complexes: Important ramifications for their application in catalysis"

26/03/03 Dr Joe Keddie, Dept of Physics, University of Surrey, "The sticky business of pressure-sensitive adhesives"

29/10/03 Prof. Roger Davey, Molecular Materials Centre, UMIST, "Stereochemical Approaches to Crystal Nucleation"

04/11/03 Dr Cliff Ludman, Dept of Chemistry, University of Durham, "Explosions - A Demonstration Lecture"

05/11/03 Prof. Colin Bain, Dept of Chemistry, University of Oxford, "Pouring Oil in Troubled Waters: Wetting Transistors and Phase Transitions in Surfactant / Alkane / Water systems

26/11/03 Dr Wilhelm Huck, Dept of Chem, University of Cambridge, "The Polymer Nanoworld - Polymers that do things at a small scale"

28/01/04 Dr Lesley Yellowlees, Dept of Chemistry, University of Edinburgh, "Electrochemical and Spectrochemical Studies on Transition Metal Complexes"

04/02/04 Prof. Paul O'Brien, Dept of Chemistry, University of Manchester, "Quantum Dots, Unlocking the Potential: Working in lost dimensions"

17/03/04 Dr Ian Fairlamb, Dept of Chemistry, University of York, "New Pd Catalysts for the Stille Reaction – Exploitation of a serendipitous discovery"

25/01/05 Prof. Sir Harry Kroto, Department of Chemistry and Biochemistry, Florida State University, "Want to Save the World? Do Chemistry - It's the only show in town for you!"

08/02/05 Dr. Geraint Morgan, Open University, "From the Moon to Mars: The story of Beagle2 and beyond!"

28/06/05 Prof. Anil Kumar, Dept of Chemistry, IIT Bombay, "Novel New Materials and Applications Based on Poly(3,4-Alkylenedioxythiophene)s"

B.5 - Periods Spent Working Away From Durham

Ultrafast Spectroscopy Lab, Central Laser Facility, CCLRC, Rutherford Appleton Laboratory, Chilton, Didcot, Oxfordshire.
05/03/03 - 07/03/03; 08/09/03 - 12/09/03; 05/01/04 - 07/01/04; 01/03/04 - 05/03/04